

**MODIFICATION OF SEMICONDUCTOR SURFACES THROUGH Si-N
LINKAGES BY WET-CHEMISTRY APPROACHES**

AND

**MODULAR FUNCTIONALIZATION OF ZINC OXIDE SURFACES FOR
CHEMICAL PROTECTION OF MATERIAL MORPHOLOGY**

by

Fei Gao

A dissertation submitted to the Faculty of the University of Delaware in partial fulfillment of the requirements for the degree of Doctor of Philosophy in Chemistry and Biochemistry

Summer 2017

© 2017 Fei Gao
All Rights Reserved

**MODIFICATION OF SEMICONDUCTOR SURFACES THROUGH Si-N
LINKAGES BY WET-CHEMISTRY APPROACHES**

AND

**MODULAR FUNCTIONALIZATION OF ZINC OXIDE SURFACES FOR
CHEMICAL PROTECTION OF MATERIAL MORPHOLOGY**

by

Fei Gao

Approved: _____
Murray V. Johnston, Ph.D.
Chair of the Department of Chemistry and Biochemistry

Approved: _____
George H. Watson, Ph.D.
Dean of the College of Arts and Sciences

Approved: _____
Ann L. Ardis, Ph.D.
Senior Vice Provost for Graduate and Professional Education

I certify that I have read this dissertation and that in my opinion it meets the academic and professional standard required by the University as a dissertation for the degree of Doctor of Philosophy.

Signed:

Andrew V. Teplyakov, Ph.D.
Professor in charge of dissertation

I certify that I have read this dissertation and that in my opinion it meets the academic and professional standard required by the University as a dissertation for the degree of Doctor of Philosophy.

Signed:

Lars Gundlach, Ph.D.
Member of dissertation committee

I certify that I have read this dissertation and that in my opinion it meets the academic and professional standard required by the University as a dissertation for the degree of Doctor of Philosophy.

Signed:

Karl Booksh, Ph.D.
Member of dissertation committee

I certify that I have read this dissertation and that in my opinion it meets the academic and professional standard required by the University as a dissertation for the degree of Doctor of Philosophy.

Signed:

S. Ismat Shah, Ph.D.
Member of dissertation committee

ACKNOWLEDGMENTS

Firstly, I want to express gratitude to my research advisor Professor Andrew Teplyakov, an extraordinary advisor from our department and an exceptional mentor among the faculty, for all the support and help throughout my Ph.D. study. As an exceptional mentor, Professor Teplyakov provides a friendly and interesting lab environment for everyone, I totally enjoyed every day in my life working in the lab. More importantly, with Professor Teplyakov's direct instruction and effective guidance, I finished the transition from a student into an independent researcher. Under influence of his enthusiasm for science, I will continue making contribution to the field of surface science in my job.

I would like to say thank you to my committee members Professor Lars Gundlach, Professor Karl Booksh and S. Ismat Shah for the helpful and insightful suggestions for my research projects.

I would like to thank the research group of Professor Thomas Beebe, Jr., especially Dr. Zachary Voras and Ms Rachel Pupillo for their continuous support of XPS and ToF-SIMS instrument.

I want to say thank you to Professor Robert Opila and Mr. Kevin Jones, Mr. Abhishek Iyer and Mr. Jimmy Hack for their their help with charge carrier lifetime measurements.

I want to thank Dr. Chaoying Ni, Dr. Jennifer Sloppy, Dr. Fei Deng for their continuous support with microscopy instrumentation.

I also really appreciate the help from Professor Steve Bai for the instruction and help with solid-state NMR

Thank you to Professor Burnaby Munson and Dr. Federico Cruz for their complete support in my teaching class. Such incredible experience taught me how to deliver knowledge effectively to young students and also helped me develop deeper understanding about physical chemistry from a different perspective.

Thanks to everyone in Professor Andrew Teplyakov's group, including the previous and current group members: Dr. Fangyuan Tian, Mr. Jiaming Lin, Mr. Timothy Miller, Dr. Jia Gao, Dr. Yue Liu, Dr. Hsuan Kung, Dr. Yichen Duan, Miss Jing Zhao, Miss Mackenzie Williams, Mr. Yuexing Cui, River (Chuan) He, Mahsa Konh and Ruth Mandel. We always work together as a team and our office is always filled with happy memories. I am so proud to be a member of Teplyakov Group!

I will not forget to thank our visiting scholars who I have been working together, Miss Ibtihel BenDhiab and Miss Soraya Aminane, for their amazing hard working and creative ideas.

The University of Delaware and its Dissertation Fellowship Program are acknowledged for partial support of this research presented here. Remaining support is allocated from the National Science Foundation (CHE 1057374) and Petroleum Research Fund administered by the American Chemical Society. The National Science Foundation (9724307; 1428149) and the NIH NIGMS COBRE program (P30-GM110758) are also acknowledge for partial support of activities in the University of Delaware Surface Analysis Facility and W. M. Keck Center for Advanced Microscopy and Microanalysis.

I want to thank all the facility and administrative staff members, Mr. Doug Nixon, Mr. Brandon Calitree, Mr. Jim Draper, Mr. John Famiglietti, Mr. Pat McMahon, Mr. Rick Bernard, Mr. Mark Schrader, Miss Susan Cheadle and other staff members in the Department of Chemistry and Biochemistry for their kind help with everything throughout my PhD study at UD.

At last, I feel so grateful to my family, my boyfriend Yi Li, and all my friends all over the world for their endless support, love and encouragement that give me the strength to study abroad, to become a better person bringing positive energy to the society. I probably don't have enough space to name you all here, but you are all deep in my heart throughout my life!

TABLE OF CONTENTS

LIST OF TABLES	xii
LIST OF FIGURES	xiii
ABSTRACT	xxii
Chapter	
1 INTRODUCTION	1
1.1 Chemical Functionalization of Semiconductor Surfaces	1
1.1.1 Organic Functionalization of Silicon Surface	3
1.1.2 Passivation of Gold Surface	4
1.1.3 Functionalization of Zinc Oxide Surface	4
1.2 Analytical Techniques to Study the Surface Modification Process	5
1.2.1 Fourier-Transform Infrared Spectroscopy (FT-IR)	6
1.2.2 X-ray Photoelectron Spectroscopy (XPS)	7
1.2.3 Time-of-Flight Secondary-Ion Mass Spectrometry (ToF-SIMS)	8
1.2.4 Atomic Force Microscopy (AFM).....	9
1.2.5 Scanning Electron Microscopy (SEM).....	11
1.2.6 Transmission Electron Microscopy (TEM).....	11
1.2.7 Nuclear Magnetic Resonance Spectroscopy (NMR).....	12
1.2.8 Charge-Carrier Lifetime Measurements	13
1.2.9 Density Functional Theory (DFT) Calculations	14
1.3 Summary.....	15
REFERENCES	16
2 EXPERIMENTAL	19
2.1 Organic Synthesis	19
2.1.1 Synthesis of <i>t</i> -Butyloxycarbonyl (t-BOC)-Protected 11-Amino-1-Undecene.	19

2.1.1.1	Materials	19
2.1.1.2	Synthetic Procedure	20
2.2	Surface Modification of Silicon and Gold.....	21
2.2.1	Materials	21
2.2.2	Preparation of Hydrogen-Terminated Si(111) Surface.	22
2.2.3	Preparation of Chlorine-Terminated Si (111) Surface.	23
2.2.4	Preparation of Hydrazine-Functionalized Si(111) Surface.	23
2.2.5	Reaction of Phenylhydrazine with Chlorine-Terminated Si (111) Surface.	24
2.2.6	Reaction of C ₆₀ with Hydrazine-Terminated Si(111) Surface. ...	24
2.2.7	Preparation of Amine-Terminated SAM on Si (111) Substrate ..	25
2.2.8	Preparation of Amine-Terminated SAM on Gold Substrate	25
2.2.9	Carbon Nanotube Attached to Functionalized Silicon and Gold Substrates.....	26
2.3	Surface Modification of Zinc Oxide.....	26
2.3.1	Materials	26
2.3.2	Preparation of Propiolic Acid-modified ZnO Surface.....	27
2.3.3	Click Reaction with Propiolic Acid-modified ZnO Surface in Gas Phase.....	27
2.3.4	Click Reaction with Propiolic Acid-modified ZnO Surface in Liquid Phase	28
2.4	Surface Analytical Techniques.....	28
2.4.1	Fourier-Transform Infrared Spectroscopy (FT-IR)	28
2.4.2	X-ray Photoelectron Spectroscopy (XPS)	29
2.4.3	Time-of-Flight Secondary Ion Mass Spectrometry (ToF-SIMS)	30
2.4.4	Scanning Electron Microscopy (SEM).....	31
2.4.5	Atomic Force Microscopy (AFM).....	31
2.4.6	Transmission Electron Microscopy (TEM).....	32
2.4.7	Nuclear Magnetic Resonance Spectroscopy (NMR).....	32
2.4.8	Charge-Carrier Lifetime Measurements	32
2.4.9	Computational Details	33
2.4.9.1	Models calculated with 6-311+G(d,p) basis set.	34
2.4.9.2	Models calculated with LANL2DZ basis set.	41
REFERENCES		58

3	REACTION OF HYDRAZINE WITH A Cl-TERMINATED Si(111) SURFACE AND ITS APPLICATION FOR DIRECT COVALENT ATTACHMENT OF C ₆₀ FULLERENE	61
3.1	Introduction	61
3.2	Results and discussion	67
3.2.1	Reaction of Hydrazine with Cl-terminated Si(111) Surface	67
3.2.1.1	Infrared Spectroscopy Studies of Hydrazine Modification of the Si(111) Surface.....	67
3.2.1.2	Analysis of Surface Reactions and Quantification of Surface Elemental Concentration by X-Ray Photoelectron Spectroscopy.	71
3.2.1.3	ToF-SIMS Identification of Surface Species on the Hydrazine-Modified Si(111) Surface.	78
3.2.1.4	DFT Computational Investigation of Surface Reaction Mechanism	80
3.2.2	Stability and Reactivity of the Hydrazine-modified Si(111) Surface	82
3.2.2.1	Stability of the Hydrazine-modified Si(111) Surface in Ambient Environment	82
3.2.2.2	Reactivity of the Hydrazine-modified Si(111) Surface with Metal Precursor	85
3.2.3	A Monolayer of Hydrazine Facilitates Direct Covalent Attachment of C ₆₀ Fullerene to Silicon Surface	87
3.2.3.1	Confirmation of Fullerenes C ₆₀ Adsorption on Hydrazine-Terminated Si(111) Surface by Atomic Force Microscopy.	87
3.2.3.2	Confirmation of Fullerenes C ₆₀ Chemically-Bound to the Hydrazine-Terminated Si(111) Surface by Time-of-Flight Secondary Ion Mass Spectrometry.....	91
3.2.3.3	Confirmation of Fullerenes C ₆₀ Covalently Bound to Hydrazine-Terminated Si(111) Surface by X-ray Photoelectron Spectroscopy.	94
3.2.3.4	Surface recombination velocity measurements of C ₆₀ -modified Si(111) Surface.	101
3.3	Conclusion	102

REFERENCES	104
4 DEHYDROHALOGENATION CONDENSATION REACTION OF PHENYLHYDRAZINE WITH Cl-TERMINATED Si(111) SURFACE	114
4.1 Introduction	114
4.2 Results and discussion	117
4.2.1 Confirmation of Phenylhydrazine Reaction with Cl-Si(111) Surface by Infrared Spectroscopy.	117
4.2.2 X-ray photoelectron spectroscopy investigation of the extent of the reaction and additional information on surface species formed during phenylhydrazine interaction with the Cl-Si(111) surface.....	121
4.2.3 Identification of surface species formed during phenylhydrazine interaction with the Cl-Si(111) surface by ToF-SIMS.....	128
4.2.4 Computational explanation of the initial steps of the surface reaction mechanism for phenylhydrazine interaction with a Cl- Si(111) surface.....	132
4.3 Conclusion	135
REFERENCES	136
5 CARBON NANOTUBES COVALENTLY ATTACHED TO FUNCTIONALIZED SURFACES DIRECTLY THROUGH THE CARBON CAGE.....	144
5.1 Introduction	144
5.2 Results and discussion	147
5.2.1 Confirmation of Nanotube Presence on the Surface	148
5.2.2 Submonolayer Coverage of Nanotubes on the Functionalized Substrate Surfaces	152
5.2.3 Spectroscopic Evidence of Covalent Binding between Functionalized Surfaces and CNTs	155
5.2.4 Confirmation that Attachment through the Cage is Energetically Feasible	161
5.2.5 Evidence of Covalent Attachment through the Cage	164
5.3 Conclusion	170
REFERENCES	171

6	CHEMICAL PROTECTION OF MATERIAL MORPHOLOGY: ROBUST AND GENTLE GAS-PHASE SURFACE FUNCTIONALIZATION OF ZnO WITH PROPIOLIC ACID	177
6.1	Introduction	177
6.2	Results and Discussion	180
6.2.1	Morphology Change of ZnO Surface during Propiolic Acid Treatment and Following “Click” Reaction.	180
6.2.2	Confirmation of Carboxylate Linkage to ZnO Surface by Infrared Investigation.	183
6.2.3	Confirmation of “Click” Reaction on Modified ZnO Surface by IR and XPS.	186
6.2.4	Multistep Functionalization of the ZnO surfaces followed by NMR	197
6.3	Conclusion	200
	REFERENCES	201
7	SUMMARY AND FUTURE OPPORTUNITIES	206
7.1	Summary.....	206
7.2	Future Opportunities.....	206
	REFERENCES	209
	Appendix	
A	COPYRIGHT PERMISSON LETTERS.....	210

LIST OF TABLES

Table 2.1 Parameters used to calculate surface coverages of nitrogen and chlorine from the XPS spectra based on the overlayer model. ¹⁴⁻¹⁵	30
Table 3.1 Charge carrier lifetime and surface recombination velocities for Si(111) surface following the reaction scheme: (a) hydrogen-terminated Si(111) surface; (b) chlorine-terminated Si(111) surface; (c) hydrazine-terminated Si(111) surface; (d) hydrazine-terminated Si(111) surface reacted with 1 mM C ₆₀ solution.	101
Table 4.1 Summary of the infrared investigation of phenylhydrazine treated Cl-Si(111) surface, including a comparison with previous studies of relevant experimental systems and DFT computational prediction for the two proposed structures shown in Figure 4.2 . All values are in cm ⁻¹	120
Table 5.1 Relative energies for covalent CNT interactions on the silicon and gold substrates	163

LIST OF FIGURES

Figure 1.1 Summary of surface modification schemes used to introduce a new chemical function to a surface (based on generalized reactions of silicon surfaces).....	2
Figure 1.2 Common vibration modes of IR active groups.	6
Figure 1.3 General principles of XPS instrumentation.....	8
Figure 1.4 General schematics of operation of ToF-SIMS.....	9
Figure 1.5 General principles of AFM.	10
Figure 1.6 An intuitive model of nuclei with corresponding magnetic moments. There is no energetic difference for any particular orientation (on the left), but in external magnetic field there is a high-energy state and a low-energy state depending on the relative orientations of the magnet to the external field (on the right).....	13
Figure 1.7 Simple scheme of recombination, which refers to reuniting of a free electron with a defect electron (hole) such that both charge carriers vanish.....	14
Figure 3.1 Schematic comparison of the reactions of Cl-Si(111) surface with ammonia and hydrazine, respectively. The energetic requirements are indicated according to the computational approach described in experimental part in Chapter 2.	63
Figure 3.2 Reaction scheme to form a stable interface between C ₆₀ fullerenes and silicon surface.	66
Figure 3.3 The Si-H stretching region of infrared spectroscopy studies of hydrazine reaction with silicon surface for (a) the final hydrazine-modified surface and (b) for chlorine-terminated Si(111), as well as (c) for the starting H-terminated Si(111) surface. Native-oxide covered surface is used as a background for spectra (c) and the surface terminated with hydrogen (H-Si(111)) is used as a background for spectra (a) and (b).	68

- Figure 3.4** Infrared spectroscopy studies of hydrazine reaction with silicon surface. The spectral ranges for N-H stretching region (left panel) and N-H bending signature region (right panel) are compared for (a) the final hydrazine-modified surface and (b) for chlorine-terminated Si(111), as well as (c) for the starting H-terminated Si(111) surface. Native-oxide covered surface is used as a background for spectra (c) and the surface terminated with hydrogen (H-Si(111)) is used as a background for spectra (a) and (b). Left panel summarizes the results of computational investigation for the computational cluster models considered and provides the predicted infrared spectra for these species indicated by bar plots. 69
- Figure 3.5** XPS spectra of the Si 2*p* spectral region for the Si(111) surface before and after hydrazine modification: (a) final surface modified with hydrazine compared with (b) Cl-Si(111) surface used in this modification and (c) H-Si(111) surface that is the starting point for the studies. 73
- Figure 3.6** XPS spectra of the Cl 2*p* spectral region for Si(111) surface before and after hydrazine modification: (a) starting Cl-Si(111) surface is compared with the same surface (b) following modification with hydrazine. 74
- Figure 3.7** XPS spectra of the N 1*s* spectral region for Si(111) surface before and after hydrazine modification: (a) starting Cl-Si(111) surface and (b) the same surface following modification with hydrazine compared with the N 1*s* core-level energies predicted by DFT investigations (solid bars) for the possible surface models. All the computational studies are based on a cluster model representing the two closest topmost silicon atoms on the unreconstructed Si(111) surface. 76
- Figure 3.8** ToF-SIMS positive-ion spectrum of Si(111) surface (a) before and (b) after hydrazine modification in the Si-N₂ (55.5-58.5 *m/z*), N-O-N (43.5-44.5 *m/z*), and Cl (33-38 *m/z*) species range. 79
- Figure 3.9** Computational investigation of potential reaction pathways for hydrazine on Cl-Si(111) surface with aSi₁₇H₂₄ cluster representing the silicon surface and B3LYP/6-311G+(d, p) computational approach. a) Model of a possible surface reaction pathway for hydrazine on Cl-Si(100) surface represented by a Si₁₇H₂₄ cluster terminated with two chlorine atoms; b) Correction to the final part of the computational reaction mechanism based on a reaction of the HCl product of the process with surrounding hydrazine molecules. 80

Figure 3.10 Si 2 <i>p</i> region of XPS of (a) freshly prepared hydrazine-terminated Si(111); (b) hydrazine-terminated Si(111) exposed to air for 30min; (c) hydrazine-terminated Si(111) exposed to air for 4 hours.	83
Figure 3.11 N 1 <i>s</i> region of XPS of (a) freshly prepared hydrazine-terminated Si(111); (b) hydrazine-terminated Si(111) exposed to air for 30min; (c) hydrazine-terminated Si(111) exposed to air for 4 hours.	84
Figure 3.12 AFM image of hydrazine-terminated Si(111) after reacted with Cu(acac) ₂ precursor.	86
Figure 3.13 Cu 2 <i>p</i> and Cu LMM region of XPS spectra of hydrazine-terminated Si(111) after reacted with Cu(acac) ₂ precursor.	86
Figure 3.14 Si 2 <i>p</i> region of XPS spectra of hydrazine-terminated Si(111) after reacted with Cu(acac) ₂ precursor.	87
Figure 3.15 Left panels: AFM images of (a) hydrazine-terminated Si(111) surface; (b) hydrazine-terminated Si(111) surface reacted with 0.25 mM C ₆₀ solution; (c) hydrazine-terminated Si(111) surface reacted with 1 mM C ₆₀ solution, washed without sonication; (d) hydrazine-terminated Si(111) surface reacted with 1 mM C ₆₀ solution, washed with sonication to remove multi-layered physisorbed C ₆₀ . Right panels: corresponding line profiles of the images.	90
Figure 3.16 Negative ion ToF-SIMS spectra of [C ₆₀] ⁻ species m/z range following the reaction of C ₆₀ with a hydrazine-terminated Si(111) surface. The exact positions of expected ions are shown as solid bars underneath the experimental data.	91
Figure 3.17 Negative ion ToF-SIMS spectra of representative spectral regions following the reaction of C ₆₀ with a hydrazine-terminated Si(111) surface: (a) [C ₆₀ -N] ⁻ species m/z range; (b) [C ₆₀ -N ₂] ⁻ species m/z range; (c) [C ₆₀ -N-Si] ⁻ species m/z range and (d) [C ₆₀ -N ₄ -Si ₂] ⁻ (or [C ₆₀ -N ₆ -Si] ⁻ , [C ₆₀ -N ₈] ⁻) species m/z range. The exact positions of expected ions are shown as solid bars underneath the experimental data.	93
Figure 3.18 High-resolution XPS spectra of C 1 <i>s</i> region for (a) the hydrazine-terminated Si(111) surface, and (b) hydrazine-terminated Si(111) surface reacted with 1 mM C ₆₀ solution.	95
Figure 3.19 High-resolution XPS spectra of N 1 <i>s</i> region for (a) the hydrazine-terminated Si(111) surface, and (b) hydrazine-terminated Si(111) surface	

reacted with 1 mM C ₆₀ solution. The core level energy shifts predicted by DFT for the model systems presented in the figure are shown as solid bars.	97
Figure 3.20 High-resolution XPS spectra of Si 2 <i>p</i> region for (a) hydrogen-terminated Si(111) surface, (b) hydrazine-terminated Si(111) surface and (c) hydrazine-terminated Si(111) surface reacted with 1 mM C ₆₀ solution.	100
Figure 4.1 Schematic comparison of the reactions of Cl–Si(111) surface with ammonia, hydrazine and phenylhydrazine, respectively. The reactions are balanced taking into account the formation of salts in the presence of excess molecular reactants	116
Figure 4.2 Summary of the infrared investigations of the N-H stretching region and C-H stretching region for phenylhydrazine reaction with Cl-Si(111) surface. The experimental spectrum is an average of five experiments conducted at identical conditions. The solid bars below the spectrum correspond to the vibrational frequencies predicted computationally for surface species formed, as summarized on corresponding schemes. All predicted frequencies are multiplied by a common scaling factor of 0.965.....	117
Figure 4.3 Summary of the infrared investigations for the Si-H stretching region of the Si samples following the phenylhydrazine reaction with Cl-Si(111) surface: (a) H-terminated Si(111) (with starting wafer used as a background); (b) Cl-terminated Si(111) prepared as indicated in the text (with sample in part (a) used as a background); (c) A surface in (b) reacted with phenylhydrazine for 1 hour as described in the text (with surface in (a) used as a background).	119
Figure 4.4 XPS spectra of the Si 2 <i>p</i> region of the Si(111) surface following the reaction steps: a) freshly prepared H-terminated Si(111) surface, b) freshly prepared Cl-Si(111) surface; the surface in (b) reacted with phenylhydrazine for c) 1 hour, d) 1.5 hours, e) 2.5 hours, and f) 3.5 hours. The binding energy corresponding to the formation of SiO _x following surface oxidation is indicated by a dashed line.....	122
Figure 4.5 XPS spectra of the Cl 2 <i>p</i> spectral region for the Si(111) surface following the reaction of phenylhydrazine with Cl-Si(111) surface for a) freshly prepared H-terminated Si(111) surface, b) freshly prepared Cl-Si(111) surface; the surface in (b) reacted with phenylhydrazine for c) 1 hour, d) 1.5 hours, e) 2.5 hours, and f) 3.5 hours.	123

Figure 4.6 XPS spectra of the N <i>1s</i> spectral region for the Si(111) surface following the reaction of phenylhydrazine with Cl-Si(111) surface for a) freshly prepared H-terminated Si(111) surface, b) freshly prepared Cl-Si(111) surface; the surface in (b) reacted with phenylhydrazine for c) 1 hour, d) 1.5 hours, e) 2.5 hours, and f) 3.5 hours. The positions of the expected XPS signatures computationally predicted based on the previously published calibration procedure ⁵⁹ for the model species shown in the figure are presented as solid bars underneath the experimental spectra.	125
Figure 4.7 Summary of the apparent relative coverages of N and Cl obtained based on XPS studies as a function of the reaction time between phenylhydrazine and a Cl-Si(111) surface	127
Figure 4.8 Negative ion ToF-SIMS spectra of the most informative spectral regions following the reaction of phenylhydrazine with a Cl-Si(111) surface: (a) [Si-N ₂] ⁻ species m/z range; (b) [Si-N ₂ -phenyl] ⁻ species m/z range; (c) [Si ₂ -N ₂ -phenyl] ⁻ species m/z range.	129
Figure 4.9 Negative ion ToF-SIMS spectra of phenylhydrazine treated Cl-Si(111) surface: (a) zoom-in of the [Si-NO-phenyl] ⁻ species m/z range; and (b) zoom-in of the [Si ₂ -NO-phenyl] ⁻ species m/z range. The exact positions of the ions corresponding to the selected species are indicated by solid vertical lines.	130
Figure 4.10 DFT investigation of the initial steps of a reaction of phenylhydrazine with a Cl-Si(111) surface. The proposed mechanism of interaction based on a reaction resulting in a HCl molecule bound to a surface-attached species as a product (a) is compared with a reaction pathway where the resulting HCl is bound to another phenylhydrazine molecule (b), which appear in excess in a realistic reaction mixture.	134
Figure 5.1 Summary of the direct attachment of carbon nanotubes to amine-functionalized silicon and gold surfaces through the CNT cage	147
Figure 5.2 SEM micrographs of the amine-modified silicon surface before (a) and after reaction with the NF-CNT (c) and COOH-CNT (e). Images (b), (d), and (f) show a close-up view of the surface before the reaction, and following reaction with the NF-CNT and COOH-CNT, respectively.	149
Figure 5.3 SEM micrographs of the amine-modified gold surface before (a) and after reaction with the NF-CNT (c) and COOH-CNT (e). Images (b), (d) and (f) show a close-up view of the surface before reaction, and following the reaction with the NF-CNT and COOH-CNT, respectively.	151

Figure 5.4 SEM micrographs of (a) (t-BOC)-protected AUD-terminated silicon surface and (b) amine-terminated silicon surface after sonication in the NF-CNT solution for 3 hours.	152
Figure 5.5 TEM (a) confirmation of carbon nanotube diameter, that is in agreement with manufacturer specification. AFM micrographs of (b) AUD-modified silicon surface and (c,d) AUD-modified silicon surface following reaction with NF-CNTs. The line profile of the white line in (d) shows the height of the CNTs.	154
Figure 5.6 XPS investigation of the N <i>1s</i> spectral region of AUD-modified silicon surface before (b) and after (a) reaction with the NF-CNTs, and cysteamine-modified gold surface before (d) and after (c) reaction with the NF-CNTs. Spectra of control experiments compare (e) NF-CNT powder, (f) NF-CNT reacted with neat propylamine, and (g) NF-CNT reacted with propylamine in DMF. The green bars underneath the spectra indicate the expected binding energies for selected systems, predicted by density functional theory calculations. The presence of two DFT-predicted binding energies below spectra (a) and (c) indicate the expected values for the N <i>1s</i> energies in a geometry in which the amine dissociates across a C=C bond parallel to the direction of the CNT and one in which the amine dissociates across a C=C bond that is not parallel to the direction of the CNT.	157
Figure 5.7 Summary of C <i>1s</i> spectral region of the XPS studies of carbon nanotube reaction with 11-amino-1-undecene-modified Si surface and cysteamine-covered Au surface.	160
Figure 5.8 Relative energies of parallel and non-parallel (denoted in red and blue) attachment configurations on cysteamine-modified gold surfaces for CNTs with radii of different sizes.	163
Figure 5.9 ToF-SIMS spectra in the region of the $[\text{Au-S-(CH}_2)_2 \text{N}]^-$ fragment, which is indicative of successful modification of the substrate with cysteamine or dimethylamino-ethanethiol. Features are absent in the case of the carbon nanotube powders (e, f), but can be observed for this peak on the cysteamine-terminated gold before (d) and after reaction with both the COOH-CNTs and NF-CNTs (a, b), and on the dimethylamino ethanethiol-terminated gold (c). The black bar below the spectra indicates the exact <i>m/z</i> position expected for the fragment.	165
Figure 5.10 ToF-SIMS spectra in the region of the $[\text{Au-S-(CH}_2)_2 \text{NH-C}_5]^-$ fragment, which is indicative of cysteamine bound to the substrate and to a five-carbon fragment of a carbon nanotube. Features are absent in the case of	

the samples without the substrate (e, f), on the cysteamine-terminated gold before reaction (d), and the control sample (c), but can be observed after reaction with both the COOH-CNTs and NF-CNTs (a, b). The black bar below the spectra indicates the exact m/z position expected for the fragment..... 167

Figure 5.11 ToF-SIMS spectra in the region of the $[\text{Au-S-(CH}_2)_2\text{N-CO-C}_5]^+$ fragment, which is indicative of amide formation resulting from carboxylic acid (attached to a five-carbon fragment) reacting with the primary amine of cysteamine. These features are absent in the case of the samples without the substrate (e, f), the modified gold surface (d), and the control sample (c). A small peak can be observed on the cysteamine-terminated gold after reaction with the NF-CNTs (b) and a large peak is observed on the amine-modified gold after reaction with the COOH-CNTs (a). The black bar below the spectra indicates the exact m/z position expected for the fragment..... 169

Figure 6.1 Reaction scheme for ZnO surface modification with propiolic acid followed by benzyl azide test reaction via gas phase and liquid phase modification..... 179

Figure 6.2 SEM studies of ZnO surface modification. (a) Clean ZnO nanopowder; (b) Gas phase propiolic acid-functionalized ZnO surface; (c) Propiolic acid functionalized ZnO surface depicted in (b) followed by copper-free gas phase “click” reaction with benzyl azide; (d) Propiolic acid functionalized ZnO surface depicted in (b) followed by copper-catalyzed liquid phase “click” reaction with benzyl azide; (e) ZnO powder directly exposed to liquid phase propiolic acid. 182

Figure 6.3 Infrared spectroscopy studies of propiolic acid reaction with ZnO surface. (a) Gas phase propiolic acid; (b) Computationally predicted infrared spectra for the cluster model schematically represented in the figure (frequencies are scaled by a common scaling factor of 0.94); (c) Propiolic acid-functionalized ZnO surface (molecularly adsorbed propiolic acid is removed following extended pumping time). Clean ZnO surface is used as a background for spectrum (c). 185

Figure 6.4 IR studies of propiolic acid reaction with ZnO surface.(a) Propiolic acid physisorbed mixed with chemisorbed ZnO surface (after 30-min pumping); (b) Propiolic acid-functionalized ZnO surface (after 16-hour pumping, same as Figure 6.3c). Clean ZnO surface is used as a background for both. 186

- Figure 6.5** Infrared spectroscopy studies of copper-free “click” reaction with propiolic acid functionalized ZnO surface. (a) Gas phase benzyl azide; (b) Computationally predicted infrared spectra for the considered cluster model shown (frequencies are scaled by a common scaling factor of 0.94); (c) Benzyl azide reacted with propiolic acid-functionalized ZnO surface; (d) Propiolic acid-functionalized ZnO surface (same as Figure 6.3c and 6.4b). Propiolic acid functionalized ZnO surface is used as a background for spectrum (c). 188
- Figure 6.6** High-resolution XPS spectra of C *1s* region for (a) Gas phase propiolic acid-functionalized ZnO surface; (b) Copper-free “click” reaction of gas phase benzyl azide with propiolic acid-functionalized ZnO surface; (c) Copper-catalyzed “click” reaction of liquid phase benzyl azide with propiolic acid functionalized ZnO surface. 189
- Figure 6.7** High-resolution XPS spectra of N *1s* region for (a) Gas phase propiolic acid-functionalized ZnO surface; (b) Copper-free “click” reaction of gas phase benzyl azide with propiolic acid functionalized ZnO surface; (c) Copper-catalyzed “click” reaction of liquid phase benzyl azide with propiolic acid functionalized ZnO surface; (d) Benzyl azide adsorbed directly onto ZnO surface. The core level energy shifts predicted by DFT for the model systems presented in the figure are shown as solid bars. 191
- Figure 6.8** High-resolution XPS spectra of Cu *2p* region for (a) Gas phase propiolic acid-functionalized ZnO surface; (b) Copper-free “click” reaction of gas phase benzyl azide with propiolic acid-functionalized ZnO surface; (c) Copper-catalyzed “click” reaction of liquid phase benzyl azide with propiolic acid functionalized ZnO surface, confirming the removal of copper catalyst following the procedure. 194
- Figure 6.9** EDX analysis of Copper-catalyzed “click” reaction of liquid phase benzyl azide with propiolic acid functionalized ZnO surface, confirming the removal of copper catalyst following the procedure. 194
- Figure 6.10** High-resolution XPS spectra of O *1s* region for (a) Gas phase propiolic acid-functionalized ZnO surface; (b) Copper-free “click” reaction of gas phase benzyl azide with propiolic acid-functionalized ZnO surface; (c) Copper-catalyzed “click” reaction of liquid phase benzyl azide with propiolic acid functionalized ZnO surface. 195
- Figure 6.11** High-resolution XPS spectra of Zn *2p* region for (a) Gas phase propiolic acid-functionalized ZnO surface; (b) Copper-free “click” reaction of gas phase benzyl azide with propiolic acid-functionalized ZnO surface; (c)

Copper-catalyzed “click” reaction of liquid phase benzyl azide with propiolic acid functionalized ZnO surface.	196
Figure 6.12 ^{13}C NMR spectroscopy studies of the reaction of propiolic acid with ZnO surface and the following copper-free “click” reaction. (a) gas phase propiolic acid-functionalized ZnO surface; (b) liquid phase propiolic acid-modified ZnO powder; (c) benzyl azide reacted with propiolic acid-functionalized ZnO surface; (d) liquid phase propiolic acid.	197
Figure 7.1 Reaction scheme to form a stable interface between C_{60} fullerenes and silicon surface.	207
Figure 7.2 Illustration of possible reactions with the hydrazine-modified silicon surface.	208

ABSTRACT

Semiconductor substrates are widely used in many applications. Multiple practical uses involving these materials require the ability to tune their physical and chemical properties to adjust those to a specific application. In recent years, surface and interface reactions have affected dramatically device fabrication and material design. Novel surface functionalization techniques with diverse chemical approaches make the desired physical, thermal, electrical, and mechanical properties attainable. Meanwhile, the modified surface can serve as one of the most important key steps for further assembly process in order to make novel devices and materials.

In the following chapters, novel chemical approaches to the functionalization of silicon and zinc oxide substrates will be reviewed and discussed. The specific functionalities including amines, azides, and alkynes on surfaces of different materials will be applied to address subsequent attachment of large molecules and assembly processes. This research is aimed to develop new strategies for manipulating the surface properties of semiconductor materials in a controlled way. The findings of these investigations will be relevant for future applications in molecular and nanoelectronics, sensing, and solar energy conversion.

The ultimate goals of the projects are:

1) *Preparation of an oxygen-and carbon-free silicon surface based exclusively on Si-N linkages for further modification protocols.*

This project involves designing the surface reaction of hydrazine on chlorine-terminated silicon surface, introduction of additional functional group through dehydrohalogenation condensation reaction and direct covalent attachment of C₆₀.

2) Demonstrating alternative method to anchor carbon nanotubes to solid substrates directly through the carbon cage.

This project targets surface modification of silicon and gold substrates with amine-terminated organic monolayers and the covalent attachment of nonfunctionalized and carboxylic acid-functionalized carbon nanotubes.

3) Designing a universal method for the modular functionalization of zinc oxide surface for the chemical protection of material morphology.

This project involves surface modification of zinc oxide nanopowder under vacuum condition with propiolic acid, followed by “click” reaction.

A combination of spectroscopy and microscopy techniques was utilized to study the surface functionalization and assembly processes. Fourier-transform infrared spectroscopy (FT-IR), X-ray photoelectron spectroscopy (XPS) and time of flight secondary ion mass spectroscopy (ToF-SIMS) were employed to elucidate the chemical structure of the modified surface. Atomic force microscopy (AFM), transmission electron microscopy (TEM) and scanning electron microscopy (SEM) were combined to obtain the surface morphological information. Density functional theory (DFT) calculations were applied to confirm the experimental results and to suggest plausible reaction mechanisms. Other complementary techniques for these

projects also include nuclear magnetic resonance (NMR) spectroscopy to identify the chemical species on the surface and charge-carrier lifetime measurements to evaluate the electronic property of C₆₀-modified silicon surface.

Chapter 1

INTRODUCTION

1.1 Chemical Functionalization of Semiconductor Surfaces

Semiconductor materials, especially silicon, have been extensively used in modern microelectronics industry. Silicon continues to be the starting platform for device manufacturing in this field. Shrinking size of the components of these devices requires controlling reactions at the interfaces and surfaces to prevent contamination and to increase device efficiency by manipulating the properties of the target interfaces. Therefore, chemical functionalization of semiconductor surface turns to become a practical method that can be widely applied to tailor the surface and interface properties of semiconductors such as conductivity, corrosion resistance, wettability and so on to the corresponding application.¹

Common surface functionalization schemes are summarized in Figure 1.1, which also reveals that surface functionalization and chemistry can serve as a preliminary step for further modification protocols.² The potential applications of functionalized surface include novel materials for catalysis, molecular and nanoelectronics, sensing, and solar energy conversion.³⁻⁶

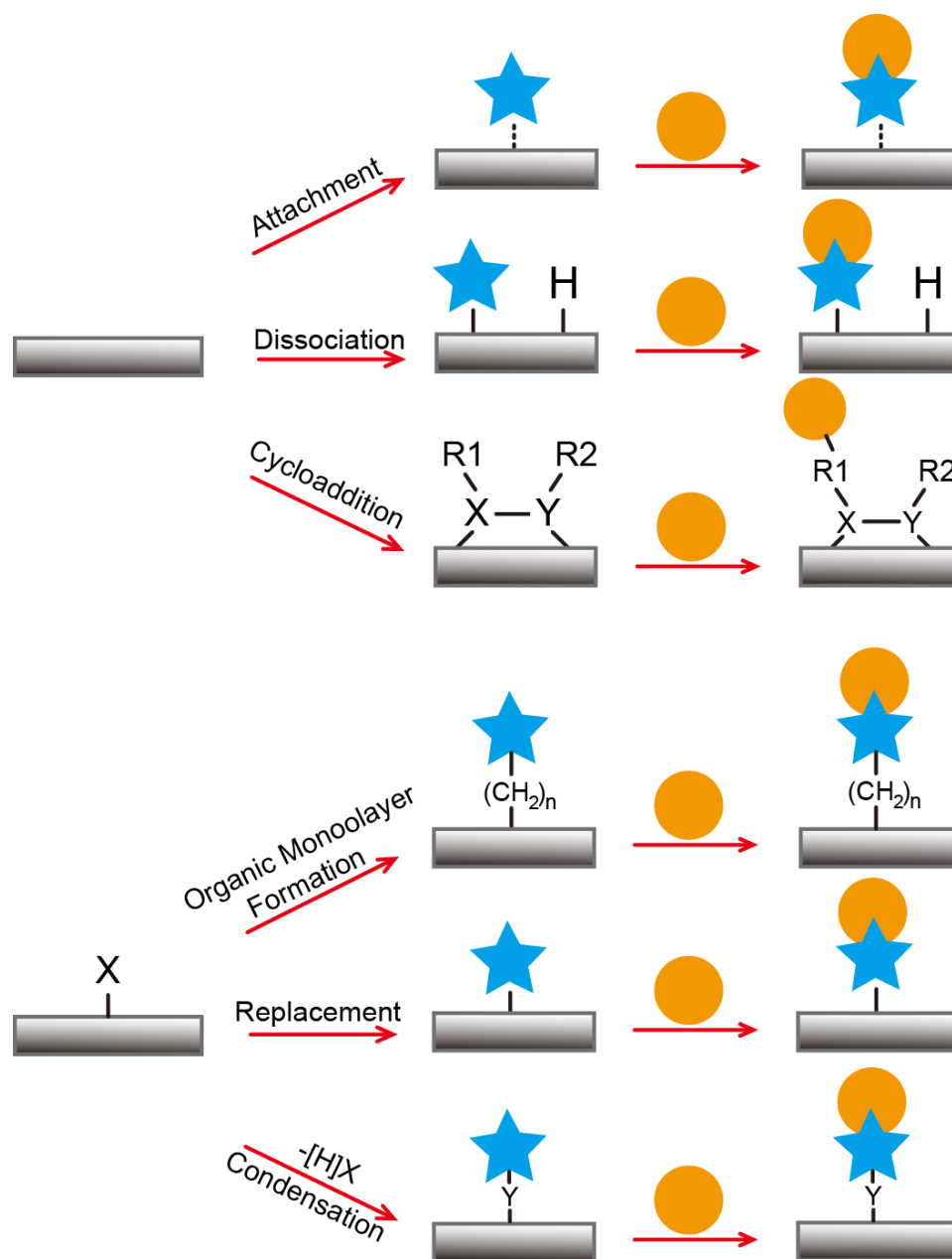


Figure 1.1 Summary of surface modification schemes used to introduce a new chemical function to a surface (based on generalized reactions of silicon surfaces).

In this thesis, the chemical functionalization utilized will be mostly based on the reaction of amine-containing compounds with surface chlorine, carbon

nanosstructure (CNTs and C₆₀) covalent binding with surface amine and azide-alkyne cycloaddition “click” reaction. The projects in this thesis involve substantial work on developing surface modification schemes for different materials and the characterization of surface species and morphology. Different materials and functionalization methods will be introduced in detail.

1.1.1 Organic Functionalization of Silicon Surface

The atomically flat hydrogen terminated Si(111) single crystalline surface can be prepared following a well-established modified RCA procedure^{2, 7-8}. This surface has long been a perfectly-defined golden standard for a number of further chemical modifications.² As summarized in Figure 1.1 above, three major types of surface modification can be developed based on the appropriately terminated semiconductor surfaces: replacement, condensation, and the direct formation of organic monolayer.

The formation of organic monolayers is probably the most common technique to introduce functional groups and to control their distribution and concentration on a surface of not only silicon but also a large number of other materials. In this thesis, a self-assembled monolayer, 11- amino-1-undecene, was introduced to H-Si(111) surface. Replacement of surface termination is an alternative approach for semiconductor surface functionalization. For the most part, those processes use direct chlorination of H-terminated surface to replace the surface hydrogen with chlorine, forming Cl-Si(111), which is also a very common surface used for further chemical modification. Finally, a very important class of surface modification processes can be generalized as condensation reactions. For example, chlorine-terminated silicon surfaces reacted with amines produce similar groups and yield HCl as side products.

In this thesis, hydrazine and phenylhydrazine reactions with Cl-Si(111) surface lead to the formation of amine species on the surface and hydrazine salt byproducts.

1.1.2 Passivation of Gold Surface

It is well known that gold is an inert and stable material with high biocompatibility. Gold and gold thin films deposited on different substrates have been widely used for both industrial and research purposes, from jewelry⁹ to drug delivery.¹⁰⁻¹¹ Common surface functionalization schemes for gold surface involve self-assembled monolayers (SAMs) containing thiol groups.¹ In this thesis, cysteamine-functionalized gold surface was prepared by immersing cleaned gold substrate in cysteamine solution for 24 hours. Gold substrate is always cleaned using piranha solution or annealing under high vacuum condition to eliminate the impurities. Experimental details for cleaning process and surface modification of gold substrates can be found in the next chapter.

1.1.3 Functionalization of Zinc Oxide Surface

ZnO is a complex material with rich and intricate defect chemistry. The properties of ZnO can be extremely sensitive to processing methods, ingredients and conditions;¹² consequently, surface modification of ZnO using both inorganic and organic species has been explored to control and regulate its surface properties, particularly at heterointerfaces in electronic devices.¹³

Molecular modification of ZnO has been employed in many applications to alter its surface properties.¹²⁻¹³ Generally, common methods utilize polar groups on the

modifying species such as carboxyl ($-\text{COOH}$),¹⁴ phosphonic acid ($-\text{P}(\text{O})(\text{OH})_2$),¹⁵ amine ($-\text{NH}_2$),¹⁶ and thiol ($-\text{SH}$)¹⁷⁻¹⁸ to anchor the functional group to the zinc oxide surface. Different compounds lead to different modes of bonding to the surface, for example, carboxyl and thiol linkers favor dissociative absorption.¹⁹ In this thesis, ZnO surface was functionalized with a carboxylic acid, propionic acid, with alkyne group on the end to enable the following “click” reaction.

1.2 Analytical Techniques to Study the Surface Modification Process

Due to the complexity of the surface modification processes, multiple analytical techniques including spectroscopic and microscopic methods are required.

To study the chemical/biological interactions and to identify the chemical structure on the surface, spectroscopic techniques such as Fourier-transform infrared spectroscopy (FT-IR), X-ray photoelectron Spectroscopy (XPS) and Time of Flight Secondary Ion Mass Spectrometry (TOF-SIMS) were combined to investigate the linkage between molecules and substrates. For certain samples, nuclear magnetic Resonance Spectroscopy (NMR) was used as a precise technique to identify the chemical species on the surface. Microscopic studies with Atomic Force Microscopy (AFM), Scanning Electron Microscopy (SEM) and Transmission Electron Microscopy (TEM) were performed to visualize the topographical and morphological information of the modified surface. Computational methods such as Density Functional Theory (DFT) calculations were utilized to confirm the experimental results and to offer possible reaction pathways. Additionally, electronic properties of the material produced may be investigated by Charge-Carrier Lifetime Measurements. A brief introduction for each analytical technique is given below.

1.2.1 Fourier-Transform Infrared Spectroscopy (FT-IR)

FT-IR is an important spectroscopic technique used to identify the presence of certain functional groups in a molecule and to detect the presence of specific impurities, which has been widely used in a variety of applications for IR-active samples in solid, liquid or gas phase. It measures how well a sample absorbs infrared light at different wavelengths. When the recombined beam passes through the sample, the sample absorbs all the different wavelengths characteristic of its spectrum, corresponding to the bending, stretching or contracting of a specific chemical bond as shown in Figure 1.2. The detector simultaneously reports variation in energy versus time for all wavelengths, which is later converted into an intensity-vs.-frequency spectrum using a mathematical function called a Fourier-transform. Depending on the specific functional group, the absorption vibrational frequency appears at different spectral ranges, so that chemical functionalities could be detected based on the signature absorption peaks in the recorded spectra.

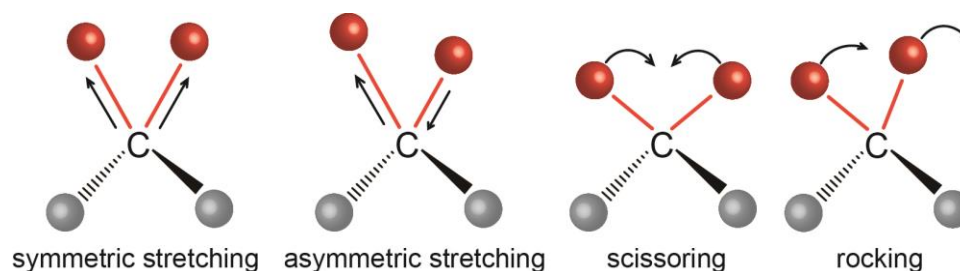


Figure 1.2 Common vibration modes of IR active groups.

1.2.2 X-ray Photoelectron Spectroscopy (XPS)

XPS is a spectroscopic technique that can sensitively measure the elemental composition, empirical formula, chemical state and electronic state of the elements with atomic numbers above three (lithium) that exist within a material. Figure 1.3 schematically presents the general principle of the XPS. When the material is irradiated with an X-ray beam, photo-emitted electrons escape from the top about 0-10 nm of the surface then captured by the analyzing system which simultaneously measures the kinetic energy and number of electrons emitted. The binding energy E_{binding} can be calculated using the equation below:

$$E_{\text{binding}} = E_{\text{photon}} - (E_{\text{kinetic}} + \Phi)$$

where E_{photon} is the energy of the X-ray photons being used, E_{kinetic} is the kinetic energy of the electrons emitted by a respective element measured by the instrument, and Φ is the work function of the spectrometer. The information of elemental composition and chemical state can be collected based on characteristic binding energy of each element associated with different chemical states.

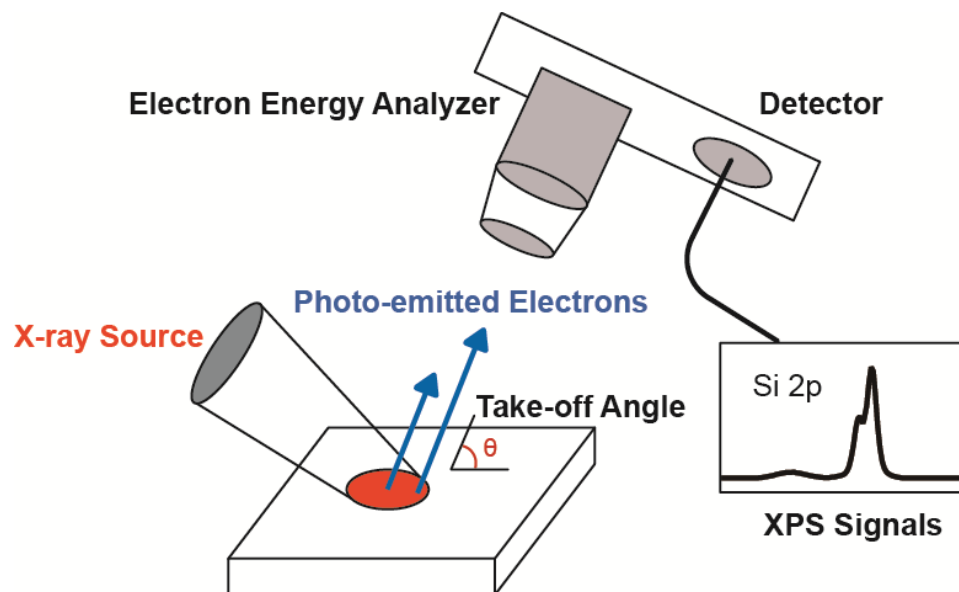


Figure 1.3 General principles of XPS instrumentation.

1.2.3 Time-of-Flight Secondary-Ion Mass Spectrometry (ToF-SIMS)

ToF-SIMS is a surface-sensitive analytical technique that can be applied to analyze the composition of solid surfaces. This technique uses a pulsed particle beam to dislodge chemical species on a materials surface, then collects and analyzes ejected secondary ions. Secondary ions generated farther from the impact site tend to be molecular compounds. They are then accelerated into a flight path on their way towards a detector. The mass/charge ratios of these secondary ions are measured with a mass spectrometer to determine the elemental, isotopic, or molecular composition of the surface to a depth of approximately 1 to 2 nm.

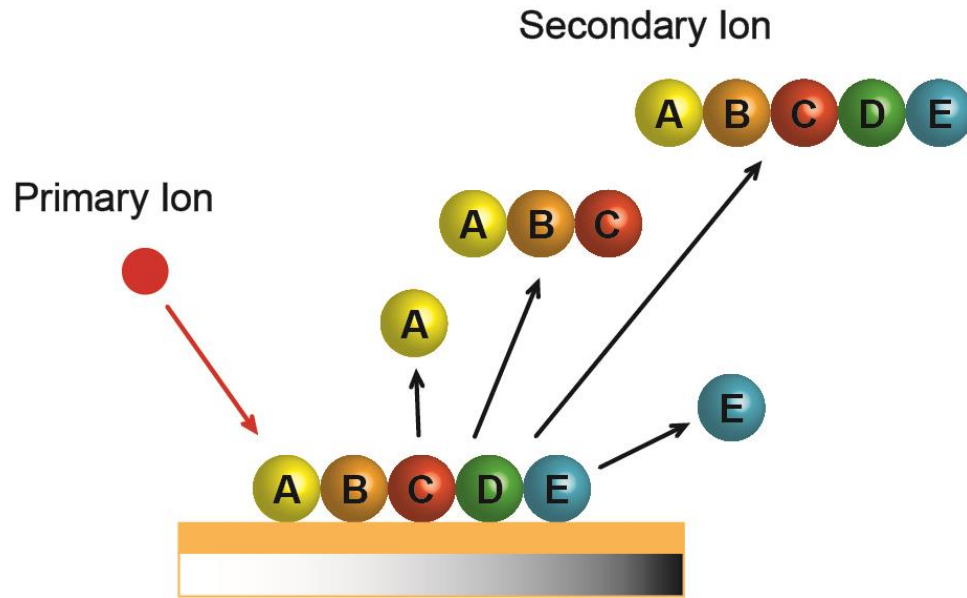


Figure 1.4 General schematics of operation of ToF-SIMS.

1.2.4 Atomic Force Microscopy (AFM)

AFM is a type of scanning force microscopy technique that measures the surface profile of a sample with very high resolution; it was developed to overcome a basic drawback with STM: STM can only image conducting or semiconducting surfaces. The AFM has the advantage of imaging almost any type of surface, based on a force measurement between a sharp tip raster-scanned over a surface called cantilever and the sample. The general scheme of an AFM measurement is summarized in Figure 1.5. When a laser is reflected from the back of the cantilever, the laser deflection is measured accurately to control the force and tip position, with the signals transferred to a computer to visualize the images. Local properties of the surfaces including feature height, electrical forces, capacitance, magnetic forces, conductivity, viscoelasticity, surface potential, and resistance can be investigated. The

vertical resolution of the AFM can reach as high as 0.1 nm; however, due to the tip effect, the lateral resolution of the AFM is generally lower and the size of features on the surface may depend on the sharpness of the tip. Thus, a different analytical technique, SEM, could be used to get a comprehensive view of the surface.

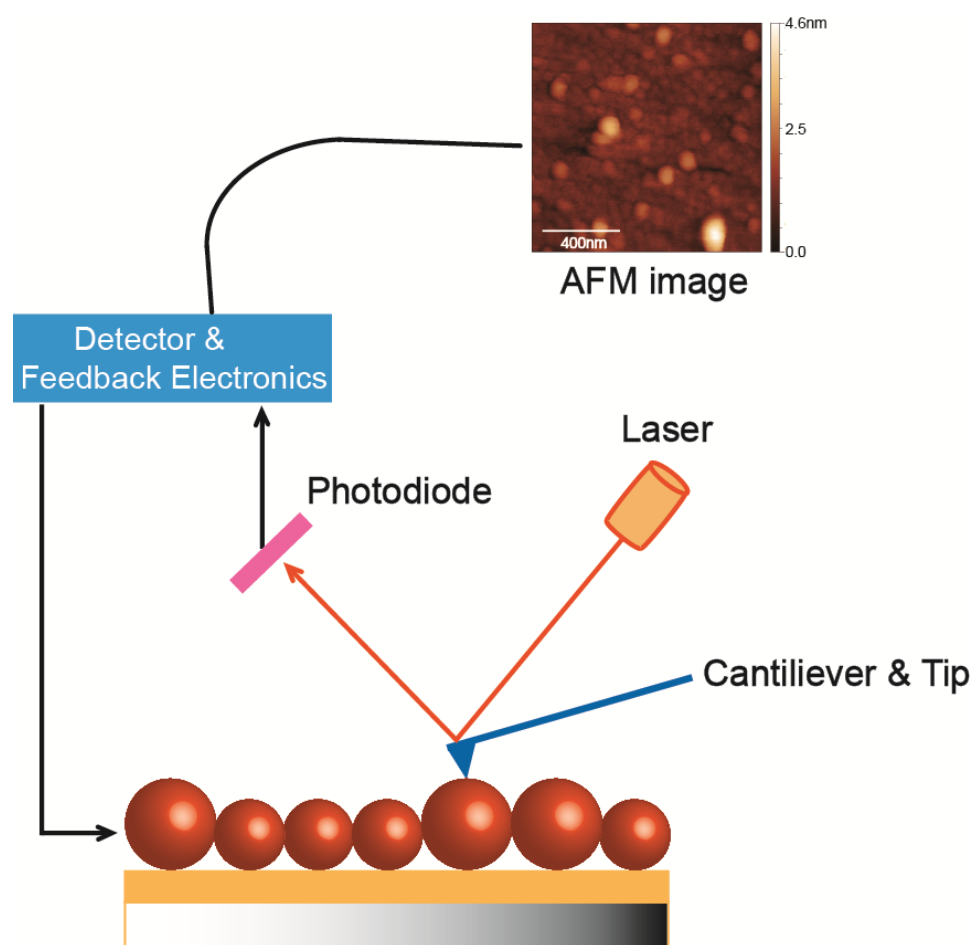


Figure 1.5 General principles of AFM.

1.2.5 Scanning Electron Microscopy (SEM)

SEM is an electron microscopy technique that scans the surface using a focused beam of electrons to produce images of a sample. Various signals that contain information about the sample surface topography and composition can be collected based on the interaction of electrons with the atoms in the sample. The resolution of the SEM can reach as high as to 1 nm. Commonly SEM is performed to detect secondary electrons emitted by atoms excited by the electron beam, providing excellent lateral information about the surface. In recent years, focused ion beam is usually incorporated with SEM to get topographical information at the cross section. The top layers of materials can be removed or patterned in a controlled way which leads to nanofabrication applications.

1.2.6 Transmission Electron Microscopy (TEM)

TEM is a microscopy technique widely applied in the physical, chemical and biological sciences. It forms the image by transmitting a beam of electrons through a specimen; the specimen is commonly a suspension on a grid, copper grid in our study. The basic principle of TEM is the same as that of the light microscope, but TEM uses electrons, which makes it capable of imaging at a significantly higher resolution than light microscopes. The electrons emitted from a "light source" at the top of the microscope travel through vacuum in the column of the microscope, get focused into a thin beam by electromagnetic lenses, which then goes through the specimen/ sample. Due to different densities of the material present, some of the electrons are scattered to some degree and disappear from the beam path, while the unscattered electrons reach a fluorescent screen at the bottom of the microscope. This leads to a "shadow image"

of the specimen with different parts displayed in varied darkness according to their density. The image is collected directly by the operator and photographed with a camera.

1.2.7 Nuclear Magnetic Resonance Spectroscopy (NMR)

NMR is a spectroscopic technique that has become the preeminent method for determining the structure of organic compounds. Of all the spectroscopic methods, it is the only one for which a complete analysis and interpretation of the entire spectrum is normally expected. The NMR is based on a physical phenomenon in which nuclei in a magnetic field absorb and re-emit electromagnetic radiation, as indicated in the simple scheme in Figure 1.6. The locations of different NMR resonance signals are reported in a spectrum relative to a reference signal from a standard compound added to the sample, tetramethylsilane usually. Since different functional groups are observed at distinguishable unique locations in NMR spectra, such well-resolved and analytically tractable analysis serves as a highly precise technique to confirm the identity of a substance. Compared to common solution NMR, solid-state NMR spectra are very broad, as the full effects of anisotropic or orientation-dependent interactions are observed in the spectrum. However, high-resolution solid-state NMR can be achieved with a number of methods including magic-angle spinning, dilution, multiple-pulse sequences, cross polarization and etc.²⁰ Thus it serve as one of the most precise method for identification of chemical species on solid nanomaterials.

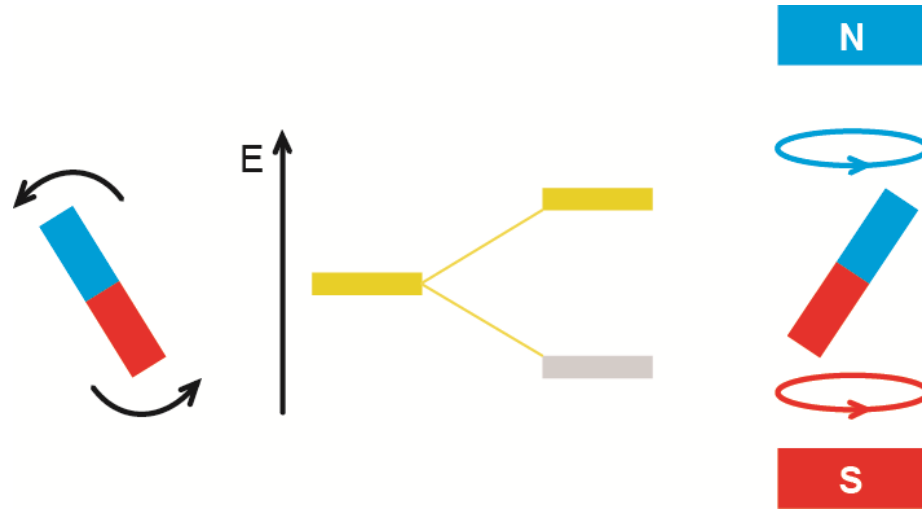


Figure 1.6 An intuitive model of nuclei with corresponding magnetic moments. There is no energetic difference for any particular orientation (on the left), but in external magnetic field there is a high-energy state and a low-energy state depending on the relative orientations of the magnet to the external field (on the right).

1.2.8 Charge-Carrier Lifetime Measurements

Charge carrier lifetime is defined as the average time taken for a minority charge carrier (electron or hole) to recombine with one of its counterparts (with opposite charge), as displayed in Figure 1.7. The ability to calibrate charge carrier lifetime in semiconductors provides a means of controlling certain properties when producing power semiconductor devices. Charge carrier lifetime in semiconductors is adjusted by many ways, such as inducing defects in the semiconductor crystal lattice, or inducing electron traps (C_{60} in our case) to the semiconductor surface. Shortening charge carrier lifetime leads to reduced storage charging. In other words, the turn-off losses in the component are reduced.

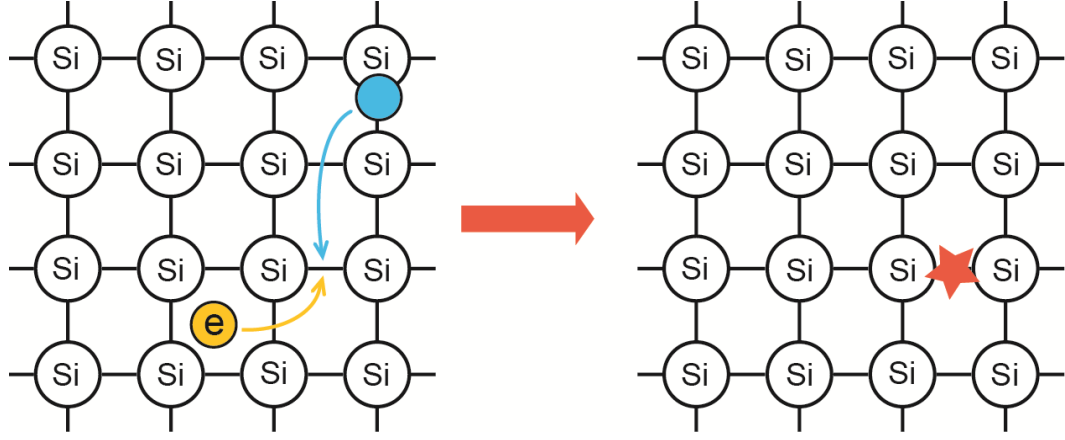


Figure 1.7 Simple scheme of recombination, which refers to reuniting of a free electron with a defect electron (hole) such that both charge carriers vanish.

In our study, the surface recombination velocity (S) can be expressed by the following equation²¹:

$$\frac{1}{\tau_{\text{eff}}} = \frac{1}{\tau_{\text{bulk}}} + \frac{2S}{W}$$

where τ_{eff} is effective minority carrier lifetime, τ_{bulk} is the minority carrier lifetime within bulk and W is the thickness of the silicon wafer (1000 μm). Surface recombination velocity can be calculated by assuming the bulk lifetime τ_{bulk} is infinite for float zone intrinsic silicon wafers.

1.2.9 Density Functional Theory (DFT) Calculations

As a versatile quantum mechanical modeling method, DFT has been very popular for calculations in physics, chemistry and materials science to describe the properties of insulators, semiconductors and metals. The DFT simulation is based on the molecular density, not via many-body wave function. With the help of DFT calculations, frequency and core-level energy of the elements are predicted to compare

with experimental FT-IR and XPS data, to support peak assignments and to offer possible reaction mechanisms.

1.3 Summary

This research is aimed to develop new strategies for manipulating the surface properties of semiconductor materials in a controlled way. The findings of these investigations will be relevant for future applications in molecular and nanoelectronics, sensing, and solar energy conversion.

The goal of this thesis work is to apply surface functionalization for designing novel biosensor interfaces and materials. Chapter one introduced the different substrates, nanoparticles and their chemical modification methods; chemical and biological ways to assemble and immobilize nanoparticles, and analytical techniques to study the assembled process. Later chapters will be focused on each individual project related to sensing, material design and surface coating.

REFERENCES

1. Love, J. C.; Estroff, L. A.; Kriebel, J. K.; Nuzzo, R. G.; Whitesides, G. M. Self-Assembled Monolayers of Thiolates on Metals as a Form of Nanotechnology. *Chem. Rev.* **2005**, *105*, 1103-1170.
2. Gao, F.; Teplyakov, A. V. Challenges and Opportunities in Chemical Functionalization of Semiconductor Surfaces. *Appl. Surf. Sci.* **2017**, *399*, 375-386.
3. Bent, S. F.; Teplyakov, A. V. Semiconductor Surface Functionalization for Advances in Electronics, Energy Conversion and Dynamic Systems. *J. Vac. Sci Technol. A* **2013**, *31*, 050810-1-12.
4. Schechter, I.; Ben-Chorin, M.; Kux, A. Gas Sensing Properties of Porous Silicon. *Anal. Chem.* **1995**, *67*, 3727-3732.
5. Zhao, J.; Wang, A.; Green, M. A. 24.5% Efficiency Silicon Pert Cells on MCZ Substrates and 24.7% Efficiency Perl Cells on FZ Substrates. *Prog. Photovolt: Res. Appl.* **1999**, *7*, 471-474.
6. Margelefsky, E.; Zeidan, R.; Davis, M. Cooperative Catalysis by Silica-Supported Organic Functional Groups. *Chem. Soc. Rev* **2008**, *37*, 1118-1126.
7. Chabal, Y. J.; Higashi, G. S.; Small, R. J., *Handbook of Semiconductor Wafer Cleaning Technology*; William Andrew: Norwich, NY, 2007.
8. Higashi, G. S.; Chabal, Y. J.; Trucks, G. W.; Raghavachari, K. Ideal Hydrogen Termination of the Si(111) Surface. *Appl. Phys. Lett.* **1990**, *56*, 656-658.

9. Liu, Y. Application of Surface Functionalization for Designing Novel Interfaces and Materials. University of Delaware, Newark, DE, 2014.
10. Ganeshkumar, M.; Ponrasu, T.; Raja, M. D.; Subamekala, M. K.; Suguna, L. Green Synthesis of Pullulan Stabilized Gold Nanoparticles for Cancer Targeted Drug Delivery. *Spectrochimica Acta Part A: Molecular and Biomolecular Spectroscopy* **2014**, *130*, 64-71.
11. Chithrani, B. D.; Chan, W. C. W. Elucidating the Mechanism of Cellular Uptake and Removal of Protein-Coated Gold Nanoparticles of Different Sizes and Shapes. *Nano Lett.* **2007**, *7*, 1542-1550.
12. Gao, F.; Aminane, S.; Bai, S.; Teplyakov, A. V. Chemical Protection of Material Morphology: Robust and Gentle Gas-Phase Surface Functionalization of ZnO with Propiolic Acid. *Chem. Mater.* **2017**, *29*, 4063–4071.
13. Hewlett, R. M.; McLachlan, M. A. Surface Structure Modification of ZnO and the Impact on Electronic Properties. *Adv. Mater.* **2016**, *28*, 3893-3921.
14. Keis, K.; Lindgren, J.; Lindquist, S.-E.; Hagfeldt, A. Studies of the Adsorption Process of Ru Complexes in Nanoporous ZnO Electrodes. *Langmuir* **2000**, *16*, 4688-4694.
15. Zhang, B.; Kong, T.; Xu, W.; Su, R.; Gao, Y.; Cheng, G. Surface Functionalization of Zinc Oxide by Carboxyalkylphosphonic Acid Self-Assembled Monolayers. *Langmuir* **2010**, *26*, 4514-4522.
16. Norberg, N. S.; Gamelin, D. R. Influence of Surface Modification on the Luminescence of Colloidal ZnO Nanocrystals. *J. Phys. Chem. B* **2005**, *109*, 20810-20816.

17. Ogata, K.; Hama, T.; Hama, K.; Koike, K.; Sasa, S.; Inoue, M.; Yano, M. Characterization of Alkanethiol/ZnO Structures by X-ray Photoelectron Spectroscopy. *Appl. Surf. Sci.* **2005**, *241*, 146-149.
18. Sadik, P. W.; Pearton, S. J.; Norton, D. P.; Lambers, E.; Ren, F. Functionalizing Zn- and O-Terminated ZnO with Thiols. *J. Appl. Phys.* **2007**, *101*, 104514.
19. Moreira, N. H.; Dominguez, A.; Frauenheim, T.; da Rosa, A. L. On the Stabilization Mechanisms of Organic Functional Groups on ZnO Surfaces. *PCCP* **2012**, *14*, 15445-15451.
20. Alia, A.; Ganapathy, S.; de Groot, H. J. M. Magic Angle Spinning (Mas) NMR: A New Tool to Study the Spatial and Electronic Structure of Photosynthetic Complexes. *Photosynth. Res.* **2009**, *102*, 415-425.
21. Gao, F.; Teplyakov, A. V. Monolayer of Hydrazine Facilitates the Direct Covalent Attachment of C₆₀ Fullerene to a Silicon Surface. *Langmuir* **2017**, 10.1021/acs.langmuir.6b03975.

Chapter 2

EXPERIMENTAL

The projects throughout my Ph.D. study involve a combination work on surface modification, organic synthesis, DFT simulation and analysis. In this chapter, detailed experimental procedures are provided.

2.1 Organic Synthesis

The silicon substrate was modified with *t*-BOC protected 11-amino-1-undecene, which was synthesized based on previously published work.¹⁻² The detailed synthetic procedure is described below.

2.1.1 Synthesis of *t*-Butyloxycarbonyl (*t*-BOC)-Protected 11-Amino-1-Undecene.

2.1.1.1 Materials

All chemicals were reagent grade or better and used as received: 11-chloro-1-undecene (Aldrich, 97%), trifluoroacetic acid (TFA) (Aldrich, 99%), potassium phthalimide (Fluka, 99.0%), hydrazine monohydrate (hydrazine, 64%, Acros Organics), di-*tert*-butyl dicarbonate (Sigma-Aldrich, 99%), dimethyl formamide (DMF) (Fisher, 99.8%), methylene chloride (Fisher, 99.9%), petroleum ether (Fisher, Certified ACS), ethyl ether (Fisher, Laboratory Grade), methanol (Fisher, 99.9%),

ethanol (Pharmco, 99.5%), ammonium hydroxide (Fisher, 14.8 N), and toluene (Fisher, 99.9%).

2.1.1.2 Synthetic Procedure

The *t*-BOC-protected 11-amino-1-undecene was prepared by standard organic synthesis methods.¹⁻³ Potassium phthalimide (12.8 g) was added to a solution of 10.0 g of 1-chloro-10-undecene in 25 mL of dry DMF. The resulting suspension was kept stirring at 90 °C for 24 h. The obtained reaction mixture was cooled to room temperature, and 75 mL of water was added. The aqueous layer was extracted once with 75 mL and subsequently twice with 30 mL of ether. The combined organic layers were washed with 25 mL of a 0.2 M NaOH solution and with 25 mL of brine and dried over anhydrous MgSO₄. Evaporation of the solvent yielded the crude product as a yellow solid. Recrystallization from 50 mL of distilled methanol after standing at 18-20 °C in a closed flask for 18 h yielded *N*-(ω -undecylenyl)-phthalimide as white needles. Hydrazine (2.5 g) was added to a solution of 10.0 g of *N*-(ω -undecylenyl)-phthalimide in 100 mL of ethanol. The resulting mixture was heated to reflux for 3 h. The solution was then cooled to room temperature and acidified to pH 1 to 2 with 1 M HCl. The white suspension was filtered carefully and the residue was washed twice with 20 mL of 1 M HCl. The combined filtrates were made alkaline (pH 10 to 11) by the addition of NaOH (tablets) and concentrated to a volume of 100 mL by evaporation under reduced pressure. The resulting turbid aqueous layer was extracted four times with 50 mL of ether. The combined organic layers were washed once with 20 mL of a 0.2 M NaOH solution and once with 20 mL of brine, to which a few milliliters of the 0.2M NaOH solution were added.

The organic layer was dried over NaOH (solid) for 1 to 2 h. Evaporation of the solvent yielded crude 1-amino-10-undecene as yellow oil. About 5 g of 1-amino-10-undecene was dissolved in 60 mL of chloroform that was added to a solution of 3 g of NaHCO₃ in 50 mL of water. Sodium chloride (6.45 g) was added along with 7.18 g of di-*tert*-butyl dicarbonate dissolved in a few milliliters of chloroform. This mixture was refluxed for 90 min and extracted twice with 50 mL of ether. The collected organic extracts were dried over magnesium sulfate and filtered, and the ether was removed by rotary evaporation. The *t*-BOC-protected product was purified by vacuum distillation. NMR confirmed the identity of each step's product: *N*-(ω -undecylenyl)-phthalimide, 1-amino-10-undecene, and *t*-butyloxycarbonyl (*t*-BOC)-protected 11-amino-1-undecene.

2.2 Surface Modification of Silicon and Gold

2.2.1 Materials

The silicon samples used for charge-carrier lifetime measurements were float zone grown, double-side polished (111)-oriented Si with thickness of 1000 μm . Phosphorus-doped, n-type single-side polished Si(111) wafers (Virginia Semiconductor Inc., 1-10 $\Omega\cdot\text{cm}$ resistivity, 325 μm thickness), n-type double-side polished Si(111) wafers (Virginia Semiconductor, >0.1 $\Omega\cdot\text{cm}$ resistivity, 500 μm thickness) and prefabricated gold-coated wafers (1000 Å gold thickness on a silicon wafer support with titanium adhesion layer, Sigma Aldrich) were used as substrates for other experiments and characterizations.

All chemicals were reagent grade or better: non-functionalized carbon nanotubes (NF-CNTs) (>90%, 1-4 nm diameter, cheaptubes.com), single walled carboxylic acid-functionalized carbon nanotubes (COOH-CNTs) (95%, 1-2 nm diameter, Nanostructured & Amorphous Materials, Inc.), Nitrogen (Praxair, boiled off from liquid nitrogen), Ar (Matheson, research purity), hydrogen peroxide (Fisher, 30% certified ACS grade), ammonium hydroxide (Fisher, 29% certified ACS plus grade), hydrochloric acid (Fisher, 37.3% certified ACS grade), buffer-HF improved (Transene Company, Inc.), chlorobenzene (99+%, Acros), phosphorus pentachloride ($\geq 98.0\%$ Sigma-Aldrich), benzoyl peroxide (Acros, $\geq 98.0\%$), anhydrous hydrazine (98%, Sigma-Aldrich), phenylhydrazine (Acros, 97%), methanol (Fisher, $\geq 99.8\%$), fullerene C₆₀ (Acros, 99.9%), toluene (Fisher, 99.9%), dichloromethane (Fisher, 99.9%), tetrahydrofuran (THF) (Fisher, distilled from Na/benzophenone) cysteamine hydrochloride (98%, Acros Organics), propylamine (Aldrich, 98%), 2-dimethylamino ethanethiol hydrochloride (Acros, 95%), N,N-dimethyl formamide (DMF) (certified ACS, Fisher Scientific), ethanol (Decon Labs, 200 proof). The deionized water used to rinse the surfaces and containers was from a first-generation Milli-Q water system (Millipore) with 18 M Ω ·cm resistivity.

2.2.2 Preparation of Hydrogen-Terminated Si(111) Surface.

The hydrogen-modified Si(111) surface was prepared by a modified RCA cleaning procedure.⁴⁻⁶ SC-1 solution was freshly prepared by mixing Milli-Q water, hydrogen peroxide, and ammonium hydroxide (volume ration 4:1:1), SC-2 solution was freshly prepared by Milli-Q water, hydrogen peroxide, and hydrochloric acid (volume ration 4:1:1). The Teflon beakers and Si(111) wafers were cleaned in SC-1

solution for 30 and 10 min, respectively, on an 80 °C water bath. After rinsing with Milli-Q water, the clean wafers were etched in HF buffer solution for 2 min and rinsed again with Milli-Q water. Then, the wafers were placed in SC-2 solution for 10 min to grow a silicon oxide layer. After that, the rinsed silicon wafers were etched in HF buffer solution again for 1 min, followed by a 6-min etching process in ammonium fluoride solution to form a well-ordered hydrogen-terminated Si(111) surface, as confirmed by a sharp 2083 cm⁻¹ peak in the infrared spectra,⁵⁻⁶ as described in detail below.

2.2.3 Preparation of Chlorine-Terminated Si (111) Surface.

The chlorine-terminated Si(111) surface was prepared by a well-established procedure using PCl₅.⁷ Phosphorus pentachloride powder was dissolved in chlorobenzene solvent to form PCl₅ solution, with trace amount of benzoyl peroxide as a reaction initiator. This solution was purged with nitrogen gas under N₂ atmosphere for at least 30 min to remove gaseous impurities. A hydrogen-terminated Si(111) wafer was placed into this solution immediately after etching procedure. The entire setup was placed in an oil bath at 110 °C for 1 h to prepare the stable chlorine-terminated Si(111) sample. Freshly generated samples were kept under freshly distilled THF.

2.2.4 Preparation of Hydrazine-Functionalized Si(111) Surface.

The freshly prepared chlorine-terminated Si(111) sample was transferred into a clean Schlenck flask filled with argon, then evacuated. This fill-evacuate procedure

was repeated three times. Anhydrous hydrazine solution was injected into the Schlenk flask, which was placed in an oil bath at 35-38 °C, using clean and dry syringe. The chlorine-terminated silicon wafer was stirred in the anhydrous hydrazine for 1 h to form a hydrazine-modified Si(111) surface.⁸ After the reaction, hydrazine-modified Si(111) surface was rinsed with dry methanol to remove any residues from the surface, dried with argon, then kept under fresh THF for further spectroscopic investigations.

2.2.5 Reaction of Phenylhydrazine with Chlorine-Terminated Si (111) Surface.

The freshly prepared chlorine-terminated Si(111) sample was transferred into a clean Schlenk flask containing phenylhydrazine solution bubbled with Ar for 30 minutes and was placed in an oil bath at room temperature. The phenylhydrazine solution was prepared by mixing phenylhydrazine and THF (volume ratio 1:2). The chlorine-terminated silicon wafer was stirred in the phenylhydrazine solution under N₂ at 35~38 °C for 1 h to form a phenylhydrazine-reacted Si(111) surface. After the reaction, the phenylhydrazine-reacted Si(111) surface was rinsed with dry methanol, dried with Ar gas and kept under fresh THF.

2.2.6 Reaction of C₆₀ with Hydrazine-Terminated Si(111) Surface.

Fullerene C₆₀ was dissolved in toluene to create a C₆₀ solution with concentration at either 1 mM or 0.25 mM. The silicon wafer modified with the hydrazine monolayer was placed in a 25 mL round-bottomed flask filled with this C₆₀ solution, then refluxed at 110 °C under N₂ for 48 hours. Then the surface was

sonicated in toluene for 5 minutes and rinsed with dichloromethane, methanol and MilliQ water for several times and to remove physisorbed C₆₀ and dried with N₂ before characterization. Each characterization method was repeated on at least three C₆₀-modified silicon samples following above experimental procedure.

2.2.7 Preparation of Amine-Terminated SAM on Si (111) Substrate

The tert-butyloxycarbonyl (t-BOC)-protected 11-amino-1-undecene (AUD) was prepared by standard organic synthesis methods.^{2-3, 9} A 5 mL quantity of a solution of the t-BOC-protected 1-amino-10-undecene was placed into a 25 mL flask fitted with a reflux condenser and kept under flowing N₂. The solution was deoxygenated with dry N₂ for at least 1 h. The hydrogen-modified Si(111) surface was prepared by a modified RCA cleaning procedure. The flask was immersed in an oil bath, and the solution was maintained at 110 °C for 2 h under a slow N₂ flow. The sample was then removed from the solution and cleaned in petroleum ether (40-60 °C), methanol, and dichloromethane. Afterward, treating the surface with 25% TFA in dichloromethane for 1 h was followed by a 5 min rinse in 10% NH₄OH to remove the t-BOC protecting group and to form the primary amine-terminated surface. The surface was then rinsed with deionized water and dried with N₂.

2.2.8 Preparation of Amine-Terminated SAM on Gold Substrate

A pre-fabricated gold-coated wafer was annealed to 400 K at 10⁻⁵ Torr for two hours. The wafer was immersed in a solution of 2 mg cysteamine hydrochloride in 10

mL DMF for 24 hours followed by rinsing with DMF to remove physically adsorbed cysteamine.²⁻³

2.2.9 Carbon Nanotube Attached to Functionalized Silicon and Gold Substrates

A 50% (w/v) solution of either single walled non-functionalized carbon nanotubes or single wall carboxylic acid-functionalized carbon nanotubes in DMF was prepared and sonicated in ice water for at least one hour to achieve good dispersion.³ To promote attachment between the carbon nanotubes and functionalized gold and silicon surfaces, the cysteamine-covered Au surface and 11-amino-1-undecene-modified Si surface were immersed in the CNT/DMF solution and sonicated (40 kHz, Branson 1510) in an ice water bath for three hours. They were then rinsed with methanol and deionized water, and dried in a stream of nitrogen. In order to confirm that this preparation procedure does not induce the reaction with a chemically inert monolayer, a control experiment with the CNT reaction with (t-BOC)-protected AUD was performed and the resulting SEM micrographs confirming this assessment are presented in the Chapter 5.

2.3 Surface Modification of Zinc Oxide

2.3.1 Materials

All ZnO powder samples (99.99% purity, Acros organics) were prepared as described previously¹⁰⁻¹¹ and used as substrates for all other experiments and characterizations. All chemicals were reagent grade or as indicated: Argon (Keen

Compressed Gas, research purity), propiolic acid (Acros organics, 98%), benzyl azide (Alfa Aesar, 94%), tetrahydrofuran (THF) (Fisher, distilled from Na/benzophenone), copper(I) acetate (Sigma-Aldrich, 97%), methanol (Fisher, $\geq 99.8\%$) and acetonitrile (Fisher, 99.9%). The deionized water used to rinse the surfaces and containers was from a first-generation Milli-Q water system (Millipore) with $18\text{ M}\Omega\cdot\text{cm}$ resistivity.

2.3.2 Preparation of Propiolic Acid-modified ZnO Surface

The ZnO samples in this study were prepared by pressing about 20 mg of ZnO powder on the tungsten mesh and then mounting it on a sample holder between two tantalum clamps that allowed for resistive heating of the sample, as described in detail previously.¹⁰ To remove the adsorbed impurities, the ZnO sample was transferred into a high-vacuum chamber with a base pressure about 1×10^{-6} Torr and annealed to 850 K for 15 minutes. After cooling down to room temperature, the sample was exposed to propiolic acid at 1 Torr for 5 minutes. The propiolic acid-modified sample was kept in high-vacuum chamber under 1×10^{-6} Torr for at least 16 hours to pump away non-chemically bound propiolic acid.

2.3.3 Click Reaction with Propiolic Acid-modified ZnO Surface in Gas Phase

After gas phase benzyl azide was dosed into the system at 1 Torr, the propiolic acid-modified ZnO sample was exposed to the benzyl azide at 100 °C for 45 minutes to thermally activate the in-situ copper-free click reaction.¹² Following this procedure, the remaining reagent was pumped away.

2.3.4 Click Reaction with Propiolic Acid-modified ZnO Surface in Liquid Phase

A propiolic acid-modified ZnO sample was removed from the high vacuum chamber, taken off the tungsten mesh and transferred into a 25 mL round bottom flask filled with 1.1 mg of copper (I) acetate, 0.2 mL of benzyl azide and about 5 mL of THF. The mixture was then stirred gently for 24 hours at 40 °C under Ar atmosphere. Upon reaction completion, the ZnO sample was rinsed gently with acetonitrile in water (v/v 1:1), methanol and THF several times before characterization.¹²

2.4 Surface Analytical Techniques

2.4.1 Fourier-Transform Infrared Spectroscopy (FT-IR)

For all the silicon wafer samples, a Nicolet Magna-IR 560 spectrometer with a liquid nitrogen-cooled external MCT detector was used to collect infrared spectra in the range 4000-650 cm^{-1} with an incident angle of 60 ° with respect to the incoming infrared beam. 512 scans per spectrum and a resolution of 8 cm^{-1} were used to collect all the spectra.

For the zinc oxide sample, FT-IR spectra in the range of 4000–650 cm^{-1} were collected in a high-vacuum chamber with a base pressure under 1×10^{-6} Torr interfaced with a Nicolet Magna 560 spectrometer with liquid nitrogen-cooled external MCT-detector. The entire optical path was purged by water- and CO_2 -free air. All spectra were collected with a resolution of 4.0 cm^{-1} and 512 scans per spectrum.

2.4.2 X-ray Photoelectron Spectroscopy (XPS)

XPS studies were performed on a K-Alpha+ XPS System from Thermo Scientific using Al Ka X-ray source ($h\nu=1486.6$ eV) at a 35.3° take-off angle with respect to the analyzer. The high-resolution spectra were collected over the range of 20 eV at 0.1 eV/step with the pass energy of 58.7 eV. The survey spectra were collected over the energy range of 0-1000 eV. CasaXPS (version 2.3.16) software was utilized to analyze all the raw data. The C 1s peak was set to 284.6 eV to calibrate all peak positions.

To quantify surface coverages of chlorine and nitrogen, an overlayer model was used with the following assumptions: (1) chlorine- or nitrogen-containing groups are the closest to the silicon substrate, and the adventitious hydrocarbon and oxygen layer is on top of the chlorine or nitrogen overlayer; (2) all the chlorine or nitrogen atoms in the overlayer are in the solid state. The equivalent monolayer coverage of an overlayer species was calculated from the equation:

$$\Phi_{OV} = \left[\left(\frac{\lambda \sin \theta}{a_{OV}} \right) \left(\frac{SF_{Si}}{SF_{OV}} \right) \left(\frac{\rho_{Si}}{\rho_{OV}} \right) \left(\frac{I_{OV}}{I_{Si}} \right) \right] \quad \text{Equation (1)}$$

This calculation was performed on the basis of both survey and high-resolution spectra by applying the substrate-overlayer model that was proposed by Briggs and Seah,¹³ and described in detail previously.¹⁴⁻¹⁵

In Equation (1), Φ is the overlayer coverage; λ is the penetration depth; θ is the photoelectron takeoff angle with respect to the analyzer; a_{OV} is the atomic diameter of the overlayer species. The value of a_{OV} was obtained using the following equation:

$$a_{OV} = \left(\frac{A_{OV}}{\rho_{OV} N_A} \right)^{1/3} \quad \text{Equation (2)}$$

A_{Ov} is the atomic weight of the overlayer species: 35.45 g/mol and 14.01 g/mol for Cl and N atoms, respectively; and N_A is Avogadro's constant. I is the integrated area under the overlayer or substrate peaks, as determined by Casa XPS software. Relevant parameters are listed in Table 1 as below.

Table 2.1 Parameters used to calculate surface coverages of nitrogen and chlorine from the XPS spectra based on the overlayer model.¹⁴⁻¹⁵

component	SF (sensitivity factor)	ρ (volumetric density, g/cm ³)	ρ (atomic density, atom/cm ³)
Si 2p	0.90	2.33	5.0×10^{22}
Cl 2p	2.38	2.00	3.43×10^{22}
N 1s	1.69	1.26	5.41×10^{22}

2.4.3 Time-of-Flight Secondary Ion Mass Spectrometry (ToF-SIMS)

The ToF-SIMS analysis was performed on a TOF-SIMS V (ION-TOF, Münster, Germany), equipped with a bismuth primary ion source. The 25 kV Bi³⁺ primary ion beam was run in 'high current bunched-mode' to the static SIMS limit of 1×10^{12} ions/cm² beam dosage for each spectrum collected. The spectra collected had a mass resolution of $m/\Delta m = 9000$ recorded at $m/z = 29$. The Bi³⁺ primary ions were rastered over an area of $200 \times 200 \mu\text{m}^2$ with a 128×128 pixel density for all spectra. High resolution negative-ion mode spectra were obtained, but only the most informative regions of the negative-ion mode spectra are presented. The extraction cone of the TOF analyzer was held at +2 kV for negative-ion extraction, with a post-

acceleration of 10 kV and a detector voltage of 9 kV. The calibration of the ToF-SIMS data was performed using ION-TOF measurement explorer software (Version 6.3). All spectra were calibrated to H^+ , H_2^+ , H_3^+ , C^+ , CH^+ , CH_2^+ , CH_3^+ , C_2H_3^+ , C_3H_5^+ , C_4H_7^+ , C_5H_5^+ , C_6H_5^+ , and C_7H_7^+ in positive mode and H^- , H_2^- , C^- , CH^- , CH_2^- , CH_3^- , C_2^- , C_2H^- , C_3^- , C_4^- , C_5^- , C_6^- , C_7^- , and C_8^- in negative mode.

All spectra for carbon nanotube attached gold surfaces were further calibrated to the fragment of a single gold atom $[\text{Au}]^-$.

2.4.4 Scanning Electron Microscopy (SEM)

A Zeiss Auriga 60 scanning electron microscope (SEM) was used to confirm the presence of the carbon nanotubes on the substrates. An electron beam with an accelerating voltage of 3 kV was used and images were collected with a secondary electron (in-lens) detector at a working distance of 5.0 mm.

2.4.5 Atomic Force Microscopy (AFM)

Individual carbon nanotubes present on the surface were observed using tapping mode Atomic force microscopy (AFM) with a Veeco Multimode SPM with a Nanoscope V controller was performed in the tapping mode. Tap300Al-G tips (Budget Sensors) with a force constant of 40 N/m and a drive frequency of 300 kHz were used and the images were analyzed using Gwyddion software.

2.4.6 Transmission Electron Microscopy (TEM)

The average diameter of the individual nanotubes was independently confirmed via a JEOL JEM-3010 transmission electron microscope (TEM) using an incident electron energy of 300 keV.

2.4.7 Nuclear Magnetic Resonance Spectroscopy (NMR)

All solid-state NMR measurements were carried out on a 11.7 T wide-bore Bruker Avance III solid-state NMR spectrometer, operating at a Larmor frequency of 500.13 MHz for ^1H and 125.77 MHz for ^{13}C . A 3.2 mm Bruker multinuclear HCN magic angle spinning (MAS) probe was used. The CP/MAS data were acquired at 25 °C with an MAS frequency of 14 kHz, controlled to within ± 3 Hz using the Bruker MAS controller. The typical 90° pulse length was 2.85 μs for ^1H and 3.3 μs for ^{13}C . For a typical measurement, sufficient number of scans was collected for ^{13}C CP/MAS NMR spectra with a recycle delay of 3 s and a cross-polarization time of 2 ms until a spectrum with a reasonable signal-to-noise ratio was obtained. ^1H SPINAL-64 heteronuclear decoupling with field strength of approximately 100 kHz was applied during the acquisition period. The solution ^{13}C NMR spectrum was obtained on a 400 MHz Bruker Avance III instrument.

2.4.8 Charge-Carrier Lifetime Measurements

A WCT-120 Lifetime Tester with a 60 W light power source was utilized to measure the effective minority carrier lifetime. The carrier lifetime is determined at an injection level of $5 \times 10^{13} \text{ cm}^{-3}$. An RF-bridge circuit, which is coupled by a coil to the measured specimen, senses the conductance in terms of permeability. For the

measurement, the sample is cut into 2 cm \times 2 cm pieces and covered with a 1 cm \times 1.7 cm aperture. The time dependence of illumination and excess photoconductance of the measured sample are calibrated by a larger area silicon wafer of the same type, following the small sample size calibration procedure provided by Sinton Instruments.

2.4.9 Computational Details

Density Function Theory (DFT) calculations were performed with the Gaussian 09 suite of programs¹⁶ utilizing the B3LYP functional¹⁷⁻¹⁸ and either 6-311+G(d,p) or LANL2DZ basis set.¹⁹⁻²⁰

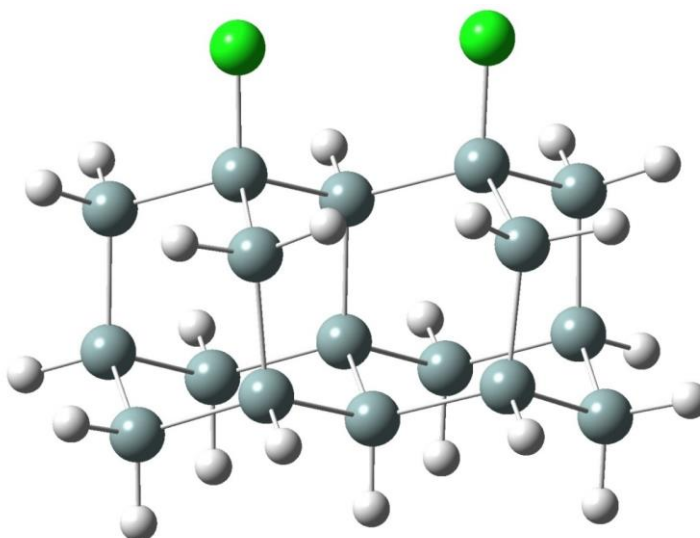
For the modification of silicon surface, a Si₁₇H₂₄ cluster model, which represents two neighboring top silicon atoms on a Si(111) surface terminated with hydrogen or chlorine, was used. The bottom three layers in this Si₁₇H₂₄ cluster model were fixed at their bulk positions in DFT calculations to avoid unrealistic distortions.

To simulate the most common surface of ZnO powder, a Zn₂₀O₂₀ cluster model based on mixed-terminated ZnO(10T0) surface was used as a substrate. This representation described the surface that corresponds to approximately 80% of the ZnO surface in the nanopowder, and is the key in chemical description of ZnO material interaction with carboxylic acids, as described in detail previously.^{10, 21} The two bottom layers of atoms in the Zn₂₀O₂₀ cluster model are “frozen” at their bulk position to prevent unrealistic distortion of the model structures.

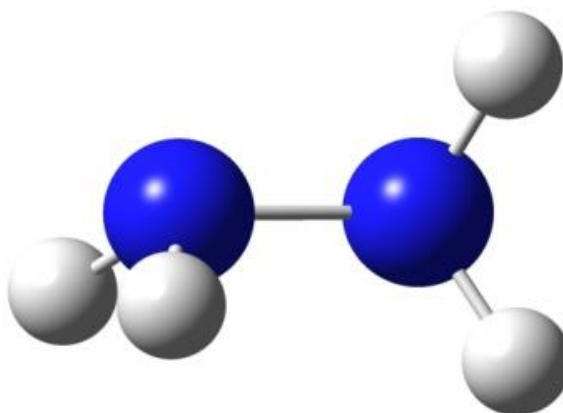
The N 1s core-level energy was predicted using Koopmans’ theorem and the correction factor to the predicted core-level energy for N 1s was 8.76 eV for 6-311+G(d,p) or 8.5 eV for LANL2DZ basis set according to our previous investigations.²²⁻²³ All the models used in this thesis are presented below.

2.4.9.1 Models calculated with 6-311+G(d,p) basis set.

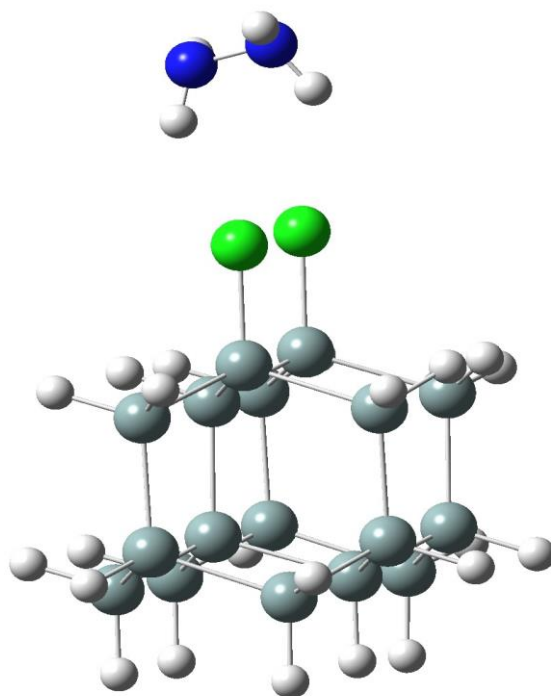
Chlorine-terminated Si(111) surface represented by a $\text{Si}_{17}\text{H}_{24}$ cluster model; Energy= -5855.75503963 a.u.



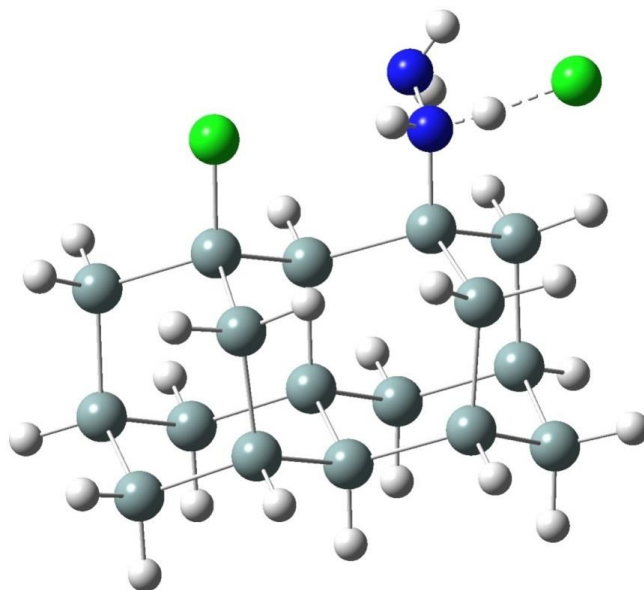
Free hydrazine molecule; Energy= -111.91057678 a.u.



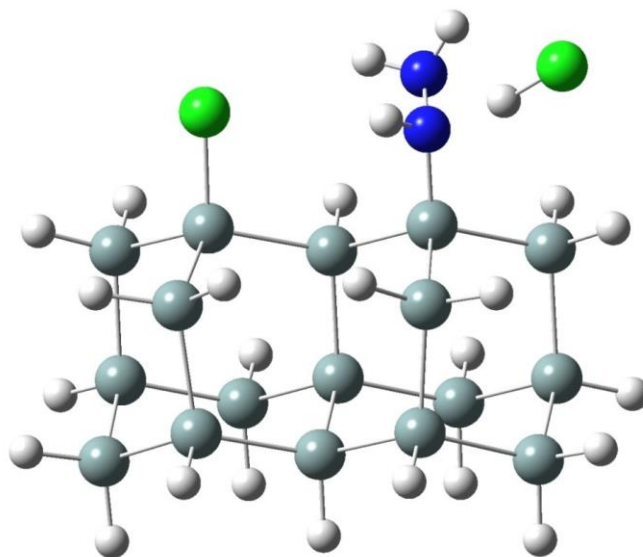
Weak interaction between a hydrazine molecule and Cl-Si(111) surface ($\text{Si}_{17}\text{H}_{24}$ cluster model); Energy=-5967.66847605a.u.



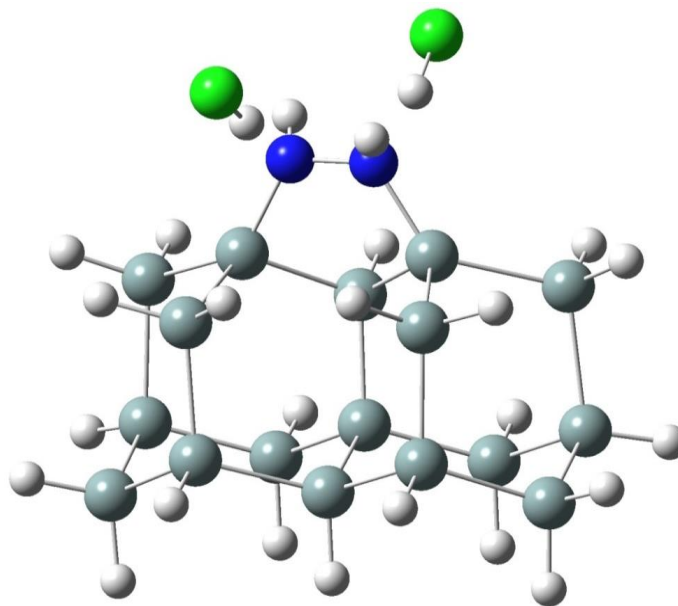
First transition state of hydrazine reaction with Cl-Si(111) surface ($\text{Si}_{17}\text{H}_{24}$ cluster model); Energy= -5967.65387574a.u.



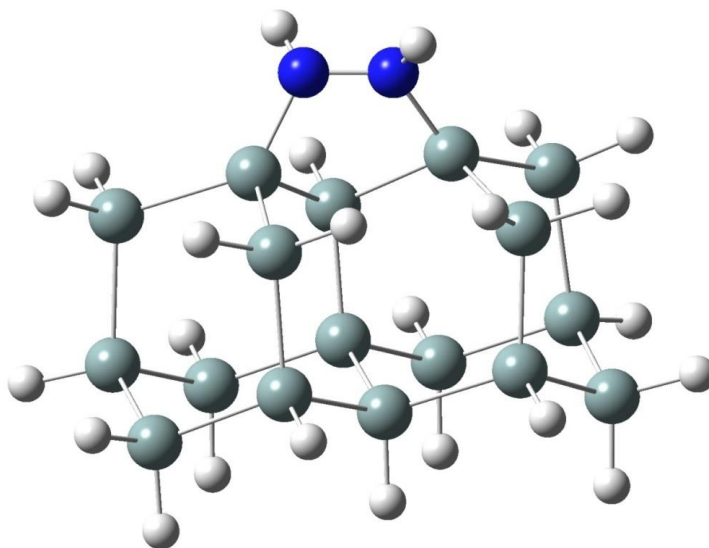
First step product of hydrazine reaction with Cl-Si(111) surface ($\text{Si}_{17}\text{H}_{24}$ cluster model); Energy= -5967.65759831a.u.



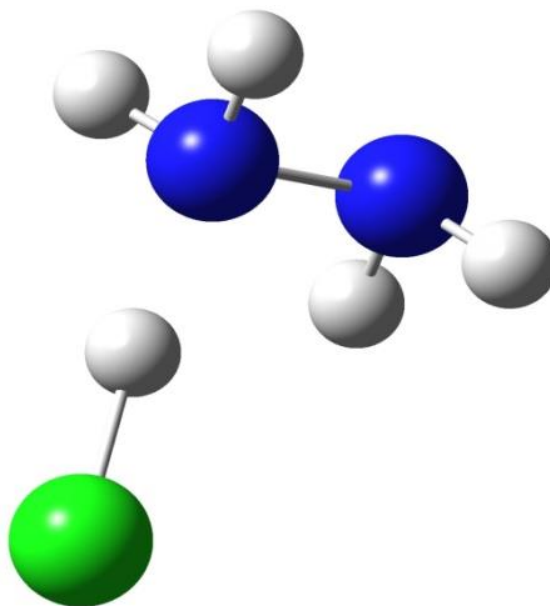
Final step product of hydrazine reaction with Cl-Si(111) surface ($\text{Si}_{17}\text{H}_{24}$ cluster model); Energy=-5967.58298457a.u



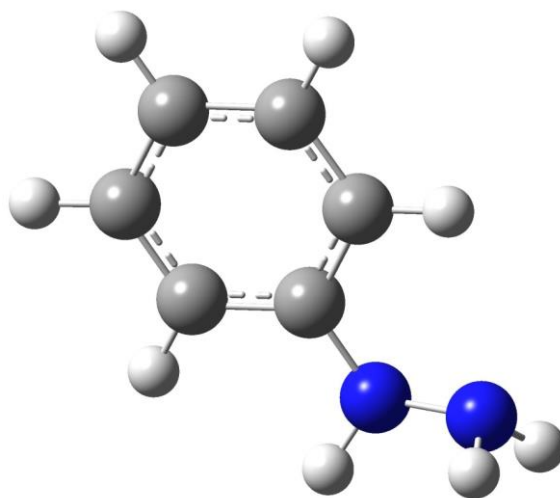
Hydrazine terminated Si(111) surface on $\text{Si}_{17}\text{H}_{24}$ cluster model; Energy= -5045.91861106 a.u



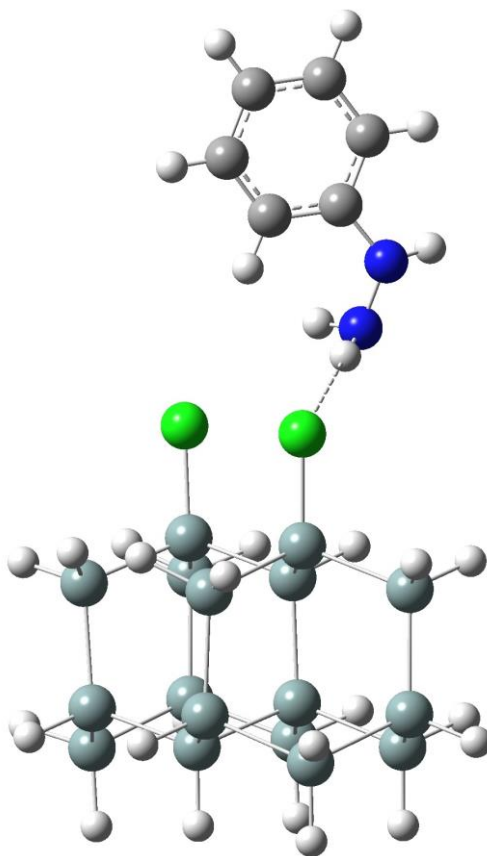
Hydrazine chloride salt molecule; Energy= -572.76036048a.u.



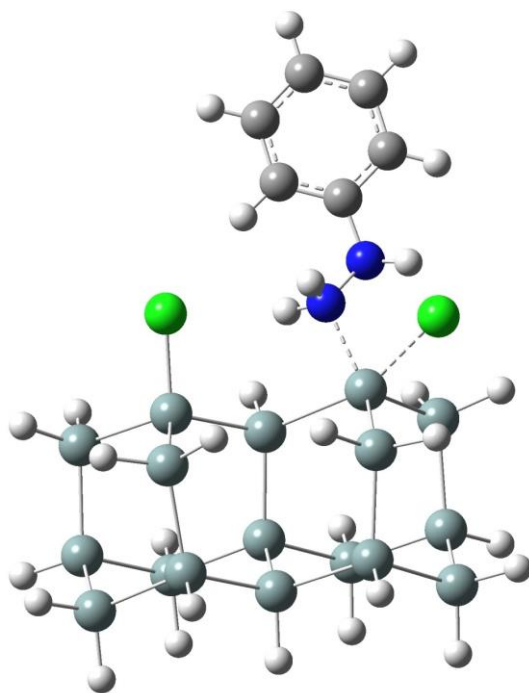
Free phenylhydrazine molecule; Energy= -343.01919594 a.u.



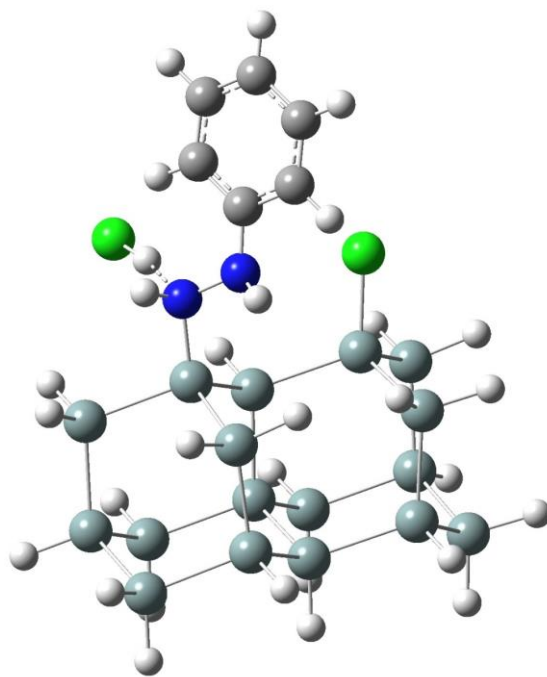
Weak interaction between a phenylhydrazine molecule and Cl-Si(111) surface ($\text{Si}_{17}\text{H}_{24}$ cluster model); Energy= -6198.7790952 a.u.



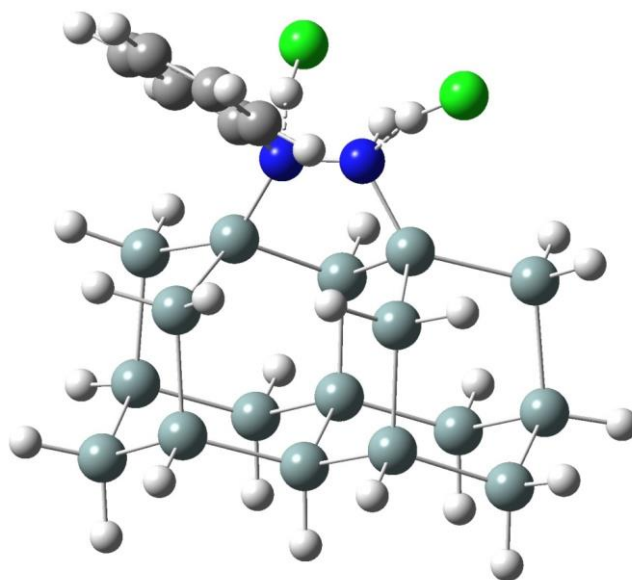
First transition state of phenylhydrazine reaction with Cl-Si(111) surface ($\text{Si}_{17}\text{H}_{24}$ cluster model); Energy= -6198.74694326 a.u.



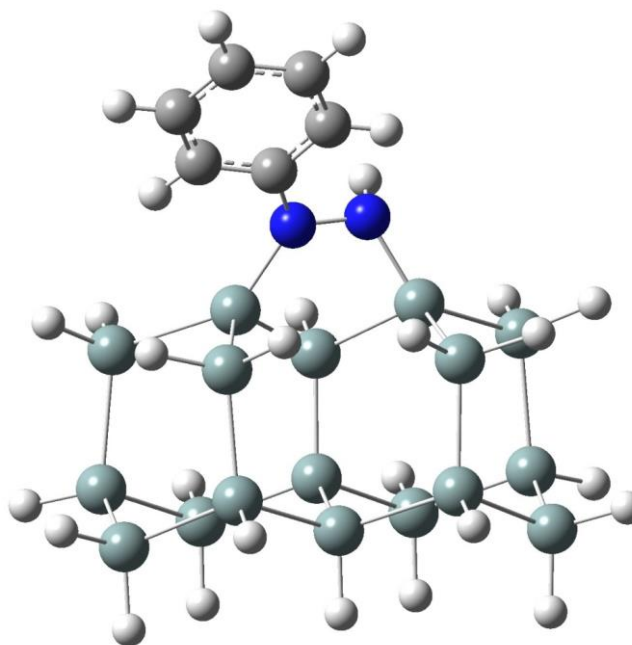
First step product of phenylhydrazine reaction with Cl-Si(111) surface ($\text{Si}_{17}\text{H}_{24}$ cluster model); Energy= -6198.75364056 a.u.



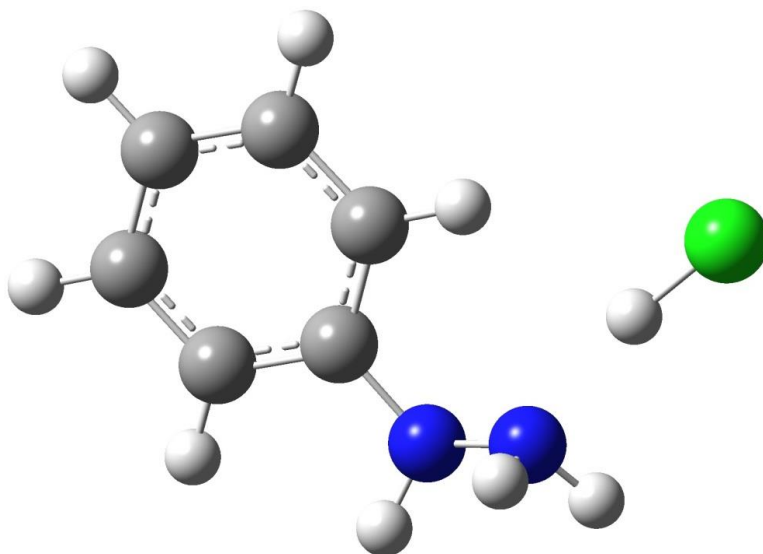
Second step product of hydrazine reaction with Cl-Si(111) surface ($\text{Si}_{17}\text{H}_{24}$ cluster model); Energy= -6198.67700491 a.u



Phenylhydrazine-terminated Si(111) surface on $\text{Si}_{17}\text{H}_{24}$ cluster model; Energy= -5276.99697241 a.u

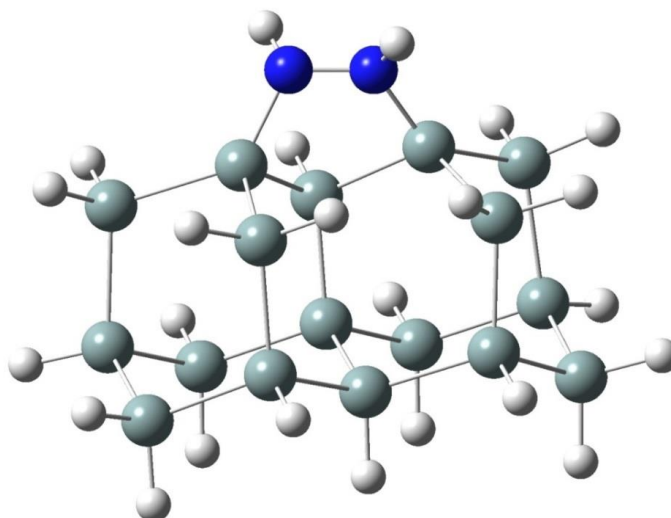


Proposed phenylhydrazine chloride salt molecule; Energy= -803.86298720 a.u.

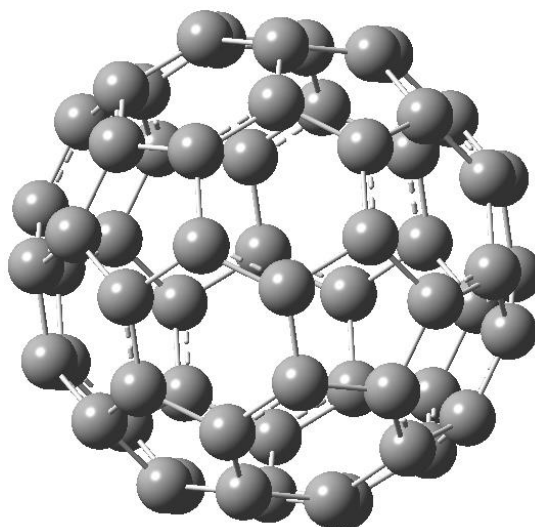


2.4.9.2 Models calculated with LANL2DZ basis set.

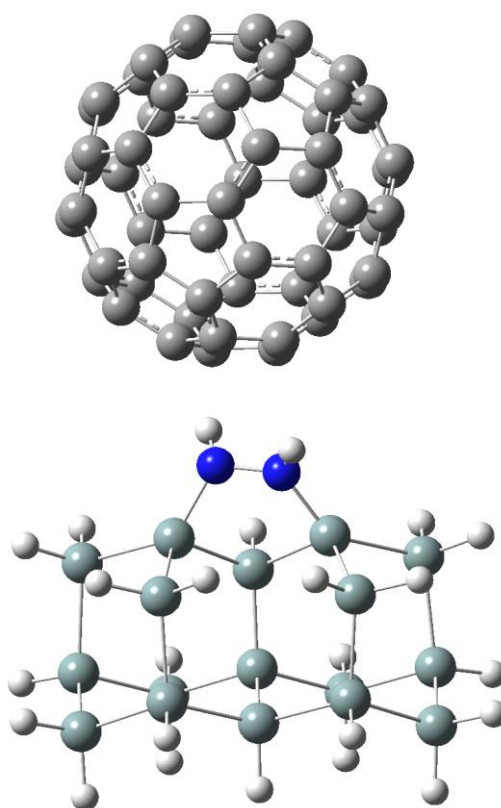
Hydrazine-terminated Si(111) surface on $\text{Si}_{17}\text{H}_{24}$ cluster model; Energy= -5045.89553175 a.u.



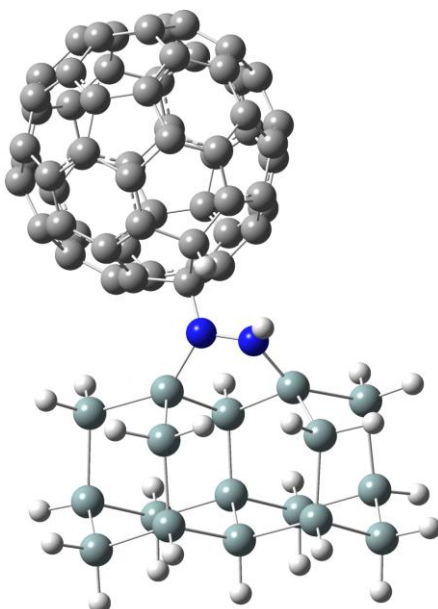
Free Buckminster fullerenes C_{60} molecule; Energy= -2286.59990866 a.u.



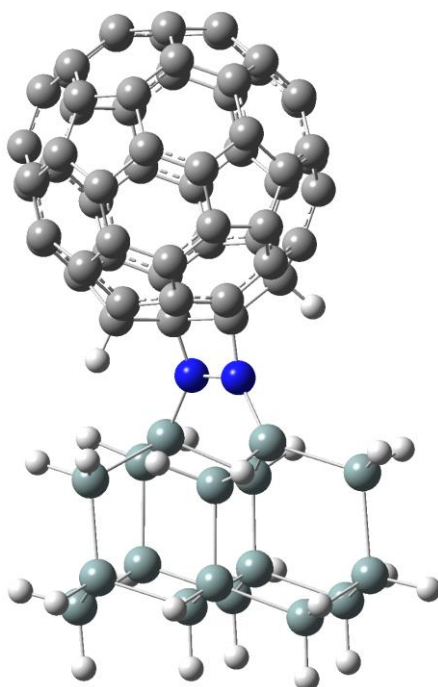
Weak interaction between a fullerenes C_{60} molecule and hydrazine-Si(111) surface ($Si_{17}H_{24}$ cluster model); Energy= -7332.49097959 a.u.



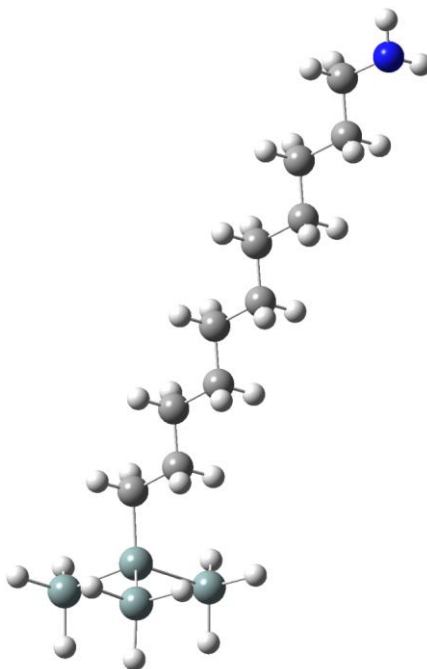
Fullerene C₆₀ attached on hydrazine-terminated Si(111) surface on Si₁₇H₂₄ cluster model, forming one C-N bond; Energy= -7332.45449790 a.u.



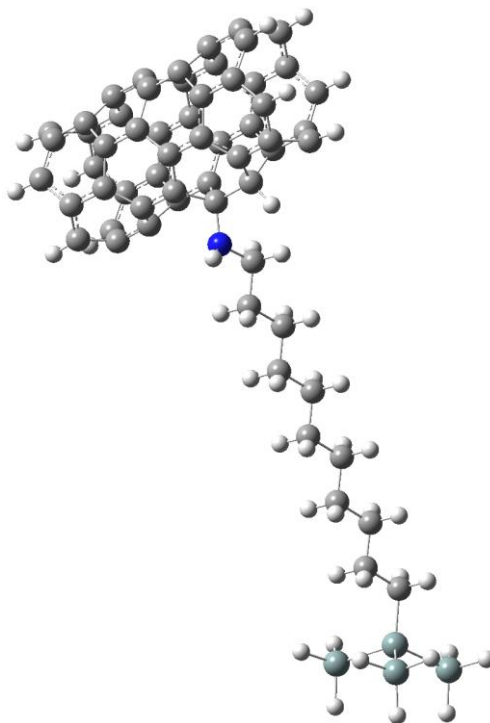
Fullerene C₆₀ attached on hydrazine-terminated Si(111) surface on Si₁₇H₂₄ cluster model, forming two C-N bonds; Energy= -7332.42645172 a.u.



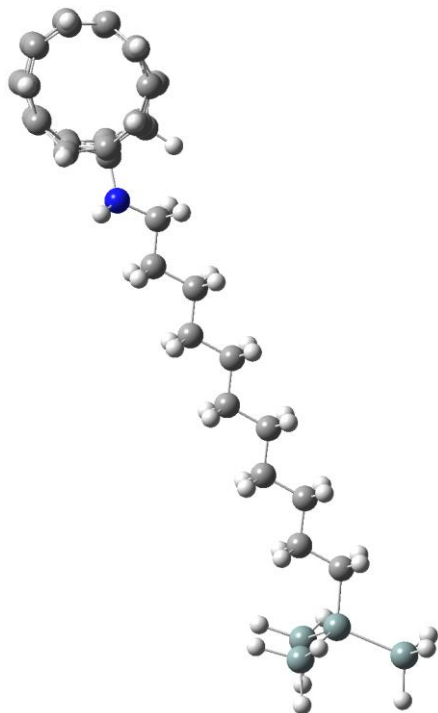
11-amino-1-undecene (AUD)-terminated Si(111) surface represented by a Si_4H_9 cluster model; Energy = -509.23494979 a.u.



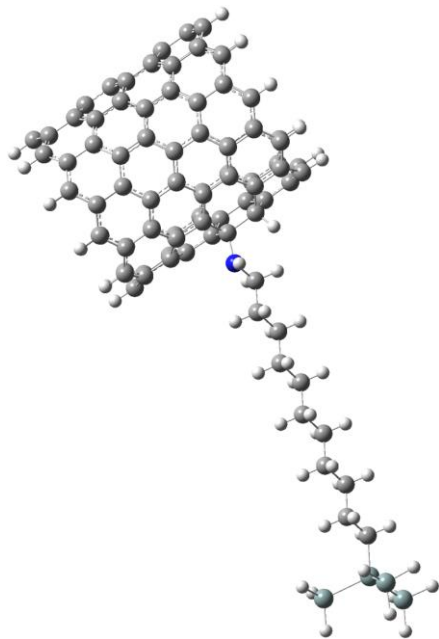
(5, 0) carbon nanotube attached to an 11-amino-1-undecene (AUD)-terminated Si(111) surface (Si_4H_9 cluster model; parallel attachment); Energy = -2419.57258502 a.u.



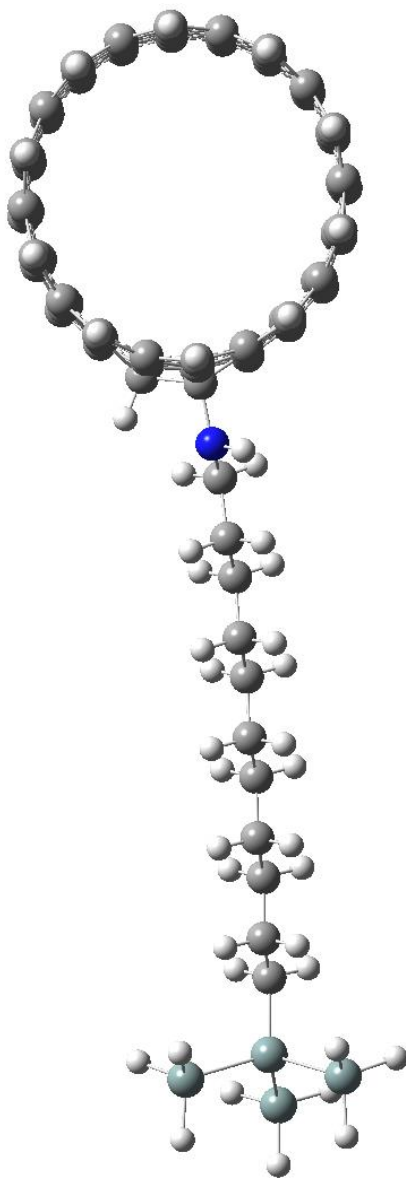
(5, 0) carbon nanotube attached to an 11-amino-1-undecene (AUD)-terminated Si(111) surface (Si_4H_9 cluster model; non-parallel attachment); Energy = -2419.54456994 a.u.



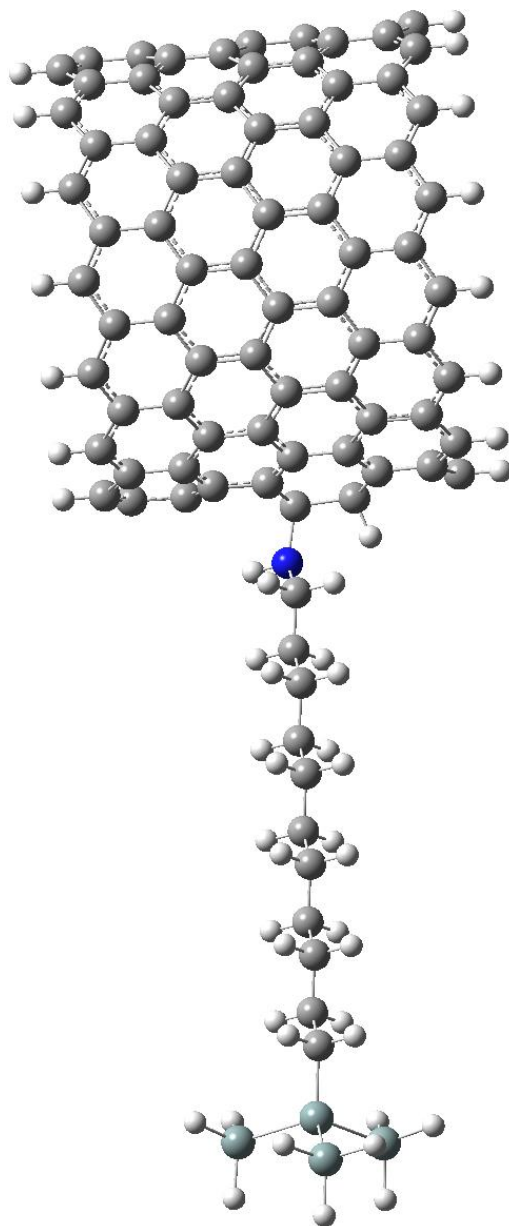
(10, 0) carbon nanotube attached to an 11-amino-1-undecene (AUD)-terminated Si(111) surface (Si_4H_9 cluster model; parallel attachment); Energy = -4331.33212240 a.u.



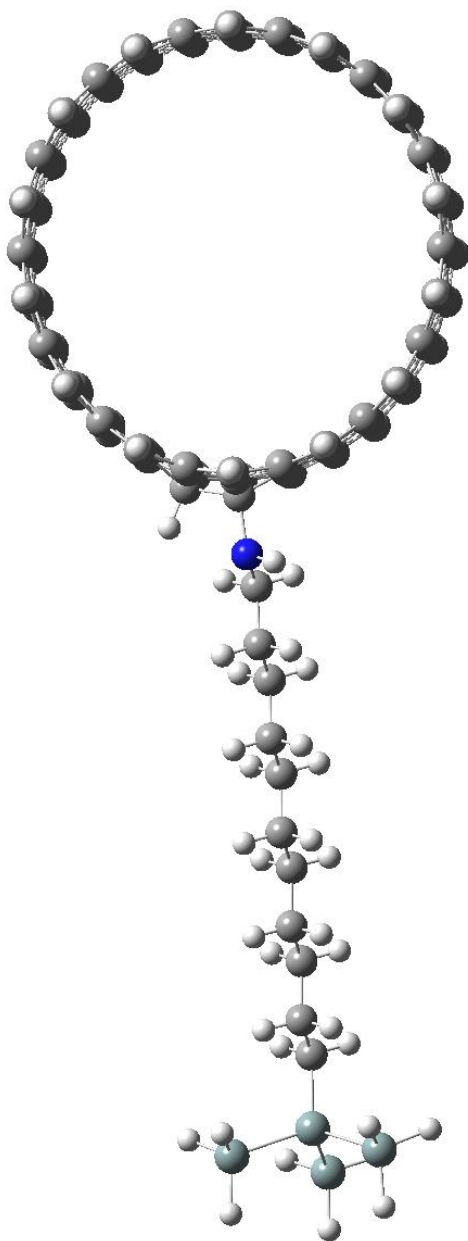
(10, 0) carbon nanotube attached to an 11-amino-1-undecene (AUD)-terminated Si(111) surface (Si_4H_9 cluster model; non-parallel attachment); Energy = -4331.33855091 a.u.



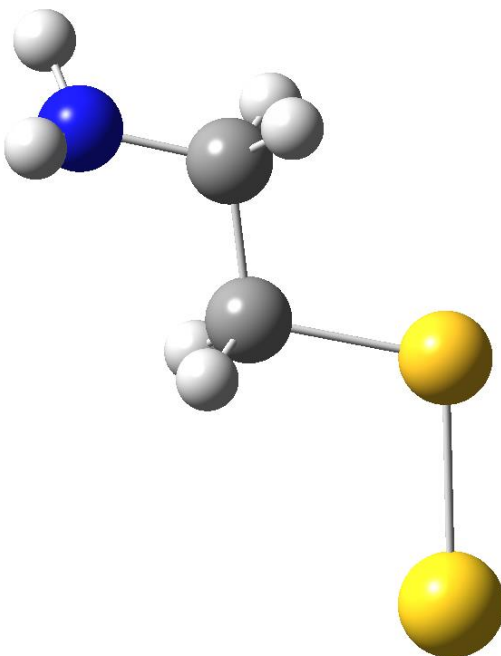
(14, 0) carbon nanotube attached to an 11-amino-1-undecene (AUD)-terminated Si(111) surface (Si_4H_9 cluster model; parallel attachment); Energy = -5860.55695975 a.u.



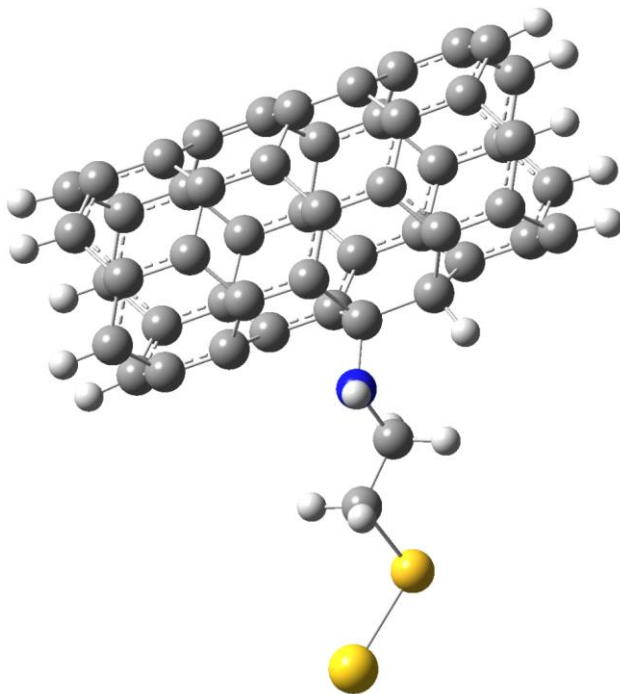
(14, 0) carbon nanotube attached to an 11-amino-1-undecene (AUD)-terminated Si(111) surface (Si_4H_9 cluster model; non-parallel attachment); Energy = -5860.56845874 a.u.



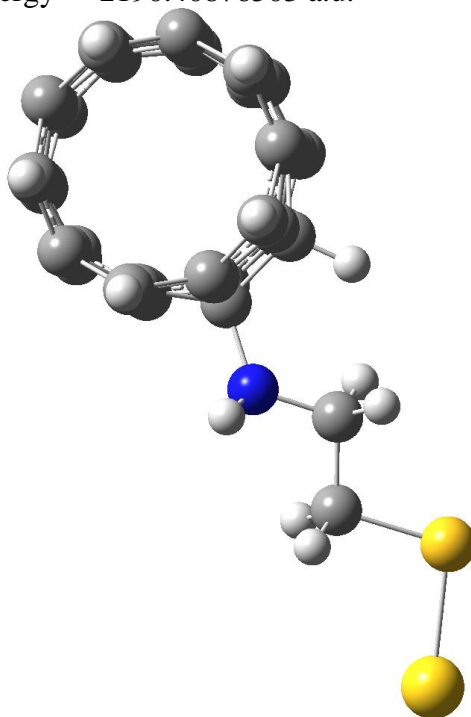
Cysteamine-covered Au surface model; Energy = -280.12123322 a.u.



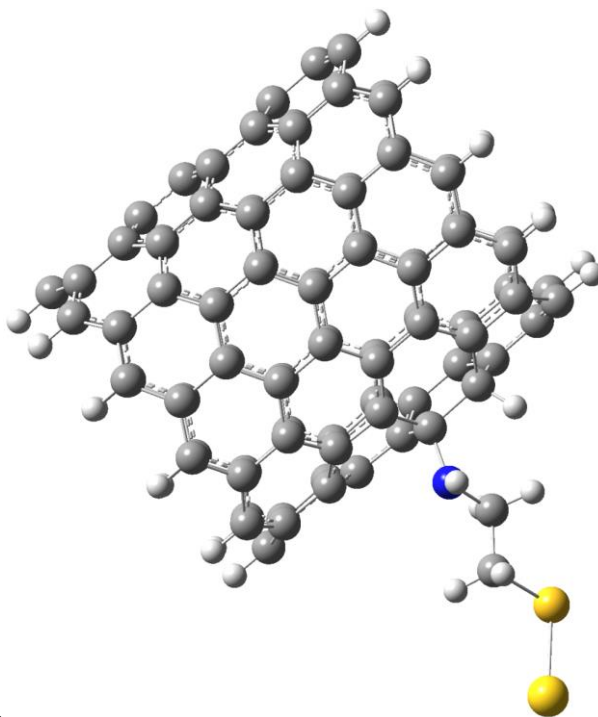
(5, 0) carbon nanotube attached to a cysteamine-covered Au surface model (parallel attachment); Energy = -2190.45754776 a.u.



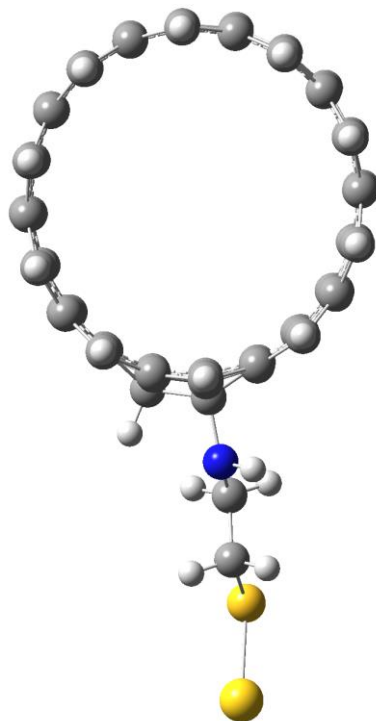
(5, 0) carbon nanotube attached to a cysteamine-covered Au surface model (non-parallel attachment); Energy = -2190.40876503 a.u.



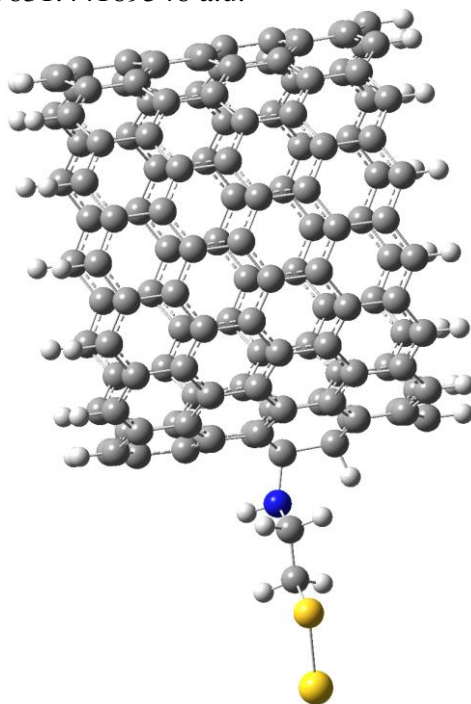
(10, 0) carbon nanotube attached to a cysteamine-covered Au surface model (parallel attachment); Energy = -4102.2159293 a.u



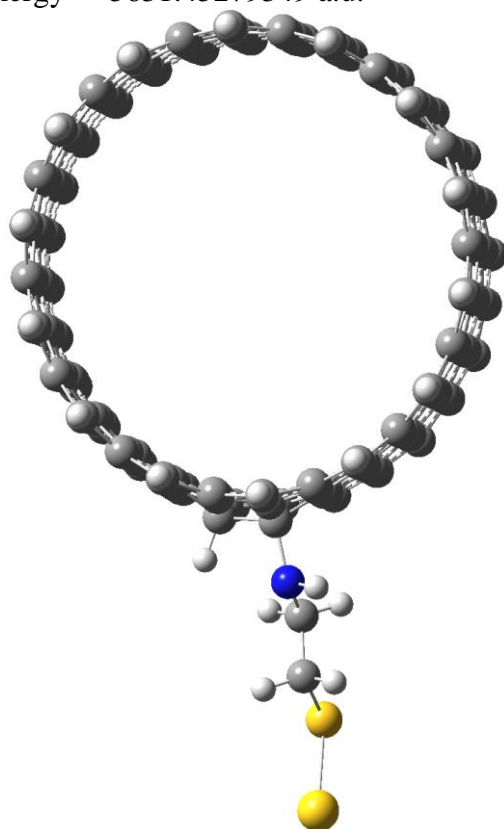
(10, 0) carbon nanotube attached to a cysteamine-covered Au surface model (non-parallel attachment); Energy = -4102.22214188 a.u.



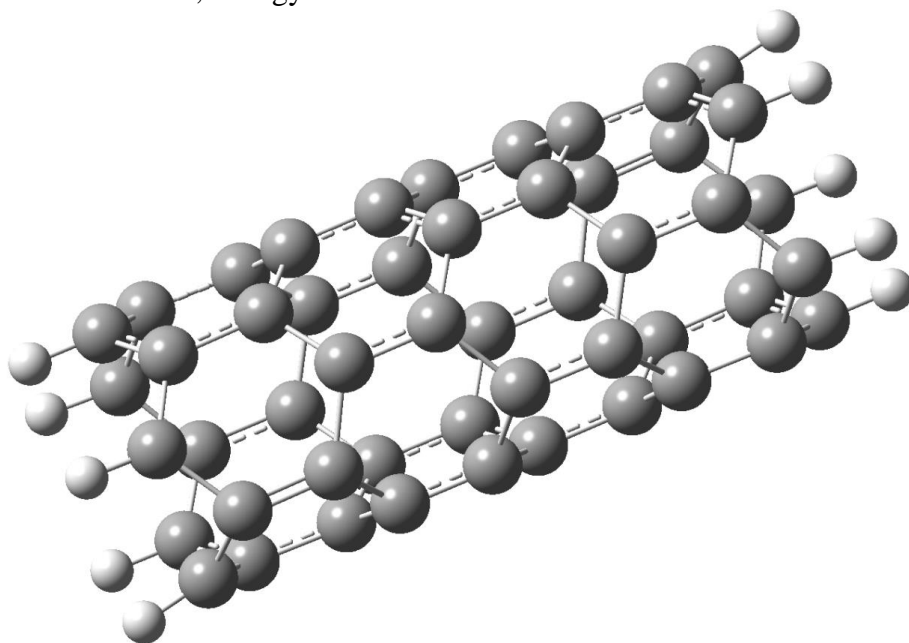
(14, 0) carbon nanotube attached to a cysteamine-covered Au surface model (parallel attachment); Energy = -5631.44169546 a.u.



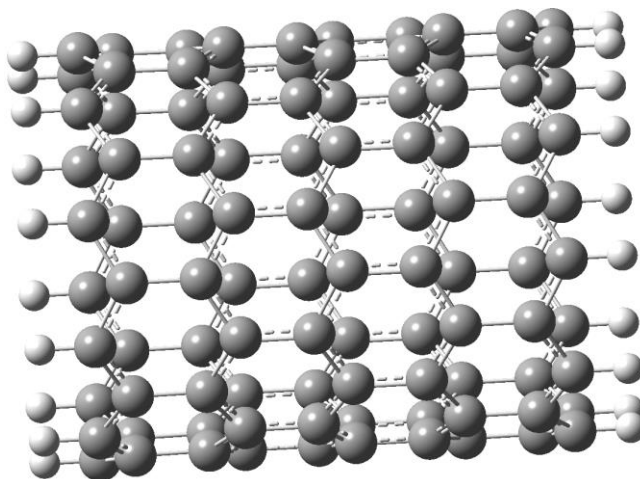
(14, 0) carbon nanotube attached to a cysteamine-covered Au surface model (non-parallel attachment); Energy = -5631.45279349 a.u.



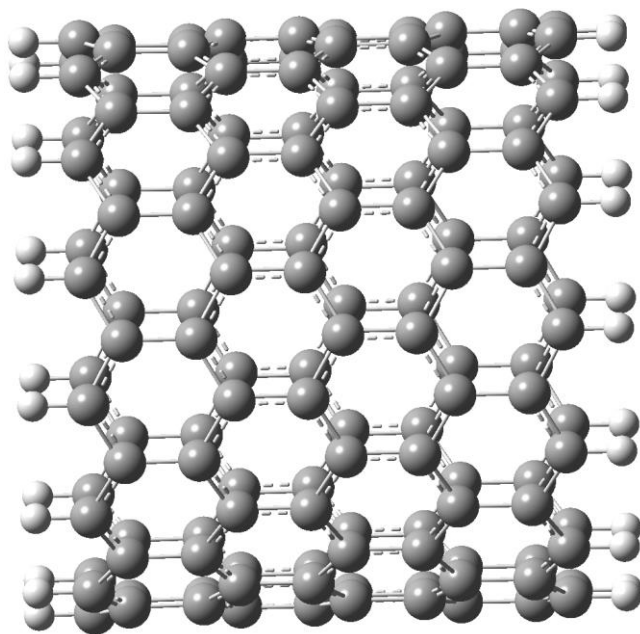
(5, 0) carbon nanotube; Energy = -1910.29763925 a.u.



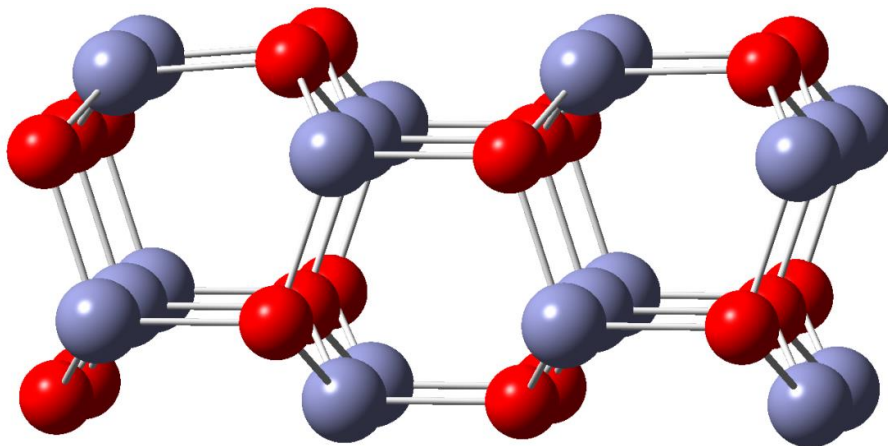
(10, 0) carbon nanotube; Energy = -3822.15469414 a.u.



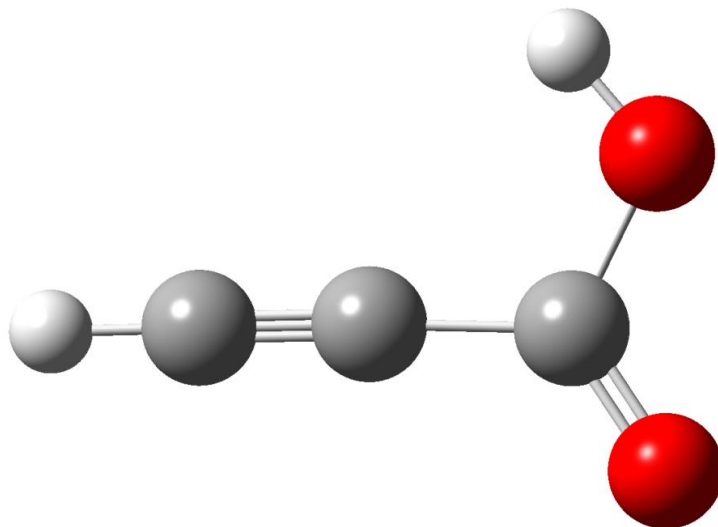
(14, 0) carbon nanotube; Energy = -5351.40204714 a.u.



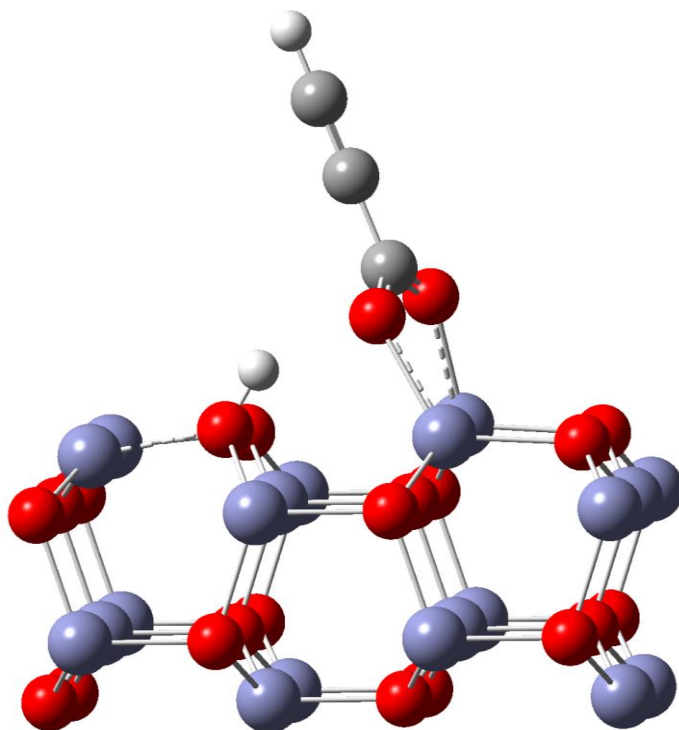
ZnO powder surface represented by a $\text{Zn}_{20}\text{O}_{20}$ cluster model; Energy = -2817.48188159 a.u



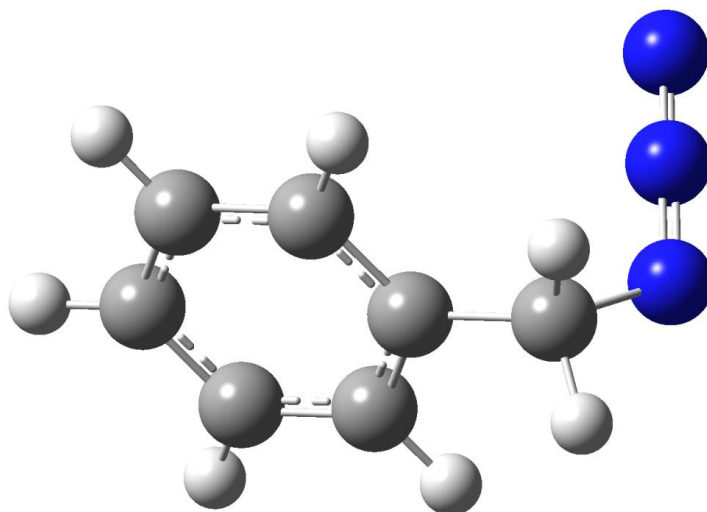
free propiolic acid molecule; Energy = -265.84961693 a.u.



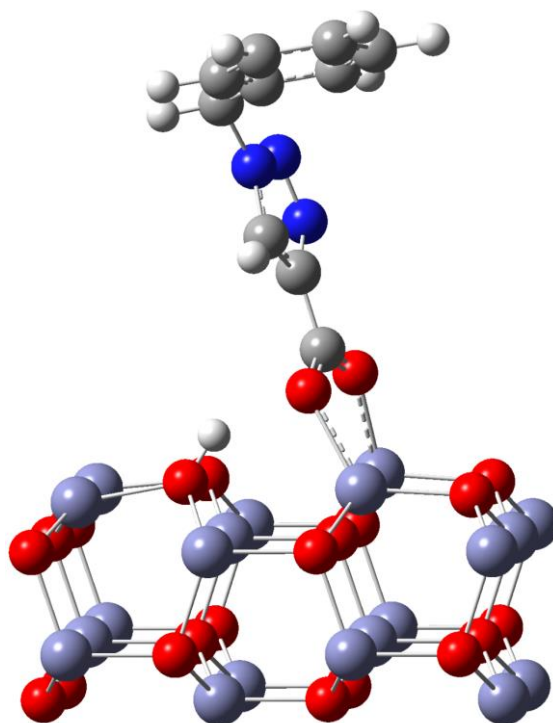
Propiolic acid reaction with ZnO surface ($\text{Zn}_{20}\text{O}_{20}$ cluster model); Energy = -3083.45551612 a.u.



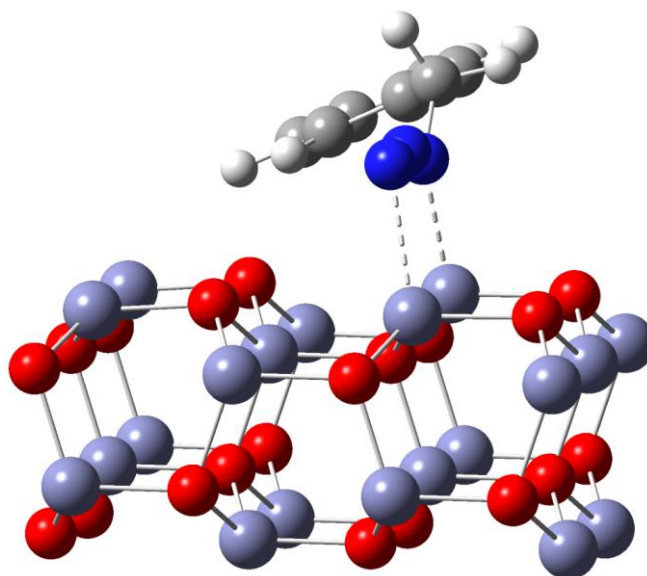
free benzyl azide molecule; Energy = -435.05402507 a.u.



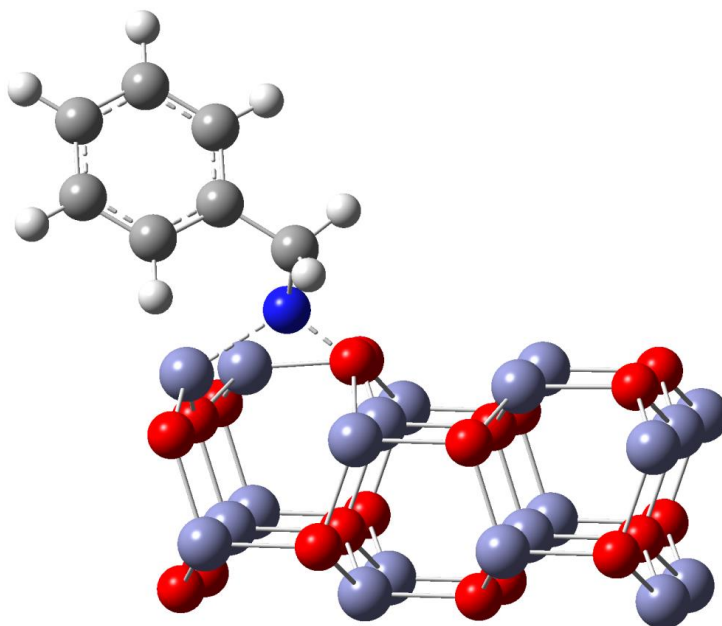
benzyl azide “clicked” with propiolic acid-functionalized ZnO surface ($\text{Zn}_{20}\text{O}_{20}$ cluster model); Energy = -3518.63190937 a.u.



Benzy azide bound to ZnO surface ($\text{Zn}_{20}\text{O}_{20}$ cluster model); Energy = -3252.56897155 a.u.



Dissociated benzyl azide bound to ZnO surface (Zn₂₀O₂₀ cluster model); Energy = -3143.09070120 a.u.



REFERENCES

1. Sieval, A. B.; Linke, R.; Heij, G.; Meijer, G.; Zuilhof, H.; Sudhölter, E. J. R. Amino-Terminated Organic Monolayers on Hydrogen-Terminated Silicon Surfaces. *Langmuir* **2001**, *17*, 7554-7559.
2. Zhang, X.; Teplyakov, A. V. Adsorption of C₆₀ Buckminster Fullerenes on an 11-Amino-1-Undecene-Covered Si(111) Substrate. *Langmuir* **2008**, *24*, 810-820.
3. Williams, M. G.; Gao, F.; BenDhiab, I.; Teplyakov, A. Carbon Nanotubes Covalently Attached to Functionalized Surfaces Directly through the Carbon Cage. *Langmuir* **2017**, *33*, 1121-1131.
4. Kern, W. The Evolution of Silicon Wafer Cleaning Technology. *J. Electrochem. Soc.* **1990**, *137*, 1887–1892.
5. Chabal, Y. J. Infrared Spectroscopy of Semiconductor Surfaces: H-Terminated Silicon Surfaces. *J. Mol. Struct.* **1993**, *292*, 65-80.
6. Chabal, Y. J.; Harris, A. L.; Raghavachari, K.; Tully, J. C. Infrared Spectroscopy of H-Terminated Silicon Surfaces. *International journal of modern physics. B, Condensed matter physics, statistical physics, applied physics* **1993**, *07*, 1031-1078.
7. Bansal, A.; Li, X. L.; Yi, S. I.; Weinberg, W. H.; Lewis, N. S. Spectroscopic Studies of the Modification of Crystalline Si(111) Surfaces with Covalently-Attached Alkyl Chains Using a Chlorination/Alkylation Method. *J. Phys. Chem. B* **2001**, *105*, 10266–10277.

8. Gao, F.; Teplyakov, A. V. Reaction of Hydrazine with a Chlorine-Terminated Si(111) Surface. *J. Phys. Chem. C* **2014**, *118*, 27998-28006.
9. Miller, T.; Teplyakov, A. V. Attachment Chemistry of PCBM to a Primary-Amine-Terminated Organic Monolayer on a Si(111) Surface. *Langmuir* **2014**, *30*, 5105-5114.
10. Kung, H.; Teplyakov, A. V. Formation of Copper Nanoparticles on ZnO Powder by a Surface-Limited Reaction. *J. Phys. Chem. C* **2014**, *118*, 1990-1998.
11. Gao, J.; Teplyakov, A. V. Surface Species Formed During Thermal Transformation of Ethanol on ZnO Powder. *J. Catal.* **2013**, *300*, 163-173.
12. Gao, F.; Aminane, S.; Bai, S.; Teplyakov, A. V. Chemical Protection of Material Morphology: Robust and Gentle Gas-Phase Surface Functionalization of ZnO with Propiolic Acid. *Chem. Mater.* **2017**, *29*, 4063–4071.
13. Briggs, D.; Seah, M. P., *Practical Surface Analysis 2nd Edition*; Wiley: New York, 1990; Vol. 1.
14. Haber, J. A.; Lewis, N. S. Infrared and X-ray Photoelectron Spectroscopic Studies of the Reactions of Hydrogen-Terminated Crystalline Si(111) and Si(100) Surfaces with Br₂, I₂, and Ferrocenium in Alcohol Solvents. *J. Phys. Chem. B* **2002**, *106*, 3639–3656.
15. Webb, L. J.; Nemanick, E. J.; Biteen, J. S.; Knapp, D. W.; Michalak, D. J.; Traub, M. C.; Chan, A. S. Y.; Brunschwig, B. S.; Lewis, N. S. High-Resolution X-ray Photoelectron Spectroscopic Studies of Alkylated Silicon(111) Surfaces. *J. Phys. Chem. B* **2005**, *109*, 3930–3937.

16. Frisch, M. J.; Trucks, G. W.; Schlegel, H. B.; Scuseria, G. E.; Robb, M. A.; Cheeseman, J. R.; Scalmani, G.; Barone, V.; Mennucci, B.; Petersson, G. A. *Gaussian 09, Revision B.01*, Gaussian, Inc.: Wallingford, CT, 2009.
17. Lee, C. T.; Yang, W. T.; Parr, R. G. Development of the Colle-Salvetti Correlation-Energy Formula into a Functional of the Electron Density. *Phys. Rev. B* **1988**, *37*, 785–789.
18. Becke, A. D. A New Mixing of Hartree–Fock and Local Densityfunctional Theories. *J. Chem. Phys.* **1993**, *98*, 1372–1377.
19. McLean, A. D.; Chandler, G. S. Contracted Gaussian Basis Sets for Molecular Calculations. I. Second Row Atoms, Z=11–18. *J. Chem. Phys.* **1980**, *72*, 5639–5648.
20. Krishnan, R.; Binkley, J. S.; Seeger, R.; Pople, J. A. Self-Consistent Molecular Orbital Methods. Xx. A Basis Set for Correlated Wavefunctions. *J. Chem. Phys.* **1980**, *72*, 650-654.
21. Kung, H.; Duan, Y.; Williams, M. G.; Teplyakov, A. V. Transmetalation Process as a Route for Preparation of Zinc-Oxide-Supported Copper Nanoparticles. *Langmuir* **2016**, *32*, 7029-7037.
22. Leftwich, T. R.; Teplyakov, A. V. Calibration of Computationally Predicted N *1s* Binding Energies by Comparison with X-ray Photoelectron Spectroscopy Measurements. *J. Electron Spectrosc. Relat. Phenom.* **2009**, *175*, 31–40.
23. Giesbers, M.; Marcelis, A. T. M.; Zuilhof, H. Simulation of XPS C *1s* Spectra of Organic Monolayers by Quantum Chemical Methods. *Langmuir* **2013**, *29*, 4782-4788.

Chapter 3

REACTION OF HYDRAZINE WITH A Cl-TERMINATED Si(111) SURFACE AND ITS APPLICATION FOR DIRECT COVALENT ATTACHMENT OF C₆₀ FULLERENE

3.1 Introduction

Modification and organic functionalization of silicon surfaces has undergone tremendous growth within the last 20 years to benefit a number of applications including electronics, heterogeneous catalysis, bio-molecular recognition and sensing, biomolecular separation and energy conversion.¹⁻⁵

The passivation or functionalization of silicon surfaces to prevent oxidation has emerged as an important requirement for a number of applications.⁶⁻¹¹ Although the majority of previous work targeted the formation of stable Si-C bonds in hydrosilylation processes, more recently substantial attention has been directed to the stable organic-inorganic interfaces on silicon with the help of Si-N bonds. However, most strategies to form surface Si-N bonds on silicon substrates also introduce additional carbon- or oxygen-containing functional groups that in turn react with the surface species to affect the stability and properties of the surface.¹²⁻¹⁹ The chemical reactivity of the produced amine-functionalized surfaces is also a crucial part of current investigations, with tunable reactivity of surface amino-groups being used as the starting points for thin film deposition²⁰⁻²² and metallic nanostructure formation²³⁻²⁴ where the precise reactivity of the surface-bound amine defines future opportunities for designing silicon-based interfaces with tunable properties.

Traditionally, a number of investigations focused on preparing Si-N based interfaces by exposing silicon surfaces to ammonia^{23, 25-31} or azides³²⁻³³ in ultra-high vacuum, recently Tian et al established wet chemistry methods to prepare carbon- and oxygen-free Si(111) surface terminated predominantly with Si-NH-Si functionality based on chlorination followed by the room temperature ammonia treatment utilizing NH₃-saturated tetrahydrofuran (THF).³⁴ However, the surface obtained was still easily oxidized in ambient conditions and the theoretical investigation of the proposed chemistry suggested that the resulting surface structures are not stable. In order to address both questions, a reaction with hydrazine, leading predominantly to the more stable surface species, compared to those obtained with ammonia, will be tested. Based on a simple computational illustration presented in Figure 3.1 (the details of the computational approach are described in chapter 2), the thermodynamic requirements for hydrazine reaction with Cl-Si(111) surface are much less substantial than those for ammonia reaction with the same Cl-Si(111) surface. The exact mechanism may be rather complex, and the formation of a variety of ammonia- or hydrazine-based salts could substantially affect the exact thermodynamics of the corresponding reactions. However, it is reasonable to expect based on the results summarized in Figure 3.1 that the reaction of hydrazine should be more facile and the resulting products more stable than in the case of ammonia chemistry.

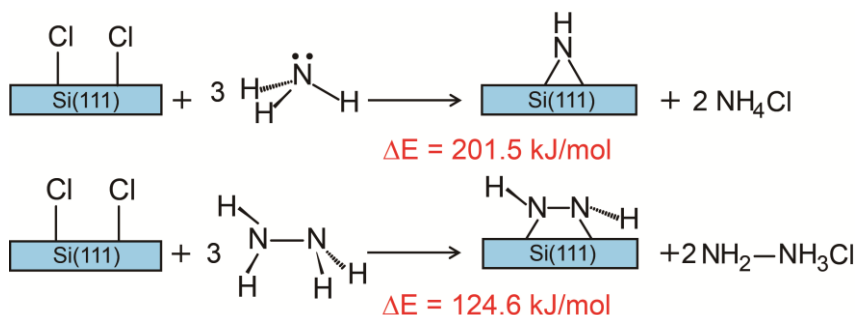


Figure 3.1 Schematic comparison of the reactions of Cl-Si(111) surface with ammonia and hydrazine, respectively. The energetic requirements are indicated according to the computational approach described in experimental part in Chapter 2.

Similarly to the research leading up to the ammonia reaction proposal, several observations can be made starting with the hydrazine chemistry on clean silicon surfaces investigated previously in UHV conditions.³⁵⁻³⁶ Following dissociation of the N-H bonds, these studies found to have the N-N bond parallel or nearly parallel to the surface. The dissociation of the N-N bond was reported on the surface defect sites.³⁵⁻³⁶ Both observations provide important implications for the research reported below for producing hydrazine-modified Si(111) surface by wet chemistry methods.

The hydrazine reaction with chlorine-terminated Si(111) surface was performed and yielded predominant Si-NH-NH-Si functionality following chlorination with PCl_5 and then by anhydrous hydrazine treatment at 35°C . Such hydrazine attachment presents a unique opportunity to yield the desired function and could serve as a well-defined platform for next-step modification based on the known chemical reactions, for example the covalent attachment of C_{60} fullerene.

C_{60} fullerenes have become important building blocks in science and technology and a key direction in nanotechnology research. Due to their properties, especially the high electron affinity and superior ability to transport charge, C_{60}

fullerenes have contributed greatly to a number of applications in energy conversion and solar cell technology,^{4, 37-38} hydrogen gas storage,³⁹ sensing³⁹⁻⁴⁰ and optics.^{39, 41} Among hundreds of studies of C₆₀ fullerenes, great efforts have been devoted to interfacing C₆₀ with semiconducting surfaces, silicon surfaces in particular, seeking novel electrically addressable and switchable functional devices,^{6, 42} because the electronic properties of silicon could easily be tuned,⁴³ and more importantly, silicon-based devices could be directly integrated within existing electronic circuitry.⁴⁴

In the past 20 years, different methods for grafting fullerenes and fullerene-based derivatives have been successfully explored on silicon surfaces. Moro et al.⁴⁵ studied the formation of silicon carbide by annealing C₆₀ films (about 200-300 nm thick) deposited on the silicon wafer up to 900 °C in a high vacuum (HV) chamber. A more recent report shows that, in an ultrahigh vacuum (UHV) system, a C₆₀ monolayer film was formed on Si(111) by depositing C₆₀ molecules at room temperature via thermal evaporation of C₆₀ powder.⁴⁶ Instead of using complex equipment, spin casting was proposed as a convenient route for preparing C₆₀ nanostructures on flat silicon wafers. Feng and Miller reported self-assembly of C₆₀ molecules by typically casting C₆₀ solution onto a Si(100) substrate to form about 5-500 monolayers of C₆₀.⁴⁷ More recently, Jeong et al. prepared C₆₀ nano-islands with various sizes and heights on silicon wafers using a spin-coating method, and an additional annealing process revealed that these nano-islands were stable during heating up to 400 °C.⁴⁸ Finally a large number of studies have investigated C₆₀ molecules covalently attached to silicon surfaces through self-assembled monolayers (SAMs). Fabre et al. reported a C₆₀ monolayer anchored on anthracene-terminated Si(100) surfaces following [4+2] Diels-Alder cycloaddition.⁴³ Our own previous study demonstrated that a fullerene C₆₀

monolayer was attached to 11-amino-1-undecene self-assembled monolayers on a Si(111) surface.⁴⁹ Despite the fact that long-alkyl-chain organic layers do lead to the formation of C₆₀ bound to the surface, they also introduce additional carbon- or oxygen-containing functional groups that in turn react with the surface itself, causing surface oxidation and leaving contaminants that affect the interface properties for any further modification protocols. Thus, a well-defined and stable Si-N-based oxygen-free interface could be important from both a fundamental and an applied standpoint.

In this thesis, a simple wet chemistry method for covalent attachment of Buckminsterfullerene C₆₀ to a hydrazine-terminated Si(111) surface is reported, according to the scheme shown in Figure 3.2. The choice of hydrazine to form the first layer instead of previously investigated ammonia^{34, 50} and amines^{49, 51} offers high stability and controlled reactivity of the resulting functional group.⁵² Thus, the two-step functionalization, where the first step is silicon modification with hydrazine and the second step is the attachment to this prepared platform should provide a more reliable path for producing the desired interface.

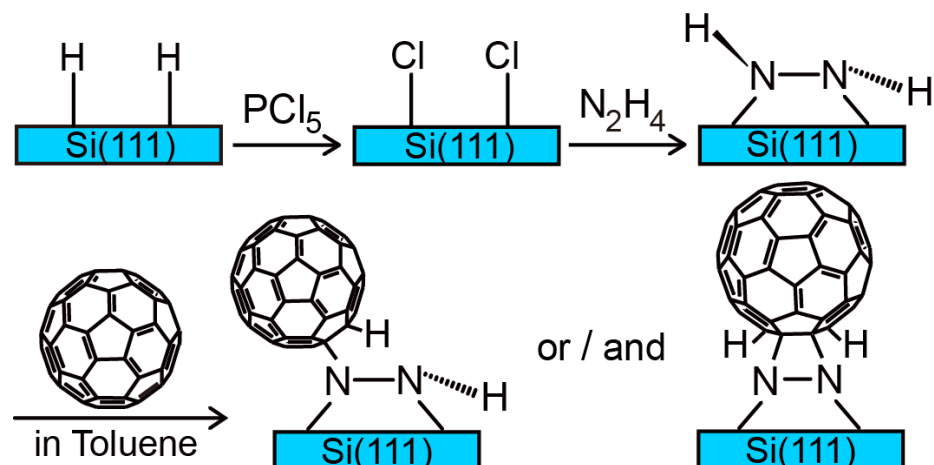


Figure 3.2 Reaction scheme to form a stable interface between C₆₀ fullerenes and silicon surface.

The surface species of hydrazine-modified Si(111) surface were identified by Fourier-transform infrared spectroscopy (FT-IR), time-of-flight secondary ion mass spectrometry (ToF-SIMS) and X-ray photoelectron spectroscopy (XPS), which was also used to quantitatively investigate the surface coverages of chlorine and nitrogen. The chemical nature and surface topography of the resulting C₆₀-modified Si(111) surfaces are investigated by X-ray photoelectron spectroscopy (XPS), time-of-flight secondary ion mass spectrometry (TOF-SIMS), and atomic-force microscopy (AFM). Density functional theory (DFT) calculations are performed with the Gaussian 09 suite of programs⁵³ to predict vibrational spectra and N *1s* core-level energy and to study the stability of surface species formed.

3.2 Results and discussion

3.2.1 Reaction of Hydrazine with Cl-terminated Si(111) Surface

3.2.1.1 Infrared Spectroscopy Studies of Hydrazine Modification of the Si(111) Surface.

In order to confirm the quality of the starting H-terminated Si(111) surface, the completeness of hydrogen removal, and to follow the reaction with hydrazine, FT-IR spectroscopy was used to interrogate the silicon surface following each modification step. Figure 3.3 and Figure 3.4 summarize the results of infrared spectroscopy studies of spectral regions representing the Si-H stretching, N-H stretching and characteristic NH_2 bending modes.

The completeness of modification process is monitored by following Si-H stretching region for H-Si(111) (Si(111) surface terminated with hydrogen); Cl-Si(111) (Cl-terminated Si(111) surface prepared by exposure of H-Si(111) to PCl_5 in the presence of benzoyl peroxide initiator), and Si-NH-NH-Si(111) (functionalized silicon surface prepared by exposure of Cl-Si(111) to $\text{NH}_2\text{-NH}_2$). For spectrum (c) in Figure 3.3 and 3.4, a clean silicon wafer with a thermal oxide is used as a background. Spectra of Cl-Si(111) (b) and Si-NH-NH-Si(111) (a) use a single beam spectrum collected for H-Si(111) as a background. The sharp Si-H stretching peak at 2083 cm^{-1} , which is well-known as a signature of a clean and well-ordered H-Si(111) surface,^{15, 54-56} shown in Figure 3.3(c), fully disappears after chlorination, and remains absent following modification with anhydrous $\text{NH}_2\text{-NH}_2$. Based on the previous studies,^{15, 54-56} this Si-H stretching mode is very sensitive both to the quality of ordering of the mono hydride-terminated Si(111) and to the purity of the H-termination. Thus, the results summarized in Figure 3.3 confirm that a clean and well-ordered H-Si(111)

surface was used as a starting point for hydrazine functionalization and that all the hydrogen atoms were replaced by chlorine during the chlorination step. No new Si-H containing species were introduced following the last step of Cl-Si(111) functionalization with hydrazine.

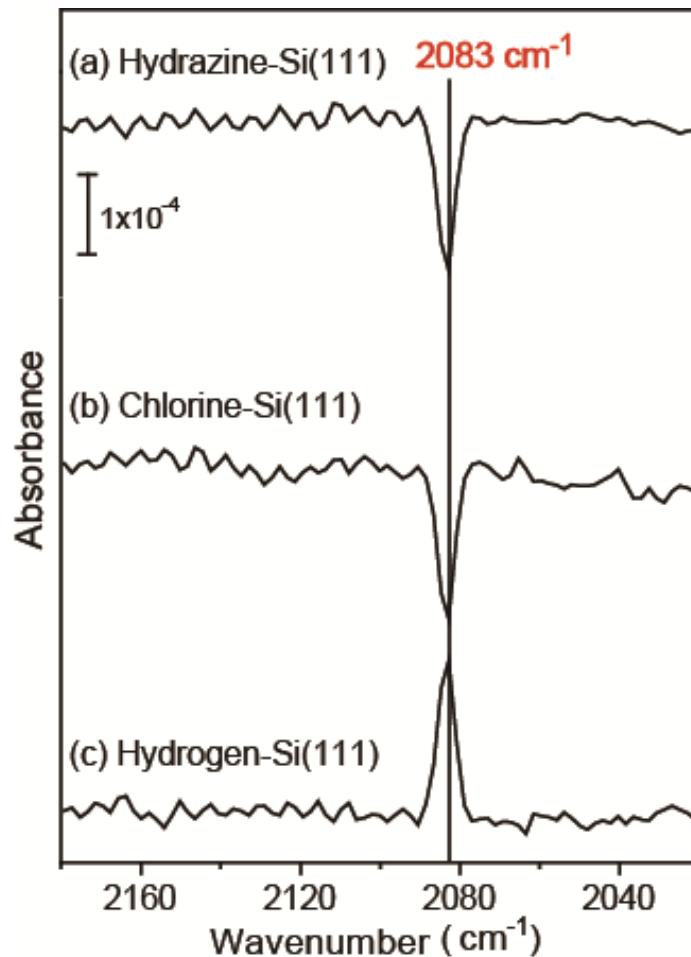


Figure 3.3 The Si-H stretching region of infrared spectroscopy studies of hydrazine reaction with silicon surface for (a) the final hydrazine-modified surface and (b) for chlorine-terminated Si(111), as well as (c) for the starting H-terminated Si(111) surface. Native-oxide covered surface is used as a background for spectra (c) and the surface terminated with hydrogen (H-Si(111)) is used as a background for spectra (a) and (b).

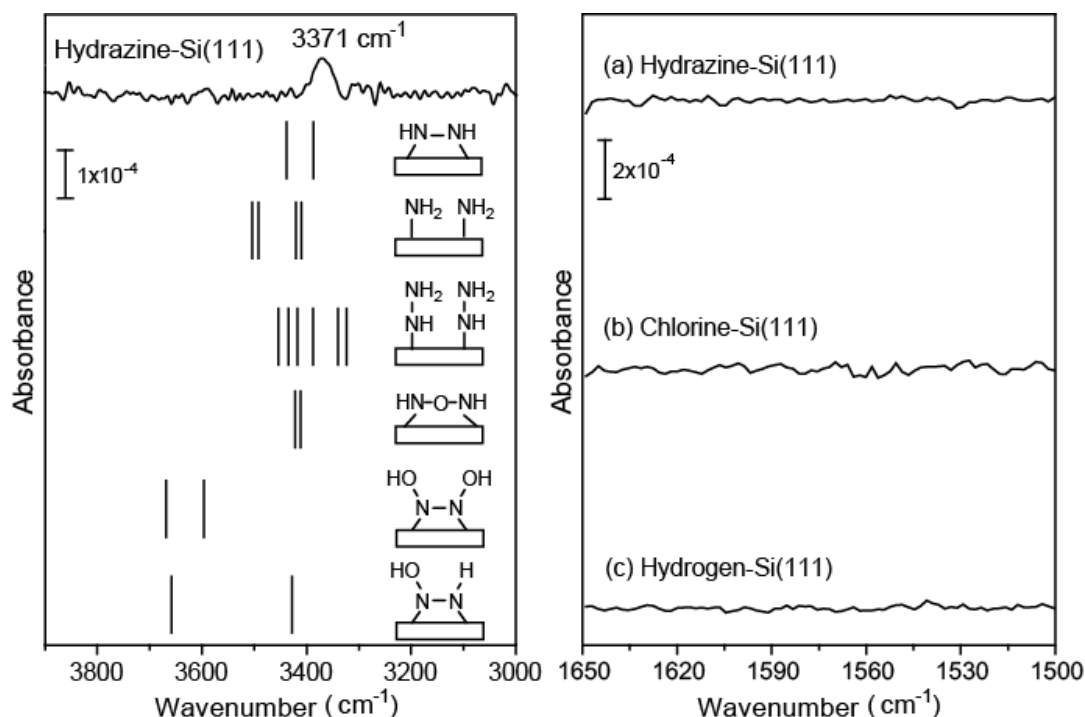


Figure 3.4 Infrared spectroscopy studies of hydrazine reaction with silicon surface. The spectral ranges for N-H stretching region (left panel) and N-H bending signature region (right panel) are compared for (a) the final hydrazine-modified surface and (b) for chlorine-terminated Si(111), as well as (c) for the starting H-terminated Si(111) surface. Native-oxide covered surface is used as a background for spectra (c) and the surface terminated with hydrogen (H-Si(111)) is used as a background for spectra (a) and (b). Left panel summarizes the results of computational investigation for the computational cluster models considered and provides the predicted infrared spectra for these species indicated by bar plots.

The left panel of Figure 3.4 presents the spectrum of the N-H stretching region for the surface modified with hydrazine. The H-Si(111) and Cl-(111) do not exhibit any absorption signals within the signal-to-noise ratio of the setup used for these experiments. The spectrum reported for Si-NH-NH-Si(111) required averaging five different experiments to achieve better signal-to-noise ratio. The solid bars below the experimentally recorded spectrum correspond to the expected vibrational frequencies

for surface -NH and -NH_2 species obtained from computational models, with frequencies scaled by a common scaling factor of 0.965.

The intensity of the stretch vibrations of submonolayer NH_x species on silicon is often small and these vibrations are difficult to use to identify specific surface species at submonolayer coverage.^{29, 57} However, a very clear peak is observed at 3371 cm^{-1} following hydrazine treatment in the left panel of Figure 3.4. In order to assign this peak, a set of computational studies have been performed for the models shown in this figure and the analysis of the predicted vibrational features can help rule out some of the possible surface as major products of the surface reaction. The surface species that have to be considered first are the target species proposed in Figure 3.1, where both nitrogen atoms of the hydrazine molecule are connected to surface silicon atoms, following replacement of two chlorine surface atoms of the Cl-Si(111) . The obtained experimental spectrum is consistent with the predicted vibrational signature of these species. Unfortunately, the presence of -NH-NH_2 species or -NH-O-NH- species cannot be ruled out based on these spectra. However, nitrogen-nitrogen bond dissociation is clearly not the dominant surface reaction pathway, as that would lead to two groups of peaks separated by over 100 cm^{-1} , which is not observed in the experimental spectrum. The presence of N-O-H functionality can also be ruled out, since that would produce an intense absorption feature above 3500 cm^{-1} . It is possible that some minority surface species of this type could yield a very weak absorption band recorded near that frequency; however, those are certainly not the majority adsorbates. Interestingly, the oxidized surface species with -NH-O-NH- functionality could be present; however, that would mean that N-N bond on those species is broken and a different analytical techniques could be used to identify that. It will also be

shown below that surface oxidation is not significant and the dominance of Si-O containing species following hydrazine exposure can be ruled out based on further XPS experiments. Thus, the computational models provided in Figure 3.4 cover all the possible types of species that can be present on a surface following reaction of hydrazine with Cl-Si(111).

One of the possible vibrational signatures that can help identifying surface –NH_x groups is a characteristic –NH₂ bending that is commonly used in surface analysis.⁵⁷⁻⁶⁰ The right panel of Figure 3.4 zooms into the corresponding spectral region; however, no signature of NH₂ bending modes, which at comparable coverage could be easily observed in previous studies,⁵⁷⁻⁶⁰ was recorded for hydrazine-treated Si(111). Thus, structures containing Si-NH₂ and Si-NH-NH₂ fragments can be ruled out as dominant on this surface.

3.2.1.2 Analysis of Surface Reactions and Quantification of Surface Elemental Concentration by X-Ray Photoelectron Spectroscopy.

To help identify surface functional groups that were difficult to pinpoint using infrared spectroscopy and to quantify surface elemental concentration for the species present on the silicon surface following each modification step, XPS measurements were performed to monitor Si 2*p*, Cl 2*p*, and N 1*s* spectral regions. These are the only elements expected to contribute to the majority of surface species. The O 1*s* spectra were also collected to confirm the cleanliness of the surface but did not yield any information that would help identify the produced surface species.

The analysis of the Si 2*p* spectra in Figure 3.5 reveals no observable silicon surface oxidation during the experimental procedure for obtaining H-terminated and

Cl-terminated Si(111) substrates. A Si 2*p* spectrum obtained following hydrazine treatment exhibits a small feature at 102.3 eV in addition to the typical signature of the clean silicon surface.^{8, 34, 49, 51, 61-63} This feature corresponds to the minority defect SiN_x surface species, similarly to those observed previously following ammonia treatment of Cl-Si(111).³⁴ A detailed investigation of this feature suggests that it is possible to overlap partially with the signature of silicon surface oxidation that is normally manifested in a broad feature at 103 eV corresponding to SiO_x⁶⁴; however, the position and the low overall intensity suggest that neither species correspond to the surface majority.

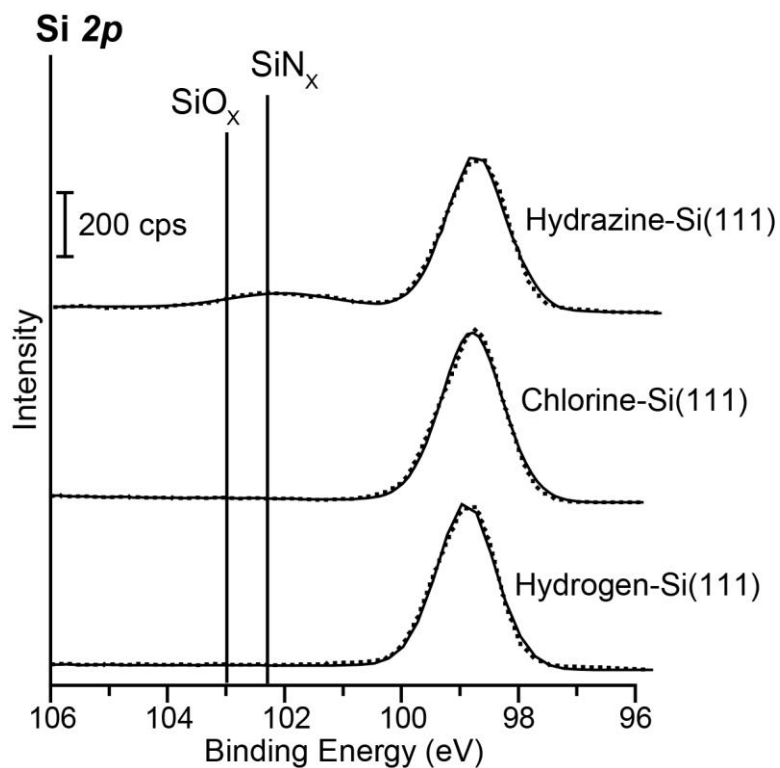


Figure 3.5 XPS spectra of the Si 2*p* spectral region for the Si(111) surface before and after hydrazine modification: (a) final surface modified with hydrazine compared with (b) Cl-Si(111) surface used in this modification and (c) H-Si(111) surface that is the starting point for the studies.

Representative Cl 2*p* spectra of the Si(111) surface before and after hydrazine modification are shown in Figure 3.6. Only one type of chlorine-containing species is observed on the surface following the chlorination step. Since the infrared signature of hydrogen-terminated silicon surface shown in Figure 3.3(c) fully disappeared following chlorination, it is expected that a fully chlorinated Cl-Si(111) surface was prepared following the second step of experimental procedure outlined above. According to the coverage analysis based on the overlayer model performed according

to Lewis et al.,^{61, 65-66} the chlorine coverage observed in the experiments presented here is fully consistent with the previously reported data for ~99 % of a monolayer.

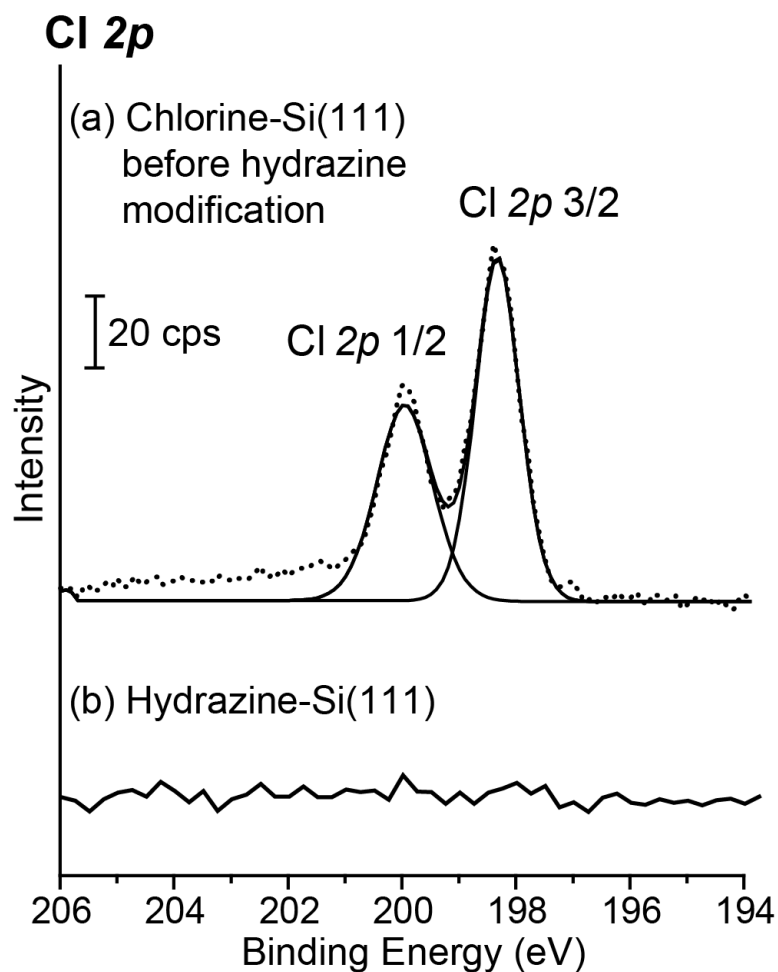


Figure 3.6 XPS spectra of the Cl 2p spectral region for Si(111) surface before and after hydrazine modification: (a) starting Cl-Si(111) surface is compared with the same surface (b) following modification with hydrazine.

The N 1s experimental spectrum shown for the hydrazine-modified Cl-Si(111) surface in Figure 3.7 indicates a predominant N-containing functionality at 399.6 eV

and a minor species at 397.5 eV. The binding energy that corresponds to the observed feature was compared to the selected results of the DFT study, on the basis of different possible chemical models, same as those utilized above for FT-IR study. The predicted N *1s* binding energies for the main expected possible geometry, Si-NH-NH-Si, on the surface following hydrazine treatment are 398.95 eV and 398.87 eV. Another possible NH_x functionality on the surface, Si-NH-NH₂, is expected to produce features at 398.61 eV, 398.96 eV, 398.71 eV and 399.02 eV (for a model containing two Si-NH-NH₂ species on neighboring surface sites). Compared with experimental result, Si-NH-NH-Si and Si-NH-NH₂ are both possible resulting species on the hydrazine-treated surface. As discussed above, no -NH₂ bending vibrations were observed in infrared study and Si-NH-NH₂ has been ruled out to be predominant species on the hydrazine-treated surface.

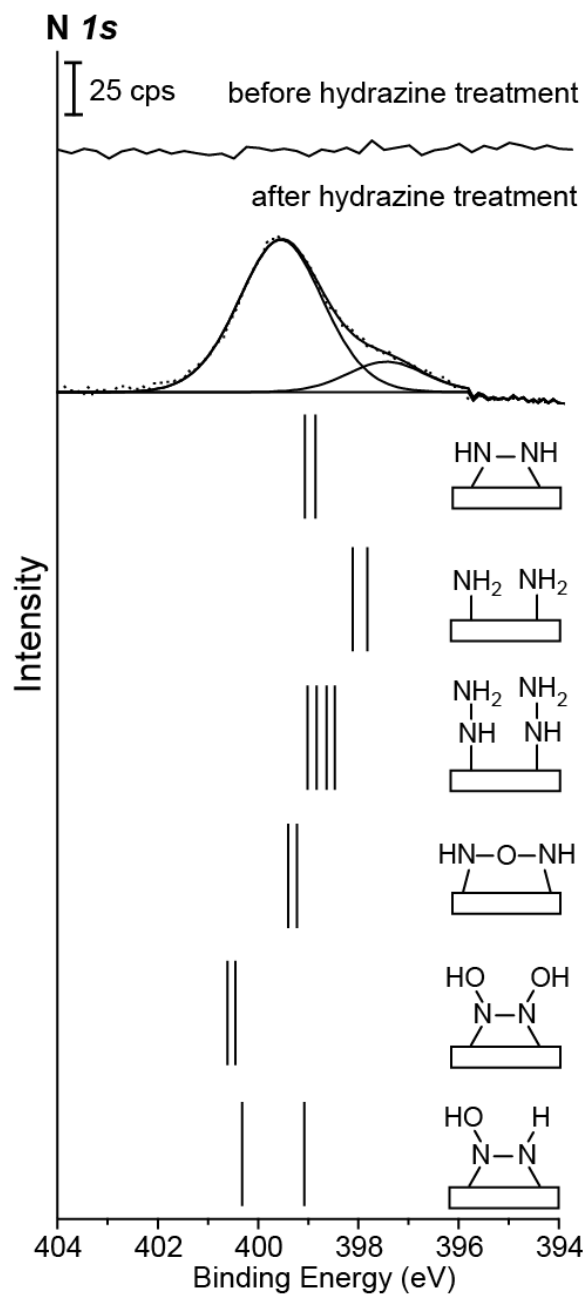


Figure 3.7 XPS spectra of the N 1s spectral region for Si(111) surface before and after hydrazine modification: (a) starting Cl-Si(111) surface and (b) the same surface following modification with hydrazine compared with the N 1s core-level energies predicted by DFT investigations (solid bars) for the possible surface models. All the computational studies are based on a cluster model representing the two closest topmost silicon atoms on the unreconstructed Si(111) surface.

More importantly, however, the studies of the model clusters representing possible surface oxidation pathways with oxygen atoms inserted into the Si-N linkage suggest that any of these species would cause the N *1s* peak to shift by about 1 eV or even more to higher energy: the N *1s* spectrum of Si-N(OH)-N(OH)-Si model was predicted to yield two closely spaced features at 400.5 eV, and that of Si-N(OH)-NH-Si model was calculated to yield 399.1 eV and 400.3 eV peaks. The predicted core level energies of Si-NH-O-NH-Si model, where oxygen is inserted into the N-N bridge, are closely spaced at 399.4 eV and do not differ substantially from the experimentally observed peak. This is the only species, in addition to the target ones, that could not be ruled out as dominant based on either infrared studies or XPS investigation. However, ToF-SIMS interrogation described in the next section should shed some light on the possible presence of this species on hydrazine-modified silicon surface.

Previous work⁶⁷ reported a broad overlapped peak centered at 399.6 eV for the Si-NH-NH-Si structure observed in vacuum following hydrazine exposure to a clean Si(100) surface, where N-N bond is parallel or nearly parallel to the surface. This peak value is consistent with the major peak shown in Figure 3.7. Based on the same computational analysis, it is very likely that the minority surface species correspond to the N-N bond dissociation. The assignment of the major peak at 399.6 eV can also be supported by the quantitative analysis of XPS spectra. Comparison of the ratio of N *1s* feature and Si *2p* feature for the hydrazine-treated surface with that of the Cl *2p* feature and Si *2p* feature on the Cl-terminated Si(111) (where ~99% of the surface is covered with Cl atoms), applying the quantification approach described by N. Lewis et al.,^{61, 65-66} can be used to determine that the ratio of nitrogen coverage on a hydrazine-

treated Si(111) surface to chlorine coverage on Cl-Si(111) is $107 \pm 8\%$. According to Figure 3.6(b), all the chlorine is removed following hydrazine treatment. Thus, in an exchange reaction, one Si-NH-NH-Si group replaces two Si-Cl groups, which is fully consistent with the proposed reaction scheme and with producing target species shown in Figure 3.1.

3.2.1.3 ToF-SIMS Identification of Surface Species on the Hydrazine-Modified Si(111) Surface.

Two questions that were not fully addressed by infrared or XPS studies are the presence of N-N-containing surface species and the possibility of oxygen insertion into the N-N bond. A sensitive and effective technique that can address this problem is ToF-SIMS. ToF-SIMS within a mass-to-charge range of 0-100 m/z was used to help this identification.

Figure 3.8 summarizes the ToF-SIMS spectra before and after surface modification with $\text{NH}_2\text{-NH}_2$. Before hydrazine treatment, Cl signature is clearly observed, as shown in the right panel of Figure 3.8, and only trace amounts of background species show up in the 56 m/z range, as indicated in the left panel. Following hydrazine treatment, the Si-N-N signature is clearly observed, suggesting that N-N bond is retained during surface modification process. To investigate the presence of Si-N-O-N species on the surface, 44 m/z region presented in the middle panel of Figure 3.8 was analyzed and suggests that only trace amount of N-O-N species mixed with contamination background species are observed on the surface, which confirms that Si-NH-O-NH-Si model is not the majority species. This finding

fully supports the hypothesis that the major species present on a silicon surface following the hydrazine treatment are of the Si-NH-NH-Si type.

The noticeable minority surface species observed in the infrared and XPS studies are likely the result of the N-N bond dissociation following the hydrazine modification. Thus, the silicon surface terminated with Si-NH-NH-Si species is prepared and stable, and the resulting functionality is available for further modification.

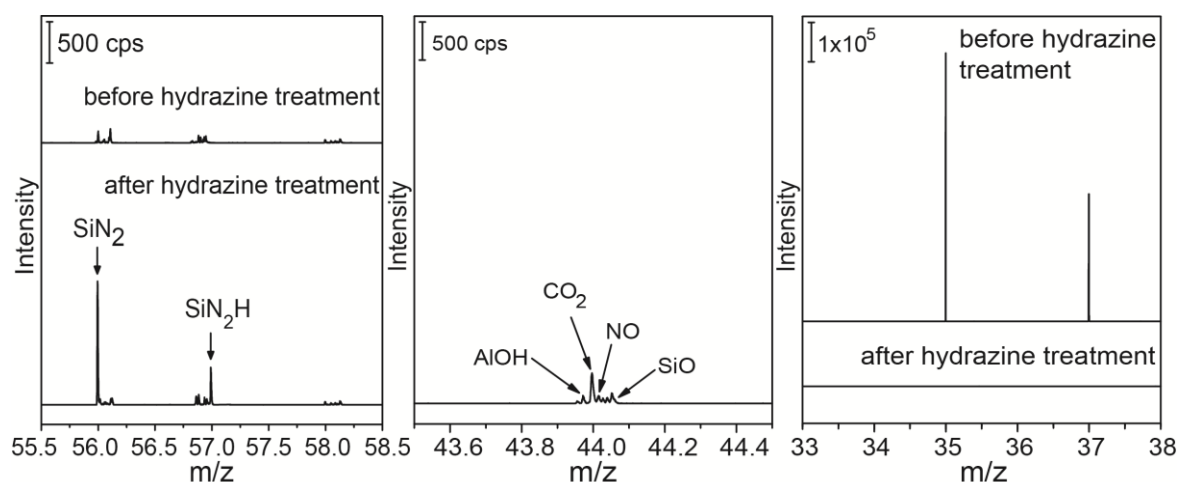


Figure 3.8 ToF-SIMS positive-ion spectrum of Si(111) surface (a) before and (b) after hydrazine modification in the Si-N₂ (55.5-58.5 m/z), N-O-N (43.5-44.5 m/z), and Cl (33-38 m/z) species range.

3.2.1.4 DFT Computational Investigation of Surface Reaction Mechanism

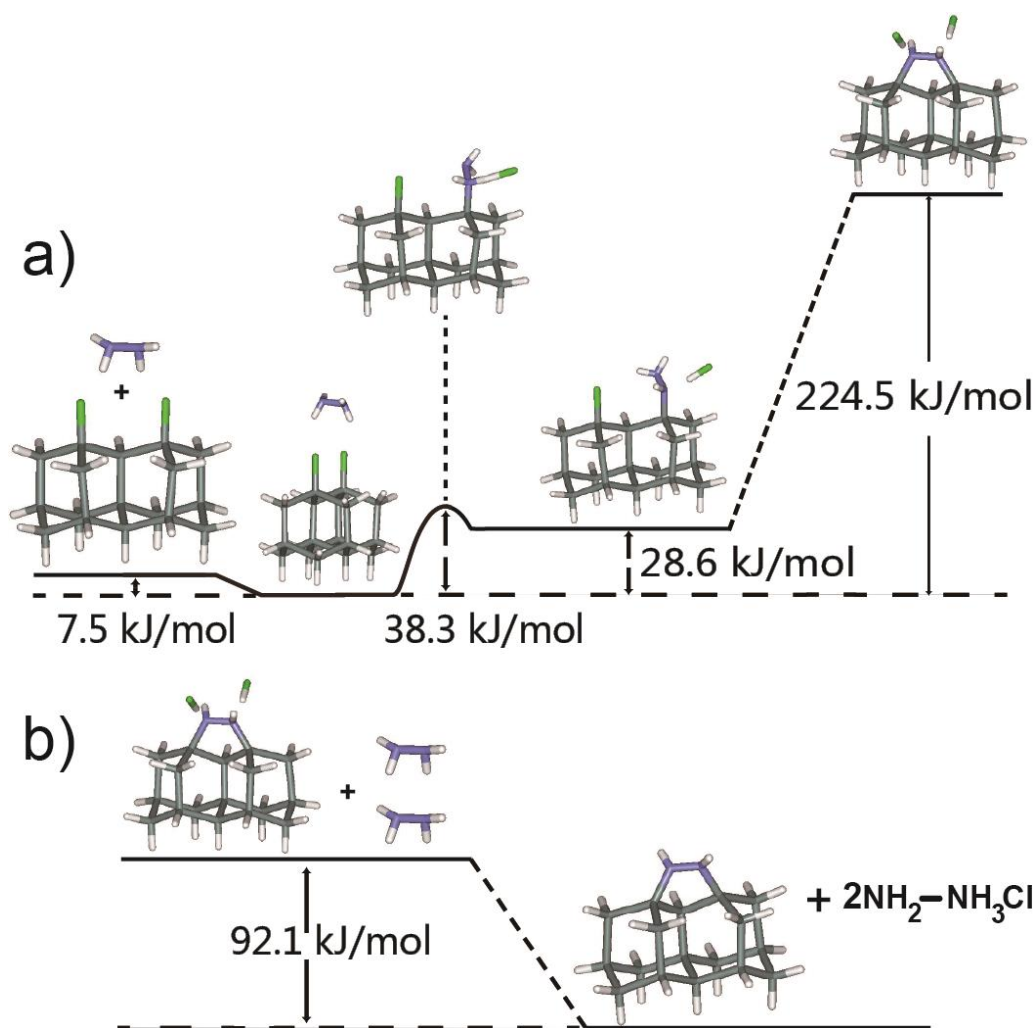


Figure 3.9 Computational investigation of potential reaction pathways for hydrazine on Cl-Si(111) surface with aSi₁₇H₂₄ cluster representing the silicon surface and B3LYP /6-311G+(d, p) computational approach. a) Model of a possible surface reaction pathway for hydrazine on Cl-Si(100) surface represented by a Si₁₇H₂₄ cluster terminated with two chlorine atoms; b) Correction to the final part of the computational reaction mechanism based on a reaction of the HCl product of the process with surrounding hydrazine molecules.

Based on the experimental results discussed above, the dominant surface species appears to be Si-NH-NH-Si. The question remains, however, if this surface species is thermodynamically stable and if it is possible to obtain it at relatively low temperatures. The main problem is that based on the results outlined in Figure 3.9(a), the final proposed species is predicted to be unstable. This issue is very similar to the one reported for ammonia reaction on Cl-Si(111) surface previously.³⁴ Two problems preclude one from constructing a more appropriate complete reaction diagram. One is related to the fact that the HCl resulting from the surface modification process is probably not present as a separate product. Since there is an excess of hydrazine present on the solution, this HCl may immediately react with either one or two separate hydrazine molecules. The effect of the reaction of hydrazine with the HCl on the stability of the surface species produced in a reaction of hydrazine with the Cl-Si(111) surface is illustrated in Figure 3.9(b). Here, the removal of HCl from a fully optimized resulting structure by surrounding hydrazine increases the stability of this structure by about 92 kJ/mol. The other problem is much more subtle. The exact arrangement of surface Si-NH-NH-Si species is not known. It is very likely that it is a complex surface reconstruction that stabilizes the resulting product even further. That is why the most appropriate way to compare the feasibility of hydrazine reaction is with the previous investigation of the similar ammonia modification that produced predominantly type of Si-NH-Si species on the same surface.³⁴ The first striking difference is based on the overall stability of the resulting species. When a proper comparison is made as shown in Figure 3.1 above, it is clear that the reaction of hydrazine is expected to be much more efficient than that of ammonia. The second important observation, is that the first step of the proposed reaction, replacement of

one surface chlorine with either -NH_2 group (in the case of ammonia) or -NH-NH_2 species (in the case of hydrazine), is actually much more kinetically accessible for the hydrazine modification. Thus, the presence of the Si-NH-NH-Si species observed experimentally is fully consistent with the higher efficiency of the proposed modification of the Cl-Si(111) surface with hydrazine compared to that previously reported for ammonia.

3.2.2 Stability and Reactivity of the Hydrazine-modified Si(111) Surface

3.2.2.1 Stability of the Hydrazine-modified Si(111) Surface in Ambient Environment

Despite the fact that, the produced hydrazine-terminated surface does get oxidized in ambient, it is still important to study how “stable” this surface really is. XPS studies shown in Figure 3.10 and 3.11 reveal that this hydrazine-terminated Si surface starts to show surface oxidation, similar to what was observed in ammonia-modified Si surface,³⁴ as in silicon surface having oxygen inserted into its backbond, after being exposed to ambient conditions for over 30 minutes. When the oxidation happens on the surface nitrogen, the major peak of hydrazine species was still observed at 399.6 eV with an additional peak shown around 402 eV corresponding to oxidized nitrogen. Eventually the surface nitrogen completely turn into NO species after being exposed to air for 4 hours.

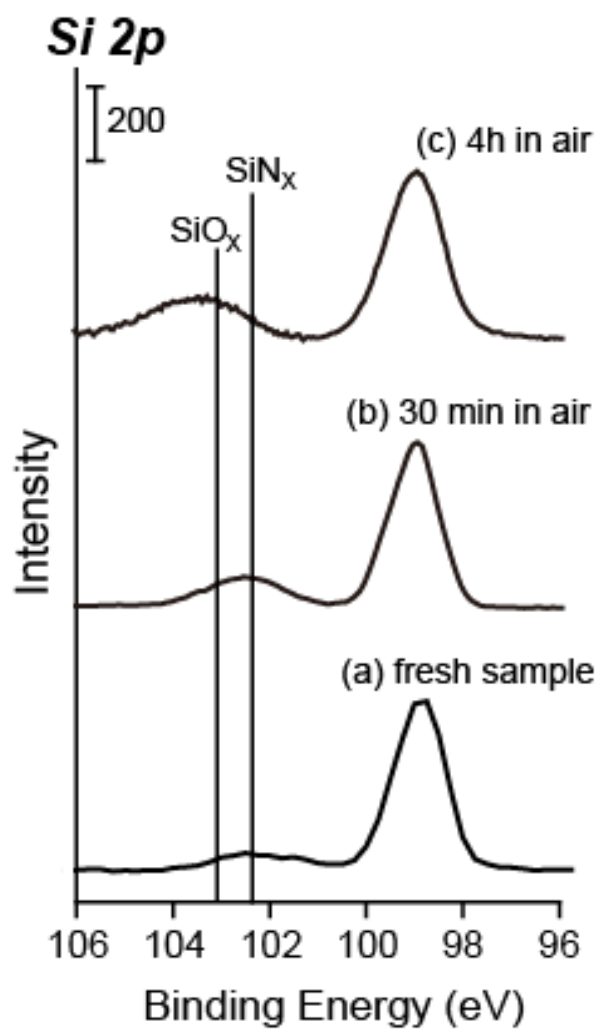


Figure 3.10 Si 2*p* region of XPS of (a) freshly prepared hydrazine-terminated Si(111); (b) hydrazine-terminated Si(111) exposed to air for 30min; (c) hydrazine-terminated Si(111) exposed to air for 4 hours.

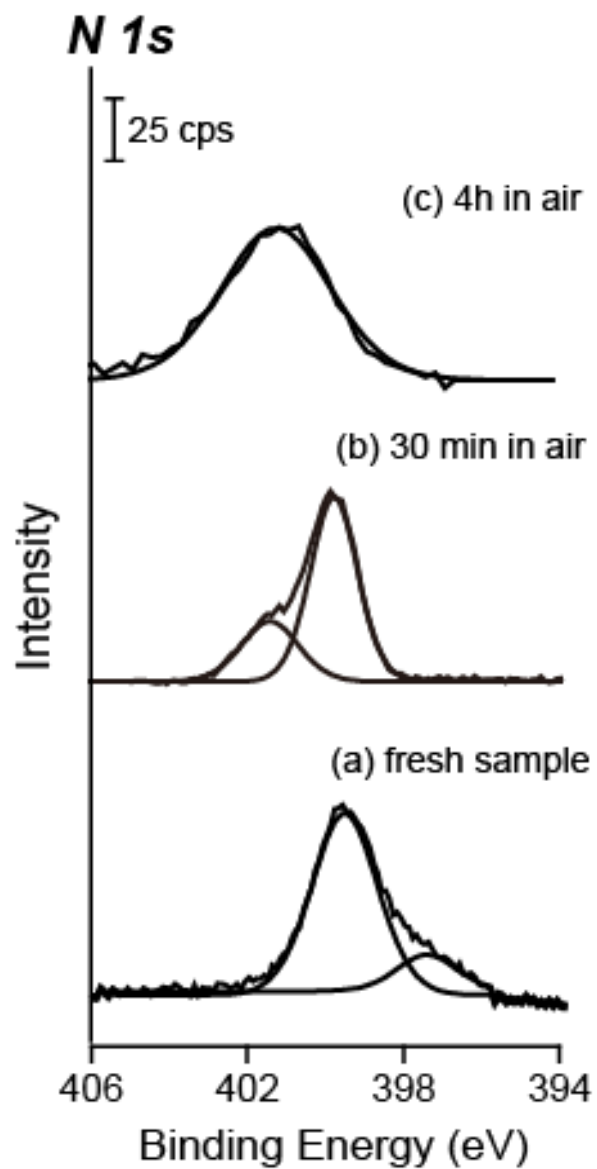


Figure 3.11 N 1s region of XPS of (a) freshly prepared hydrazine-terminated Si(111); (b) hydrazine-terminated Si(111) exposed to air for 30min; (c) hydrazine-terminated Si(111) exposed to air for 4 hours.

3.2.2.2 Reactivity of the Hydrazine-modified Si(111) Surface with Metal Precursor

The reactivity of this hydrazine-modified Si(111) surface was investigated with the deposition of copper precursor, $\text{Cu}(\text{acac})_2$ at room temperature under high vacuum condition.

The preliminary results shown in Figure 3.12, 3.13 and 3.14 definitely confirm the reaction between $\text{Cu}(\text{acac})_2$ and hydrazine-terminated Si(111) surface. The copper nanoparticles were observed on the surface after the deposition as shown in Figure 3.11. The XPS studies confirmed the presence of copper species after deposition and more importantly the formation of a bond between Cu and Si, in Figure 3.12 and 3.13. Although similar study has been successfully explored on hydrogen-terminated Si(111) surface,⁶⁸ for the deposition on hydrazine-modified silicon surface, further studies will be necessary to elucidate the mechanism of the deposition, but it proves that this unique hydrazine-modified silicon surface can serve as a platform for many different further modification protocols.

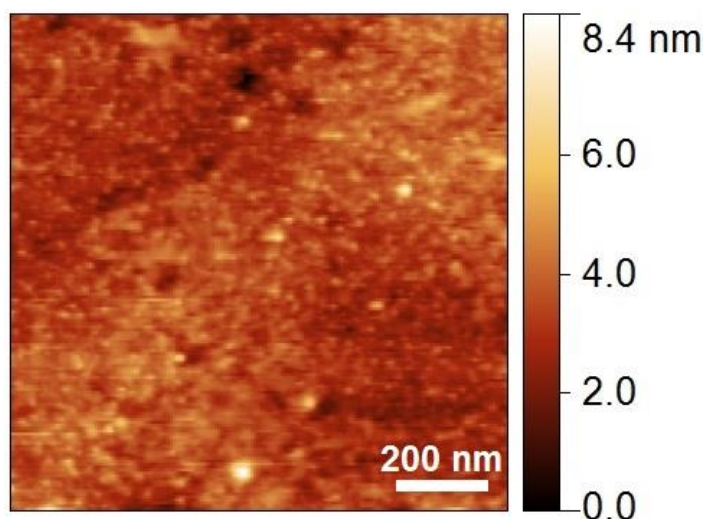


Figure 3.12 AFM image of hydrazine-terminated Si(111) after reacted with Cu(acac)₂ precursor.

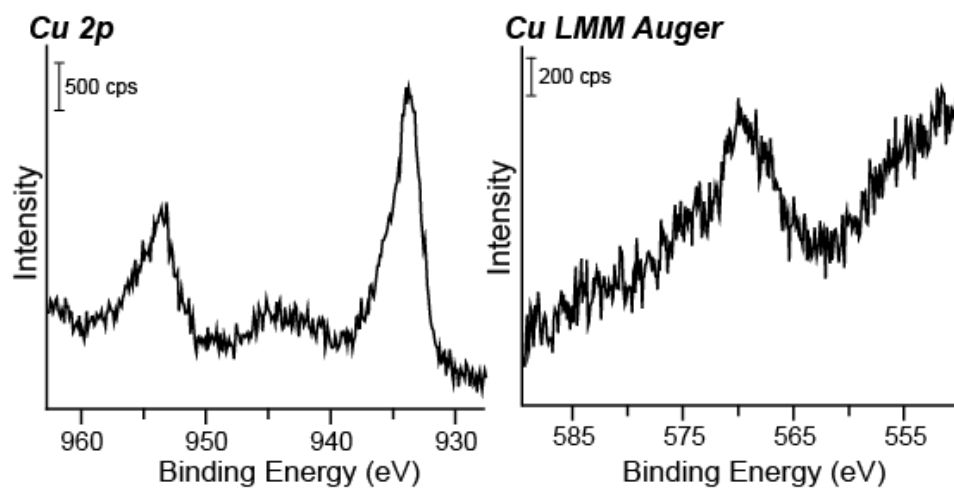


Figure 3.13 Cu 2*p* and Cu LMM region of XPS spectra of hydrazine-terminated Si(111) after reacted with Cu(acac)₂ precursor.

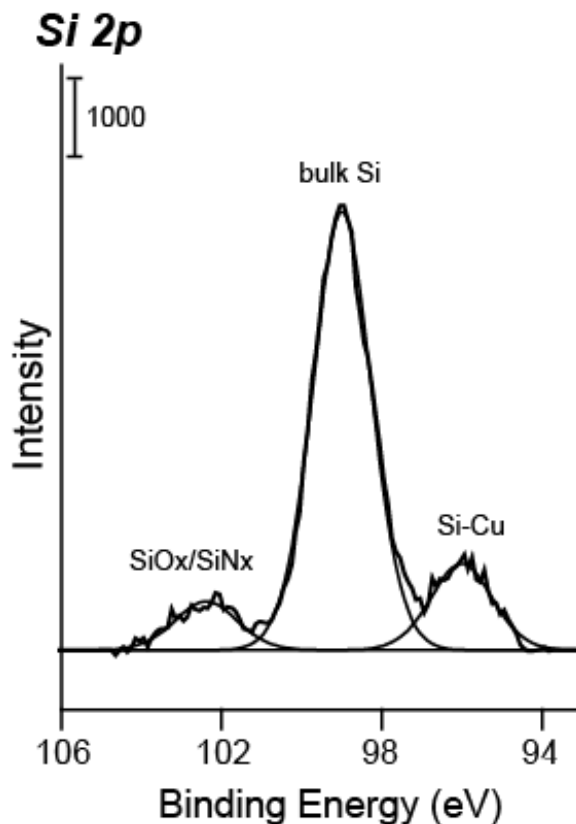


Figure 3.14 Si 2*p* region of XPS spectra of hydrazine-terminated Si(111) after reacted with Cu(acac)₂ precursor.

3.2.3 A Monolayer of Hydrazine Facilitates Direct Covalent Attachment of C₆₀ Fullerene to Silicon Surface

3.2.3.1 Confirmation of Fullerenes C₆₀ Adsorption on Hydrazine-Terminated Si(111) Surface by Atomic Force Microscopy.

Since the first step, silicon modification with hydrazine, has been confirmed, the second step which is the attachment of C₆₀ Fullerenes is firstly studied by microscopic methods. AFM images shown in Figure 3.15 were collected following the reaction of the C₆₀ solution with the hydrazine-terminated Si(111) surface. The corresponding line profiles are displayed on the right of the figure. As a starting point, the hydrazine-terminated Si(111) surface in Figure 3.15(a) shows no nanostructured

features at the nanometer scale and exhibits an RMS roughness of 0.28 nm. After reacting with low concentration (0.25 mM) C_{60} solution followed by a 5-minute sonication, the C_{60} -modified surface in Figure 3.15(b) shows substantial change in surface topography. The silicon substrate now shows a small number of ad clusters with a height commensurate with a single buckyball molecule. The RMS roughness increased to 1.11 nm and, as will be shown further, this image corresponds to a monolayer of C_{60} covering the hydrazine-modified surface and a few ad molecules on top of this system or possibly on small number of protruding defect sites. The sonication approach seems to work nicely with buckyballs and does not induce any additional surface oxidation or C_{60} monolayer desorption in our case. To see the effect of fullerene concentration on the size of the clusters on the surface, a higher concentrated (1 mM) C_{60} solution is used as the reagent, and the resulting images are presented in Figures 3.15(c) and (d). In Figure 3.15(c), when the sample is washed by a stream of methanol and Milli-Q water with no sonication, the image exhibits the formation of large clusters, up to 12 nm in height, along with increased RMS roughness, which clearly correspond to multiple layers of buckyballs. This is consistent with agglomeration of C_{60} molecules into relatively large and stable clusters at a high concentration of the solution.⁴⁹ To get rid of these additional physisorbed C_{60} structures on the surface, the sample was sonicated in toluene for 5 minutes and then rinsed with dichloromethane, methanol and MilliQ water several times. As observed in Figure 3.15(d), this sample exhibits essentially the same density of ad clusters as the low concentration C_{60} -modified surface, with nearly identical height of the clusters and RMS roughness. The observation is consistent with previous investigations of C_{60} aggregate formation.^{42, 69} In addition, given the similarity of the samples shown in

Figures 3.15(b) and 3.15(d), it is expected that their spectroscopic signatures will also be very similar, as confirmed below in the ToF-SIMS investigation. Since the multi-layered physisorbed C_{60} clusters are removed after sonication and rinsing, and since the high-concentration C_{60} -modified surface then shows nearly the same surface morphology as that of the low-concentration C_{60} -modified surface, the C_{60} molecule reacts with the hydrazine-modified silicon surface in a self-limiting manner.

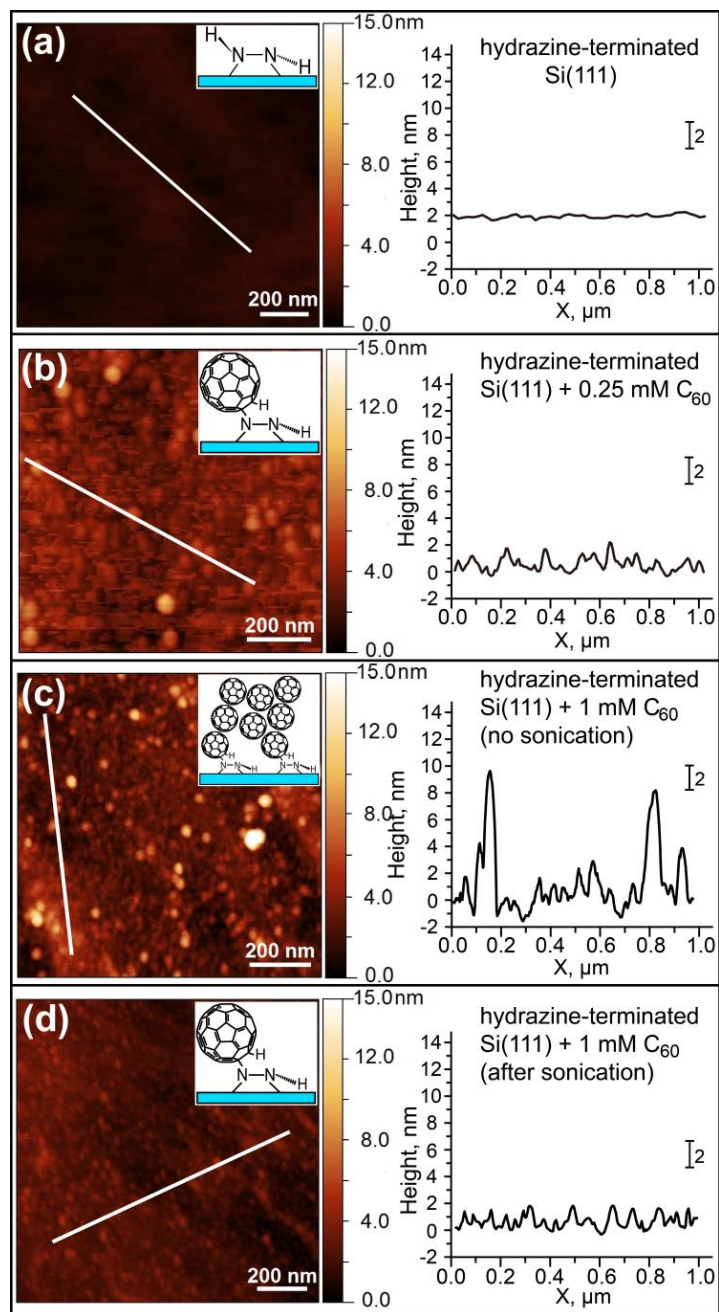


Figure 3.15 Left panels: AFM images of (a) hydrazine-terminated Si(111) surface; (b) hydrazine-terminated Si(111) surface reacted with 0.25 mM C_{60} solution; (c) hydrazine-terminated Si(111) surface reacted with 1 mM C_{60} solution, washed without sonication; (d) hydrazine-terminated Si(111) surface reacted with 1 mM C_{60} solution, washed with sonication to remove multi-layered physisorbed C_{60} . Right panels: corresponding line profiles of the images.

3.2.3.2 Confirmation of Fullerenes C_{60} Chemically-Bound to the Hydrazine-Terminated Si(111) Surface by Time-of-Flight Secondary Ion Mass Spectrometry.

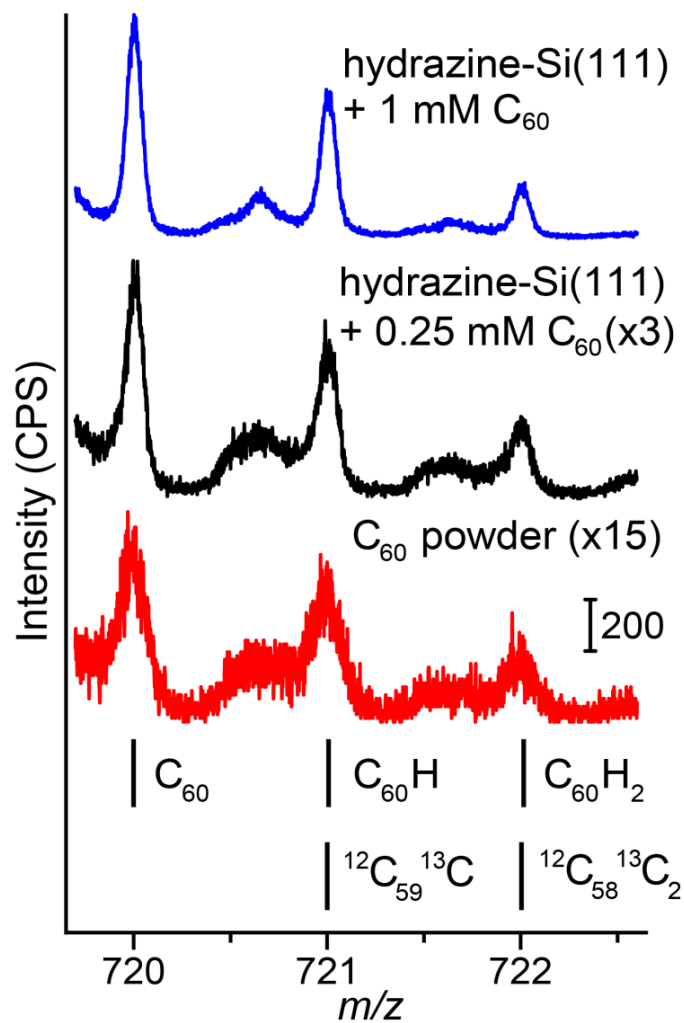


Figure 3.16 Negative ion ToF-SIMS spectra of $[C_{60}]^-$ species m/z range following the reaction of C_{60} with a hydrazine-terminated Si(111) surface. The exact positions of expected ions are shown as solid bars underneath the experimental data.

To identify the structure of the species formed by fullerenes on a surface, ToF-SIMS data are collected for both high and low-concentration C₆₀ solution-treated surface and C₆₀ powder itself for comparison. Negative ion m/z range of 719.5 to 722.5 is displayed in Figure 3.16. Compared with the spectra of pristine C₆₀ powder, the hydrazine-terminated Si(111) surface treated with C₆₀ solution at either high or low concentration shows identical characteristic features at m/z 720, m/z 721 and m/z 722, as is expected based on the microscopy studies presented above. Considering that SIMS is generally treated as a semiquantitative technique, the signal intensities have been calibrated to be shown at the same scale. Although here it is impossible to distinguish the peaks at m/z 721 and m/z 722 to be [C₆₀-H]⁻ and [C₆₀-H₂]⁻, or C₆₀ with different amount of ¹³C isotopes, they are still the strongest evidence that confirms the existence of C₆₀ on the C₆₀ solution-treated surface.

Figure 3.17 presents a summary of the other relevant spectral ranges studied by this surface analytical technique. Negative ion m/z ranges of 733.6 to 734.5, 747.6 to 748.4, 761.6 to 762.4 and 831.5 to 832.5 are carefully studied and summarized in this figure. The zoom-in of the [C₆₀-N]⁻ feature, [C₆₀-N₂]⁻ feature, [C₆₀-N-Si]⁻ feature are displayed in Figure 3.17(a), (b) and (c) with vertical bars indicating the expected positions of corresponding molecular fragments. These results confirm that C₆₀ is chemically bound to one or two nitrogen atoms, that the N-N bond of the surface bound hydrazine remains intact after reaction with C₆₀, and that the formation of a bond between C₆₀ and surface nitrogen does not disrupt the presence of Si-N-based interface. Thus, it is confirmed that C₆₀ is chemically attached onto the hydrazine-terminated Si surface through the bond formed between the C₆₀ cage and nitrogen. It

must be pointed out that the presence of three or more nitrogen atoms connected to a fullerene molecule was not confirmed within the signal-to-noise ratio of the current experiments since no noticeable feature was observed in m/z region of 831.5 to 832.5, shown in Figure 3.17(d).

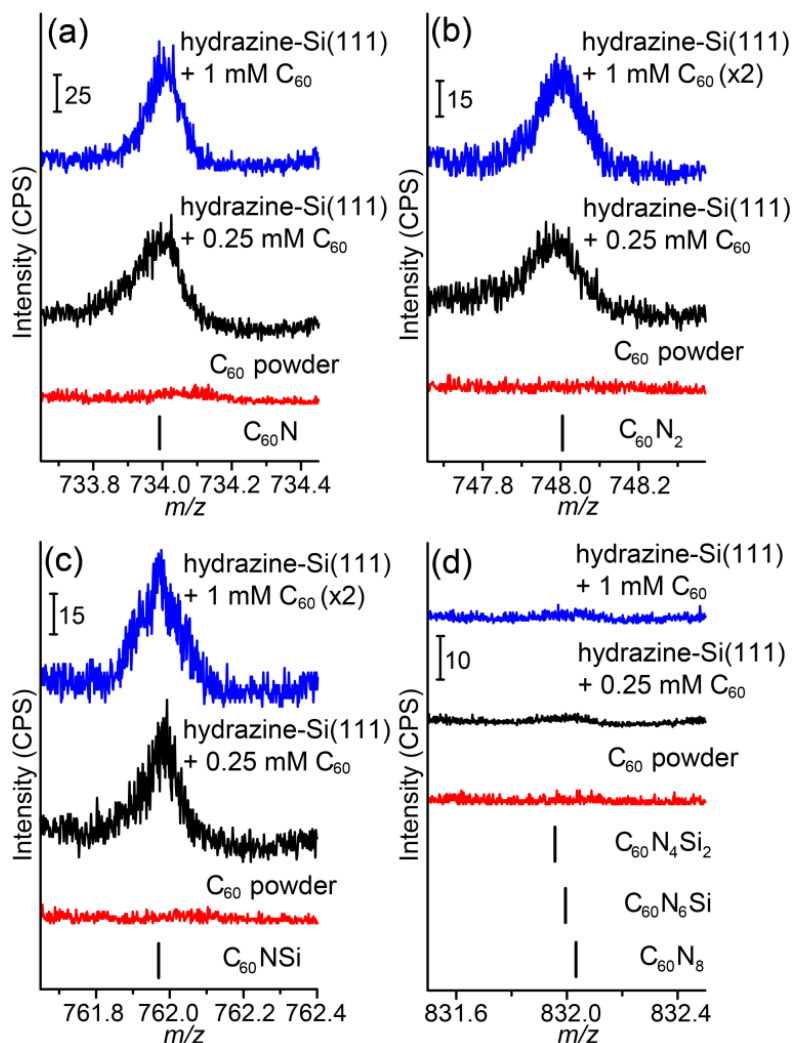


Figure 3.17 Negative ion ToF-SIMS spectra of representative spectral regions following the reaction of C_{60} with a hydrazine-terminated Si(111) surface: (a) $[C_{60}-N]^-$ species m/z range; (b) $[C_{60}-N_2]^-$ species m/z range; (c) $[C_{60}-N-Si]^-$ species m/z range and (d) $[C_{60}-N_4-Si_2]^-$ (or $[C_{60}-N_6-Si]^-$, $[C_{60}-N_8]^-$) species m/z range. The exact positions of expected ions are shown as solid bars underneath the experimental data.

3.2.3.3 Confirmation of Fullerenes C₆₀ Covalently Bound to Hydrazine-Terminated Si(111) Surface by X-ray Photoelectron Spectroscopy.

XPS is used to address the reaction more quantitatively. The studies of the C 1s spectral region following the reaction of C₆₀ solution with hydrazine-terminated Si(111) surface are presented in Figure 3.18. Both for hydrazine-terminated Si(111) surface (3.18a) and 1 mM C₆₀ solution modified surface (3.18b), three peaks at 284.6 eV, 286.4 eV and 288.5 eV are discerned and assigned to C–C bonds, C–O/C–N bonds and C=O bonds. The considerable increase of these peaks is a result of fullerene C₆₀ interacting with the hydrazine-terminated silicon surface, forming C–N bonds in addition to surface oxidation (C–O species) or adsorption of adventitious hydrocarbons (C=O species) that may occur during sample transfer. However, the most important observation is the peak at 291.3 eV, which corresponds to the π – π^* shake-up in aromatic functional groups,⁷⁰⁻⁷¹ confirming the presence of the aromatic entities on the modified surface following its reaction with C₆₀. Since this peak is not observed for the hydrazine-terminated silicon sample, there is only one possible source of aromaticity in this sample: the presence of C₆₀.

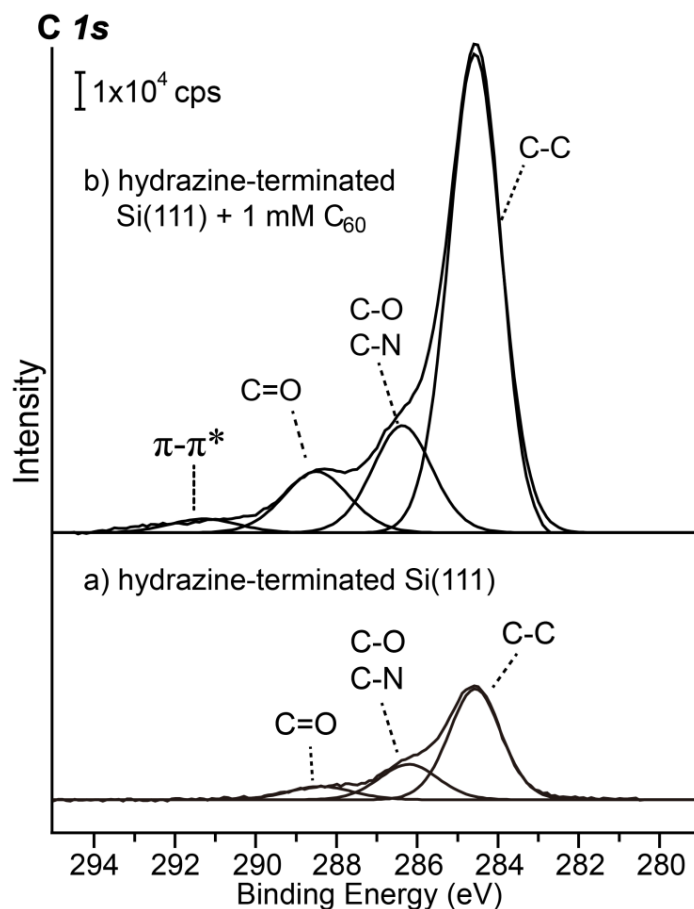


Figure 3.18 High-resolution XPS spectra of C *1s* region for (a) the hydrazine-terminated Si(111) surface, and (b) hydrazine-terminated Si(111) surface reacted with 1 mM C₆₀ solution.

Figure 3.19 shows the N *1s* spectral region of the hydrazine-terminated silicon and C₆₀ monolayer on silicon, respectively, along with the DFT-predicted N *1s* core level energies shown as solid bars for the models indicated in the figure. The N *1s* experimental spectra shown for the hydrazine-modified Cl-Si(111) surface in Figure 3.19(a) indicate a predominant N-containing functionality at 399.6 eV (FWHM=1.5 eV) and a minor species at 397.5 eV. Previous studies have identified the major peak

at 399.6 eV to be Si–NH–NH–Si,^{52, 67} with the N–N bond being parallel or nearly parallel to the surface.^{52, 67} The minority surface species has been assigned to the N–N bond dissociation, predominantly on surface defect sites;^{34, 52} this assignment is supported by the DFT studies. Figure 3.19(b) shows the N *1s* region for the sample modified with C₆₀. This spectrum is clearly different from that of the hydrazine-modified surface. First, the maximum of the main peak is shifted towards higher energy, and the peak itself becomes substantially broader, suggesting that this feature encompasses several different spectral signatures. If the main feature in Figure 3.19(b) is fitted with a peak of the same full width at half maximum as the main feature on the hydrazine-terminated silicon surface (399.6 eV, FWHM = 1.5 eV), the remaining intensity of this feature can be fitted with a peak at 400.3 eV. Its area is nearly double of that for the feature at 399.6 eV. The peak at 400.3 eV (FWHM = 1.6 eV) can be assigned to the nitrogen atoms connected to silicon and the C₆₀ cage. This assignment is made based on the comparison of the experimental spectra with the core level shifts predicted for the models indicated in Figure 3.19 for the C₆₀ molecule bound to either one or two nitrogen atoms of the surface-bound hydrazine functionality. It is also fully consistent with the previous investigations of amino-modified buckyballs.^{51, 69, 72}

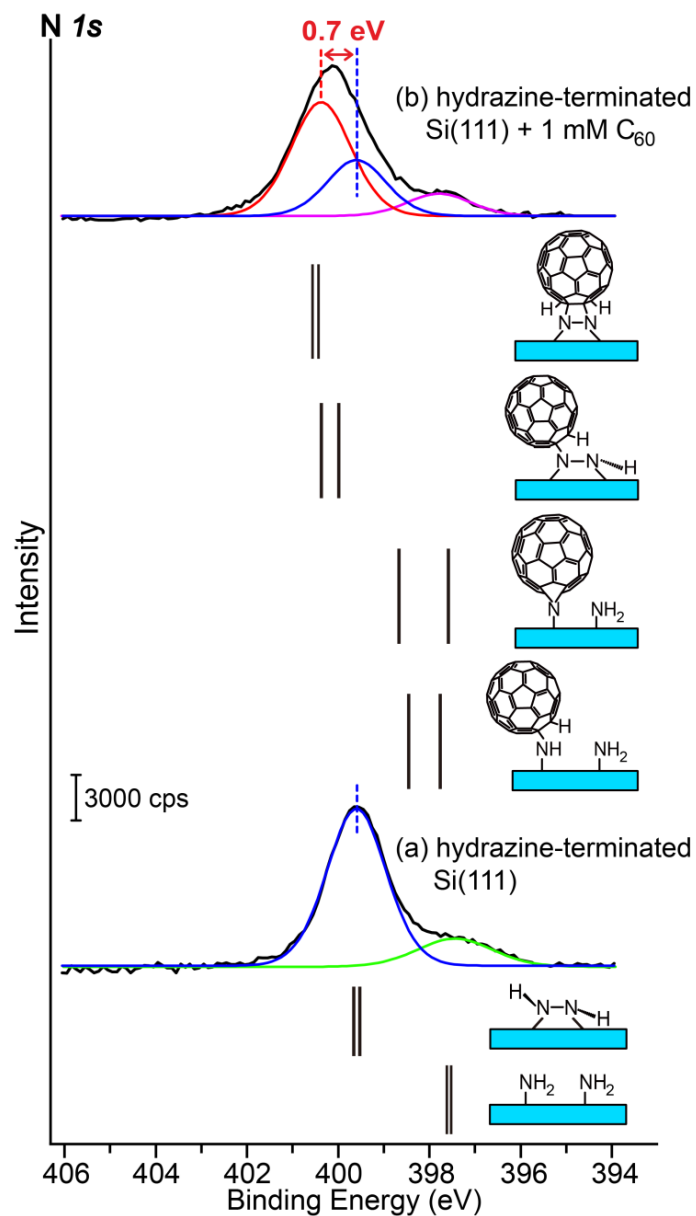


Figure 3.19 High-resolution XPS spectra of N 1s region for (a) the hydrazine-terminated Si(111) surface, and (b) hydrazine-terminated Si(111) surface reacted with 1 mM C₆₀ solution. The core level energy shifts predicted by DFT for the model systems presented in the figure are shown as solid bars.

Thus, the feature at 399.6 eV in Figure 3.19 belongs to the unreacted nitrogen-containing surface sites; the peak at 400.3 eV corresponds to the nitrogen atoms connected to silicon and the C₆₀ cage. This assignment is also supported by the DFT studies summarized in Figure 3.19. This thesis suggests that the attachment of C₆₀ to either one or two surface –NH functionalities is expected to shift the N *1s* level towards a higher binding energy, with reacted N shifting by 0.8~0.9 eV, and the unreacted nitrogen atom of the same functional group shifting by 0.4 eV. The positions of the computationally predicted values in Figure 3.19 are relative to the peak predicted for the hydrazine-terminated silicon surface (Si–NH–NH–Si) that was matched with the experimental value. The minor peak at 397.9 eV in Figure 3.19(b) is possibly a combination of the N–N dissociated minority sites on the hydrazine-modified surface and the structure with N atoms inserted into the C₆₀ cage directly, forming pyridine-like N⁷³⁻⁷⁴ or C–N–C⁷³⁻⁷⁴ entities. It is investigated by comparing with DFT studies of a proposed structure for a hydrazine-terminated surface and of two possible structures that could exist following C₆₀ modification, as models presented in Figure 3.19. The minor peak on the hydrazine-terminated surface (397.5 eV) shifts by 0.4 eV towards a higher binding energy region after reaction with C₆₀ (397.9 eV). This observation is fully consistent with the result of the DFT prediction mentioned above, which demonstrates that the reaction of minor surface species with C₆₀ leads to the upward shift in binding energy.

Based on this comparison, it can be inferred that the chemical reaction has occurred and the observed binding-energy shift is explained by the C₆₀ reaction with the hydrazine-modified silicon surface. More importantly, this simple analysis confirms that approximately two thirds of surface nitrogen atoms are affected by this

reaction, meaning that the high-coverage of the C_{60} is formed on this surface. In other words, this observation reinforces the qualitative results offered above by AFM and ToF-SIMS investigations. The AFM studies are indeed consistent with a full monolayer of C_{60} molecules with observation of a very low coverage of *additional* ad atoms (or ad clusters) of the buckyballs on top of this first layer or possibly on defect sites. The ToF-SIMS work confirms that the species observed in AFM are bound to the surface covalently, with carbon atoms connected to silicon atoms via a nitrogen bridge and with some buckyballs connected with at least two surface nitrogen atoms. Finally, XPS studies suggest that the reported chemistry is very efficient, with nearly two thirds of the nitrogen atoms of the hydrazine-modified silicon surface affected by the presence of the C_{60} cage of the buckyballs: this assessment is made based on the peak ratio of the nitrogen species affected by the C_{60} reaction (400.3 eV) to unreacted nitrogen-containing species (399.6 eV). This last observation also implies a very high coverage of the buckyballs within the monolayer.

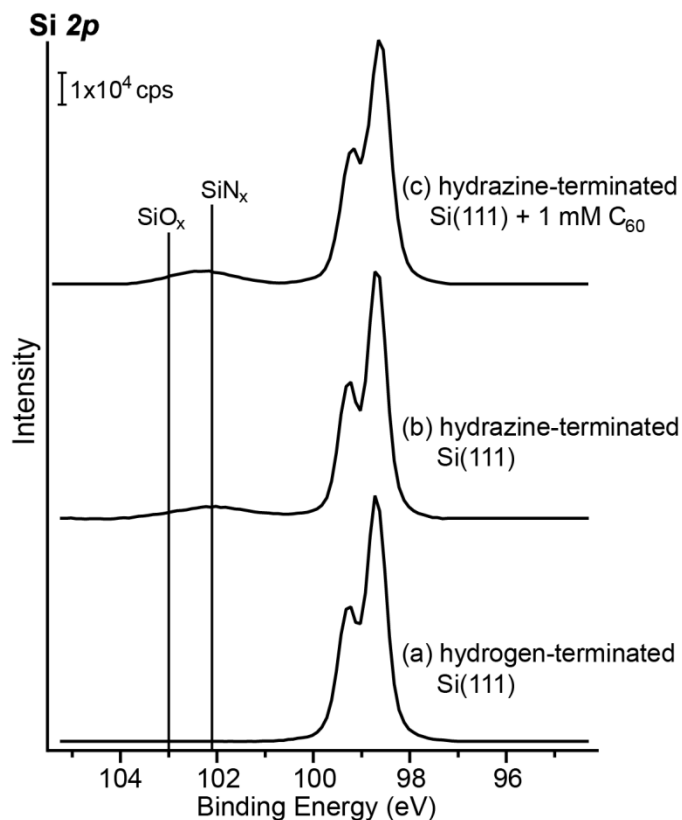


Figure 3.20 High-resolution XPS spectra of Si $2p$ region for (a) hydrogen-terminated Si(111) surface, (b) hydrazine-terminated Si(111) surface and (c) hydrazine-terminated Si(111) surface reacted with 1 mM C_{60} solution.

Figure 3.20 summarizes XPS studies of the Si $2p$ spectral region following the reaction of C_{60} solution with hydrazine-terminated Si(111) surface. Compared with a clean hydrogen-terminated Si(111) surface, the hydrazine-terminated silicon surface shows a broad feature centered at 102.2 eV, which corresponds to the minority defect SiN_x surface species.^{34, 52} After being treated by 1 mM C_{60} solution, the hydrazine-terminated silicon surface also presents a broad peak centered at 102.5 eV, possibly a mixture of SiN_x surface species and SiO_x surface oxidation;⁶⁴ however, the position

and the low overall intensity suggest that neither species correspond to the surface majority.

3.2.3.4 Surface recombination velocity measurements of C₆₀-modified Si(111) Surface.

Table 3.1 Charge carrier lifetime and surface recombination velocities for Si(111) surface following the reaction scheme: (a) hydrogen-terminated Si(111) surface; (b) chlorine-terminated Si(111) surface; (c) hydrazine-terminated Si(111) surface; (d) hydrazine-terminated Si(111) surface reacted with 1 mM C₆₀ solution.

Surface structure	Charge-carrier lifetime, τ (μ s)	Surface recombination velocity, S (cm s^{-1})
(a) Si(111)-H	35.1 ± 1.1	1426.7 ± 43.0
(b) Si(111)-Cl	39.9 ± 0.8	1254.5 ± 24.1
(c) Si(111)-NH-NH	10.4 ± 0.9	4821.7 ± 432.1
(d) Si(111)-(NH)N-C ₆₀	3.4 ± 0.1	14599.8 ± 313.8

Charge carrier lifetime measurements are conducted to evaluate the electronic properties of this C₆₀-modified silicon surface. Table 3.1 shows the minority carrier lifetime of Si(111) surfaces following the reaction and respective surface recombination velocities. The surface recombination velocity (S) is calculated following the equation and assumption detailed described in Chapter 1. The absolute values summarized in this table are not as significant as the relative comparison of the same samples at different modification steps due to the possible effects of a relatively small sample size. Nevertheless the data are consistent with the previous studies of the H-terminated Si(111) reported by our group,¹¹ but more importantly, it is clear that hydrazine-terminated Si(111) surface reacted with C₆₀ solution exhibits the lowest

minority carrier lifetime and the highest surface recombination velocity. This observation is fully consistent with the C₆₀ molecules serving as efficient electron (and exciton) traps.³⁸⁻³⁹ It can be noted that the minor surface oxidation is recorded after the 48-hour C₆₀ solution treatment as presented in Figure 3.20; however, the detailed studies of the effect of surface oxidation versus the attachment of C₆₀ molecules on charge carrier lifetime requires further investigation. Thus, the C₆₀-modified silicon surface exhibits substantially lower minority carrier lifetime than the silicon oxide surface, regardless of minor surface oxidation during reaction. This number is actually much lower than the previously reported charge-carrier lifetime measurements for C₆₀ thin films,⁷⁵ but this comparison requires further investigation.

3.3 Conclusion

In this study, a wet chemistry method was utilized to prepare a Si(111) surface terminated predominantly with Si-NH-NH-Si functionality, sequentially a novel method to covalently attach the Buckminsterfullerene C₆₀ to this hydrazine-modified Si(111) surface has been developed and shown to yield high coverage of a C₆₀ monolayer.

For the hydrazine-modified Si(111) surface, the FT-IR studies showed that all the H-terminated reactive sites were replaced after modification with chlorine and later with hydrazine. The Si-NH-NH-Si species were identified by FT-IR, ToF-SIMS and XPS, which also helps quantitatively investigate the surface coverage of chlorine and nitrogen. In addition, the XPS spectra suggested that the Si(111) surface remained unoxidized following modification steps. On the basis of the DFT calculations, the N

*I*s binding energy detected from XPS was also consistent with the presence of Si-NH-NH-Si surface species as dominant product. Finally, the DFT investigation confirmed the higher efficiency of hydrazine modification compared to that for ammonia reaction with the same surface. Precise characterization of the new approach to prepare NH_x-terminated surfaces and comprehensive identification and quantification of all chemical species on the surface will require further studies, both computationally and experimentally. The study of stability and reactivity of the hydrazine-modified Si(111) surface implies that such hydrazine-modified silicon surface can be used as an oxygen-free platform for further modification protocols, in which the C₆₀ fullerene attachment is a good example.

For the C₆₀ fullerene attachment onto hydrazine-modified silicon surface, the XPS study confirms that the reaction has occurred through the surface Si-NH-functionality. AFM investigations suggest that a monolayer of C₆₀ could be formed on this surface with only a few ad molecules on top of this monolayer or at defect sites. ToF-SIMS results indicate that the nitrogen atom of the hydrazine-modified silicon surface is attached directly to the C₆₀ cage following the surface reaction. More evaluations of this C₆₀ modified silicon surface, including C₆₀ triplet state lifetime measurements, which lead to potential future applications, are currently under investigation. This unique silicon surface with C₆₀ directly attached to silicon through a single amino-functionality circumvents the need for functionalized organic monolayers formed by hydrosilylation as a starting point for attachment, it avoids the need for ultra-high vacuum and the formation of Si-C bonds susceptible to oxidation, and it can serve as a platform for further modification based on the chemistry of C₆₀ fullerenes.

REFERENCES

1. He, T.; He, J.; Lu, M.; Chen, B.; Pang, H.; Reus, W. F.; Nolte, W. M.; Nackashi, D. P.; Franzon, P. D.; Tour, J. M. Controlled Modulation of Conductance in Silicon Devices by Molecular Monolayers. *J. Am. Chem. Soc.* **2006**, *128*, 14537-14541.
2. Margelefsky, E.; Zeidan, R.; Davis, M. Cooperative Catalysis by Silica-Supported Organic Functional Groups. *Chem. Soc. Rev* **2008**, *37*, 1118-1126.
3. Liu, Z.; Amiridis, M. D. Quantitative Ft-Irras Spectroscopic Studies of the Interaction of Avidin with Biotin on Functionalized Quartz Surfaces. *J. Phys. Chem. B* **2005**, *109*, 16866-16872.
4. Bent, S. F.; Teplyakov, A. V. Semiconductor Surface Functionalization for Advances in Electronics, Energy Conversion and Dynamic Systems. *J. Vac. Sci Technol. A* **2013**, *31*, 050810-1-12.
5. Stutz, H. Protein Attachment onto Silica Surfaces--a Survey of Molecular Fundamentals, Resulting Effects and Novel Preventive Strategies in Ce. *Electrophoresis* **2009**, *30*, 2032-2061.
6. Buriak, J. M. Organometallic Chemistry on Silicon and Germanium Surfaces. *Chem. Rev.* **2002**, *102*, 1271-1308.
7. Linford, M. R.; Fenter, P.; Eisenberger, P. M.; Chidsey, C. E. D. Alkyl Monolayers on Silicon Prepared from 1-Alkenes and Hydrogen-Terminated Silicon. *J. Am. Chem. Soc.* **1995**, *117*, 3145-3155.

8. Nemanick, E. J.; Hurley, P. T.; Webb, L. J.; Knapp, D. W.; Michalak, D. J.; Brunschwig, B. S.; Lewis, N. S. Chemical and Electrical Passivation of Single-Crystal Silicon(100) Surfaces through a Two-Step Chlorination/Alkylation Process. *J. Phys. Chem. B* **2006**, *110*, 14770–14778.
9. Yu, H. B.; Webb, L. J.; Solares, S. D.; Cao, P. G.; Goddard, W. A.; Heath, J. R.; Lewis, N. S. Scanning Tunneling Microscopy of Ethylated Si(111) Surfaces Prepared by a Chlorination/Alkylation Process. *J. Phys. Chem. B* **2006**, *110*, 23898–23903.
10. Leftwich, T. R.; Teplyakov, A. V. Chemical Manipulation of Multifunctional Hydrocarbons on Silicon Surfaces. *Surf. Sci. Rep.* **2008**, *63*, 1-71.
11. Tian, F.; Yang, D.; Opila, R. L.; Teplyakov, A. V. Chemical and Electrical Passivation of Si(111) Surfaces. *Appl. Surf. Sci.* **2012**, *258*, 3019-3026.
12. Bergerson, W. F.; Mulder, J. A.; Hsung, R. P.; Zhu, X. Y. Assembly of Organic Molecules on Silicon Surfaces via the Si-N Linkage. *J. Am. Chem. Soc.* **1999**, *121*, 454-455.
13. Bocharov, S.; Mathauser, A. T.; Teplyakov, A. V. Adsorption and Thermal Chemistry of Nitroethane on Si(100)-2x1. *J. Phys. Chem. B.* **2003**, *107*, 7776-7782.
14. Méndez De Leo, L. P.; Teplyakov, A. V. Nitro Group as a Means of Attaching Organic Molecules to Silicon: Nitrobenzene on Si(100)-2x1. *J. Phys. Chem. B* **2006**, *110*, 6899-6905.
15. Leftwich, T. R.; Madachik, M. R.; Teplyakov, A. V. Dehydrative Cyclocondensation Reactions on Hydrogen-Terminated Si(100) and Si(111): An Ex Situ Tool for the Modification of Semiconductor Surfaces. *J. Am. Chem. Soc.* **2008**, *130*, 16216-16223.

16. Perrine, K. A.; Leftwich, T. R.; Weiland, C.; Madachik, M. R.; Opila, R. L.; Teplyakov, A. V. Reactions of Aromatic Bifunctional Molecules on Silicon Surfaces: Nitrosobenzene and Nitrobenzene. *J. Phys. Chem. C* **2009**, *113*, 6643–6653.
17. Madachik, M. R.; Teplyakov, A. V. Coadsorption of Ethylene and Nitrobenzene on Si(100)-2 × 1: Toward Surface Patterning at the Molecular Level. *J. Phys. Chem. C* **2009**, *113*, 18270-18275.
18. Peng, G.; Seo, S.; Ruther, R. E.; Hamers, R. J.; Mavrikakis, M.; Evans, P. G. Molecular-Scale Structure of a Nitrobenzene Monolayer on Si(001). *J. Phys. Chem. C* **2011**, *115*, 3011–3017.
19. Tian, F.; Cui, Y.; Teplyakov, A. V. Nitroxidation of H-Terminated Si(111) Surfaces with Nitrobenzene and Nitrosobenzene. *J. Phys. Chem. C* **2014**, *118*, 502-512.
20. Bent, S. F.; Kachian, J. S.; Rodríguez-Reyes, J. C. F.; Teplyakov, A. V. Tuning the Reactivity of Semiconductor Surfaces by Functionalization with Amines of Different Basicity. *PNAS* **2011**, *108*, 956-960.
21. Lin, J.-M.; Rodríguez-Reyes, J. C. F.; Teplyakov, A. V. Competing Reactions During Metalorganic Deposition: Ligand-Exchange Versus Direct Reaction with the Substrate Surface. *J. Vac. Sci. Technol. A* **2013**, *31*, 021401-1-021401-17.
22. Lin, J.-M.; Teplyakov, A. V. Computational Investigation of Surface Reactivity of Functionalized Silicon Surfaces in Deposition Processes. *Theor. Chem. Acc.* **2013**, *132*, 1404-1-14.
23. Perrine, K. A.; Lin, J.-M.; Teplyakov, A. V. Controlling the Formation of Metallic Nanoparticles on Functionalized Silicon Surfaces. *J. Phys. Chem. C* **2012**, *116*, 14431–14444.

24. Perrine, K. A.; Teplyakov, A. V. Reactivity of Selectively Terminated Single Crystal Silicon Surfaces. *Chem. Soc. Rev.* **2010**, *39*, 3256–3274.
25. Widjaja, Y.; Mysinger, M. M.; Musgrave, C. B. Ab Initio Study of Adsorption and Decomposition of NH₃ on Si(100)-(2x1). *J. Phys. Chem. B* **2000**, *104*, 2527–2533.
26. Widjaja, Y.; Musgrave, C. B. A Density Functional Theory Study of the Nonlocal Effects of NH₃ Adsorption and Dissociation on Si(100)-(2x1). *Surf. Sci.* **2000**, *469*, 9-20.
27. Kubler, L.; Bischoff, J. L.; Bolmont, D. General Comparison of the Surface Processes Involved in Nitridation of Si(100)-2x1 by NH₃ and in Sin_x Film Deposition: A Photoemission Study. *Phys. Rev. B* **1988**, *38*, 13113–13123.
28. Rangelov, G.; Stober, J.; Eisenhut, B.; Fauster, T. NH₃ and No Interaction with Si(100)-(2x1) Surfaces. *Phys. Rev. B* **1991**, *44*, 1954–1957.
29. Rodríguez-Reyes, J. C. F.; Teplyakov, A. V. Cooperative Nitrogen Insertion Processes: Thermal Transformation of NH₃ on a Si(100) Surface. *Phys. Rev. B* **2007**, *76*, 075348-1-16.
30. Rodríguez-Reyes, J. C. F.; Teplyakov, A. V. Role of Surface Strain in the Subsurface Migration of Adsorbates on Silicon. *Phys. Rev. B* **2008**, *78*, 165314-1-14.
31. Tian, F.; Teplyakov, A. V. Silicon Surface Functionalization Targeting Si-N Linkages. *Langmuir* **2013**, *29*, 13-28.
32. Bocharov, S.; Dmytrenko, O.; Méndez De Leo, L. P.; Teplyakov, A. V. Azide Reactions for Controlling Clean Silicon Surface Chemistry: Benzylazide on Si(100)-2x1. *J. Am. Chem. Soc.* **2006**, *128*, 9300-9301.
33. Leftwich, T. R.; Teplyakov, A. V. Cycloaddition Reactions of Phenylazide and Benzylazide on a Si(100)-2x1 Surface. *J. Phys. Chem. C* **2008**, *112*, 4297-4303.

34. Tian, F.; Taber, D. F.; Teplyakov, A. V. NH-Termination of the Si(111) Surface by Wet Chemistry. *J. Am. Chem. Soc.* **2011**, *133*, 20769–20777.
35. Bu, Y.; Shinn, D. W.; Lin, M. C. Adsorption and Thermal Decomposition of N₂h₄ and Ch₃n₂h₃ on Si(111)7x7. *Surf. Sci.* **1992**, *276*, 184-199.
36. Tindall, C.; Li, L.; Takaoka, O.; Hasegawa, Y.; Sakurai, T. Adsorption of N₂h₄ on Silicon Surfaces. *J. Vac. Sci. Technol. A* **1997**, *15*, 1155-1158.
37. Sullivan, P.; Jones, T. S. Pentacene/Fullerene (C₆₀) Heterojunction Solar Cells: Device Performance and Degradation Mechanisms. *Org. Electron.* **2008**, *9*, 656-660.
38. Tong, X.; Wang, N.; Slootsky, M.; Yu, J.; Forrest, S. R. Intrinsic Burn-in Efficiency Loss of Small-Molecule Organic Photovoltaic Cells Due to Exciton-Induced Trap Formation. *Sol. Energy Mater. Sol. Cells* **2013**, *118*, 116-123.
39. Withers, J. C.; Loutfy, R. O.; Lowe, T. P. Fullerene Commercial Vision. *Fullerene Sci. Technol.* **1997**, *5*, 1-31.
40. Rather, J. A.; De Wael, K. Fullerene-C₆₀ Sensor for Ultra-High Sensitive Detection of Bisphenol-a and Its Treatment by Green Technology. *Sensors Actuators B: Chem.* **2013**, *176*, 110-117.
41. Qaiser, D.; Khan, M. S.; Singh, R. D.; Khan, Z. H. Comparative Study of Optical Parameters of Fullerene C₆₀ Film at Different Temperatures. *Opt. Commun.* **2010**, *283*, 3437-3440.
42. Guerin, D.; Lenfant, S.; Godey, S.; Vuillaume, D. Synthesis and Electrical Properties of Fullerene-Based Molecular Junctions on Silicon Substrate. *J. Mater. Chem.* **2010**, *20*, 2680-2690.

43. Fabre, B.; Bassani, D. M.; Liang, C.-K.; Ray, D.; Hui, F.; Hapiot, P. Anthracene and Anthracene: C₆₀ Adduct-Terminated Monolayers Covalently Bound to Hydrogen-Terminated Silicon Surfaces. *J. Phys. Chem. C* **2011**, *115*, 14786-14796.
44. Sze, S. M.; Ng, K. K., *Physics of Semiconductor Devices, 3rd Edition*; J. Wiley & Sons: New York, 2006.
45. Moro, L.; Paul, A.; Lorents, D. C.; Malhotra, R.; Ruoff, R. S.; Lazzeri, P.; Vanzetti, L.; Lui, A.; Subramoney, S. Silicon Carbide Formation by Annealing C₆₀ Films on Silicon. *J. Appl. Phys.* **1997**, *81*, 6141-6146.
46. Nakaya, M.; Iwasa, T.; Tsunoyama, H.; Eguchi, T.; Nakajima, A. Heterodimerization via the Covalent Bonding of Ta@Si₁₆ Nanoclusters and C₆₀ Molecules. *J. Phys. Chem. C* **2015**, *119*, 10962-10968.
47. Feng, W.; Miller, B. Self-Assembly and Characterization of Fullerene Monolayers on Si(100) Surfaces. *Langmuir* **1999**, *15*, 3152-3156.
48. Jeong, J.; Chung, D. J.; Ahn, J.; Park, J. Y.; Chung, B. H. Size-Controllable C₆₀ Nano-Islands Prepared on Silicon Wafers via Spin-Coating and the Effect of Annealing. *Carbon* **2015**, *94*, 120-123.
49. Zhang, X.; Teplyakov, A. V. Adsorption of C₆₀ Buckminster Fullerenes on an 11-Amino-1-Undecene-Covered Si(111) Substrate. *Langmuir* **2008**, *24*, 810-820.
50. Chopra, T. P.; Longo, R. C.; Cho, K.; Chabal, Y. J. Ammonia Modification of Oxide-Free Si(111) Surfaces. *Surf. Sci.* **2016**, *650*, 285-294.
51. Miller, T.; Teplyakov, A. V. Attachment Chemistry of PCBM to a Primary-Amine-Terminated Organic Monolayer on a Si(111) Surface. *Langmuir* **2014**, *30*, 5105-5114.

52. Gao, F.; Teplyakov, A. V. Reaction of Hydrazine with a Chlorine-Terminated Si(111) Surface. *J. Phys. Chem. C* **2014**, *118*, 27998-28006.
53. Frisch, M. J.; Trucks, G. W.; Schlegel, H. B.; Scuseria, G. E.; Robb, M. A.; Cheeseman, J. R.; Scalmani, G.; Barone, V.; Mennucci, B.; Petersson, G. A. *Gaussian 09, Revision B.01*, Gaussian, Inc.: Wallingford, CT, 2009.
54. Chabal, Y. J.; Harris, A. L.; Raghavachari, K.; Tully, J. C. Infrared Spectroscopy of H-Terminated Silicon Surfaces. *International journal of modern physics. B, Condensed matter physics, statistical physics, applied physics* **1993**, *07*, 1031-1078.
55. Michalak, D. J.; Amy, S. R.; Aureau, D.; Dai, M.; Estève, A.; Chabal, Y. J. Nanopatterning Si(111) Surfaces as a Selective Surface-Chemistry Route. *Nat. Mater.* **2010**, *9*, 266-271.
56. Michalak, D. J.; Rivillon, S.; Chabal, Y. J.; Estève, A.; Lewis, N. S. Infrared Spectroscopic Investigation of the Reaction of Hydrogen-Terminated, (111)-Oriented, Silicon Surfaces with Liquid Methanol. *J. Phys. Chem. B* **2006**, *110*, 20426-20434.
57. Queeney, K. T.; Chabal, Y. J.; Raghavachari, K. Role of Interdimer Interactions in NH₃ Dissociation on Si(100)-(2x1). *Phys. Rev. Lett.* **2001**, *86*, 1046-1049.
58. Dai, M.; Wang, Y.; Kwon, J.; Halls, M. D.; Chabal, Y. J. Nitrogen Interaction with Hydrogen-Terminated Silicon Surfaces at the Atomic Scale. *Nat. Mater.* **2009**, *8*, 825-830.
59. Dillon, A. C.; Gupta, P.; Robinson, M. B.; Bracher, A. S.; George, S. M. Ammonia Decomposition on Silicon Surfaces Studied Using Transmission Fourier Transform Infrared Spectroscopy. *J. Vac. Sci. Technol. A* **1991**, *9*, 2222-2230.

60. Bater, C.; Sanders, M.; Craig, J. H. J. Ammonia as a Precursor in Electron-Enhanced Nitridation of Si(100). *Surf. Interface Anal.* **2000**, 29, 208-214.
61. Bansal, A.; Li, X. L.; Yi, S. I.; Weinberg, W. H.; Lewis, N. S. Spectroscopic Studies of the Modification of Crystalline Si(111) Surfaces with Covalently-Attached Alkyl Chains Using a Chlorination/Alkylation Method. *J. Phys. Chem. B* **2001**, 105, 10266–10277.
62. Liu, Y.; Chen, J.; Teplyakov, A. V. Chemical Passivation Processes for Biofunctionalization Schemes on Semiconductors Surfaces. *Langmuir* **2012**, 28, 15521-15528.
63. Zhang, X.; Antonopoulos, I. H.; Kumar, S.; Chen, J.; Teplyakov, A. V. Tuning the Geometry of Shape-Restricted DNA Molecules on the Functionalized Si(111) *Appl. Surf. Sci.* **2009**, 256, 815-818.
64. Queeney, K. T.; Weldon, M. K.; Chang, J. P.; Chabal, Y. J.; Gurevich, A. B.; Sapjeta, J.; Opila, R. L. Infrared Spectroscopic Analysis of the Si/SiO₂ Interface Structure of Thermally Oxidized Silicon. *J. Appl. Phys.* **2000**, 87, 1322-1330.
65. Webb, L. J.; Nemanick, E. J.; Biteen, J. S.; Knapp, D. W.; Michalak, D. J.; Traub, M. C.; Chan, A. S. Y.; Brunschwig, B. S.; Lewis, N. S. High-Resolution X-ray Photoelectron Spectroscopic Studies of Alkylated Silicon(111) Surfaces. *J. Phys. Chem. B* **2005**, 109, 3930–3937.
66. Webb, L. J.; Lewis, N. S. Comparison of the Electrical Properties and Chemical Stability of Crystalline Silicon(111) Surfaces Alkylated Using Grignard Reagents or Olefins with Lewis Acid Catalysts. *J. Phys. Chem. B* **2003**, 107, 5404-5412.
67. Bu, Y.; Lin, M. C. Surface Chemistry of N₂h₄ on Si(100)-2x1. *Surf. Sci.* **1994**, 311, 385-394.

68. Duan, Y.; Gao, F.; Teplyakov, A. V. Role of the Deposition Precursor Molecules in Defining Oxidation State of Deposited Copper in Surface Reduction Reactions on H-Terminated Si(111) Surface. *J. Phys. Chem. C* **2015**, *119*, 27018-27027.
69. Sahoo, R. R.; Patnaik, A. Surface Confined Self-Assembled Fullerene Nanoclusters: A Microscopic Study. *Appl. Surf. Sci.* **2005**, *245*, 26-38.
70. Sakai, Y.; Iijima, Y.; Asakawa, D.; Hiraoka, K. XPS Depth Profiling of Polystyrene Etched by Electrospray Droplet Impact. *Surf. Interface Anal.* **2010**, *42*, 658-661.
71. Enkvist, C.; Lunell, S.; Sjögren, B.; Brühwiler, P. A.; Svensson, S. The C 1s Shakeup Spectra of Buckminsterfullerene, Acenaphthylene, and Naphthalene, Studied by High Resolution X-ray Photoelectron Spectroscopy and Quantum Mechanical Calculations. *J. Chem. Phys.* **1995**, *103*, 6333-6342.
72. Sahoo, R. R.; Patnaik, A. Binding of Fullerene C₆₀ to Gold Surface Functionalized by Self-Assembled Monolayers of 8-Amino-1-Octane Thiol: A Structure Elucidation. *J. Colloid Interface Sci.* **2003**, *268*, 43-49.
73. Matsuoka, M.; Isotani, S.; Mansano, R.; Sucasaire, W.; Pinto, R.; Mittani, J.; Ogata, K.; Kuratani, N. X-Ray Photoelectron Spectroscopy and Raman Spectroscopy Studies on Thin Carbon Nitride Films Deposited by Reactive Rf Magnetron Sputtering. *World Journal of Nano Science and Engineering* **2012**, *2*, 92-102.
74. Le Normand, F.; Hommet, J.; Szörényi, T.; Fuchs, C.; Fogarassy, E. XPS Study of Pulsed Laser Deposited Cn_x Films. *Phys. Rev. B* **2001**, *64*, 235416.
75. Ziehlke, H.; Burtone, L.; Koerner, C.; Fitzner, R.; Reinold, E.; Bäuerle, P.; Leo, K.; Riede, M. Increase of Charge Carrier Lifetime in Dicyanovinyl-

Quinquethiophene: Fullerene Blends Upon Deposition on Heated Substrates. *Org. Electron.* **2011**, *12*, 2258-2267.

Chapter 4

DEHYDROHALOGENATION CONDENSATION REACTION OF PHENYLHYDRAZINE WITH Cl-TERMINATED Si(111) SURFACE

4.1 Introduction

The studies of silicon-based materials and interfaces expand in a number of fields, including electronics, heterogeneous catalysis, biomolecular recognition and sensing, biomolecular separation, and energy conversion.¹⁻⁵

In order to produce the desired stable interfaces, silicon surfaces terminated with hydrogen or halogen are commonly used as starting points. Recent work on preparation and characterization of H-terminated⁶⁻¹¹ and Cl-terminated¹²⁻¹⁷ Si(100) and Si(111) single crystalline surfaces allows for detailed understanding of the chemical processes with a truly molecular level precision. The functionalization step commonly includes the reactions of these modified silicon surfaces with appropriate organic reagents to produce stable organic monolayers that can in turn be further modified to yield nearly any chemical or biological functionality needed.¹⁷⁻²⁰

Although the majority of previous work in surface modification of silicon material targeted the formation of stable Si-C bonds in hydrosilylation processes²¹⁻²², more recently substantial attention has been directed to avoid the presence of both carbon and oxygen directly at the interface with silicon. Considerable efforts have been focused on stable organic-inorganic interfaces on silicon with the help of Si-N bonds. Thermodynamic stability and chemical versatility of such interfaces drove the initial investigations of ammonia,^{13, 18-19, 23-27} amines,^{17, 28-29} nitro- and nitroso-

compounds³⁰⁻³³ as well as azides,³⁴⁻³⁶ with clean silicon single crystalline surfaces in vacuum towards more practical, cheap, and robust reactions of the same compounds with H- or Cl-terminated silicon surfaces by wet chemistry methods.^{13, 30, 36-38} Tian et al.¹³ established a strategy to prepare a carbon- and oxygen-free monolayer on Si(111) surface terminated predominantly with Si-NH-Si functionality based on chlorination of H-terminated Si(111) surface followed by the room temperature ammonia treatment with NH₃-saturated tetrahydrofuran (THF). More recently, carbon- and oxygen-free Si(111) surface terminated mostly with Si-NH-NH-Si functionality was prepared in a similar reaction with anhydrous hydrazine treatment at 35°C.²⁸ The amines have been used in reactions with Cl-terminated silicon to introduce a variety of functionalities;^{8, 13-16, 28-29, 39} however, hydrazine attachment presents a unique opportunity to yield the desired function, as will be demonstrated below.

Among the possible functional groups, the phenyl ring can be used as a good test-probe for surface reactions from a fundamental stand point. The aromatic ring presents a nice target for spectroscopic characterization and quantitative analysis.²⁹⁻³⁰ Compared to unfunctionalized hydrazine, phenylhydrazine is more stable and easier to handle. At the same time, phenyl-based organic monolayers possess a number of attractive properties, including their resistance to surface oxidation.⁴⁰⁻⁴¹ In other words, this substituent can be used to tune chemical, mechanical, and electronic properties of a semiconductor surface.

This thesis aims at a well-defined surface of silicon functionalized with phenylhydrazine to produce an oxygen-free platform for further investigation. A phenylhydrazine-functionalized Si(111) sample is obtained from a Cl-Si(111) surface with phenylhydrazine at 35~38 °C under N₂ atmosphere. A schematic comparison of

the main proposed products for reactions of ammonia, hydrazine, and phenylhydrazine is provided in Figure 4.1. This type of reactions involves HCl elimination and the formation of new N-Si bonds, thus they can serve as examples of dehydrohalogenation condensation process.

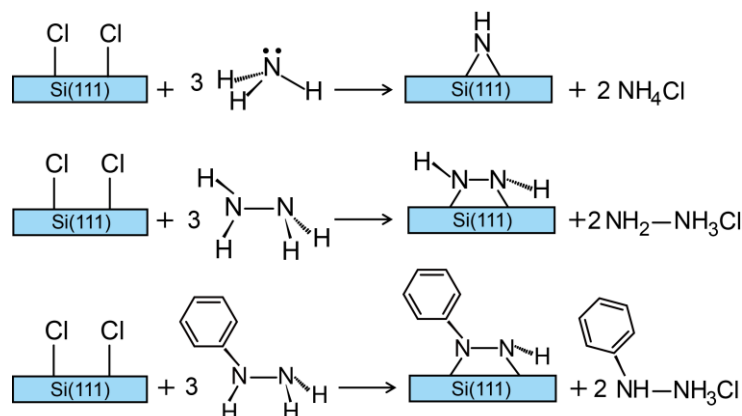


Figure 4.1 Schematic comparison of the reactions of Cl-Si(111) surface with ammonia, hydrazine and phenylhydrazine, respectively. The reactions are balanced taking into account the formation of salts in the presence of excess molecular reactants

To confirm the presence of Si-N bonds following this procedure and to establish the structures of surface species produced, every step of modification was followed by Fourier-transform infrared spectroscopy (FT-IR), X-ray photoelectron spectroscopy (XPS), and time-of-flight secondary ion mass spectrometry (ToF-SIMS). Density functional theory (DFT) calculations were performed to propose a plausible mechanism of surface reaction and to produce a set of appropriate spectroscopic observables, including vibrational spectra and core-level energies, to compare with the results of experimental studies.

4.2 Results and discussion

4.2.1 Confirmation of Phenylhydrazine Reaction with Cl-Si(111) Surface by Infrared Spectroscopy.

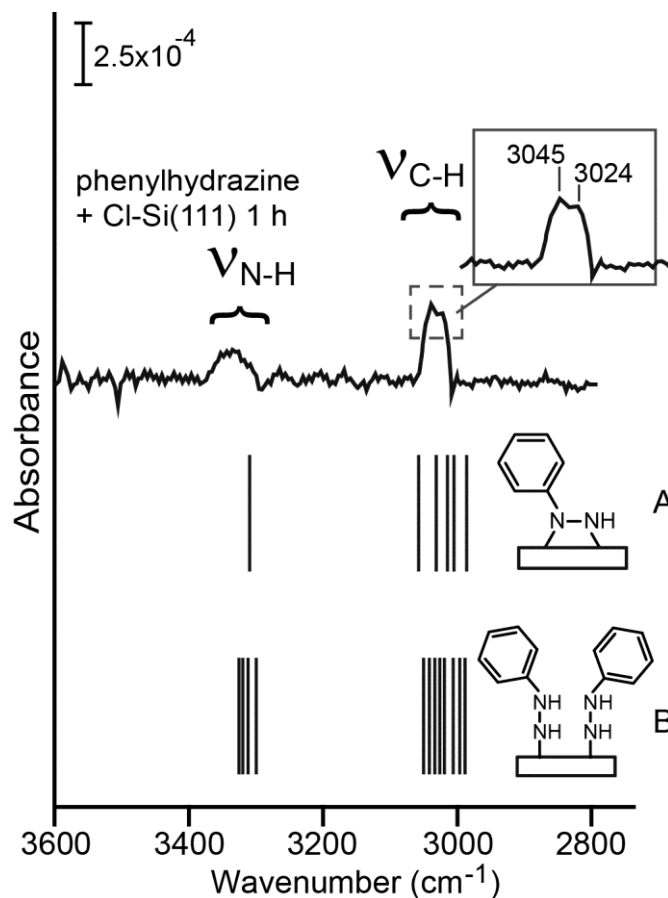


Figure 4.2 Summary of the infrared investigations of the N-H stretching region and C-H stretching region for phenylhydrazine reaction with Cl-Si(111) surface. The experimental spectrum is an average of five experiments conducted at identical conditions. The solid bars below the spectrum correspond to the vibrational frequencies predicted computationally for surface species formed, as summarized on corresponding schemes. All predicted frequencies are multiplied by a common scaling factor of 0.965.

In order to confirm the reaction of phenylhydrazine with a Cl-Si(111) surface and to possibly identify the products of this reaction, infrared spectra of the resulting

surface were interrogated. Figure 4.2 summarizes the most informative spectral region confirming the presence of C-H and N-H containing chemical groups following the reaction. The N-H stretching vibrations corresponding to -NH_x species are recorded around 3328 cm^{-1} and an obvious feature just above 3000 cm^{-1} corresponding to the C-H stretching of the phenyl ring is clearly observed. Even based on these results alone, it is possible to infer that the phenyl ring remains intact following the reaction of phenylhydrazine with a Cl-Si(111) surface. Otherwise, the C-H vibrations corresponding to the rehybridized species containing sp^2 and sp^3 carbon would be observed below 3000 cm^{-1} .⁴²⁻⁴⁵ In order to attempt precise identification of the surface, comparison of the experimental spectra with the computationally predicted vibrational signatures of the proposed surface species is needed, as also summarized in Figure 4.2. The possible surface models of the resulting species with a restriction that they must maintain the intact phenyl ring and possess some N-H bonds include all the species presented in the figure. However, it appears that based on these predictions alone it is impossible to distinguish them. Nevertheless, the fact that the phenyl ring remains intact and that the surface species possess N-H bonds will be important for further studies outlined below.

The infrared studies of the Si-H region following the phenylhydrazine reaction with the Cl-Si(111) surface are provided for reference in Figure 4.3. As well-studied in previous literature,^{9-10, 13, 28, 37, 46} the IR results confirm that the reaction started with a clean and well-ordered H-Si(111) surface and that all the hydrogen atoms were replaced by chlorine during the chlorination step. In last step of Cl-Si(111) treated by phenylhydrazine, no new Si-H containing species were introduced.

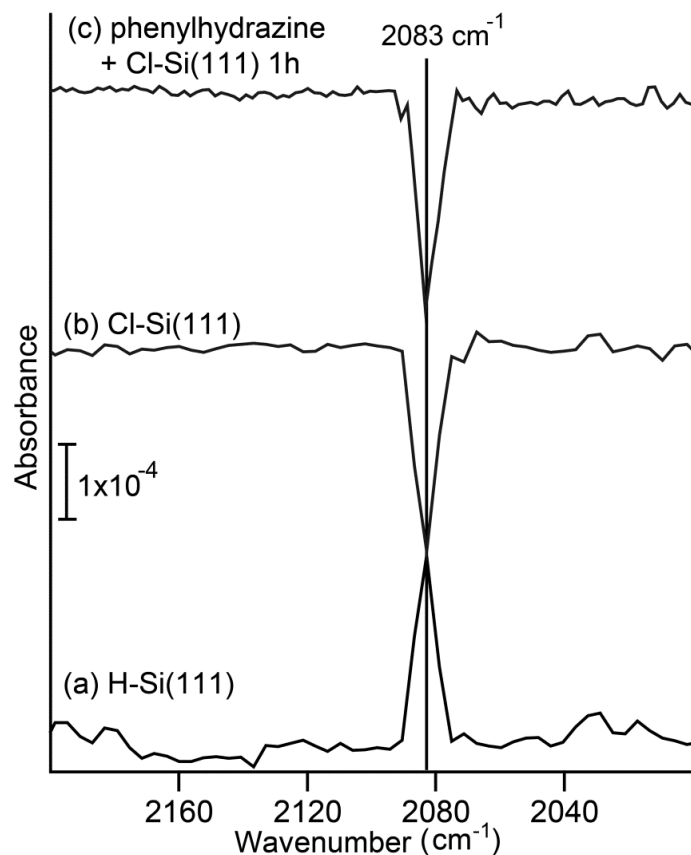


Figure 4.3 Summary of the infrared investigations for the Si-H stretching region of the Si samples following the phenylhydrazine reaction with Cl-Si(111) surface: (a) H-terminated Si(111) (with starting wafer used as a background); (b) Cl-terminated Si(111) prepared as indicated in the text (with sample in part (a) used as a background); (c) A surface in (b) reacted with phenylhydrazine for 1 hour as described in the text (with surface in (a) used as a background).

The rest of the spectral features are summarized in Table 4.1. Although the computational study suggests that there may be some subtle spectroscopic differences between the two possible models shown in Figure 4.2, especially within the fingerprint region, distinguishing them based on the experimental spectra collected in this study is not feasible, as the spectra are complicated by the effect of partial oxidation during the collection time on the absorption features.

Table 4.1 Summary of the infrared investigation of phenylhydrazine treated Cl-Si(111) surface, including a comparison with previous studies of relevant experimental systems and DFT computational prediction for the two proposed structures shown in **Figure 4.2**. All values are in cm^{-1} .

Experimental Value	Previous Investigation		Approximate Assignment	Calculated based on structure A in Fig. 4.1	Calculated based on structure B in Fig. 4.1
	Reported Value	System Studied			
3320	3290 ⁸	Ethylenediamine + Cl-Si(111) ⁸	Si-NH-C ₆ H ₅	3304	3296-3322
3045, 3024	3069, ⁴⁷ 3032 ⁴⁷	Phenyl isothiocyanate monolayer on Si(001) ⁴⁷	aromatic CH stretching	3031, 3015	3004-3045
1607	1595, ⁴⁸ 1600 ³⁰	Aromatic SAM on Si(111), ⁴⁸ Nitrobenzene + H-Si(111) ³⁰	aromatic CC	1551, 1530	1551, 1558, 1560, 1545
1450	1493, ⁴⁸ 1480 ³⁰	Aromatic SAM on Si(111), ⁴⁸ Nitrobenzene + H-Si(111) ³⁰	aromatic CC		
1265	1200~1300, ³⁸ 1150~1280 ³⁰	Nitrosobenzene + clean Si(100), ³⁸ Nitrosobenzene + H-Si(111) ³⁰	C-N(O)-Si		1261, 1267, 1285, 1286
1136	1110, ³⁹ 1209 ³⁹	CH ₃ MgCl + Cl-Si(111), ³⁹ C ₂ H ₅ MgBr + Cl-Si(111) ³⁹	Si-O-Si TO		
1120	1112 ⁸	Ethylenediamine + Cl-Si(111) ⁸	C-N-H	1200	1198, 1224
1101	1073-1109 ³⁹	CH ₃ MgCl / C ₂ H ₅ MgBr + Cl-Si(111) ³⁹	SiO-C		
1043	1034, ³⁹ 1025 ³⁹	CH ₃ MgCl + Cl-Si(111), ³⁹ C ₂ H ₅ MgBr + Cl-Si(111) ³⁹	Si-O-Si LO		
891	906-912, ⁴⁹ 880 ⁵⁰	Condensed phase Phenylcopper, ⁴⁹ Iodobenzene Adsorbed on Cu(111) ⁵⁰	aromatic C-H out-of-plane bending	927, 945	949, 940, 933, 922
821	849, ⁵¹ 845 ⁵¹	Gas phase Benzene, ⁵¹ Benzene Adsorbed on Cu(111) ⁵¹	aromatic C-H out-of-plane bending	856	863, 849, 832, 814
	820, ⁸ 825 ⁸	Ethylenediamine + Cl-Si(111) ⁸	Si-N	842	
773, 724	722-725, ⁴⁹ 725 ⁵⁰	Condensed phase Phenylcopper, ⁴⁹ Iodobenzene Adsorbed on Cu(111) ⁵⁰	aromatic C-H out-of-plane bending	788, 731	798, 790, 736, 723

4.2.2 X-ray photoelectron spectroscopy investigation of the extent of the reaction and additional information on surface species formed during phenylhydrazine interaction with the Cl-Si(111) surface.

In this study, a number of important conclusions can be reached based on XPS investigation. The first question that can be answered by this surface analytical technique is the quality of the surface with respect to surface oxidation. The analysis of the Si $2p$ spectra presented in Figure 4.4 reveals that no silicon surface oxidation was observed during the experimental procedure for obtaining H-terminated and Cl-terminated Si(111) substrates, as shown in spectra (a) and (b). The dashed line in Figure 4.4 indicates the expected position for the XPS feature corresponding to SiO_x at approximately 103 eV.^{13, 16, 28, 52-57} A Si $2p$ spectrum obtained following phenylhydrazine treatment exhibits a very minor feature at 102.2 eV in addition to the typical signature of the clean silicon surface, and as reaction time increases from 1 hour in Figure 4.4(c) to 3.5 hours in Figure 4.4(f), this minor feature increases in intensity and also shifts to the higher energy. Previous investigations of the feature observed at 102.2 eV suggest that it is most likely a signature of surface nitride^{13, 28, 58} formed at the surface defect sites. The position of this feature is clearly different from the 103 eV peak corresponding to SiO_x .⁵² Prolonged exposure to ambient conditions does result in surface oxidation. The signs of this oxidation are definitely noticeable in Figure 4.4(f) for a 3.5 hours contact time with phenylhydrazine, suggesting that even in nearly oxygen-free atmosphere, surface oxide is formed if the reaction time is increased substantially.²⁹

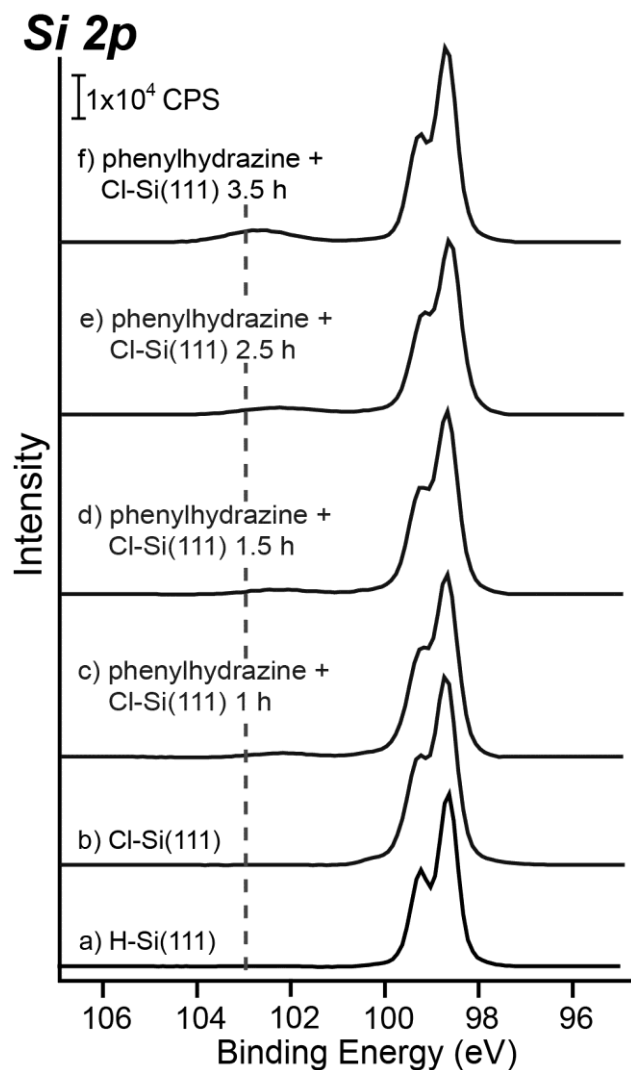


Figure 4.4 XPS spectra of the Si 2p region of the Si(111) surface following the reaction steps: a) freshly prepared H-terminated Si(111) surface, b) freshly prepared Cl-Si(111) surface; the surface in (b) reacted with phenylhydrazine for c) 1 hour, d) 1.5 hours, e) 2.5 hours, and f) 3.5 hours. The binding energy corresponding to the formation of SiO_x following surface oxidation is indicated by a dashed line.

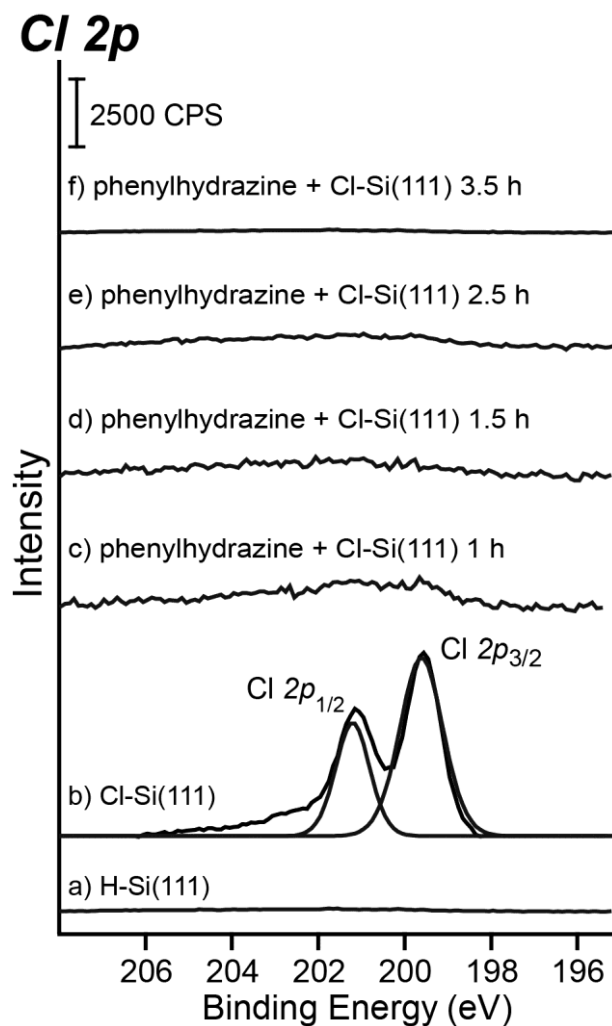


Figure 4.5 XPS spectra of the Cl 2p spectral region for the Si(111) surface following the reaction of phenylhydrazine with Cl-Si(111) surface for a) freshly prepared H-terminated Si(111) surface, b) freshly prepared Cl-Si(111) surface; the surface in (b) reacted with phenylhydrazine for c) 1 hour, d) 1.5 hours, e) 2.5 hours, and f) 3.5 hours.

Although silicon surface oxidation does not seem to pose substantial problems to the proposed surface modification approach at relatively short reaction times, it is important to understand how effective chlorine removal is during this process. Representative Cl 2*p* spectra of the Si(111) surface before and after phenylhydrazine modification are shown in Figure 4.5. As expected, no chlorine is present on the H-terminated Si(111) shown in Figure 4.5(a); the signature of this element appears only following silicon modification with PCl₅. After this modification step, only one type of chlorine-containing species is observed on the surface, as shown in Figure 4.5(b). Based on the coverage analysis following the overlayer model applied to this system according to Lewis et al.,¹⁴⁻¹⁶ the chlorine coverage observed in this experiment is consistent with the previously reported data for ~99 % of a monolayer.^{13, 28} Following the 1 hour reaction of the Cl-Si(111) surface with phenylhydrazine shown in Figure 4.5(c), the amount of surface chlorine is drastically reduced and the concentration of this element on a surface quickly approaches zero at longer reaction times shown in Figure 4.5(d)-(f).

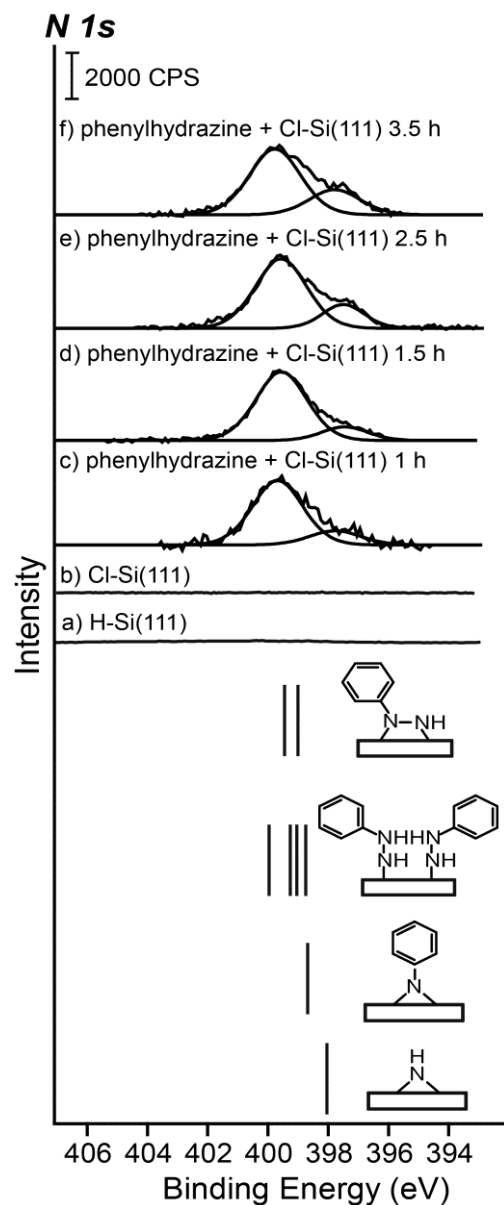


Figure 4.6 XPS spectra of the N *1s* spectral region for the Si(111) surface following the reaction of phenylhydrazine with Cl-Si(111) surface for a) freshly prepared H-terminated Si(111) surface, b) freshly prepared Cl-Si(111) surface; the surface in (b) reacted with phenylhydrazine for c) 1 hour, d) 1.5 hours, e) 2.5 hours, and f) 3.5 hours. The positions of the expected XPS signatures computationally predicted based on the previously published calibration procedure⁵⁹ for the model species shown in the figure are presented as solid bars underneath the experimental spectra.

Figure 4.6 presents a summary of the N *1s* investigations for the reaction of phenylhydrazine with a Cl-Si(111) surface. Figures 4.6(a) and 4.6(b) show that no nitrogen is present on H-terminated or Cl-terminated Si(111), respectively. Figure 4.6(c) clearly shows a dominant feature at 399.7 eV. The binding energy that corresponds to this observed feature is compared to the selected results of the DFT investigation of the models presented in Figure 4.6. The predictions of the N *1s* binding energies for the main expected possible geometry, Si-N-NH(phenyl)-Si, on the surface following phenylhydrazine treatment are 399.44 eV and 399.00 eV. Another possible NH_x functionality on the surface, Si-NH-NH-phenyl, is predicted to exhibit peaks at 398.73 eV, 399.04 eV, 399.25 eV and 399.96 eV (for a model containing two Si-NH-NH-phenyl species on neighboring surface sites). The third possible structure for NH_x species on the surface, Si-N(Si)-NH-phenyl, is predicted to exhibit peaks at 399.63 eV and 399.02 eV.

Based on the comparison of experimental and computationally-predicted spectra, it again appears that all the proposed species would have spectral signatures consistent with the experiment. It is important to highlight that the main feature observed experimentally is very different in energy from those that would originate from N-Si or N-N bond oxidation^{13, 17, 28} or the formation of a hydrazine salt.²⁸

The minor peak observed at 397.7 eV does increase with the reaction time. Based on the previous studies, it is likely a signature of a minor channel of a hydrazine reaction – N-N dissociation. This assignment is supported by comparing the observed energy with those reported for hydrazine and ammonia reacting with a Cl-Si(111) surface^{13, 28} and by an illustration of a possible position for such a species in Figure 4.6.

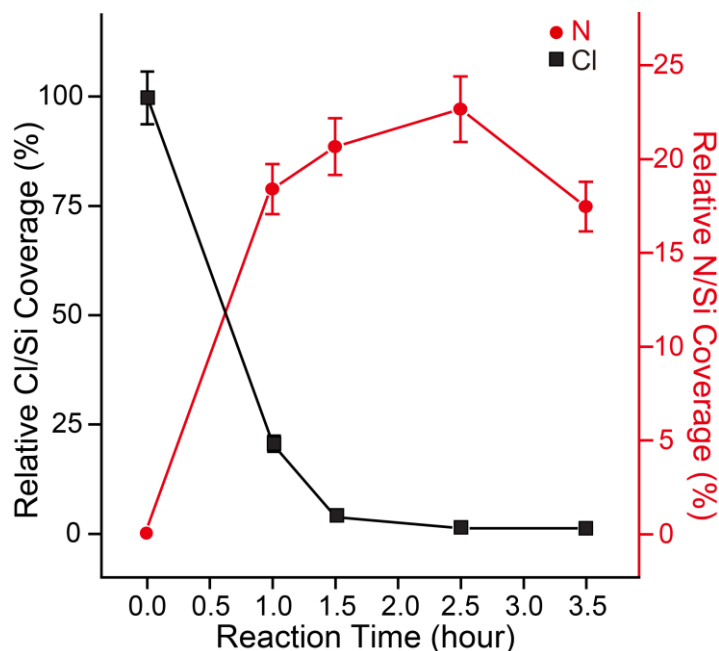


Figure 4.7 Summary of the apparent relative coverages of N and Cl obtained based on XPS studies as a function of the reaction time between phenylhydrazine and a Cl-Si(111) surface

By applying the quantitative analysis described by Lewis et al.,^{14, 16, 60} the ratio of the N *1s* feature and Si *2p* feature on the phenylhydrazine-treated surface can be calibrated with the corresponding ratio of the Cl *2p* feature and Si *2p* feature on the Cl-terminated Si(111) (where ~99% of the surface is covered with Cl atoms). This procedure yields nitrogen coverage of $21 \pm 5\%$ following 1 hour contact time.

The quantitative results of apparent relative surface coverages of N and Cl are summarized in Figure 4.7. The trends shown in this figure reveal that the apparent coverage of N increases up to 2.5 hours of the reaction time and decreases at longer exposure. The decrease is likely caused by surface oxidation observed at very long reaction times even in the controlled conditions used in this work. The apparent coverage of Cl decreases quickly and approaches zero for reaction times longer than

1.5 hours. The analysis of these trends suggests that chlorine removal is a relatively easy process, which will be further supported by computational studies. However, it is apparent that the reaction becomes very complicated and is affected substantially by surface reconstruction and surface oxidation processes for contact times longer than 2.5 hours.

4.2.3 Identification of surface species formed during phenylhydrazine interaction with the Cl-Si(111) surface by ToF-SIMS.

The infrared spectroscopy and XPS investigations reported above help rule out the presence of certain surface species as a result of the reaction of phenylhydrazine with a Cl-Si(111) surface. A comparison with selected DFT models also suggested that their expected vibrational and XPS signatures are consistent with the recorded experimental spectra. However, based on these studies alone it is practically impossible to identify the actual species present on a surface following this reaction. In order to further identify the species present on a surface following the phenylhydrazine reaction, ToF-SIMS traces were recorded before and after surface modification. Figure 4.8 presents a summary of the most relevant spectral ranges studied by this surface analytical technique.

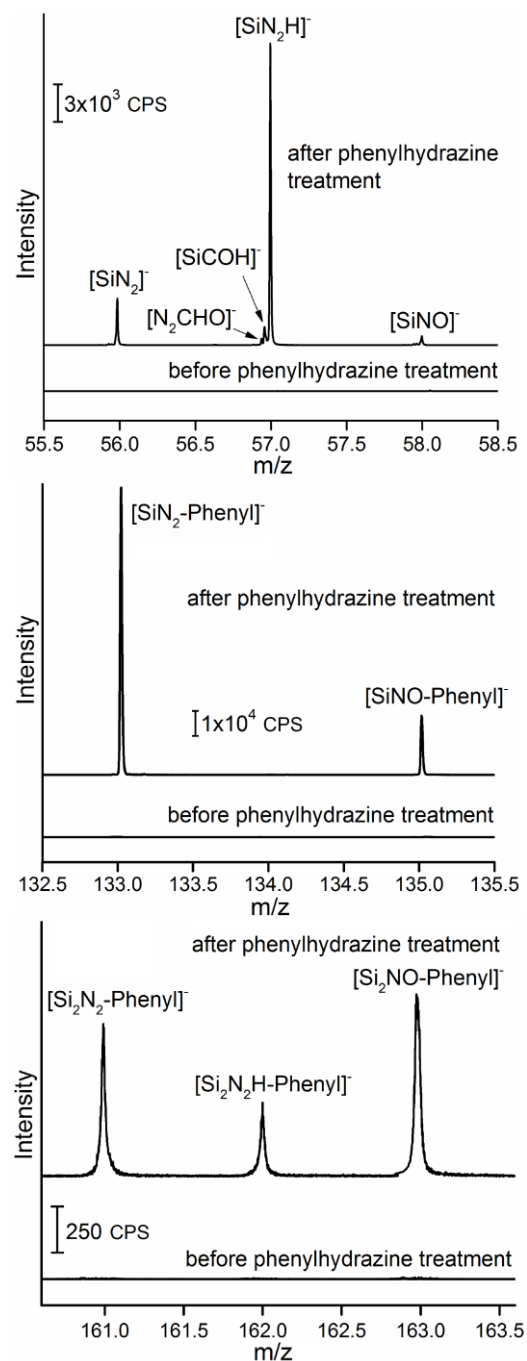


Figure 4.8 Negative ion ToF-SIMS spectra of the most informative spectral regions following the reaction of phenylhydrazine with a Cl-Si(111) surface: (a) $[\text{Si-N}_2]^-$ species m/z range; (b) $[\text{Si-N}_2\text{-phenyl}]^-$ species m/z range; (c) $[\text{Si}_2\text{-N}_2\text{-phenyl}]^-$ species m/z range.

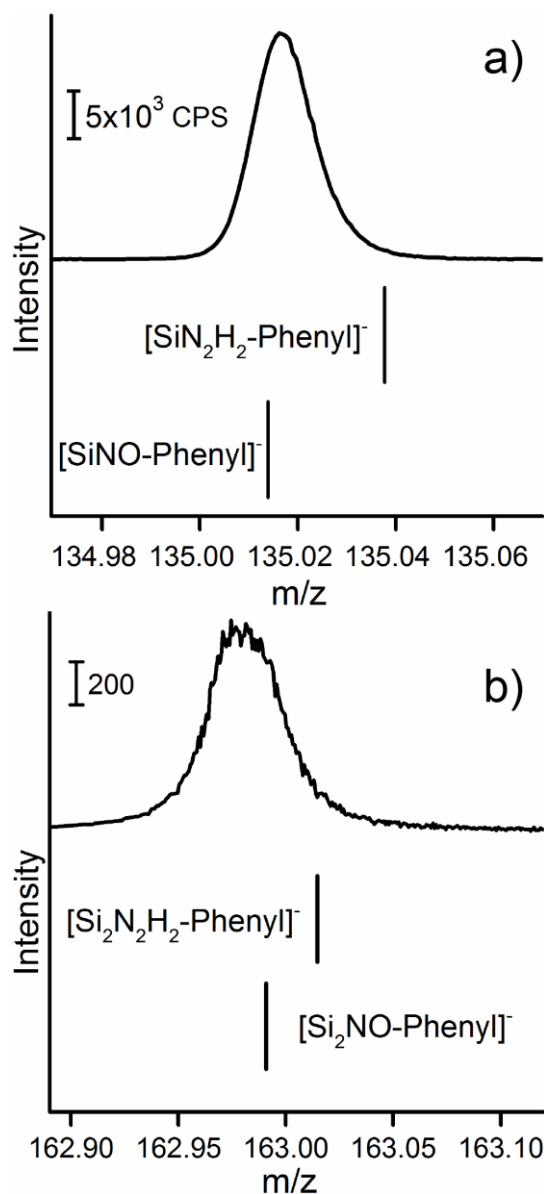


Figure 4.9 Negative ion ToF-SIMS spectra of phenylhydrazine treated Cl-Si(111) surface: (a) zoom-in of the $[\text{Si-NO-phenyl}]^-$ species m/z range; and (b) zoom-in of the $[\text{Si}_2\text{-NO-phenyl}]^-$ species m/z range. The exact positions of the ions corresponding to the selected species are indicated by solid vertical lines.

Negative ion ToF-SIMS spectra are used for plots (a)-(c) in Figure 4.8, which confirm that only following phenylhydrazine treatment, are the signatures for surface

bound phenylhydrazine reaction products observed. Specifically, negative ion m/z ranges of 55.5 to 58.5, 132.5 to 135.5 and 160.5 to 163.5 are summarized in these plots. Following the phenylhydrazine treatment, the $[\text{Si-N}_2\text{H}]^-$ fragment is clearly present and corresponds to the highest intensity feature in Figure 4.8(a). Generally, ToF-SIMS cannot be used for a quantitative comparison of different but closely related surface species; however, if the ionization cross sections of the $[\text{Si-N}_2\text{H}]^-$ and $[\text{Si-N}_2\text{H}_2]^-$ species are similar, the intensity difference between the two corresponding peaks in Figure 4.8(a) suggests that most of them are originated from $\text{Si-N}_2\text{H-Si}$ surface fragments and not from the $\text{Si-N}_2\text{H}_2$ surface species. There are $[\text{Si-N}_2\text{-phenyl}]^-$ and $[\text{Si-NO-phenyl}]^-$ species observed to be present in Figure 4.8(b). The oxidized species are generally observed to be present in this experimental setup since oxygen gas is always present in the background, albeit in very small quantities. Signatures of $[\text{Si}_2\text{-N}_2\text{-phenyl}]^-$, $[\text{Si}_2\text{-N}_2\text{H-phenyl}]^-$ and $[\text{Si}_2\text{-NO-phenyl}]^-$ species are presented in Figure 4.8(c).

To clarify and confirm the observed signatures, a zoom-in of $[\text{Si-NO-phenyl}]^-$ feature at 135.02 m/z is presented in Figure 4.9(a), with the vertical line indicating the expected position of the $[\text{Si-N}_2\text{H}_2\text{-phenyl}]^-$ species, which is clearly absent. This comparison rules out the structure of $[\text{Si-NH-NH-phenyl}]^-$ as a signature of a dominant surface species. Similarly, the zoom-in in Figure 4.9(b) clearly shows a peak at 162.98 corresponding to the minor oxidized $[\text{Si}_2\text{-NO-phenyl}]^-$ species and not the $[\text{Si}_2\text{-N}_2\text{H}_2\text{-phenyl}]^-$ group, whose expected position is also indicated by a vertical line.

Together with the infrared and XPS results described above, the ToF-SIMS studies zero in on a dominant surface species. Although infrared and XPS results could not identify this species unambiguously, they confirmed the presence of the

intact phenyl ring, the absence of major surface oxidation, and the relatively low coverage of nitrogen even at the optimal set of conditions. ToF-SIMS confirmed that the N-N bond is intact in the majority surface species and that the Si-N-NH(phenyl)-Si structure is indeed the dominant one.

4.2.4 Computational explanation of the initial steps of the surface reaction mechanism for phenylhydrazine interaction with a Cl-Si(111) surface.

The proposed mechanism of the initial steps of phenylhydrazine interaction with a Cl-Si(111) surface is depicted in Figure 4.10. The initial adsorption of phenylhydrazine on a Cl-Si(111) surface is a slightly exothermic process and the first reaction step is endothermic, with a very modest reaction barrier. The proposed second step leads to a much more endothermic product; however, it is overall consistent with the previously interrogated reactions of ammonia and unfunctionalized hydrazine on the Cl-Si(111) surface. It is likely that the endothermicity of this reaction is greatly moderated by a surface reconstruction and also by the fact that the HCl molecule released as a consequence of the reaction is bound to a phenylhydrazine molecule, since phenylhydrazine is present in excess in the reaction mixture. The stability of the resulting product is similar for this model to the stability of the unfunctionalized hydrazine in a similar reaction.²⁸ However, the different stabilities of the final salts ($\text{NH}_2\text{-NH}_3\text{Cl}$ vs. $\text{Ph-NH-NH}_3\text{Cl}$) will definitely affect the overall thermodynamics of the process. What makes the process involving phenylhydrazine different is the resulting efficiency of the process, with only approximately a quarter of surface silicon atoms connected to a nitrogen atom of the incoming phenylhydrazine molecule. The most straightforward explanation for such a difference is in the bulkiness of

phenylhydrazine. Specifically, if the structure of the first step product (where a single Si-N linkage is formed and a single HCl molecule is released) is considered carefully, it becomes apparent that the substituent phenyl ring is hindering the possible approach of another phenylhydrazine molecule to engage in a chemical interaction with the surface. Once the reaction goes to completion with both nitrogen atoms of the phenylhydrazine forming Si-N linkers and two HCl molecules released, this hindrance does not disappear, and in fact becomes even more pronounced. Further investigations of the surface reconstruction, consistent with a rather low surface coverage of nitrogen and at the same time essentially absent surface oxidation that could potentially stabilize this reconstruction, are necessary.

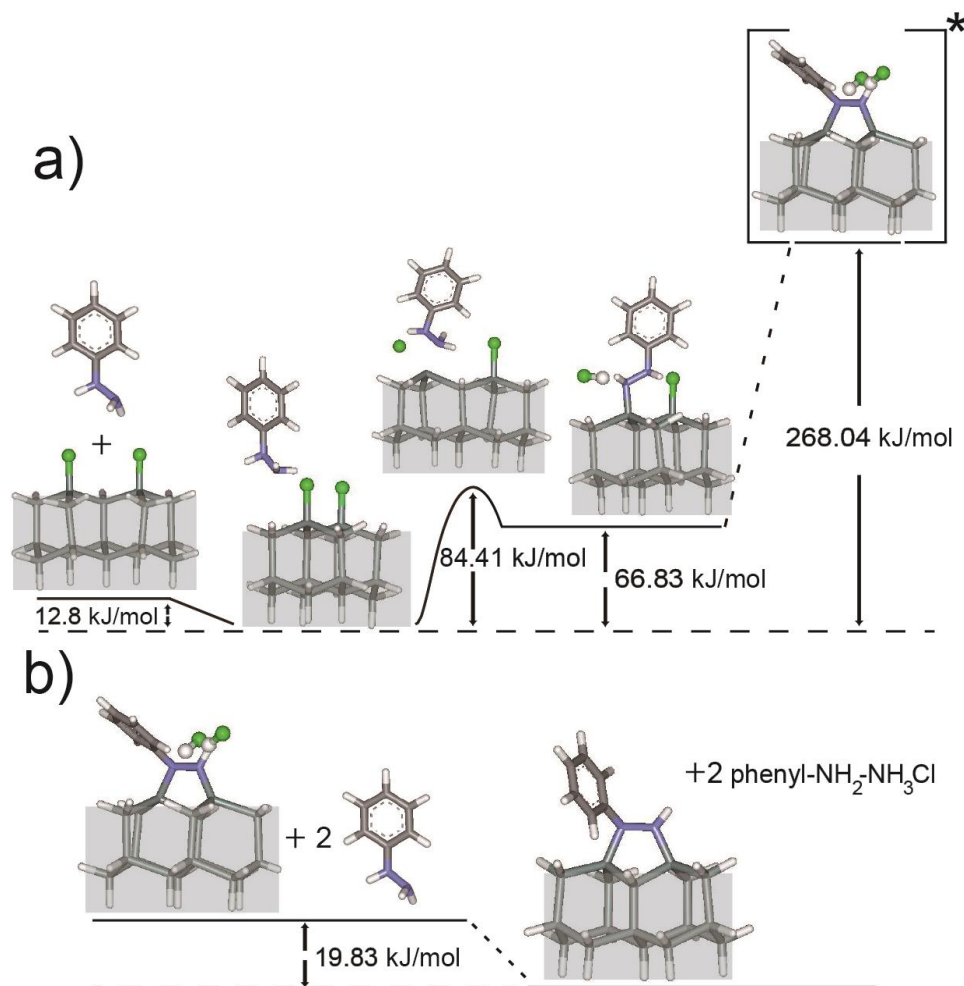


Figure 4.10 DFT investigation of the initial steps of a reaction of phenylhydrazine with a Cl-Si(111) surface. The proposed mechanism of interaction based on a reaction resulting in a HCl molecule bound to a surface-attached species as a product (a) is compared with a reaction pathway where the resulting HCl is bound to another phenylhydrazine molecule (b), which appear in excess in a realistic reaction mixture.

4.3 Conclusion

The work described in this thesis attempts to understand a complex process of phenylhydrazine interaction with a Cl-Si(111) surface to introduce a chemical functionality based on a dehydrohalogenation process. The ultimate goal of this approach would be to introduce high coverage of a target functionality based exclusively on Si-N linkers and without surface oxidation. The infrared investigation confirms the reaction and also confirms that the introduced functionality remains intact following the modification procedure. XPS studies are consistent with the proposed surface species and also confirm the absence of substantial surface oxidation unless the reaction time exceeds 2.5 hours. ToF-SIMS allows for identification of the majority species formed and the DFT studies offer a possible mechanism for the initial interaction steps for phenylhydrazine. However, increase of surface coverage of functionalized hydrazines or at least the reasons behind such a high stability of the modified surface with respect to oxidation, likely a stable reconstruction, in ambient have to be understood in further studies.

REFERENCES

1. Bent, S. F.; Teplyakov, A. V. Semiconductor Surface Functionalization for Advances in Electronics, Energy Conversion and Dynamic Systems. *J. Vac. Sci Technol. A* **2013**, *31*, 050810-1-12.
2. Liu, Z.; Amiridis, M. D. Quantitative Ft-Irras Spectroscopic Studies of the Interaction of Avidin with Biotin on Functionalized Quartz Surfaces. *J. Phys. Chem. B* **2005**, *109*, 16866-16872.
3. Margelefsky, E.; Zeidan, R.; Davis, M. Cooperative Catalysis by Silica-Supported Organic Functional Groups. *Chem. Soc. Rev* **2008**, *37*, 1118-1126.
4. Zhao, J.; Wang, A.; Green, M. A. 24.5% Efficiency Silicon Pert Cells on MCZ Substrates and 24.7% Efficiency Perl Cells on FZ Substrates. *Prog. Photovolt: Res. Appl.* **1999**, *7*, 471-474.
5. Stutz, H. Protein Attachment onto Silica Surfaces--a Survey of Molecular Fundamentals, Resulting Effects and Novel Preventive Strategies in Ce. *Electrophoresis* **2009**, *30*, 2032-2061.
6. Aldinger, B. S.; Hines, M. A. Si(100) Etching in Aqueous Fluoride Solutions: Parallel Etching Reactions Lead to pH-Dependent Nanohillock Formation or Atomically Flat Surfaces. *J. Phys. Chem. C* **2012**, *116*, 21499-21507.
7. Clark, I. T.; Aldinger, B. S.; Gupta, A.; Hines, M. A. Aqueous Etching Produces Si(100) Surfaces of near-Atomic Flatness: Strain Minimization Does Not Predict Surface Morphology. *J. Phys. Chem. C* **2010**, *114*, 423-428.

8. Chopra, T. P.; Longo, R. C.; Cho, K.; Halls, M. D.; Thissen, P.; Chabal, Y. J. Ethylenediamine Grafting on Oxide-Free H-, 1/3 ML F-, and Cl-Terminated Si(111) Surfaces. *Chem. Mater.* **2015**, *27*, 6268–6281.
9. Michalak, D. J.; Amy, S. R.; Aureau, D.; Dai, M.; Estève, A.; Chabal, Y. J. Nanopatterning Si(111) Surfaces as a Selective Surface-Chemistry Route. *Nat. Mater.* **2010**, *9*, 266–271.
10. Michalak, D. J.; Rivillon, S.; Chabal, Y. J.; Estève, A.; Lewis, N. S. Infrared Spectroscopic Investigation of the Reaction of Hydrogen-Terminated, (111)-Oriented, Silicon Surfaces with Liquid Methanol. *J. Phys. Chem. B* **2006**, *110*, 20426–20434.
11. Perrine, K. A.; Teplyakov, A. V. Reactivity of Selectively Terminated Single Crystal Silicon Surfaces. *Chem. Soc. Rev.* **2010**, *39*, 3256–3274.
12. Gao, F.; Teplyakov, A. V. Challenges and Opportunities in Chemical Functionalization of Semiconductor Surfaces. *Appl. Surf. Sci.* **2017**, *399*, 375–386.
13. Tian, F.; Taber, D. F.; Teplyakov, A. V. NH-Termination of the Si(111) Surface by Wet Chemistry. *J. Am. Chem. Soc.* **2011**, *133*, 20769–20777.
14. Webb, L. J.; Nemanick, E. J.; Biteen, J. S.; Knapp, D. W.; Michalak, D. J.; Traub, M. C.; Chan, A. S. Y.; Brunschwig, B. S.; Lewis, N. S. High-Resolution X-ray Photoelectron Spectroscopic Studies of Alkylated Silicon(111) Surfaces. *J. Phys. Chem. B* **2005**, *109*, 3930–3937.
15. Webb, L. J.; Lewis, N. S. Comparison of the Electrical Properties and Chemical Stability of Crystalline Silicon(111) Surfaces Alkylated Using Grignard Reagents or Olefins with Lewis Acid Catalysts. *J. Phys. Chem. B* **2003**, *107*, 5404–5412.

16. Bansal, A.; Li, X. L.; Yi, S. I.; Weinberg, W. H.; Lewis, N. S. Spectroscopic Studies of the Modification of Crystalline Si(111) Surfaces with Covalently-Attached Alkyl Chains Using a Chlorination/Alkylation Method. *J. Phys. Chem. B* **2001**, *105*, 10266–10277.
17. Tian, F.; Teplyakov, A. V. Silicon Surface Functionalization Targeting Si-N Linkages. *Langmuir* **2013**, *29*, 13-28.
18. Rodríguez-Reyes, J. C. F.; Teplyakov, A. V. Role of Surface Strain in the Subsurface Migration of Adsorbates on Silicon. *Phys. Rev. B* **2008**, *78*, 165314-1-14.
19. Rodríguez-Reyes, J. C. F.; Teplyakov, A. V. Cooperative Nitrogen Insertion Processes: Thermal Transformation of NH₃ on a Si(100) Surface. *Phys. Rev. B* **2007**, *76*, 075348-1-16.
20. Gangarapu, S.; Pujari, S. P.; Alon, H.; Rijksen, B.; Sukenik, C. N.; Zuilhof, H. Effect of A-Heteroatoms on the Formation of Alkene-Derived Monolayers on H-Si(111): A Combined Experimental and Theoretical Study. *Langmuir* **2015**, *31*, 8318-8327.
21. Buriak, J. M. Organometallic Chemistry on Silicon and Germanium Surfaces. *Chem. Rev.* **2002**, *102*, 1271–1308.
22. Pujari, S. P.; Scheres, L.; Marcelis, A. T. M.; Zuilhof, H. Covalent Surface Modification of Oxide Surfaces. *Angew. Chem. Int. Ed.* **2014**, *53*, 6322-6356.
23. Widjaja, Y.; Mysinger, M. M.; Musgrave, C. B. Ab Initio Study of Adsorption and Decomposition of NH₃ on Si(100)-(2x1). *J. Phys. Chem. B* **2000**, *104*, 2527–2533.
24. Widjaja, Y.; Musgrave, C. B. A Density Functional Theory Study of the Nonlocal Effects of NH₃ Adsorption and Dissociation on Si(100)-(2x1). *Surf. Sci.* **2000**, *469*, 9-20.

25. Kubler, L.; Bischoff, J. L.; Bolmont, D. General Comparison of the Surface Processes Involved in Nitridation of Si(100)-2x1 by NH₃ and in Sin_x Film Deposition: A Photoemission Study. *Phys. Rev. B* **1988**, *38*, 13113–13123.
26. Rangelov, G.; Stober, J.; Eisenhut, B.; Fauster, T. NH₃ and No Interaction with Si(100)-(2x1) Surfaces. *Phys. Rev. B* **1991**, *44*, 1954–1957.
27. Perrine, K. A.; Lin, J.-M.; Teplyakov, A. V. Controlling the Formation of Metallic Nanoparticles on Functionalized Silicon Surfaces. *J. Phys. Chem. C* **2012**, *116*, 14431–14444.
28. Gao, F.; Teplyakov, A. V. Reaction of Hydrazine with a Chlorine-Terminated Si(111) Surface. *J. Phys. Chem. C* **2014**, *118*, 27998–28006.
29. Cui, Y.; Tian, F.; Gao, F.; Teplyakov, A. V. Building Organic Monolayers Based on Fluorinated Amines on the Si(111) Surface. *J. Phys. Chem. C* **2014**, *118*, 26721–26728.
30. Tian, F.; Cui, Y.; Teplyakov, A. V. Nitroxidation of H-Terminated Si(111) Surfaces with Nitrobenzene and Nitrosobenzene. *J. Phys. Chem. C* **2014**, *118*, 502–512.
31. Bocharov, S.; Teplyakov, A. V. Adsorption, Ordering, and Chemistry of Nitrobenzene on Si(100)-2x1. *Surf. Sci.* **2004**, *573*, 403–412.
32. Bocharov, S.; Mathauser, A. T.; Teplyakov, A. V. Adsorption and Thermal Chemistry of Nitroethane on Si(100)-2x1. *J. Phys. Chem. B* **2003**, *107*, 7776–7782.
33. Méndez De Leo, L. P.; Teplyakov, A. V. Nitro Group as a Means of Attaching Organic Molecules to Silicon: Nitrobenzene on Si(100)-2x1. *J. Phys. Chem. B* **2006**, *110*, 6899–6905.

34. Bocharov, S.; Dmytrenko, O.; Méndez De Leo, L. P.; Teplyakov, A. V. Azide Reactions for Controlling Clean Silicon Surface Chemistry: Benzylazide on Si(100)-2x1. *J. Am. Chem. Soc.* **2006**, *128*, 9300-9301.
35. Leftwich, T. R.; Teplyakov, A. V. Cycloaddition Reactions of Phenylazide and Benzylazide on a Si(100)-2x1 Surface. *J. Phys. Chem. C* **2008**, *112*, 4297-4303.
36. Cao, P.; Xu, K.; Heath, J. R. Azidation of Silicon(111) Surfaces. *J. Am. Chem. Soc.* **2008**, *130*, 14910–14911.
37. Leftwich, T. R.; Madachik, M. R.; Teplyakov, A. V. Dehydrative Cyclocondensation Reactions on Hydrogen-Terminated Si(100) and Si(111): An Ex Situ Tool for the Modification of Semiconductor Surfaces. *J. Am. Chem. Soc.* **2008**, *130*, 16216-16223.
38. Perrine, K. A.; Leftwich, T. R.; Weiland, C.; Madachik, M. R.; Opila, R. L.; Teplyakov, A. V. Reactions of Aromatic Bifunctional Molecules on Silicon Surfaces: Nitrosobenzene and Nitrobenzene. *J. Phys. Chem. C* **2009**, *113*, 6643–6653.
39. Amy, S. R.; Michalak, D. J.; Chabal, a. Y. J.; Wielunski, L.; Hurley, P. T.; Lewis, N. S. Investigation of the Reactions During Alkylation of Chlorine-Terminated Silicon (111) Surfaces. *J. Phys. Chem. C* **2007**, *111*, 13053–13061.
40. Seo, J.; Kim, H. J.; Pekarek, R. T.; Rose, M. J. Hybrid Organic/Inorganic Band-Edge Modulation of *P*-Si(111) Photoelectrodes: Effects of R, Metal Oxide, and Pt on H₂ Generation. *J. Am. Chem. Soc.* **2015**, *137*, 3173-3176.
41. Holubová, B.; Čiovák, Z. Z.; KucEROVÁ I.; Zlámal, M. Weatherability of Hybrid Organic–Inorganic Silica Protective Coatings on Glass. *Prog. Org. Coat.* **2015**, *88*, 172–180.

42. Tao, F.; Wang, Z. H.; Lai, Y. H.; Xu, G. Q. Attachment of Styrene and Phenylacetylene on Si(111)-7x7: The Influence of Substitution Groups on the Reaction Mechanism and Formation of Π -Conjugated Skeletons. *J. Am. Chem. Soc.* **2003**, *125*, 6687-6696.
43. Rodríguez-Reyes, J. C. F.; Teplyakov, A. V. Chemistry of Diffusion Barrier Film Formation: Adsorption and Dissociation of Tetrakis(Dimethylamino)Titanium on Si(100)-2x1. *J. Phys. Chem. C* **2007**, *111*, 4800-4808.
44. Mui, C.; Wang, G. T.; Bent, S. F.; Musgrave, C. B. Reactions of Methylamines at the Si(100)-2x1 Surface. *J. Chem. Phys.* **2001**, *114*, 10170-10180.
45. Schwartz, M. P.; Hamers, R. J. The Role of Π -Conjugation in Attachment of Organic Molecules to the Silicon (001) Surface. *Surf. Sci.* **2002**, *515*, 75-86.
46. Chabal, Y. J.; Harris, A. L.; Raghavachari, K.; Tully, J. C. Infrared Spectroscopy of H-Terminated Silicon Surfaces. *International journal of modern physics. B, Condensed matter physics, statistical physics, applied physics* **1993**, *07*, 1031-1078.
47. Ellison, M. D.; Hamers, R. J. Adsorption of Phenyl Isothiocyanate on Si(001): A 1,2-Dipolar Surface Addition Reaction. *J. Phys. Chem. B* **1999**, *103*, 6243-6251.
48. Harada, Y.; Koitaya, T.; Mukai, K.; Yoshimoto, S.; Yoshinobu, J. Spectroscopic Characterization and Transport Properties of Aromatic Monolayers Covalently Attached to Si(111) Surfaces. *J. Phys. Chem. C* **2013**, *117*, 7497-7505.
49. Costa, G.; Camus, A.; Gatti, L.; Marsich, N. On Phenylcopper. *J. Organomet. Chem.* **1966**, *5*, 568-572.
50. Xi, M.; Bent, B. E. Iodobenzene on Cu(111): Formation and Coupling of Adsorbed Phenyl Groups. *Surf. Sci.* **1992**, *278*, 19-32.

51. Xi, M.; Yang, M. X.; Jo, S. K.; Bent, B. E.; Stevens, P. Benzene Adsorption on Cu(111): Formation of a Stable Bilayer. *J. Chem. Phys.* **1994**, *101*, 9122-9131.
52. Queeney, K. T.; Weldon, M. K.; Chang, J. P.; Chabal, Y. J.; Gurevich, A. B.; Sapjeta, J.; Opila, R. L. Infrared Spectroscopic Analysis of the Si/SiO₂ Interface Structure of Thermally Oxidized Silicon. *J. Appl. Phys.* **2000**, *87*, 1322-1330.
53. Nemanick, E. J.; Hurley, P. T.; Webb, L. J.; Knapp, D. W.; Michalak, D. J.; Brunschwig, B. S.; Lewis, N. S. Chemical and Electrical Passivation of Single-Crystal Silicon(100) Surfaces through a Two-Step Chlorination/Alkylation Process. *J. Phys. Chem. B* **2006**, *110*, 14770–14778.
54. Miller, T.; Teplyakov, A. V. Attachment Chemistry of PCBM to a Primary-Amine-Terminated Organic Monolayer on a Si(111) Surface. *Langmuir* **2014**, *30*, 5105-5114.
55. Liu, Y.; Chen, J.; Teplyakov, A. V. Chemical Passivation Processes for Biofunctionalization Schemes on Semiconductors Surfaces. *Langmuir* **2012**, *28*, 15521-15528.
56. Zhang, X.; Antonopoulos, I. H.; Kumar, S.; Chen, J.; Teplyakov, A. V. Tuning the Geometry of Shape-Restricted DNA Molecules on the Functionalized Si(111) *Appl. Surf. Sci.* **2009**, *256*, 815-818.
57. Zhang, X.; Teplyakov, A. V. Adsorption of C₆₀ Buckminster Fullerenes on an 11-Amino-1-Undecene-Covered Si(111) Substrate. *Langmuir* **2008**, *24*, 810-820.
58. Wittberg, T. N.; Hoenigman, J. R.; Moddeman, W. E.; Cothorn, C. R.; Gullett, M. R. AES and XPS of Silicon Nitride Films of Varying Refractive Indices. *J. Vac. Sci. Technol.* **1978**, *15*, 348-352.

59. Leftwich, T. R.; Teplyakov, A. V. Calibration of Computationally Predicted N *1s* Binding Energies by Comparison with X-ray Photoelectron Spectroscopy Measurements. *J. Electron Spectrosc. Relat. Phenom.* **2009**, *175*, 31–40.
60. Haber, J. A.; Lewis, N. S. Infrared and X-ray Photoelectron Spectroscopic Studies of the Reactions of Hydrogen-Terminated Crystalline Si(111) and Si(100) Surfaces with Br₂, I₂, and Ferrocenium in Alcohol Solvents. *J. Phys. Chem. B* **2002**, *106*, 3639–3656.

Chapter 5

CARBON NANOTUBES COVALENTLY ATTACHED TO FUNCTIONALIZED SURFACES DIRECTLY THROUGH THE CARBON CAGE

5.1 Introduction

Since the initial identification and reports on carbon nanotubes,¹⁻² their properties have spurred a flurry of intense studies due to their unique structure and characteristics. The chemical reactivity, as well as the optical, mechanical, and electronic properties of carbon nanotubes (CNTs), have resulted in integration of these materials into various fields and applications, including sensors,³⁻⁵ nanoelectronic devices,⁶ hydrogen storage,⁷⁻⁸ and field emission devices.⁹⁻¹⁰ For such applications, the ability to control and fine-tune the attachment and placement of carbon nanotubes onto a solid substrate is necessary.

The immobilization of CNTs onto gold substrates, typically following the formation of alkylthiol self-assembled monolayers (SAMs), has been amply reported in literature. In several cases, the presence of carboxylic acid functionality is utilized to anchor the CNTs to the thiolated gold surface via condensation or amide formation.¹¹⁻¹³ The long-term stability of the CNT-substrate interface involving thiol-gold linkages may be a concern, however, due to thermal instability and photooxidation of the SAM.¹⁴ For applications in which these challenges may pose problems, the gold-thiol interface can be circumnavigated by the sturdy attachment of CNTs onto silicon substrates. Several examples in the literature highlight CNT

attachment to amine- or hydroxyl-modified silicon surfaces.¹⁵⁻¹⁷ In order to avoid the layer of oxidized silicon, alternative methods involving the direct hydrogenation of silicon followed by modification with aliphatic alkenes for further reaction with carbon nanotubes have been proposed.¹⁸ Examples of the attachment of carbon nanotubes to other surface materials, such as polymers¹⁹ and ITO glass,²⁰ have also been reported in literature.

Thus, most of the methods in literature describing the covalent attachment of carbon nanotubes rely on interactions between the substrate surface species and functional groups (e.g. carboxylic acid) on the carbon nanotubes. In most cases, the functional group is present only on the ends of the CNTs, rather than along the length (with the exception of defects). This is ideal for applications in which vertically-aligned CNT assemblies are desired; however, in cases where a very high degree of intimate covalent contact is required between the CNTs and substrate, bonding between the substrate and the cage of the CNT may be sought instead. It has been shown that electron transfer through CNTs attached to a gold substrate via self-assembled monolayers is influenced by electrons tunneling through the SAMs.²¹ The presence of functional groups bound to a carbon nanotube can also impact the charge transport through the CNT, depending on the nature of the bonding involved.²²⁻²³ These changes are desired in some cases, such as in chemical sensor development;²⁴ in other cases, however, it may be preferable for the intrinsic electronic properties of the nanotube to be preserved.

Interestingly, the surfaces of CNTs are relatively rarely the subject of direct chemical modification. The inner surfaces of nanotubes are considered to be inert, and in fact these materials are commonly used to provide the “cage effect” for highly

controlled processes inside the nanotubes.²⁵⁻²⁷ On the other hand, a number of adsorbates have been shown to react with the outside surface of CNTs.²⁸⁻³¹ The question is whether the reactivity of the outer surface of carbon nanotubes without additional chemical functionalities could be explored to staple them covalently to chemically functionalized surfaces. This approach has been suggested for similar systems.³² The covalent bonding between the cage of a C₆₀ buckyball and solid flat semiconductor substrates has been reported and reviewed in detail,³³⁻³⁶ with one of the examples of such interactions involving the direct attachment of the C₆₀ and amine-terminated self-assembled monolayers.³⁷⁻³⁹ In another study, the attachment of [6,6] phenyl-C₆₁-butyric acid methyl ester (PCBM), structurally similar to the buckyball, to an amine-modified silicon surface showed that while both attachment through the ester to form an amide and attachment through the cage to form a secondary amine are viable, the latter is actually more favorable.⁴⁰ It stands to reason then, that direct attachment of carbon nanotubes through the cage, regardless of the presence or absence of other functional groups, might occur in a similar manner, in addition to the expected attachment through those functional groups. In this thesis, the attachment of non-functionalized carbon nanotubes to amine-modified gold and silicon substrates, as summarized in Figure 5.1, is demonstrated. Microscopic techniques confirm the presence of the CNTs on the surfaces after washing and sonication to remove physically adsorbed CNTs. X-ray photoelectron spectroscopy (XPS), coupled with density functional theory (DFT) calculations, are used to evaluate the chemistry of the system. Full computational mechanistic studies are not presented here although similar chemistry on the C₆₀ system has been reported.⁴⁰ Unlike the C₆₀ system, the final point for analyzing CNT attachment chemistry is not well-defined. Nevertheless, further

computational investigation is ongoing. Finally, time-of-flight secondary ion mass spectrometry (ToF-SIMS) is used to identify fragments from CNT attachment to the surface and to compare attachment of non-functionalized CNTs and carboxylic acid-functionalized CNTs to these surfaces.

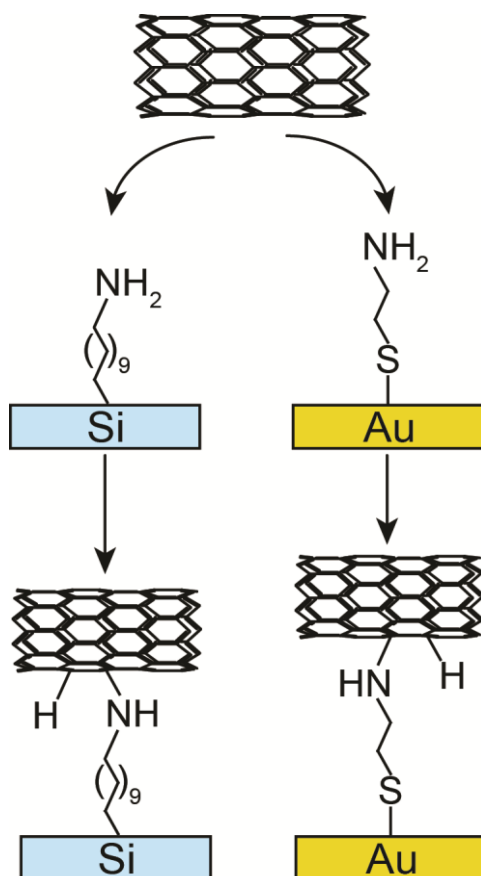


Figure 5.1 Summary of the direct attachment of carbon nanotubes to amine-functionalized silicon and gold surfaces through the CNT cage

5.2 Results and discussion

In order to provide a reliable and straightforward method for covalent bonding of carbon nanotubes to functionalized surfaces directly through the nanotube cage, it is

important to confirm that carbon nanotubes are present on a surface following the procedure, that they are deposited at a submonolayer coverage, that their binding is covalent and that the presence of surface functional groups on carbon nanotubes is not needed for this deposition but rather that the binding occurs via chemical reactions of the pre-functionalized substrate surface with the cage of the carbon nanotube directly. In order to address the first part of the process, microscopic techniques, including SEM, TEM, and AFM will be applied. The feasibility of a direct covalent link between the substrate and cage of the carbon nanotube will be investigated with DFT computational methods, and to confirm and analyze the covalent binding, XPS and ToF-SIMS will be applied.

5.2.1 Confirmation of Nanotube Presence on the Surface

Drop-casting methods are commonly used to deliver a variety of materials to the surface, and in this work the same approach is used. However, in order to remove the multilayers and bundles of nanotubes and to zero in on the nanotubes strongly bound to the surface, sonication is utilized. In order to confirm that the nanotubes remain on the surface following the sonication process, SEM was used to compare the surfaces before and after this preparation step. Figures 5.2(a) and 5.2(b) show the amine-terminated silicon surface before the addition of the CNT-NF. Following the reaction, SEM clearly confirms the presence of the nanotubes, as can be observed in Figures 5.2(c) and 5.2(d). Likewise, the presence of COOH-CNT can be observed on the surface following the deposition and sonication, as demonstrated in Figures 5.2(e) and 5.2(f).

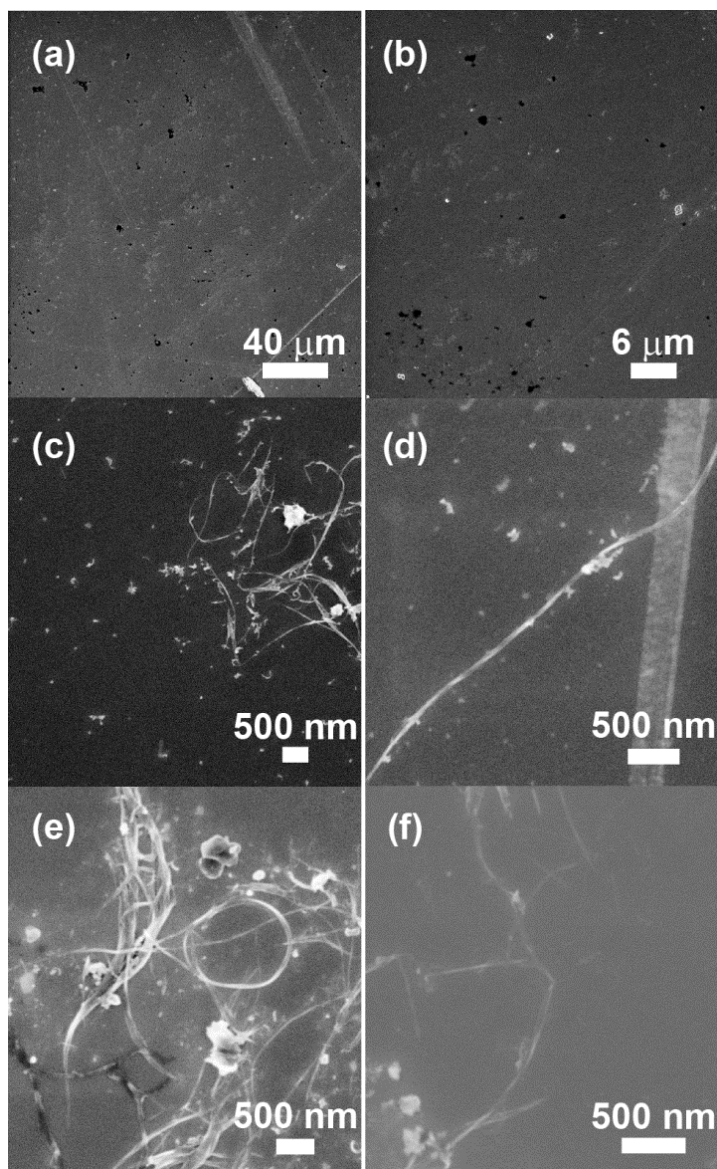


Figure 5.2 SEM micrographs of the amine-modified silicon surface before (a) and after reaction with the NF-CNT (c) and COOH-CNT (e). Images (b), (d), and (f) show a close-up view of the surface before the reaction, and following reaction with the NF-CNT and COOH-CNT, respectively.

Similar results are obtained in Figure 5.3 for the amine-modified gold surface. It is apparent from the SEM images in both Figure 5.2 and Figure 5.3 that carbon

nanotubes can be deposited on the functionalized surface and that following the sonication process, both gold and silicon surfaces retain small but reproducible coverages of both functionalized and non-functionalized nanotubes. It also appears that the nature of the substrate does not play a substantial role in the coverage of either functionalized or non-functionalized nanotubes following the sonication step. It needs to point out that, to confirm the preparation procedure described in Chapter 2 does not induce the reaction with a chemically inert monolayer, a control experiment with the CNT reaction with (t-BOC)-protected AUD was performed, and the resulting SEM micrographs confirming this assessment are displayed in Figure 5.4. SEM image of a control sample in which (5.4a) the silicon functionalized with (t-BOC)-protected AUD was allowed to sonicate in the non-functionalized CNT solution for 3 hours, followed by washing in several solvents. Image 5.4(b) shows, for reference, the test sample corresponding to this control in which the AUD has been de-protected, resulting in the amine-terminated silicon surface.

However, SEM does not indicate the type of binding between the nanotubes and the surfaces; neither does it confirm the presence of individual nanotubes or monolayers of nanotubes due to the resolution limit of the instrument. The manufacturer specifications for the diameters of the nanotubes (1-4 nm) suggest that alternative analytical techniques must be used to verify that individual carbon nanotubes are in sufficient enough contact with the surface to interact covalently.

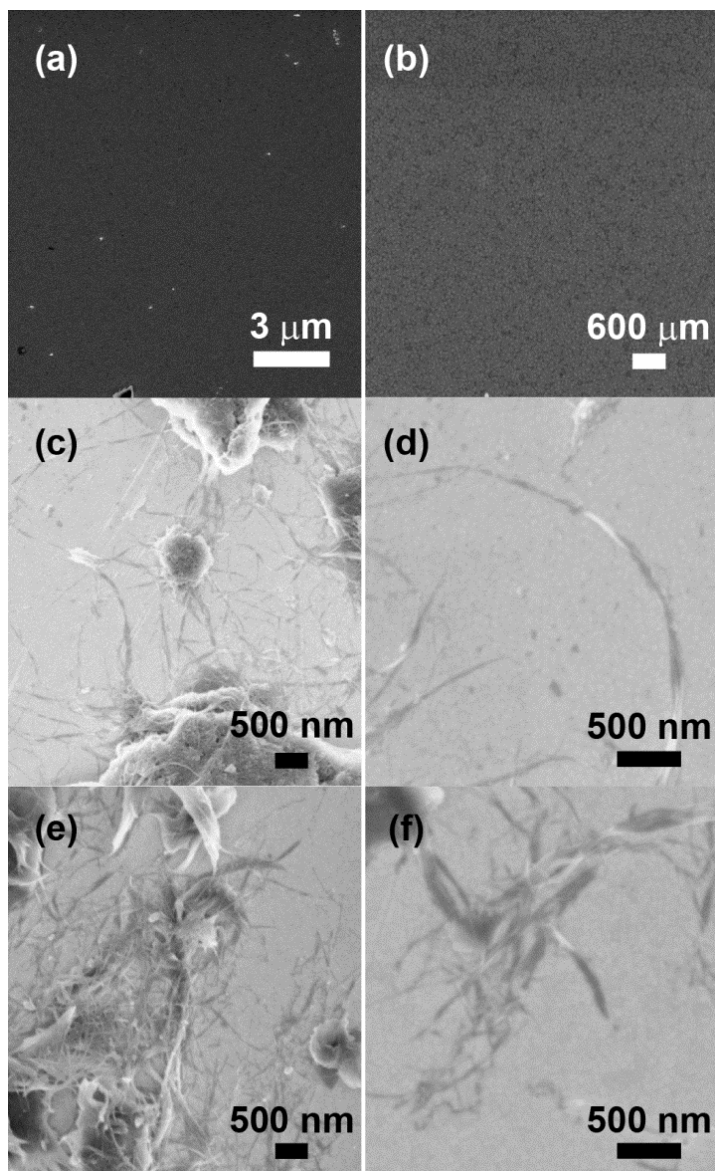


Figure 5.3 SEM micrographs of the amine-modified gold surface before (a) and after reaction with the NF-CNT (c) and COOH-CNT (e). Images (b), (d) and (f) show a close-up view of the surface before reaction, and following the reaction with the NF-CNT and COOH-CNT, respectively.

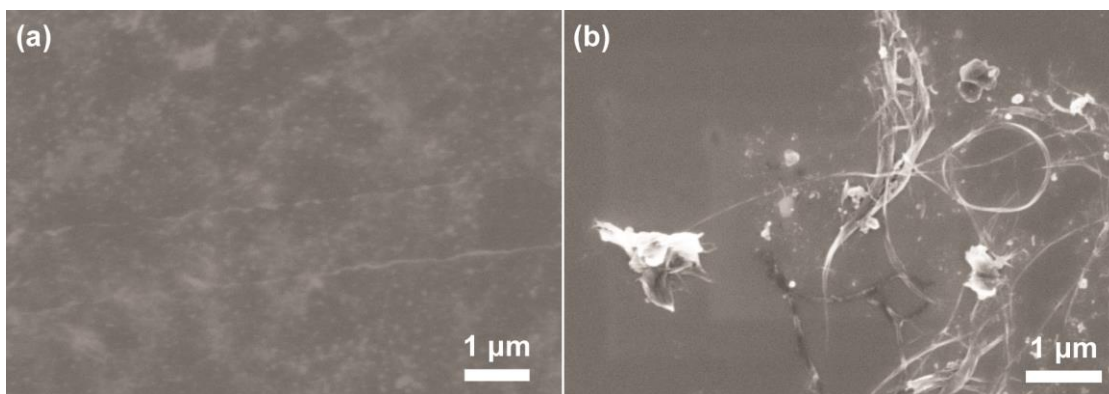


Figure 5.4 SEM micrographs of (a) (t-BOC)-protected AUD-terminated silicon surface and (b) amine-terminated silicon surface after sonication in the NF-CNT solution for 3 hours.

5.2.2 Submonolayer Coverage of Nanotubes on the Functionalized Substrate Surfaces

In order to verify the expected diameter of the carbon nanotubes, transmission electron microscopy was used to closely examine an individual bundle of nanotubes. The average diameter of the non-functionalized carbon nanotubes was calculated to be 1.7 nm from the TEM micrograph shown in Figure 5.5(a), which is consistent with the diameter reported by the manufacturer. Atomic force microscopy was then used to observe the AUD-modified silicon following its reaction with the NF-CNTs and compare it to the AUD-modified silicon surface without introducing nanotubes. Figure 5.5(b) shows the flat surface of the amine-terminated silicon whereas Figures 5.5(c) and 5.5(d) show the same surface following its reaction with the CNT. The features present in these micrographs indicate that individual carbon nanotubes can be identified on the surface. Indeed, the height of these features, compared to the manufacturer-reported and TEM-confirmed CNT diameters, confirms that the features

correspond to individual carbon nanotubes several hundreds of nanometers in length. The line profile shows that the heights of the CNTs observed in Figure 5.5(d), approximately 1.5 nm, are fully consistent with the sizes of individual nanotubes. It is noteworthy that at a junction where two nanotubes appear to cross-over in Figure 5.5(d), the observed height, about 3 nm, is double that of an individual CNT. Thus, AFM investigation is used to identify individual carbon nanotubes but more importantly, it demonstrates that these individual CNTs lie in intimate contact with the surface, which provides ample opportunities for the surface amine moieties to interact directly with the carbon nanotube cage. Thus, chemical identification techniques can be used to confirm this binding.

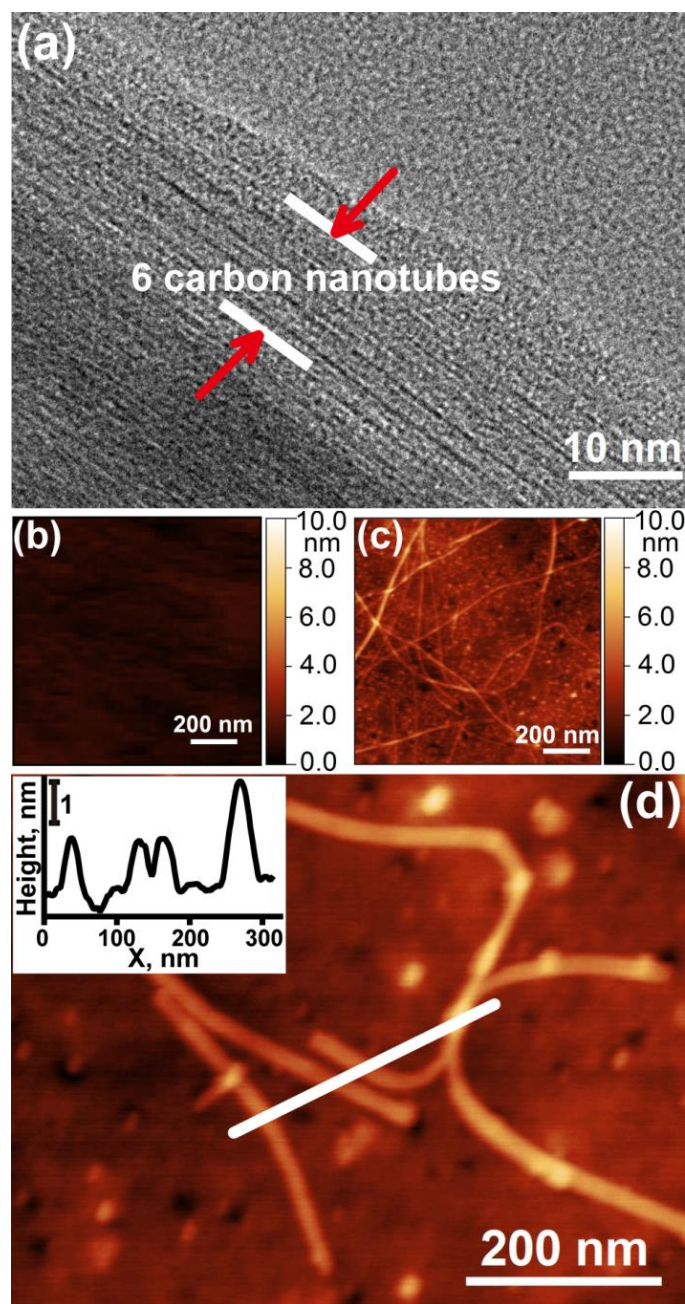


Figure 5.5 TEM (a) confirmation of carbon nanotube diameter, that is in agreement with manufacturer specification. AFM micrographs of (b) AUD-modified silicon surface and (c,d) AUD-modified silicon surface following reaction with NF-CNTs. The line profile of the white line in (d) shows the height of the CNTs.

5.2.3 Spectroscopic Evidence of Covalent Binding between Functionalized Surfaces and CNTs

X-ray photoelectron spectroscopy was used to study the surface chemistry of carbon nanotubes on amine-functionalized silicon and gold surfaces. Since the main spectroscopic signature is based on the chemical environment of the nitrogen atom of the functionalized organic layer as it reacts with the carbon nanotubes, Figure 5.6 compares the XPS results in the N *1s* region for the gold and silicon surfaces before, and after, reaction with the non-functionalized carbon nanotubes. It is obvious that the nominally non-functionalized carbon nanotubes contain a number of defect sites that are essentially the same as those for the functionalized CNTs, thus in probing the reaction of the NF-CNTs described in this section, it will be important to distinguish the chemical pathways that involved these defect sites from those that could be associated with the reaction directly through the cage of a CNT. The N *1s* spectrum in Figure 5.6(b) for the AUD-modified silicon substrate shows the main feature at 399.5 eV that represents the majority -NH_2 species and a smaller peak around 402 eV that is likely oxidized nitrogen species because the samples were transferred to the XPS in ambient conditions. These assignments are based on the previous investigations of amino-terminated organic monolayers³⁹⁻⁴² and are in a good agreement with the computational studies presented for the model systems provided in Figure 5.6, denoted by green lines below the spectra. If this spectrum is compared to that obtained following the reaction with the non-functionalized carbon nanotubes (5.6a), the large feature (which now represents a mixture of -NH_2 and -NH- species) shifts the overall binding energy by about 0.5 eV and a smaller peak around 397.5 appears. The 0.5 eV shift is fully consistent with the formation of the -NH- species by a direct covalent binding of the terminal amine of the organic layer on a substrate surface with the cage

of carbon nanotubes by a direct attachment process. This assessment is also supported by the computational investigation of the N *1s* shift following such a reaction, as summarized in Figure 5.6.

The small feature at 397.5 eV could be explained by a side reaction where nitrogen is inserted into an aromatic system of the cage structure (likely at defect sites), and the obtained binding energy is in agreement with previous investigations of similar systems reported in literature⁴³ and with the density functional theory investigations of several model systems summarized in the Appendix section. The small peak around 402 eV is a combination of oxidized nitrogen and it very likely is covering a feature indicating amide formation due to defects on the carbon nanotubes. However, a direct assignment of this feature is not possible based on these data alone. The system of cysteamine on gold, both before (5.6d) and after (5.6c) reaction with non-functionalized carbon nanotubes shows very similar spectra, with the largest peak around 399.5 eV shifting up by 0.5 eV following the reaction with the carbon nanotubes, and smaller peaks at 397 eV and 402 eV, which can be assigned similarly to the assignment provided above for the silicon system. The 0.5 eV binding energy shift following amine interactions with the carbon nanotube is in agreement with predicted N *1s* core-level energies from density functional theory calculations that were performed separately for the gold and silicon substrate systems.

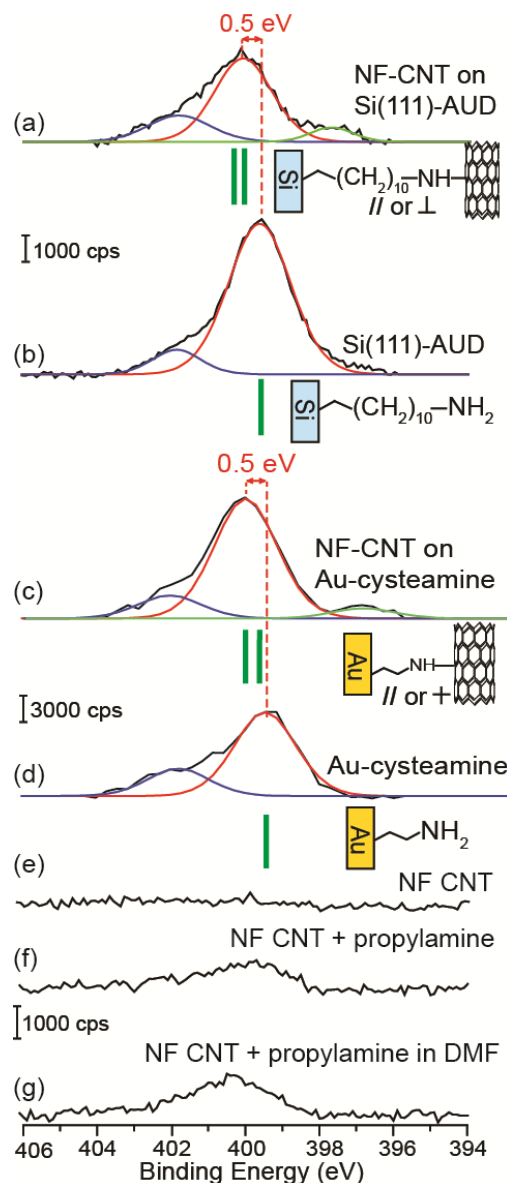


Figure 5.6 XPS investigation of the N $1s$ spectral region of AUD-modified silicon surface before (b) and after (a) reaction with the NF-CNTs, and cysteamine-modified gold surface before (d) and after (c) reaction with the NF-CNTs. Spectra of control experiments compare (e) NF-CNT powder, (f) NF-CNT reacted with neat propylamine, and (g) NF-CNT reacted with propylamine in DMF. The green bars underneath the spectra indicate the expected binding energies for selected systems, predicted by density functional theory calculations. The presence of two DFT-predicted binding energies below spectra (a) and (c) indicate the expected values for the N $1s$ energies in a geometry in which the amine dissociates across a C=C bond parallel to the direction of the CNT and one in which the amine dissociates across a C=C bond that is not parallel to the direction of the CNT.

To account for different possibilities of amine attachment to the CNT cage, the positions of the N *1s* features were compared for two different types of geometries: one in which the amine dissociates across the bond that is parallel to the CNT, and the other, in which the amine dissociates across a C=C bond that is not parallel to the direction of the nanotube. The calculated binding energies of these two possible geometries are not identical, but are very close to one another. The predicted binding energies are indicated by the green bars underneath the spectra in Figure 5.6. A complete list of model systems with several different diameters of CNTs is provided in the Supporting Information section. The main conclusions that can be drawn from this set of studies are that the chemistry of the local environment of surface amino-groups changes upon the substrate interacting with the carbon nanotubes and that neither the nature of the substrate itself nor the organic linker appear to influence the chemistry of the amino-termination with the carbon nanotubes. All of the comparisons provided in Figure 5.6 are consistent with the reaction of the amino-functionality of the surface with carbon nanotubes directly via the attachment through the carbon cage; however, in order to confirm this, better understanding of the reaction conditions and specific identification of the surface species produced is needed.

A series of control experiments were performed to confirm the nature of the nitrogen species observed following surface attachment of carbon nanotubes. First, Figure 5.6(e) shows that the non-functionalized carbon nanotube powder analyzed, as received, exhibits no features in the N *1s* spectral region. Thus, the N *1s* features recorded are solely the signatures of the nitrogen species originating from the functionalized surface. To make sure that the reactivity is based on the -NH_2

attachment, the carbon nanotubes were allowed to sonicate with neat propylamine and with propylamine in DMF solvent for three hours (the same reaction conditions as with the amine-terminated substrates); after washing to remove unreacted propylamine and solvent, they were dried and analyzed via XPS. The CNTs reacted with neat propylamine (5.6f) and with propylamine in DMF (5.6g) show the presence of nitrogen. From the comparison of the peak positions of the spectra 5.6(f) and 5.6(g) with those for amino-functionalized surfaces in Figures 5.6(a) and 5.6(c), it is clear that the reactions result in the formation of similar species in all the cases and that this reaction corresponds to the upward shift of the binding energy of the surface primary amino group. Of course, the differences in intensity and the presence of other features in the surface spectra can be related to the different geometry of interaction, where neat propylamine or propylamine in a solvent would have easy access to all the functionalities and the entire surface of carbon nanotubes, while the amino-functionalized surfaces could not possibly react all the surface amino groups with submonolayer coverages of carbon nanotubes, and at the same time, the reactivity of the surface could influence the efficiency of the entire process. For example, the carbon nanotube that is efficiently immobilized on an amino-functionalized surface could produce additional linkages via sequential attachment reactions.

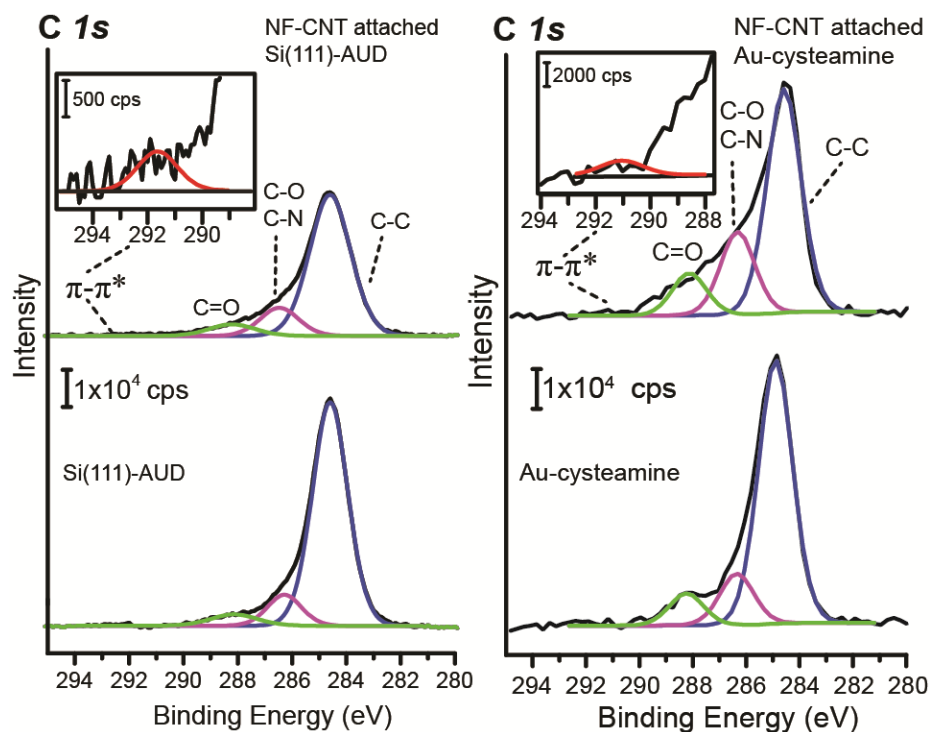


Figure 5.7 Summary of C *1s* spectral region of the XPS studies of carbon nanotube reaction with 11-amino-1-undecene-modified Si surface and cysteamine-covered Au surface.

Overall, the XPS results suggest four important points: 1) the nitrogen observed in these experiments originates only from the amine-modified silicon and gold substrates and not from impurities in CNTs or from interactions with a solvent, 2) the surface chemistries on the silicon and gold systems are very similar to one another, 3) the interaction between the surface and the carbon nanotubes results in a chemical change, and 4) the spectroscopic signature of the surface species formed is consistent with the direct attachment of surface amino groups to the cage of the carbon nanotubes; however, the nature of this bonding has to be confirmed independently. It should also be pointed out that the C *1s* spectral region has also been scrutinized in this thesis. The resulting spectra are presented in Figure 5.7; however, because of the

presence of organic monolayer and because of a brief exposure to ambient conditions during sample transfer, the detailed quantitative assignment of all the observed features is not practical. Nevertheless, there are indeed noticeable changes in the C 1s spectral regions on both gold and silicon surfaces following attachment of the NF-CNTs and the π - π^* shake-up suggests that aromatic structures are attached in the process, fully consistent with the results of microscopy studies described above.

5.2.4 Confirmation that Attachment through the Cage is Energetically Feasible

Computational investigations utilizing density functional theory were undertaken to determine whether covalent binding between the CNT cage and modified substrate is possible. Modified model substrates (gold and silicon) and (10,0) carbon nanotubes were modeled and optimized, and the energies of different covalent bonding configurations were computed. CNTs with three different radii (but with identical geometries otherwise) were chosen to compare radius effects on covalent binding to the flat substrate. Two types of binding between the substrate and the cage were considered (and described above): “Parallel” and “non-parallel” to the longitudinal direction of the CNT. The relative energy (ΔE) of each configuration is compared to its initial optimized components (CNT and amine-terminated substrate). Figure 5.8 summarizes these relative energies for the CNTs on gold. The attachment of the smallest radius CNT is exothermic for the parallel configuration, but slightly endothermic for the non-parallel structure. In contrast, the ΔE for the two larger radii CNTs are endothermic for both geometries, with the smaller ΔE belonging to the non-parallel arrangement. This contrast is likely due to the differences in the radius of

curvature and thus in the strain of the resulting adducts. For the smaller radius CNT, the carbons that make up the π -bond that interacts with the substrate amine are not in the same plane and do not greatly interfere with one another. As the radius increases, these carbon atoms in the cage become more similar to those in the graphene sheet. These relative energies suggest that, while some energy input is required to bind the surface to the CNT cage, this interaction is feasible. Very similar results were obtained for calculations on the silicon surface and are summarized in Table 5.1 as below, with the differences largely arising from the description of the cluster models for gold and silicon surfaces rather than from the geometrical differences of the structures resulting from attachment of an amine functional group to the cage of the carbon nanotube. The computational studies suggest that this type of attachment is possible, but in order to experimentally confirm this, further spectroscopic investigation must be performed.

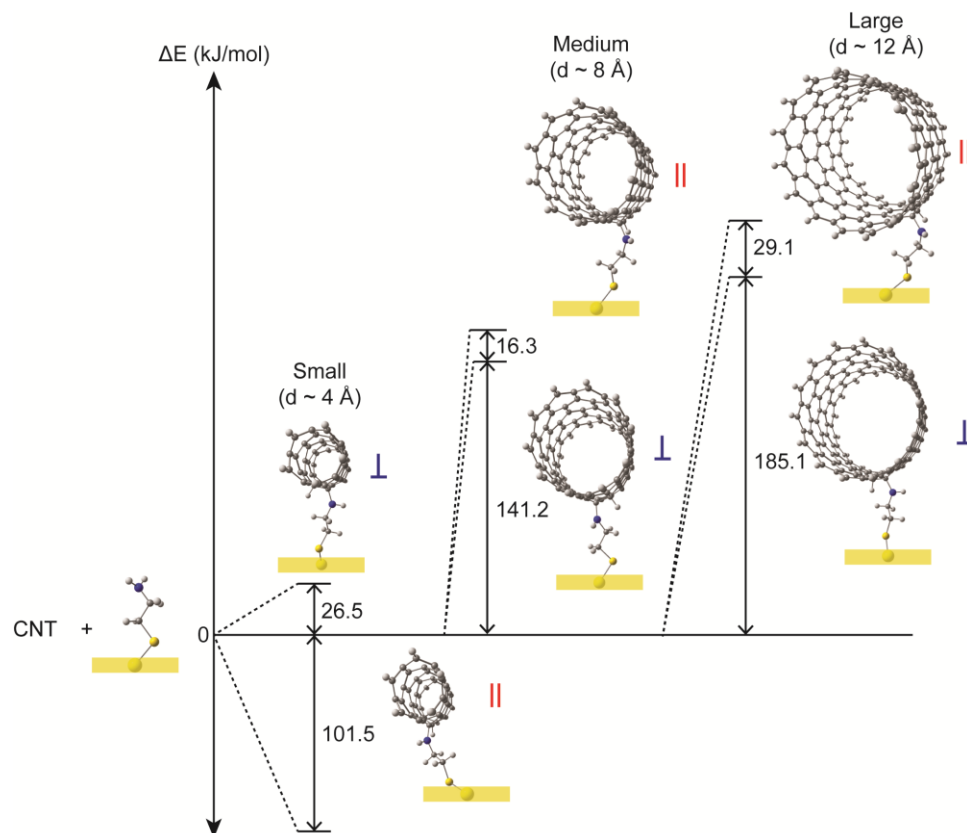


Figure 5.8 Relative energies of parallel and non-parallel (denoted in red and blue) attachment configurations on cysteamine-modified gold surfaces for CNTs with radii of different sizes.

Table 5.1 Relative energies for covalent CNT interactions on the silicon and gold substrates

CNT Size	Attachment ΔE (kJ/mol)		⊥ Configuration ΔE (kJ/mol)	
	Silicon	Gold	Silicon	Gold
Small (d ~ 4 Å)	-105.0	-101.5	-31.5	26.5
Medium (d ~ 8 Å)	151.0	157.5	134.1	141.2
Large (d ~ 12 Å)	210.1	214.2	180.0	185.1

5.2.5 Evidence of Covalent Attachment through the Cage

ToF-SIMS was used to identify specific fragments associated with attachment on the surface. Due to the complex nature of the carbon nanotube system and all the fragments possible, the assessment of the covalent attachment of carbon nanotubes on the surfaces is very difficult. This is even more complicated in the case of the silicon substrate due to the long carbon AUD chain and three stable isotopes of silicon. On the other hand, using a gold substrate may simplify the fragment assignments since a single gold isotope provides an excellent marker for such a complex system. At the same time, as described above in the XPS investigation, the attachment chemistry is essentially identical on amino-terminated gold and silicon substrates. Thus, the ToF-SIMS analysis presented below is focused on gold substrates.

Figure 5.9 shows the ToF-SIMS spectra for the $[\text{Au-S-(CH}_2)_2 \text{ N}]^+$ fragment expected at 270.973006 m/z . The corresponding m/z features are not observed for carboxylic acid-functionalized or the non-functionalized carbon nanotubes (5.9e and 5.9f, respectively), as is expected. However, a very prominent peak is observed for the cysteamine-terminated gold (5.9d). The same peak is observed for the amino-terminated samples following their reaction with COOH-CNTs and with NF-CNTs (5.9a and 5.9b, respectively). This is expected because all the cysteamine-modified gold surfaces should contain this fragment even after their reaction with carbon nanotubes.

A control sample was prepared by modifying a gold substrate with dimethylamino ethanethiol and allowing it to react with the NF-CNTs; this spectrum can be observed in Figure 5.9c. In this case, the methyl groups on the dimethylamino ethanethiol should protect the amine from chemically interacting with the carbon nanotubes during sonication. The spectrum from this sample also shows a peak for the

$[\text{Au-S-(CH}_2)_2\text{ N}]^-$ fragment, which is expected. This confirms that all the gold substrates are successfully functionalized with their respective amine-containing molecules.

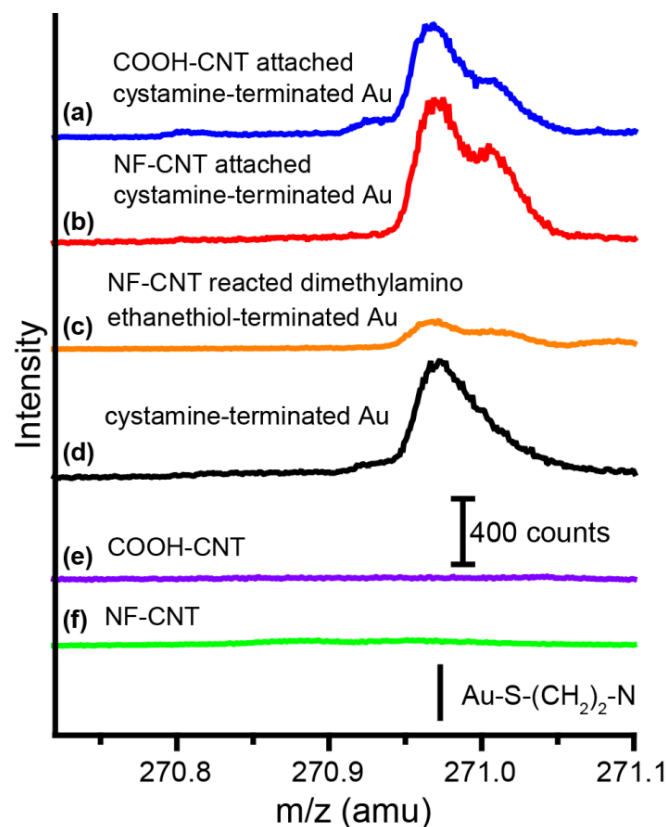


Figure 5.9 ToF-SIMS spectra in the region of the $[\text{Au-S-(CH}_2)_2\text{ N}]^-$ fragment, which is indicative of successful modification of the substrate with cysteamine or dimethylamino-ethanethiol. Features are absent in the case of the carbon nanotube powders (e, f), but can be observed for this peak on the cysteamine-terminated gold before (d) and after reaction with both the COOH-CNTs and NF-CNTs (a, b), and on the dimethylamino ethanethiol-terminated gold (c). The black bar below the spectra indicates the exact m/z position expected for the fragment.

The spectra in the region of the $[\text{Au-S-(CH}_2)_2\text{NH-C}_5]^+$ fragment at 331.980830 m/z are summarized in Figure 5.10 and correspond to cysteamine attached to the substrate and a five-carbon fragment of the carbon nanotube. As expected, no peaks at this m/z position are observed for the carbon nanotube powders (5.10e, 5.1-f), or for the cysteamine-modified gold (5.10d). A prominent feature corresponding to this fragment is observed for the cysteamine-terminated gold following its reaction with the carbon nanotubes (5.10a, 5.10b). By itself, this observation would be insufficient to conclude that the carbon nanotubes are covalently bound to the surface in this case; however, the control sample with dimethylamino ethanethiol (5.10c), which should prevent covalent bonding of carbon nanotubes to the surface amine group, does not exhibit this feature. This suggests that the five-carbon fragment from the carbon nanotubes is actually bound to the cysteamine through the primary amine.

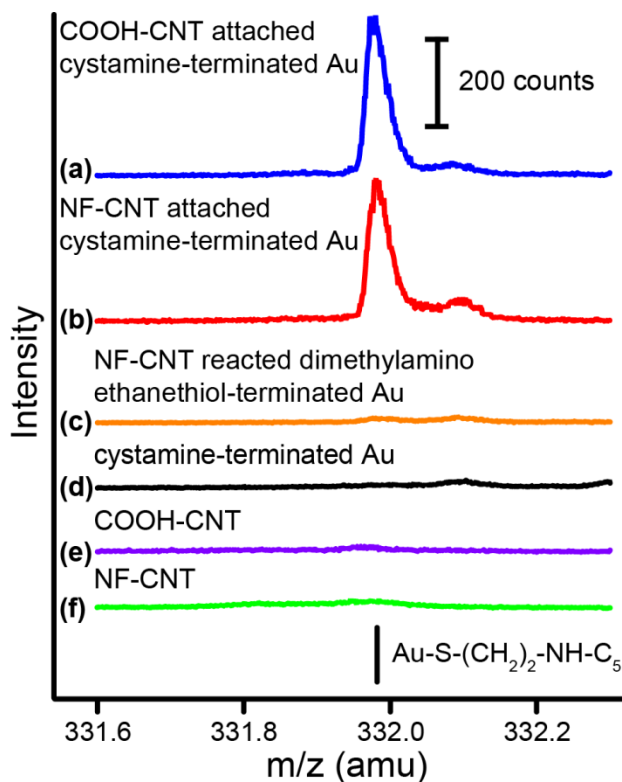


Figure 5.10 ToF-SIMS spectra in the region of the $[\text{Au-S-(CH}_2)_2 \text{NH-C}_5]^-$ fragment, which is indicative of cysteamine bound to the substrate and to a five-carbon fragment of a carbon nanotube. Features are absent in the case of the samples without the substrate (e, f), on the cysteamine-terminated gold before reaction (d), and the control sample (c), but can be observed after reaction with both the COOH-CNTs and NF-CNTs (a, b). The black bar below the spectra indicates the exact m/z position expected for the fragment.

The next set of experiments explores whether it could be concluded that the binding through the surface amino-group requires participation of the carboxylic acid of the functionalized carbon nanotubes or the participation of the defect sites of the non-functionalized carbon nanotube. Figure 5.11 shows the ToF-SIMS spectra in the region of the $[\text{Au-S-(CH}_2)_2 \text{N-CO-C}_5]^-$ fragment at $358.967921 \text{ } m/z$. This fragmentation is expected to occur when cysteamine interacts with a carboxylic acid to

form an amide, such as in the case of the carboxylic acid-functionalized CNTs or with defects on the CNTs. The C_5 portion of the fragment indicates that a five-carbon fragment from the carbon nanotube is attached to the amide. No signal is observed in the spectra for the CNT powders (5.11e and 5.11f), the cysteamine-modified gold (5.11d), or the dimethylamino ethanethiol-modified gold (5.11c). Again, this is expected, as the methyl groups on the control sample hinder the reaction between the carbon nanotubes and the amino-functionalized substrate.

In the case of the amino-terminated gold surface reacted with functionalized carbon nanotubes, the attachment through amide formation is expected and has been previously shown to occur with caged structures featuring carboxylic acid.⁴⁰ The main peak in Figure 5.11(a) confirms that this is indeed the case. It should, however, be pointed out that the intensity of this feature is very small compared to the peak for the same sample in Figure 5.11, suggesting that only a part of this reaction occurs through the amide functionality and a substantial portion leads to a direct attachment of the primary amino-group to the cage of the carbon nanotube. The ToF-SIMS intensities are only a semi-quantitative measure of the extent of a reaction; but the previous statement is also reinforced by the relatively small peak from the $[Au-S-(CH_2)_2 N-CO-C_5]^-$ fragment for the attachment of non-functionalized carbon nanotubes, as shown in Figure 5.11(b), which might occur on the defect sites. An approximation of the percentage of attachment events that occur via the cage versus the carboxylic acid can be determined by comparing the integration of the ToF-SIMS peaks corresponding to the $[Au-S-(CH_2)_2 NH-C_5]^-$ and the $[Au-S-(CH_2)_2 N-CO-C_5]^-$ fragments. This semi-quantitative comparison assumes that the ionization cross sections for the two fragments are similar and indicates that about three quarters of the COOH-

functionalized CNTs attachment takes place through the cage of the nanotube and almost 90 % of the non-functionalized CNT attachments occur through the cage. Overall, this set of studies implies that the presence of extra functionality is not necessary to covalently bind carbon nanotubes to an amine-terminated surface and that strong, covalent attachment will occur through the cage.

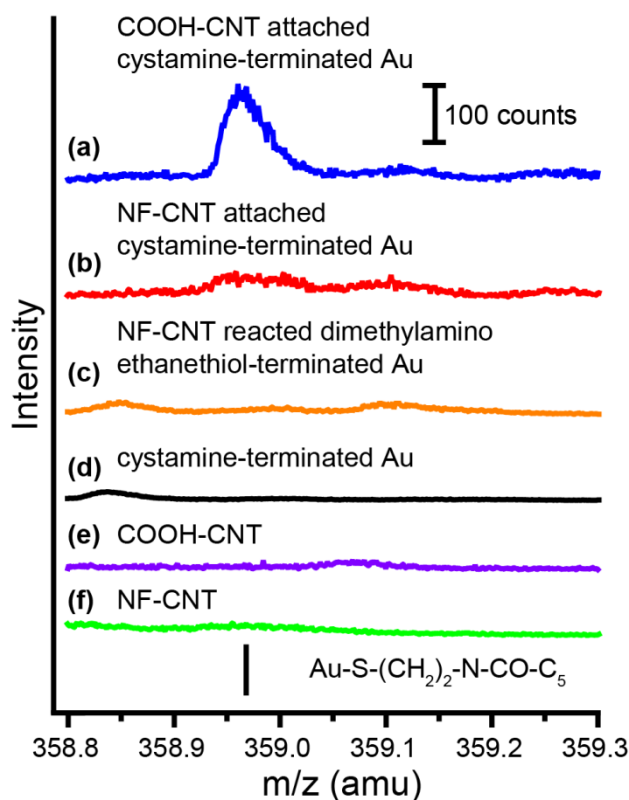


Figure 5.11 ToF-SIMS spectra in the region of the $[\text{Au-S-(CH}_2)_2\text{N-CO-C}_5]^+$ fragment, which is indicative of amide formation resulting from carboxylic acid (attached to a five-carbon fragment) reacting with the primary amine of cysteamine. These features are absent in the case of the samples without the substrate (e, f), the modified gold surface (d), and the control sample (c). A small peak can be observed on the cysteamine-terminated gold after reaction with the NF-CNTs (b) and a large peak is observed on the amine-modified gold after reaction with the COOH-CNTs (a). The black bar below the spectra indicates the exact m/z position expected for the fragment.

5.3 Conclusion

The covalent attachment of carbon nanotubes to functionalized silicon and gold surfaces has been investigated. Microscopic techniques confirm the presence of flat-lying nanotubes on both substrates and the presence of a sufficient number of nanotubes to allow for covalent binding. Spectroscopic studies suggest that regardless of the presence of functional groups on carbon nanotubes, they can attach directly through the carbon cage to the amino-functionalized surfaces by a direct addition process. The role of functional groups present on CNTs is important, as they have been shown to react with surface amines; however, the direct attachment through the cage has been demonstrated to additionally take place, both for functionalized and for non-functionalized carbon nanotubes. The experiment with the protected amino functionality of the surface reinforces the role of primary amines as an excellent anchor functional group for utilizing with carbon nanotubes.

These findings provide a novel approach for covalent and stable attachment of flat-lying carbon nanotubes to chemically functionalized substrates and to control the architecture of the attachment process, which will be important in many applications.

REFERENCES

1. Iijima, S.; Ichihashi, T. Single-Shell Carbon Nanotubes of 1-Nm Diameter. *Nature* **1993**, *363*, 603-605.
2. Bethune, D. S.; Klang, C. H.; de Vries, M. S.; Gorman, G.; Savoy, R.; Vazquez, J.; Beyers, R. Cobalt-Catalysed Growth of Carbon Nanotubes with Single-Atomic-Layer Walls. *Nature* **1993**, *363*, 605-607.
3. Jung, D.-H.; Kim, B. H.; Ko, Y. K.; Jung, M. S.; Jung, S.; Lee, S. Y.; Jung, H.-T. Covalent Attachment and Hybridization of DNA Oligonucleotides on Patterned Single-Walled Carbon Nanotube Films. *Langmuir* **2004**, *20*, 8886-8891.
4. Duan, Y.; Pirolli, L.; Teplyakov, A. V. Investigation of the H₂S Poisoning Process for Sensing Composite Material Based on Carbon Nanotubes and Metal Oxides. *Sensors and actuators. B, Chemical* **2016**, *235*, 213-221.
5. Balasubramanian, K.; Burghard, M. Chemically Functionalized Carbon Nanotubes. *Small* **2005**, *1*, 180.
6. Yu, X. F.; Mu, T.; Huang, H. Z.; Liu, Z. F.; Wu, N. Z. The Study of the Attachment of a Single-Walled Carbon Nanotube to a Self-Assembled Monolayer Using X-Ray Photoelectron Spectroscopy. *Surf. Sci.* **2000**, *461*, 199.
7. Dillon, A. C.; Jones, K. M.; Bekkedahl, T. A.; Kiang, C. H.; Bethune, D. S.; Heben, M. J. Storage of Hydrogen in Single-Walled Carbon Nanotubes. *Nature* **1997**, *386*, 377.

8. Darkrim, F. L.; Malbrunot, P.; Tartaglia, G. P. Review of Hydrogen Storage by Adsorption in Carbon Nanotubes. *Int. J. Hydrogen Energy* **2002**, 27, 193.
9. Bonard, J. M.; Kind, H.; Stöckli, T.; Nilsson, L. O. Field Emission from Carbon Nanotubes: The First Five Years. *Solid-State Electron.* **2001**, 45, 893.
10. Nakayama, Y.; Akita, S. Field-Emission Device with Carbon Nanotubes for a Flat Panel Display. *Synth. Met.* **2001**, 117, 207.
11. Liu, Z.; Shen, Z.; Zhu, T.; Hou, S.; Ying, L. Organizing Single-Walled Carbon Nanotubes on Gold Using a Wet Chemical Self-Assembling Technique. *Langmuir* **2000**, 16, 3569.
12. Lin, W.; Xiu, Y.; Jiang, H.; Zhang, R.; Hildreth, O.; Moon, K. S.; Wong, C. P. Self-Assembled Monolayer-Assisted Chemical Transfer of in Situ Functionalized Carbon Nanotubes. *J. Am. Chem. Soc.* **2008**, 130, 9636.
13. Rahman, M. M. Fabrication of Self-Assembled Monolayer Using Carbon Nanotubes Conjugated 1-Aminoundecanethiol on Gold Substrates. *Nat. Sci.* **2011**, 3, 208.
14. Schlenoff, J. B.; Li, M.; Ly, H. Stability and Self-Exchange in Alkanethiol Monolayers. *J. Am. Chem. Soc.* **1995**, 117, 12528.
15. Huang, X. J.; Ryu, S. W.; Im, H. S.; Choi, Y. K. Wet Chemical Needlelike Assemblies of Single-Walled Carbon Nanotubes on a Silicon Surface. *Langmuir* **2007**, 23, 991.
16. Yu, J.; Shapter, J. G.; Quinton, J. S.; Johnston, M. R.; Beattie, D. a. Direct Attachment of Well-Aligned Single-Walled Carbon Nanotube Architectures to Silicon (100) Surfaces: A Simple Approach for Device Assembly. *Phys. Chem. Chem. Phys.* **2007**, 9, 510.

17. Shearer, C. J.; Ellis, A. V.; Shapter, J. G.; Voelcker, N. H. Chemically Grafted Carbon Nanotube Surface Coverage Gradients. *Langmuir* **2010**, *26*, 18468.
18. Yu, J. X.; Losic, D.; Marshall, M.; Böcking, T.; Gooding, J. J.; Shapter, J. G. Preparation and Characterisation of an Aligned Carbon Nanotube Array on the Silicon (100) Surface. *Soft Matter* **2006**, *2*, 1081.
19. Choi, S. W.; Kang, W. S.; Lee, J. H.; Najeeb, C. K.; Chun, H. S.; Kim, J. H. Patterning of Hierarchically Aligned Single-Walled Carbon Nanotube Langmuir-Blodgett Films by Microcontact Printing. *Langmuir* **2010**, *26*, 15680.
20. Wang, Q.; Moriyama, H. [60]-Fullerene and Single-Walled Carbon Nanotube-Based Ultrathin Films Stepwise Grafted onto a Self-Assembled Monolayer on ITO. *Langmuir* **2009**, *25*, 10834.
21. Chou, A.; Eggers, P. K.; Paddon-Row, M. N.; Gooding, J. J. Self-Assembled Carbon Nanotube Electrode Arrays: Effect of Length of the Linker between Nanotubes and Electrode. *J. Phys. Chem. C* **2009**, *113*, 3203.
22. López-Bezanilla, A.; Triozon, F.; Latil, S.; Blase, X.; Roche, S. Effect of the Chemical Functionalization on Charge Transport in Carbon Nanotubes at the Mesoscopic Scale. *Nano Lett.* **2009**, *9*, 940.
23. Peng, S.; Cho, K. Chemical Control of Nanotube Electronics. *Nanotechnology* **2000**, *11*, 57.
24. Kong, J.; Franklin, N. R.; Zhou, C.; Chapline, M. G.; Peng, S.; Cho, K.; Dai, H. Nanotube Molecular Wires as Chemical Sensors. *Science* **2000**, *287*, 622.
25. Chamberlain, T. W.; Meyer, J. C.; Biskupek, J.; Leschner, J.; Santana, A.; Besley, N. A.; Bichoutskaia, E.; Kaiser, U.; Khlobystov, A. N. Reactions of the Inner

Surface of Carbon Nanotubes and Nanoprotrusion Processes Imaged at the Atomic Scale. *Nat. Chem.* **2011**, *3*, 732.

26. Nakanishi, Y.; Omachi, H.; Fokina, N. A.; Schreiner, P. R.; Kitaura, R.; Dahl, J. E. P.; Carlson, R. M. K.; Shinohara, H. Template Synthesis of Linear-Chain Nanodiamonds inside Carbon Nanotubes from Bridgehead-Halogenated Diamantane Precursors. *Angew. Chem., Int. Ed.* **2015**, *54*, 10802.

27. Xiu, P.; Xia, Z.; Zhou, R.; Suzuki, D. S., *Physical and Chemical Properties of Carbon Nanotubes*, 2013, p 197.

28. Lin, T.; Bajpai, V.; Ji, T.; Dai, L. Chemistry of Carbon Nanotubes. *Aust. J. Chem.* **2003**, *56*, 635.

29. Park, E.; Suzuki, D. S., *Physical and Chemical Properties of Carbon Nanotubes*, 2013, p 225.

30. Landis, E. C.; Hamers, R. J. Covalent Grafting of Ferrocene to Vertically Aligned Carbon Nanofibers: Electron-Transfer Processes at Nanostructured Electrodes. *J. Phys. Chem. C* **2008**, *112*, 16910.

31. Hauquier, F.; Pastorin, G.; Hapiot, P.; Prato, M.; Bianco, A.; Fabre, B. Carbon Nanotube-Functionalized Silicon Surfaces with Efficient Redox Communication. *Chem. Commun.* **2006**, 4536.

32. Liu, J.; Casavant, M. J.; Cox, M.; Walters, D. A.; Boul, P.; Lu, W.; Rimberg, A. J.; Smith, K. A.; Colbert, D. T.; Smalley, R. E. Controlled Deposition of Individual Single-Walled Carbon Nanotubes on Chemically Functionalized Templates. *Chem. Phys. Lett.* **1999**, *303*, 125.

33. Moriarty, P. J. Fullerene Adsorption on Semiconductor Surfaces. *Surf. Sci. Rep.* **2010**, *65*, 175.

34. Cattaruzza, F.; Llanes-Pallas, A.; Marrani, A. G.; Dalchiele, E. A.; Decker, F.; Zanoni, R.; Prato, M.; Bonifazi, D. Redox-Active Si(100) Surfaces Covalently Functionalised with [60]Fullerene Conjugates: New Hybrid Materials for Molecular-Based Devices. *J. Mater. Chem.* **2008**, *18*, 1570.
35. Gu érin, D.; Lenfant, S.; Godey, S.; Vuillaume, D. Synthesis and Electrical Properties of Fullerene-Based Molecular Junctions on Silicon Substrate. *J. Mater. Chem.* **2010**, *20*, 2680.
36. Fabre, B.; Bassani, D. M.; Liang, C.-K.; Ray, D.; Hui, F.; Hapiot, P. Anthracene and Anthracene: C₆₀ Adduct-Terminated Monolayers Covalently Bound to Hydrogen-Terminated Silicon Surfaces. *J. Phys. Chem. C* **2011**, *115*, 14786-14796.
37. Sahoo, R. R.; Patnaik, A. Binding of Fullerene C₆₀ to Gold Surface Functionalized by Self-Assembled Monolayers of 8-Amino-1-Octane Thiol: A Structure Elucidation. *J. Colloid Interface Sci.* **2003**, *268*, 43-49.
38. Tsukruk, V. V.; Everson, M. P.; Lander, L. M.; Brittain, W. J. Nanotribological Properties of Composite Molecular Films: C-60 Anchored to a Self-Assembled. *Langmuir* **1996**, *12*, 3905.
39. Zhang, X.; Teplyakov, A. V. Adsorption of C₆₀ Buckminster Fullerenes on an 11-Amino-1-Undecene-Covered Si(111) Substrate. *Langmuir* **2008**, *24*, 810-820.
40. Miller, T.; Teplyakov, A. V. Attachment Chemistry of PCBM to a Primary-Amine-Terminated Organic Monolayer on a Si(111) Surface. *Langmuir* **2014**, *30*, 5105-5114.
41. Gao, F.; Teplyakov, A. V. Reaction of Hydrazine with a Chlorine-Terminated Si(111) Surface. *J. Phys. Chem. C* **2014**, *118*, 27998-28006.

42. Tian, F.; Taber, D. F.; Teplyakov, A. V. NH-Termination of the Si(111) Surface by Wet Chemistry. *J. Am. Chem. Soc.* **2011**, *133*, 20769–20777.
43. Choi, H. C.; Park, J.; Kim, B. Distribution and Structure of N Atoms in Multiwalled Carbon Nanotubes Using Variable-Energy X-Ray Photoelectron Spectroscopy. *J. Phys. Chem. B* **2005**, *109*, 4333.

Chapter 6

CHEMICAL PROTECTION OF MATERIAL MORPHOLOGY: ROBUST AND GENTLE GAS-PHASE SURFACE FUNCTIONALIZATION OF ZnO WITH PROPIOLIC ACID

6.1 Introduction

Within the last several years, metal oxides have attracted increasing attention to benefit a number of novel applications including solid state lighting, hybrid organic-inorganic light-emitting diodes and dye-sensitized solar cells.¹⁻² Among these materials, zinc oxide, with a wide band gap of 3.3 eV at room temperature and photoluminescence emission centered at ~ 287 nm,³ has attracted substantial interest, specifically targeting research on interfacing it with small molecules, dyes, or biomolecules,⁴ because the resulting organic-inorganic hybrids can be employed in devices such as solar cells and sensors.⁵ In fact, precise control and molecular-level understanding of the interface between ZnO and molecules has become fundamentally and technologically important challenge for a very wide range of possible future applications.

The most common approach to functionalize ZnO surface with small molecules usually utilizes wet chemistry reactions with functionalized carboxylic^{4, 6-8} and phosphonic acids.⁸⁻¹² Bishop et al. reported an approach to form stable, multidentate carboxylate linkages to a variety of metal oxide nanoparticles including ZnO, Fe₂O₃, TiO₂, and WO₃, while also enabling subsequent multistep chemistry via the Cu(I)-catalyzed “click” reaction.¹ Later, Cao et al. investigated ZnO nanorod films

functionalized with carboxylic acid capped with an azide end group followed by copper-free “click” chemistry.⁴ More recently, Tudisco et al. obtained nanostructured ZnO fibers functionalized through the grafting of a bifunctional phosphonic linker with azide terminations, followed by the anchoring of a specific cavitand receptor having four alkyne groups via “click” reaction.¹² Although carboxylic and phosphonic acids do lead to the formation of stable linkages on ZnO surface, multiple species are always formed during the attachment process, which makes it difficult to apply further modification protocols onto the resulting surfaces. More importantly, solution-based methods, despite sometimes being successful in applications to nanoparticles, alter the structures of thin films or nanostructured materials because ZnO is easily dissolved in a wide number of solvents and especially prone to dissolution in acids.¹³⁻¹⁵ This point is especially detrimental to chemical modification of delicate ZnO nanostructures that can be grown on a variety of substrates and possess a wide range of very attractive properties.¹⁶⁻¹⁸

Despite recent advances in solution ZnO surface modification, even successful and carefully optimized conditions for processes utilizing wet chemistry methods are normally associated with some changes in material morphology caused by etching processes.¹⁹ Thus, an alternative method for surface modification that produces stable and robust surface linkages and at the same time does not dissolve (or influences the structure) of ZnO features, has to be developed. Hence, the necessity to develop a well-controlled interfacial strategy on ZnO surface is highly desired. Here we report a simple and precise method to achieve stable bidentate carboxylate linkage to ZnO surface, which has an azide group available for further modification that can be tested, for example, by “click” chemistry, as summarized in Figure 6.1. This alkyne–azide

click reaction has been successfully explored under ultrahigh vacuum condition, where the azide is stable upon adsorption, yet maintains sufficient reactivity.²⁰

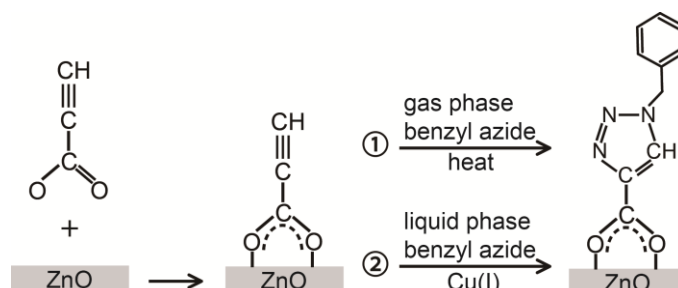


Figure 6.1 Reaction scheme for ZnO surface modification with propiolic acid followed by benzyl azide test reaction via gas phase and liquid phase modification.

There are a number of advantages of the gas-phase modification as opposed to the solution-based chemistry. First, the preparation of the ZnO surface can be controlled much better compared to the solution methods, since vacuum annealing and exposure to additional co-reagents can provide a better set of conditions for a reaction with a selected adsorbate. Second, as will be shown below, the chemistry of the adsorbate can be controlled to deliver a perfectly preserved functional group to the surface and at the same time the adsorbate created can be anchored to the surface in a highly selective manner. Finally, the functional group delivered by this gas-phase exposure can be further modified either by subsequent exposures to a desired reagent in a gas phase or by wet-chemistry modification procedures, as the ZnO surface modified in the first step becomes structurally stable with respect to both of these approaches.

In this thesis, to confirm the reaction of gas phase carboxylic acid with ZnO surface followed by azide–alkyne cycloaddition “click” reaction and to establish the

structures of surface species produced, each step of modification was characterized by scanning electron microscopy (SEM), solid-state nuclear magnetic resonance spectroscopy (SSNMR), Fourier-transform infrared spectroscopy (FT-IR) and X-ray photoelectron spectroscopy (XPS). Density functional theory (DFT) calculations were performed to propose a plausible mechanism of surface reaction and to produce a set of appropriate spectroscopic observables, including vibrational spectra and core-level energies to compare with the results of experimental studies.

The successful functionalization of the ZnO surface by exposure to gas-phase propiolic acid apparently stabilizes the oxide surface, so that further modification, for example, by “click” chemistry can be performed either in liquid phase or, again, by a gas-phase exposure to a probe azide. This universal method opens up new possibilities for working with a multitude of different modification schemes following the initial surface preparation and for developing new chemistries for ZnO-based nanomaterials and nanostructures.

6.2 Results and Discussion

6.2.1 Morphology Change of ZnO Surface during Propiolic Acid Treatment and Following “Click” Reaction.

In addressing any treatment approaches for solid state materials in powder or nanostructure form, it is always important to understand the effects of these treatments on the morphology of the material studied. Given that ZnO can easily dissolve in acidic solutions,¹³⁻¹⁵ and acidic surface modifiers including thiol, carboxyl, and phosphonate linkers have been observed to alter the surface chemistry and to etch the

zinc oxide surface,¹⁵ it is critical to confirm that gas-phase exposure of this material to propiolic acid does not influence the surface morphology. A set of studies exploring this statement is presented in Figure 6.2, where the morphology of ZnO powder following various treatments is investigated by SEM to uncover any potential “etching” by a carboxylic acid. Following the exposure of pristine ZnO powder (shown in Figure 6.2a) to the gas phase treatment with propiolic acid at 1 Torr for 8 minutes, the structure of the material is fully preserved, as shown in Figure 6.2(b). However, if the treatment is performed by the propiolic acid in liquid phase, the structure of the nanopowder is largely destroyed, as demonstrated in Figure 6.2(e), meaning that further surface modification based on the surface shown in Figure 6.2(e) would definitely lead to a different morphology, compared to the pristine surface. Most importantly, if the first step is the gas-phase exposure of ZnO nanopowder to propiolic acid (where the morphology is preserved), further chemical reactions, such as either gas-phase thermal “click” with benzyl azide (shown in Figure 6.2c) or the copper-catalyzed “click” process in the liquid phase (Figure 6.2d) do not appear to affect the morphology of ZnO material at all. Thus, the propiolic acid-functionalized ZnO surface formed in the first step is sufficiently stable to withstand the annealing and solution-based processing. In other words, such gas-phase modification of ZnO provides an alternative pathway to modify the ZnO surface with a carboxylic acid at a high degree of control over the morphology, without any noticeable impact on the surface structure, offering a solution for the common challenge posed by acidic modifiers for ZnO functionalization.

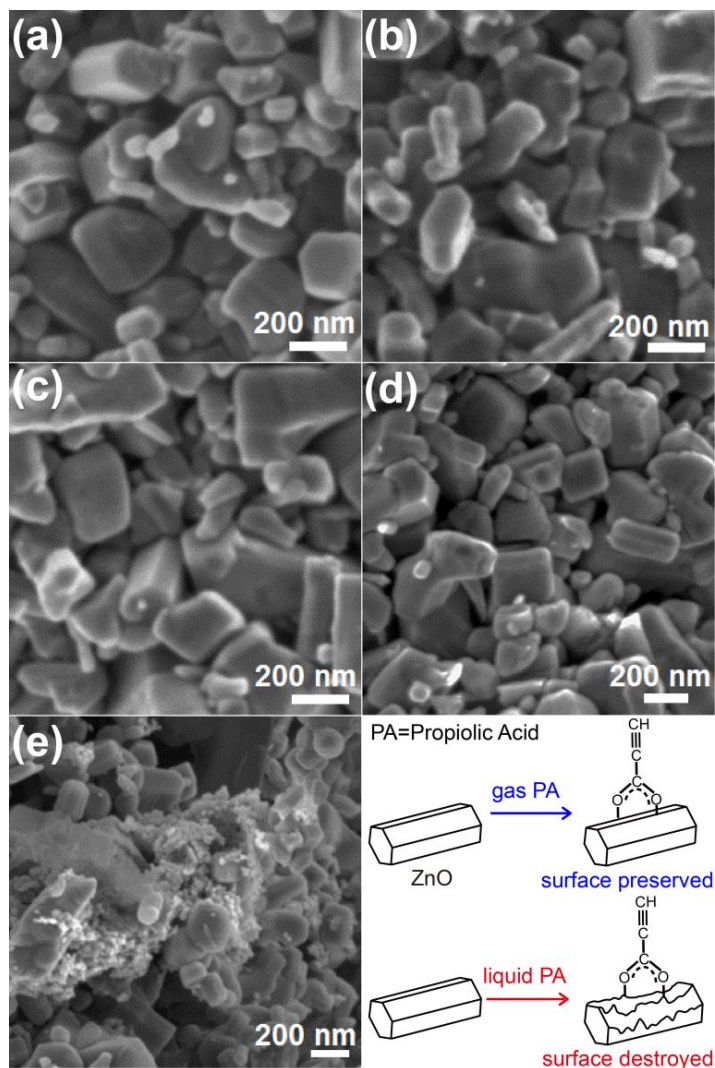


Figure 6.2 SEM studies of ZnO surface modification. (a) Clean ZnO nanopowder; (b) Gas phase propiolic acid-functionalized ZnO surface; (c) Propiolic acid functionalized ZnO surface depicted in (b) followed by copper-free gas phase “click” reaction with benzyl azide; (d) Propiolic acid functionalized ZnO surface depicted in (b) followed by copper-catalyzed liquid phase “click” reaction with benzyl azide; (e) ZnO powder directly exposed to liquid phase propiolic acid.

6.2.2 Confirmation of Carboxylate Linkage to ZnO Surface by Infrared Investigation.

Although structural integrity of the ZnO material studied is confirmed by SEM, in order to be practical, the modification schemes proposed have to be verified spectroscopically. The initial assessment of the successful surface modification can be made based on in-situ infrared investigations. Figure 6.3 summarizes the spectral region of 1000-3800 cm^{-1} for gas phase propiolic acid (7.3a), propiolic acid-functionalized ZnO surface (6.3c), along with DFT predicted vibrations of a single propiolic acid molecule chemisorbed on the model cluster representing ZnO surface (7.3b) provided for comparison. The chemical reaction between the gas-phase propiolic acid and ZnO can be confirmed by the disappearance of the hydroxyl group absorption at around 3600 cm^{-1} following the room-temperature exposure of ZnO powder to the gas-phase propiolic acid, as would be expected, since the most common reaction pathway would be the dissociation of the carboxylic group to form a carboxylate and a surface-bound hydrogen,¹⁵ with vibrational signature substantially different from the unreacted $-\text{COOH}$.²¹⁻²² At the same time, the produced adsorbate clearly exhibits the characteristic absorption features of the $\text{C}\equiv\text{C}$ stretching vibration around 2100 cm^{-1} and an obvious feature just above 3250 cm^{-1} corresponding to the C-H stretching of the alkyne group. The spectrum 6.3c was recorded following extensive (16 hours) pumping in vacuum to remove all the non-chemically adsorbed propiolic acid. Shortened pumping time leads to multiple species physisorbed on the ZnO surface including molecular propiolic acid, as observed by infrared spectroscopy in Figure 6.4. Such comparison emphasizes the necessity of the removal of physisorbed species by additional pumping and it will be further elaborated by SSNMR and discussed later to demonstrate that only one type of zinc carboxylate species is formed

on the a surface during gas-phase reaction with propiolic acid. The chemisorbed propiolic acid also exhibits a strong absorption peak at 1608 cm^{-1} and weaker split peaks centered at 1375 cm^{-1} , consistent with the asymmetric and symmetric stretches of a zinc carboxylate species.^{1, 5, 7, 23-24} It also shows a relatively weak broad absorption feature around 1710 to 1685 cm^{-1} likely associated with the differences in O-C-O vibrations in multiple structurally similar surface species present.^{1, 25-27} The nature of the chemisorbed product is also confirmed by comparing the experimentally recorded infrared spectrum to that predicted computationally for a model proposed surface species shown in Figure 6.3b. Based on this comparison, the predicted spectrum is consistent with the experimental results for the signatures of $\text{C}\equiv\text{C}$, $\text{C}\equiv\text{C}-\text{H}$. A noticeable shift in the vibrations corresponding to the carboxylate linkage can be explained by the simplicity of the computational model used, as the realistic structures will be affected by their neighbors and by the likely interactions with available surface hydroxyl groups, affecting the vibrational frequencies of both species. Overall, this set of infrared studies confirms the $-\text{COOH}$ dissociation and the presence of $\text{C}\equiv\text{C}$, $\text{C}\equiv\text{C}-\text{H}$ and zinc carboxylate containing chemical groups following the reaction of gas phase propiolic acid with ZnO surface, forming a bidentate carboxylate linkage to ZnO.

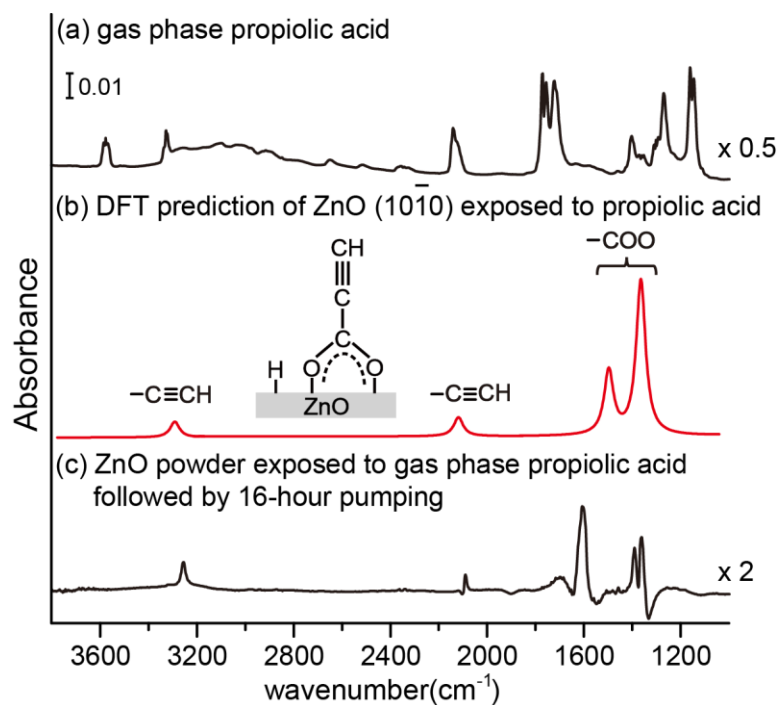


Figure 6.3 Infrared spectroscopy studies of propiolic acid reaction with ZnO surface. (a) Gas phase propiolic acid; (b) Computationally predicted infrared spectra for the cluster model schematically represented in the figure (frequencies are scaled by a common scaling factor of 0.94); (c) Propiolic acid-functionalized ZnO surface (molecularly adsorbed propiolic acid is removed following extended pumping time). Clean ZnO surface is used as a background for spectrum (c).

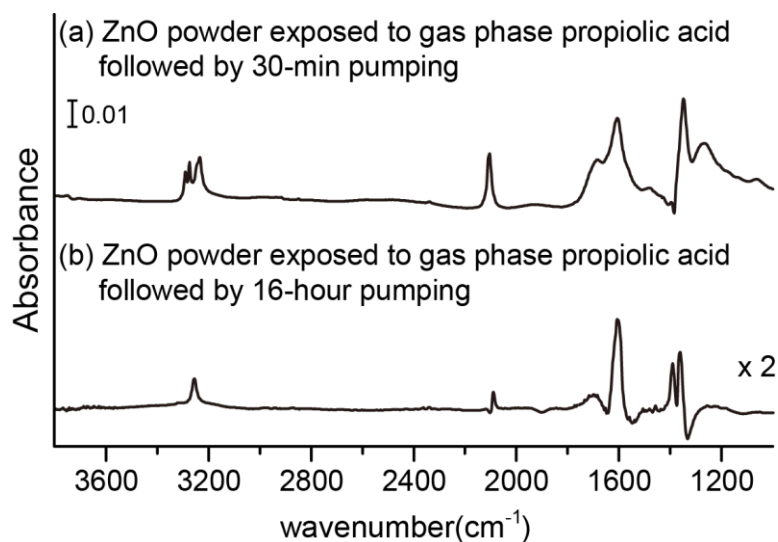


Figure 6.4 IR studies of propiolic acid reaction with ZnO surface.(a) Propiolic acid physisorbed mixed with chemisorbed ZnO surface (after 30-min pumping); (b) Propiolic acid-functionalized ZnO surface (after 16-hour pumping, same as Figure 6.3c). Clean ZnO surface is used as a background for both.

6.2.3 Confirmation of “Click” Reaction on Modified ZnO Surface by IR and XPS.

To explore the possibility of performing multistep functionalization of the ZnO surfaces based on the initial chemisorption of a functionalized carboxylic acid, the propiolic acid-modified ZnO was exposed to gas-phase benzyl azide, at elevated temperature to thermally activate copper-free click chemistry.^{4, 28} Reaction with benzyl azide is expected to provide a phenyl group as an indicator of chemical modification for IR and XPS analysis. The spectral region of 1000-3800 cm^{-1} for gas phase benzyl azide (6.5a) and benzyl azide “clicked” propiolic acid-functionalized ZnO surface (6.5c) are presented in Figure 6.5. When benzyl azide is introduced into

the reaction chamber, strong signatures of azide group and phenyl ring at 2110 cm^{-1} and 3050 cm^{-1} , respectively, are clearly recorded for the gas-phase benzyl azide (6.5a). Based on the DFT prediction for a product of thermal “click” chemistry between the model ZnO cluster and benzyl azide (Figure 6.5b), the signature of this chemical modification should be very different from the gas-phase species. The spectrum recorded following this thermal “click” resulting from the gas-phase exposure of benzyl azide is shown in Figure 6.5c using propiolic acid-modified surface as a background. If this spectrum is compared with the spectrum of the propiolic acid-modified surface (spectrum 6.5d) replotted from Figure 6.3, it is clear that this signature is a combination of the absorption features corresponding to the benzyl azide reaction and the decrease in intensity of the selected features corresponding to chemisorbed propiolic acid. Specifically, the decreased intensity of the 3250 cm^{-1} feature corresponds to the loss of the alkyne functionality. The decrease in intensity of several features corresponding to the very specific vibrations of the surface-bound carboxylate/ $\text{C}\equiv\text{C}$ such as the decreased intensity of the peaks at 1608 cm^{-1} and 1375 cm^{-1} also suggests that the triple bond participates in a reaction with benzyl azide. At the same time, several key vibrations associated with the formation of a triazole ring and a successful “click” reaction are recorded to appear within the fingerprint vibrational region.²⁹⁻³¹ The small peaks above 3000 cm^{-1} and around 1130 cm^{-1} corresponding to aromatic C–H are observed as the evidence of phenyl ring attachment. Two strong peaks at 1403 cm^{-1} and 1228 cm^{-1} are the signature of C–N in the triazole ring as suggested by the DFT-predicted spectra.

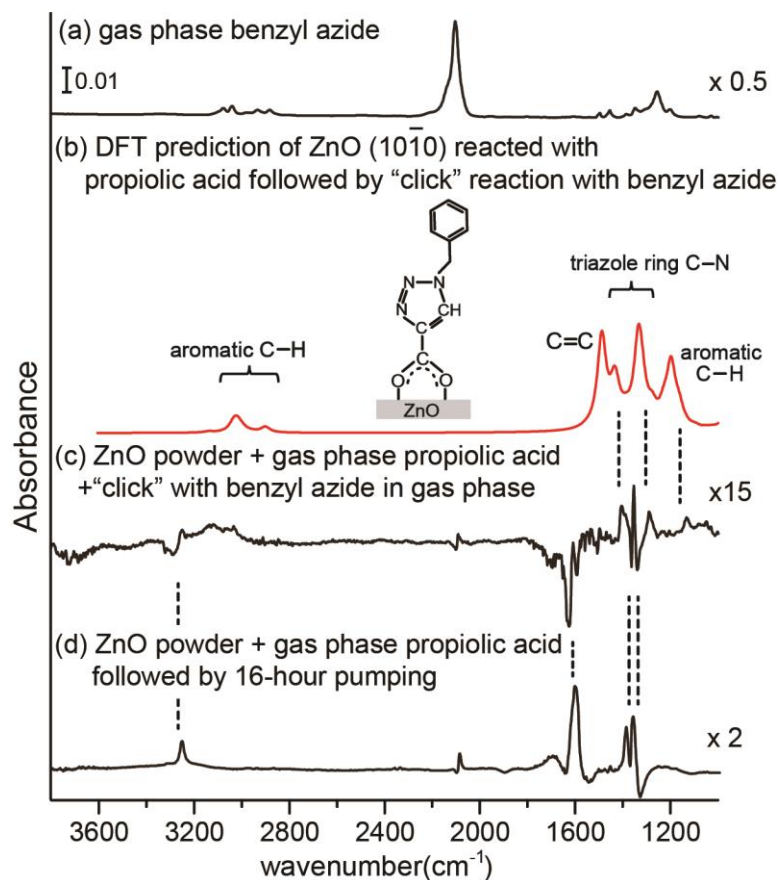


Figure 6.5 Infrared spectroscopy studies of copper-free “click” reaction with propiolic acid functionalized ZnO surface. (a) Gas phase benzyl azide; (b) Computationally predicted infrared spectra for the considered cluster model shown (frequencies are scaled by a common scaling factor of 0.94); (c) Benzyl azide reacted with propiolic acid-functionalized ZnO surface; (d) Propiolic acid-functionalized ZnO surface (same as Figure 6.3c and 6.4b). Propiolic acid functionalized ZnO surface is used as a background for spectrum (c).

Thus, the infrared study of copper-free click reaction indicates the presence of phenyl groups and triazole linkage following the copper-free click reaction of benzyl azide with propiolic acid-modified ZnO surface. One question that is more difficult to address based solely on the infrared spectra is if some of the benzyl azide may directly react with the ZnO surface, forming a nitrene-type species and possibly displacing

surface carboxylates. This question can be addressed using XPS. This technique could also help us in identifying the difference in gas-phase and liquid-phase modification processes following the initial gas-phase exposure of ZnO to propiolic acid.

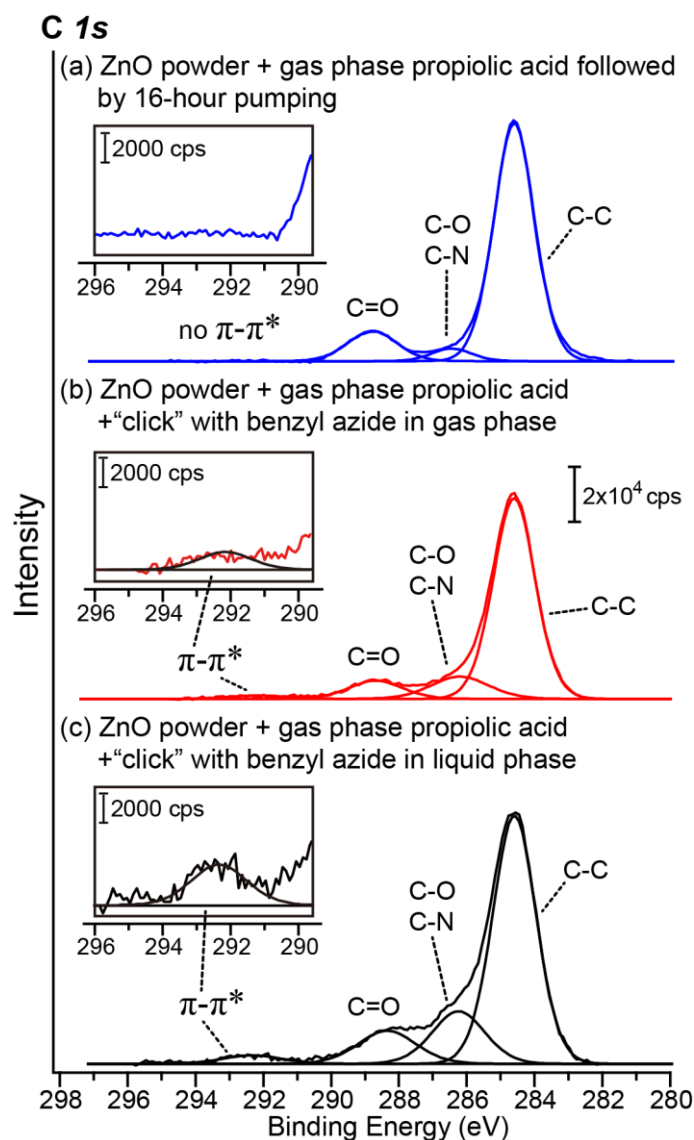


Figure 6.6 High-resolution XPS spectra of C 1s region for (a) Gas phase propiolic acid-functionalized ZnO surface; (b) Copper-free “click” reaction of gas phase benzyl azide with propiolic acid-functionalized ZnO surface; (c) Copper-catalyzed “click” reaction of liquid phase benzyl azide with propiolic acid functionalized ZnO surface.

The spectra of C *1s* region of propiolic acid-functionalized ZnO surface and the surface following the “click” reaction with benzyl azide are presented in Figure 6.6. This figure also compares the results of the copper-free gas-phase click reaction and the copper-catalyzed azide–alkyne cycloaddition (CuAAC) reaction conducted using liquid phase benzyl azide with the propiolic acid functionalized ZnO surface.^{1, 32} As shown in Figure 6.6, for all three samples, three peaks at 284.6 eV, 286.3 eV and 288.6 eV are fit and assigned to C–C bonds, C–O/C–N bonds and C=O bonds. It needs to be noted that the peak at 286.3 eV, associated with C–O/C–N bonds on propiolic acid functionalized ZnO surface, increases after copper-free “click” reaction with gas phase benzyl azide and increases in intensity even more following CuAAC reaction with liquid phase benzyl azide, as a result of benzyl azide interacting with the propiolic acid-functionalized ZnO surface forming the triazole ring. This observation is also consistent with the expectation that CuAAC reaction is substantially faster than thermal attachment. But the most important observation is the peak at 292.1 eV, which corresponds to the π – π^* shake-up in aromatic functional groups, confirming the presence of the aromatic entities on the modified surface following the “click” reaction with benzyl azide. Since this peak is not observed for propiolic acid functionalized ZnO surface, there is only one possible source of aromaticity in this sample: the presence of the phenyl ring from benzyl azide.

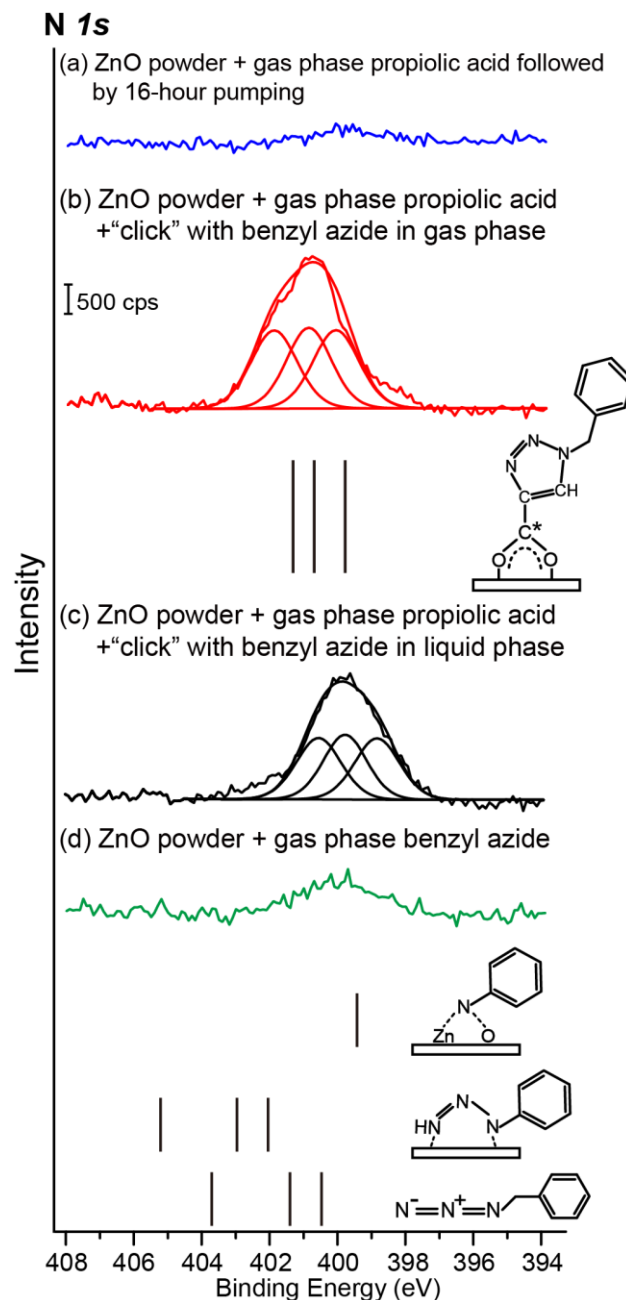


Figure 6.7 High-resolution XPS spectra of N 1s region for (a) Gas phase propiolic acid-functionalized ZnO surface; (b) Copper-free “click” reaction of gas phase benzyl azide with propiolic acid functionalized ZnO surface; (c) Copper-catalyzed “click” reaction of liquid phase benzyl azide with propiolic acid functionalized ZnO surface; (d) Benzyl azide adsorbed directly onto ZnO surface. The core level energy shifts predicted by DFT for the model systems presented in the figure are shown as solid bars.

Another spectral region that should be very informative is the one corresponding to N *1s*. Figure 6.7 shows the N *1s* spectral region of propiolic acid-functionalized ZnO surface and benzyl azide “clicked” ZnO surface by two different methods, respectively, along with the DFT-predicted N *1s* core level energies shown as solid bars for the models indicated in the figure. The N *1s* experimental spectrum shown for the propiolic acid-functionalized ZnO surface in Figure 6.7a exhibits no feature of nitrogen containing species, as would be expected. In Figure 6.7b, following copper-free “click” reaction with gas phase benzyl azide, propiolic acid functionalized ZnO surface shows a strong and broad peak centered at 401 eV, which is discerned into three peaks attributed to the triazole ring.^{30-31, 33} Furthermore, the experimental results match consistently the computational prediction of N *1s* core level for the triazole model structure shown in Figure 6.7. Another comparison is given by the N *1s* experimental spectra of propiolic acid functionalized ZnO surface “clicked” with benzyl azide through CuAAC reaction, as shown in Figure 6.7c. Although the features appear to be shifted slightly towards lower binding energy region, this spectrum shows a very similar strong and broad feature, fit with three peaks for the triazole ring as well.³¹ According to the DFT calculation, the two possible isomers resulted from copper-free “click” reaction, as opposed to catalyzed liquid-phase process, would result in species differentiated by 0.8~0.9 eV in XPS spectra, which may explain the observed peak shift and the small differences in peak shape resulted from CuAAC reaction, which only leads to a single triazole-ring isomer produced.^{32, 34} It is also worth pointing out that the results of gas-phase thermal “click” in Figure 6.7b and liquid phase copper catalyzed “click” attachment in Figure 6.7c exhibit low intensity

broad shoulders in addition to the main features. Given the high reactivity of benzyl azide, a number of additional investigations summarized in Figure 6.7 were performed to evaluate the direct reaction of this compound with ZnO surface. Based on the DFT prediction of proposed models shown in Figure 6.7, the shoulders observed in Figure 7.7b and 7.7c are possible results of the direct attachment of a nitrene entity inserted into ZnO bond following the loss of N₂ by an azide molecule and other reactions occurring on surface defect sites. Other possible attachments appear to correspond to much higher binding energies than what is observed experimentally. In order to test this hypothesis, a control experiment for benzyl azide adsorbed directly on a ZnO surface is presented in Figure 6.7d. It shows a broad low intensity feature above 400 eV, likely corresponding to surface-bound nitrene species according to the comparison with the DFT models in Figure 6.7. The shape and intensity of the observed feature suggest that it is not the major species in the reaction of benzyl azide with the ZnO surface modified with propiolic acid.

The XPS spectra of other relevant regions including Cu 2*p*, O 1*s* and Zn 2*p* regions are also collected and shown in Figure 6.8, 6.10, 6.11, however, these spectral regions are not very informative in that they only present the expected largely unchanged features in Zn and O region. It should be noted that the Cu 2*p* region was recorded to confirm the absence of copper catalyst: the copper catalyst was removed following the CuAAC “click” reaction, as shown in Figure 6.8 and also confirmed by SEM/EDX measurements in Figure 6.9.

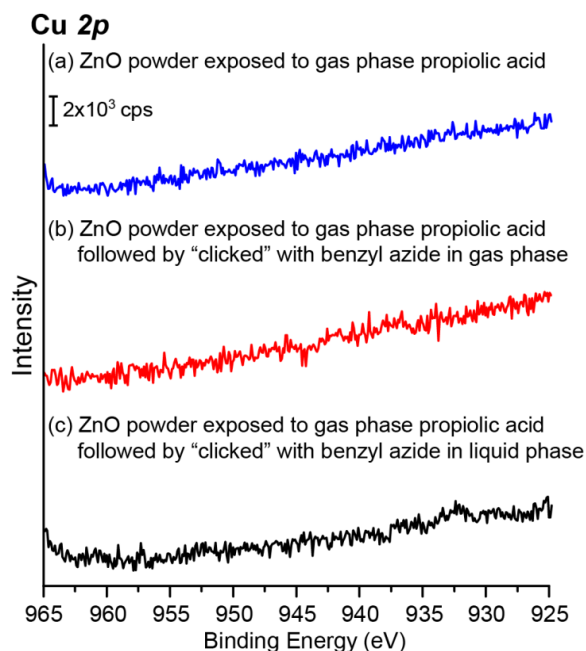


Figure 6.8 High-resolution XPS spectra of Cu 2p region for (a) Gas phase propiolic acid-functionalized ZnO surface; (b) Copper-free “click” reaction of gas phase benzyl azide with propiolic acid-functionalized ZnO surface; (c) Copper-catalyzed “click” reaction of liquid phase benzyl azide with propiolic acid functionalized ZnO surface, confirming the removal of copper catalyst following the procedure.

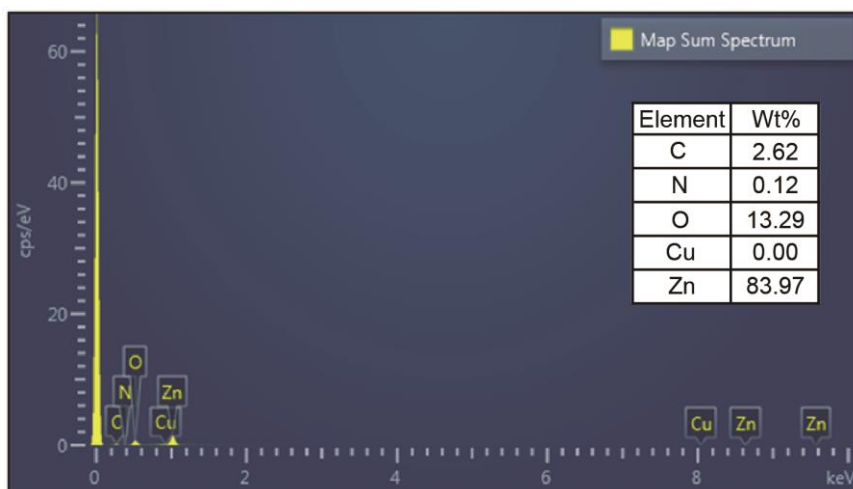


Figure 6.9 EDX analysis of Copper-catalyzed “click” reaction of liquid phase benzyl azide with propiolic acid functionalized ZnO surface, confirming the removal of copper catalyst following the procedure.

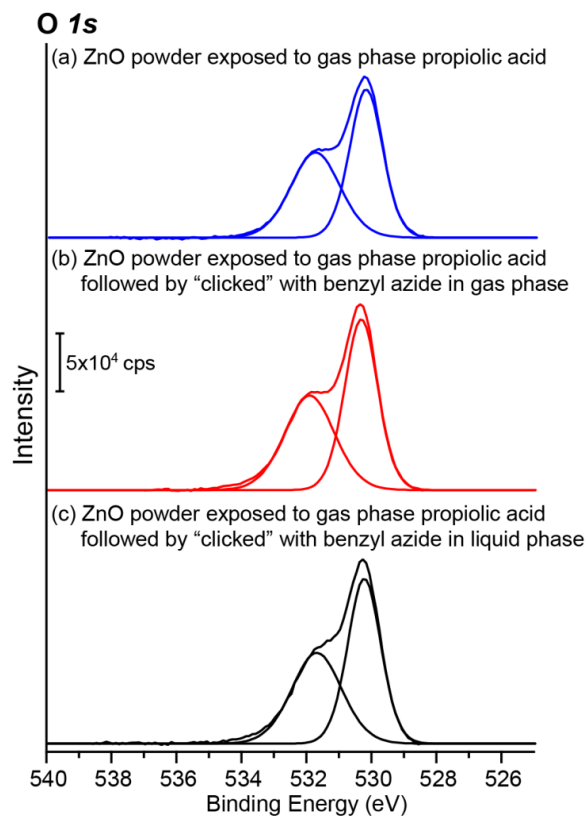


Figure 6.10 High-resolution XPS spectra of O 1s region for (a) Gas phase propiolic acid-functionalized ZnO surface; (b) Copper-free “click” reaction of gas phase benzyl azide with propiolic acid-functionalized ZnO surface; (c) Copper-catalyzed “click” reaction of liquid phase benzyl azide with propiolic acid functionalized ZnO surface.

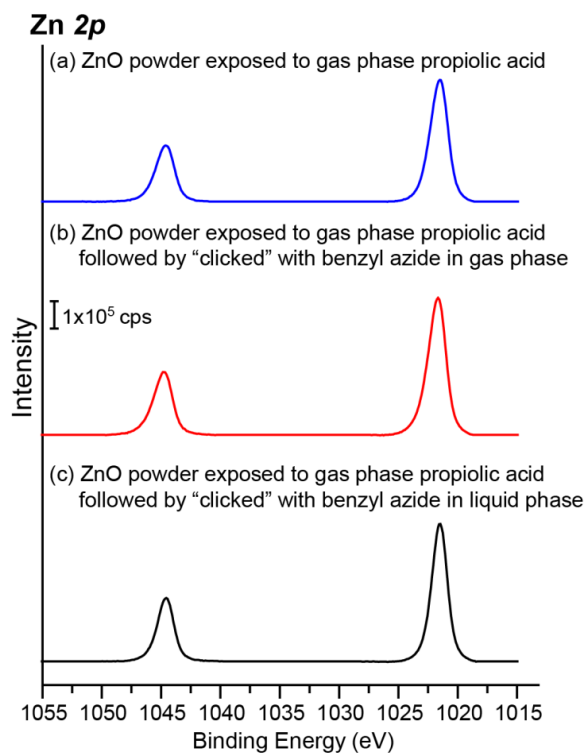


Figure 6.11 High-resolution XPS spectra of Zn 2p region for (a) Gas phase propiolic acid-functionalized ZnO surface; (b) Copper-free “click” reaction of gas phase benzyl azide with propiolic acid-functionalized ZnO surface; (c) Copper-catalyzed “click” reaction of liquid phase benzyl azide with propiolic acid functionalized ZnO surface.

Thus, the XPS results summarized above confirm that both CuAAC and copper-free “click” reactions are successfully performed on the propiolic acid-functionalized ZnO surface and the results of both “click” approaches appear to be essentially the same.

6.2.4 Multistep Functionalization of the ZnO surfaces followed by NMR

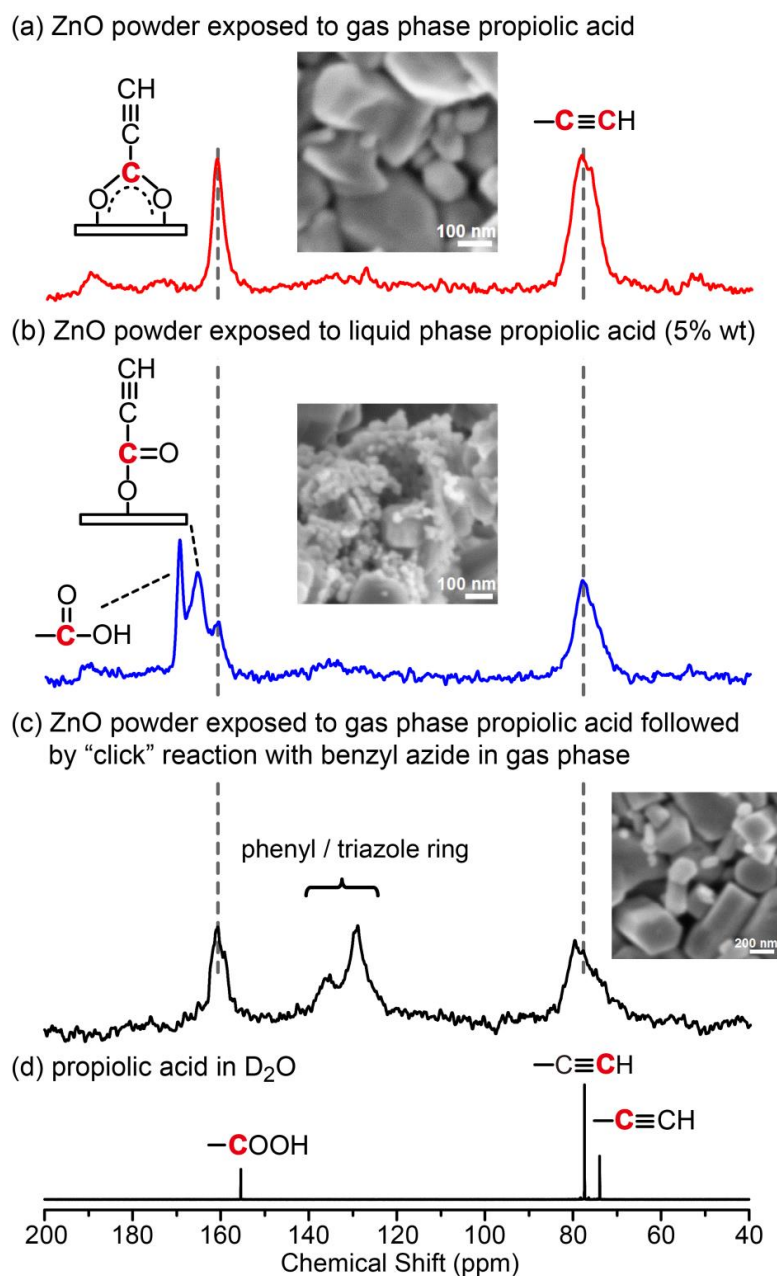


Figure 6.12 ^{13}C NMR spectroscopy studies of the reaction of propiolic acid with ZnO surface and the following copper-free “click” reaction. (a) gas phase propiolic acid-functionalized ZnO surface; (b) liquid phase propiolic acid-modified ZnO powder; (c) benzyl azide reacted with propiolic acid-functionalized ZnO surface; (d) liquid phase propiolic acid.

Although the IR and XPS confirmed the modification of ZnO with gas-phase propiolic acid and also confirmed that the resulting surface can be further functionalized by “click” chemistry, they did not answer the question of why the liquid phase reaction with propiolic acid is so different from gas-phase exposure and also whether there is any difference between the anchoring of propiolic acid onto ZnO in liquid and gas phase attachment. NMR spectroscopy will help us address these questions.

Figure 6.12 displays the ^{13}C solid-state NMR spectra for gas phase propiolic acid-functionalized ZnO surface (6.12a); ZnO powder reacted with liquid phase propiolic acid (6.12b) and gas-phase benzyl azide “clicked” propiolic acid-functionalized ZnO surface (6.12c). To better interpret the results, solution ^{13}C NMR spectrum of propiolic acid in D_2O (6.12d) is shown for comparison. Despite the anisotropic broadening effect, these studies clearly show the signature of alkyne group at 79 ppm for the propiolic acid-functionalized ZnO surface (6.12a), fully consistent with that of propiolic acid in solution (77.5 and 73.9 ppm for alkyne carbons; 6.12d). A sharp peak is recorded at 161 ppm (6.12a), corresponding to zinc bidentate carboxylate linkage.³⁵ These observations support the success of propiolic acid modification of the ZnO surface. When the ZnO powder is directly exposed to the liquid phase propiolic acid (6.12b), two additional peaks are observed at 165 ppm and 169 ppm. These two peaks can be attributed to zinc monodentate carboxylate linkage and the physisorbed propiolic acid molecule;³⁶ the peak at 169 ppm is noticeably sharper, likely indicating that the mobility of this physisorbed propiolic acid is much higher than that of the species corresponding to the features of 161 and 165 ppm. This

set of studies is extremely important in that it uncovers the main differences in liquid phase vs. gas-phase modification of ZnO. The gas phase modification offers a much better control of the surface, when the ZnO powder (and by extension many thin films or nanostructures) can be annealed in vacuum prior to exposure to propiolic acid. Thus, a single type of anchoring, the carboxylate formation, is dominant. However, if the ZnO modification is performed in ambient conditions or in a solution, the presence of surface hydroxyl groups and the possibility to form a physisorbed layer of propiolic acid prevents one from preparing well-defined surface with a single type of functionality. Thus, further modification processes are applied not only to the target carboxylate groups on a ZnO surface but also to other functionalities and possibly surface defects, leading to the formation of a much less well-defined mixture of surface species.

So what about the “click” chemistry confirmation by NMR? After being “clicked” with benzyl azide, the propiolic acid-functionalized ZnO surface (7.12c) shows the characteristic peaks of phenyl group and triazole ring at 128 ppm and 135 ppm, clearly showing that the “click” reaction occurred.³⁷ It has to be pointed out that the alkyne carbons at 79 ppm and zinc bidentate carboxylate linkage at 161 ppm do not completely disappear following the click reaction. The former is likely caused by the relatively low efficiency of copper-free “click” reaction and a low apparent yield of gas phase “click” chemistry.²⁰ The latter confirms that the bidentate structure is preserved on the surface following the click reaction. Thus, the ¹³C NMR spectroscopy studies strongly confirm the reaction of propiolic acid with ZnO surface forming a single type of a bidentate carboxylate linkage on ZnO, and the occurrence of the following “click” reaction with benzyl azide.

Overall, the solid state NMR study reinforces the conclusions reached in SEM, FT-IR and XPS investigations. The SEM study suggests that the ZnO surface morphology is preserved during the gas-phase surface modification process with propiolic acid and all the reactions following this initial functionalization. The FT-IR study proves the formation of zinc carboxylate linkage capped with an alkyne group which enables the following “click” reaction. The XPS study indicates the formation of a triazole ring as a result of successful azide–alkyne cycloaddition with the propiolic acid-functionalized ZnO surface. Finally the solid state NMR study provides a strong signature for each surface modification step.

6.3 Conclusion

A simple and precise method to modify the zinc oxide surface with gas-phase propiolic acid in vacuum at room temperature is described. The SSNMR, FT-IR and XPS results prove the formation of a stable bidentate carboxylate linkage to ZnO surface, and the alkyne group on the surface enables subsequent azide–alkyne cycloaddition “click” reaction with benzyl azide. This approach avoids the utilization of carboxylic acid solutions, preserving the surface morphology for further modification protocols, as confirmed by detailed microscopy investigations. This design can serve as a universal method for the modular functionalization of zinc oxide surface following the initial surface preparation. Since this gas-phase interfacial engineering strategy allows for preserving surface structure and morphology of the modified surface from the “etching” effect of acidic modifier, it is an important method for surface modification of ZnO thin films, nanostructures and nanopowders.

REFERENCES

1. Bishop, L. M.; Yeager, J. C.; Chen, X.; Wheeler, J. N.; Torelli, M. D.; Benson, M. C.; Burke, S. D.; Pedersen, J. A.; Hamers, R. J. A Citric Acid-Derived Ligand for Modular Functionalization of Metal Oxide Surfaces via “Click” Chemistry. *Langmuir* **2012**, 28, 1322-1329.
2. Law, M.; Greene, L. E.; Johnson, J. C.; Saykally, R.; Yang, P. Nanowire Dye-Sensitized Solar Cells. *Nat Mater* **2005**, 4, 455-459.
3. Özgür, Ü.; Alivov, Y. I.; Liu, C.; Teke, A.; Reshchikov, M. A.; Doğan, S.; Avrutin, V.; Cho, S.-J.; Morkoç, H. A Comprehensive Review of ZnO Materials and Devices. *J. Appl. Phys.* **2005**, 98, 041301.
4. Cao, Y.; Galoppini, E.; Reyes, P. I.; Lu, Y. Functionalization of Nanostructured ZnO Films by Copper-Free Click Reaction. *Langmuir* **2013**, 29, 7768-7775.
5. Keis, K.; Bauer, C.; Boschloo, G.; Hagfeldt, A.; Westermarck, K.; Rensmo, H.; Siegbahn, H. Nanostructured ZnO Electrodes for Dye-Sensitized Solar Cell Applications. *J. Photochem. Photobiol. A: Chem.* **2002**, 148, 57-64.
6. Rossini, J. E.; Huss, A. S.; Bohnsack, J. N.; Blank, D. A.; Mann, K. R.; Gladfelter, W. L. Binding and Static Quenching Behavior of a Terthiophene Carboxylate on Monodispersed Zinc Oxide Nanocrystals. *J. Phys. Chem. C* **2011**, 115, 11-17.

7. Taratula, O.; Galoppini, E.; Mendelsohn, R.; Reyes, P. I.; Zhang, Z.; Duan, Z.; Zhong, J.; Lu, Y. Stepwise Functionalization of ZnO Nanotips with DNA. *Langmuir* **2009**, *25*, 2107-2113.
8. Liu, D.; Wu, W.; Qiu, Y.; Yang, S.; Xiao, S.; Wang, Q.-Q.; Ding, L.; Wang, J. Surface Functionalization of ZnO Nanotetrapods with Photoactive and Electroactive Organic Monolayers. *Langmuir* **2008**, *24*, 5052-5059.
9. Zhang, B.; Kong, T.; Xu, W.; Su, R.; Gao, Y.; Cheng, G. Surface Functionalization of Zinc Oxide by Carboxyalkylphosphonic Acid Self-Assembled Monolayers. *Langmuir* **2010**, *26*, 4514-4522.
10. Hotchkiss, P. J.; Malicki, M.; Giordano, A. J.; Armstrong, N. R.; Marder, S. R. Characterization of Phosphonic Acid Binding to Zinc Oxide. *J. Mater. Chem.* **2011**, *21*, 3107-3112.
11. Na, H. B.; Lee, I. S.; Seo, H.; Park, Y. I.; Lee, J. H.; Kim, S.-W.; Hyeon, T. Versatile Peg-Derivatized Phosphine Oxide Ligands for Water-Dispersible Metal Oxide Nanocrystals. *Chem. Commun.* **2007**, 5167-5169.
12. Tudisco, C.; Fragalà, M. E.; Giuffrida, A. E.; Bertani, F.; Pinalli, R.; Dalcanale, E.; Compagnini, G.; Condorelli, G. G. Hierarchical Route for the Fabrication of Cavitand-Modified Nanostructured ZnO Fibers for Volatile Organic Compound Detection. *J. Phys. Chem. C* **2016**, *120*, 12611-12617.
13. Greenwood, N. N.; Earnshaw, A., *Chemistry of the Elements 2nd Edition*; Butterworth-Heinemann Limited: Oxford, UK, 1997.
14. Ferracane, J. L., *Materials in Dentistry: Principles and Applications*; Lippincott Williams & Wilkins, 2001.

15. Hewlett, R. M.; McLachlan, M. A. Surface Structure Modification of ZnO and the Impact on Electronic Properties. *Adv. Mater.* **2016**, 28, 3893-3921.
16. Park, J. B.; Oh, H.; Park, J.; Kim, N.-J.; Yoon, H.; Yi, G.-C. Scalable ZnO Nanotube Arrays Grown on CVD-Graphene Films. *APL Materials* **2016**, 4, 106104.
17. Rusli, N. I.; Abdulgafour, H.; Hassan, Z.; Yam, F. K.; Ali, N. K.; Hashim, A. M.; Mahmood, M. R.; Nayan, N. In *ZnO Nanostructures Grown on Porous Silicon Substrate without Catalyst*, 2012 International Conference on Enabling Science and Nanotechnology, 5-7 Jan. 2012; 2012; pp 1-2.
18. Schmidt-Mende, L.; MacManus-Driscoll, J. L. ZnO–Nanostructures, Defects, and Devices. *Mater. Today* **2007**, 10, 40-48.
19. González-Moreno, R., et al. Attachment of Protoporphyrin Dyes to Nanostructured ZnO Surfaces: Characterization by near Edge X-ray Absorption Fine Structure Spectroscopy. *J. Phys. Chem. C* **2011**, 115, 18195-18201.
20. Bebensee, F.; Bombis, C.; Vadapoo, S.-R.; Cramer, J. R.; Besenbacher, F.; Gothelf, K. V.; Linderoth, T. R. On-Surface Azide–Alkyne Cycloaddition on Cu(111): Does It “Click” in Ultrahigh Vacuum? *J. Am. Chem. Soc.* **2013**, 135, 2136-2139.
21. Gao, J.; Teplyakov, A. V. Chemical Transformations of Acetone on ZnO Powder. *J. Catal.* **2014**, 319, 136-141.
22. Gao, J.; Teplyakov, A. V. Surface Species Formed During Thermal Transformation of Ethanol on ZnO Powder. *J. Catal.* **2013**, 300, 163-173.
23. Taratula, O.; Galoppini, E.; Wang, D.; Chu, D.; Zhang, Z.; Chen, H.; Saraf, G.; Lu, Y. Binding Studies of Molecular Linkers to ZnO and MgZnO Nanotip Films. *J. Phys. Chem. B* **2006**, 110, 6506-6515.

24. Keis, K.; Lindgren, J.; Lindquist, S.-E.; Hagfeldt, A. Studies of the Adsorption Process of Ru Complexes in Nanoporous ZnO Electrodes. *Langmuir* **2000**, *16*, 4688-4694.
25. Mudunkotuwa, I. A.; Grassian, V. H. Citric Acid Adsorption on TiO₂ Nanoparticles in Aqueous Suspensions at Acidic and Circumneutral pH: Surface Coverage, Surface Speciation, and Its Impact on Nanoparticle–Nanoparticle Interactions. *J. Am. Chem. Soc.* **2010**, *132*, 14986-14994.
26. Buchholz, M.; Xu, M.; Noei, H.; Weidler, P.; Nefedov, A.; Fink, K.; Wang, Y.; Wöl, C. Interaction of Carboxylic Acids with Rutile TiO₂(110): IR-Investigations of Terephthalic and Benzoic Acid Adsorbed on a Single Crystal Substrate. *Surf. Sci.* **2016**, *643*, 117-123.
27. Knurr, B. J.; Weber, J. M. Structural Diversity of Copper–CO₂ Complexes: Infrared Spectra and Structures of [Cu(CO₂)_n][–] Clusters. *J. Phys. Chem. A* **2014**, *118*, 10246-10251.
28. Baskin, J. M.; Prescher, J. A.; Laughlin, S. T.; Agard, N. J.; Chang, P. V.; Miller, I. A.; Lo, A.; Codelli, J. A.; Bertozzi, C. R. Copper-Free Click Chemistry for Dynamic in Vivo Imaging. *Proc. Natl. Acad. Sci. U.S.A.* **2007**, *104*, 16793-16797.
29. Upadhyay, A. P.; Behara, D. K.; Sharma, G. P.; Bajpai, A.; Sharac, N.; Ragan, R.; Pala, R. G. S.; Sivakumar, S. Generic Process for Highly Stable Metallic Nanoparticle-Semiconductor Heterostructures via Click Chemistry for Electro/Photocatalytic Applications. *ACS Appl. Mater. Interfaces* **2013**, *5*, 9554-9562.
30. Williams, M. G.; Teplyakov, A. V. Building High-Coverage Monolayers of Covalently Bound Magnetic Nanoparticles. *Appl. Surf. Sci.* **2016**, *388*, Part A, 461-467.

31. Liu, Y.; RamaRao, N.; Miller, T.; Hadjipanayis, G.; Teplyakov, A. V. Controlling Physical Properties of Iron Nanoparticles During Assembly by “Click Chemistry”. *J. Phys. Chem. C* **2013**, *117*, 19974-19983.
32. Rostovtsev, V. V.; Green, L. G.; Fokin, V. V.; Sharpless, K. B. A Stepwise Huisgen Cycloaddition Process: Copper(I)-Catalyzed Regioselective "Ligation" of Azides and Terminal Alkynes. *Angew. Chem. Int. Ed.* **2002**, *41*, 2596–2599.
33. Ciampi, S.; Böcking, T.; Kilian, K. A.; James, M.; Harper, J. B.; Gooding, J. J. Functionalization of Acetylene-Terminated Monolayers on Si(100) Surfaces: A Click Chemistry Approach. *Langmuir* **2007**, *23*, 9320-9329.
34. Liang, L.; Astruc, D. The Copper(I)-Catalyzed Alkyne-Azide Cycloaddition (CuAAC) “Click” Reaction and Its Applications. An Overview. *Coord. Chem. Rev.* **2011**, *255*, 2933-2945.
35. Jacobsen, F. E., *Bioinorganic Tools and Zinc Selective Inhibitors for Matrix Metalloproteinases*; ProQuest: University of California, San Diego, 2007.
36. Ye, B.-H.; Li, X.-Y.; Williams, I. D.; Chen, X.-M. Synthesis and Structural Characterization of Di- and Tetranuclear Zinc Complexes with Phenolate and Carboxylate Bridges. Correlations between ^{13}C NMR Chemical Shifts and Carboxylate Binding Modes. *Inorg. Chem.* **2002**, *41*, 6426-6431.
37. Creary, X.; Anderson, A.; Brophy, C.; Crowell, F.; Funk, Z. Method for Assigning Structure of 1,2,3-Triazoles. *J. Org. Chem.* **2012**, *77*, 8756-8761.

Chapter 7

SUMMARY AND FUTURE OPPORTUNITIES

7.1 Summary

In this thesis, a variety of different substrates and nanomaterials including silicon, gold and zinc oxide nanopowder have been functionalized with diverse surface modifiers, aiming at developing new strategies for manipulating the surface properties of semiconductor materials in a controlled way, to benefit future applications in molecular and nanoelectronics, sensing, and solar energy conversion.¹ Our expertise allows us to selectively tune the chemical and physical properties of semiconductor surfaces by an appropriate choice of surface chemistry based on different approaches including chemical passivation, molecular switches and on the use of self-assembled monolayers.² The surface and interface properties were investigated by a combination of spectroscopic techniques including FTIR, XPS, ToF-SIM and NMR, microscopic techniques including AFM, SEM and TEM, computational method such as DFT calculations and charge carrier lifetime measurement to evaluate the electronic property.

7.2 Future Opportunities

Based on the procedures proposed and tested in this thesis for surface modification, functionalization, and chemical assembly, a number of new devices and materials can be designed.

In Chapter 3, a simple and efficient wet chemistry method was designed to prepare a Si(111) surface terminated predominantly with Si-NH-NH-Si functionality. Subsequently, a novel method to covalently attach the Buckminsterfullerene C_{60} to this hydrazine-modified Si(111) surface has been developed and shown to yield high coverage of a C_{60} monolayer, as displayed in Figure 7.1.

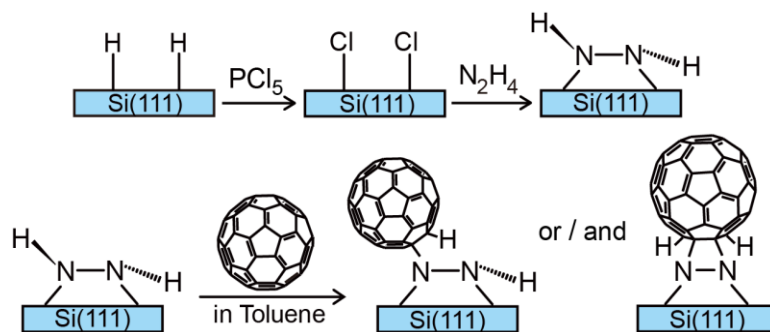


Figure 7.1 Reaction scheme to form a stable interface between C_{60} fullerenes and silicon surface.

Such unique hydrazine-modified silicon surface with high reactivity can serve as a platform for many different further modification protocols; this point has been reinforced by the test of copper precursor, as discussed in Chapter 3 and the study of phenylhydrazine with Cl-Si(111) in Chapter 4. Although in Chapter 5, the carbon nanotube is demonstrated to attach directly through the carbon cage with the amine group of self-assemble monolayer on the surface, same type of chemistry can be applied onto the hydrazine-modified silicon surface.² As illustrated in Figure 7.2, many different types of functionality have been studied on this unique interface, more importantly; we started to learn how to use such surfaces to induce different chemical reactions.

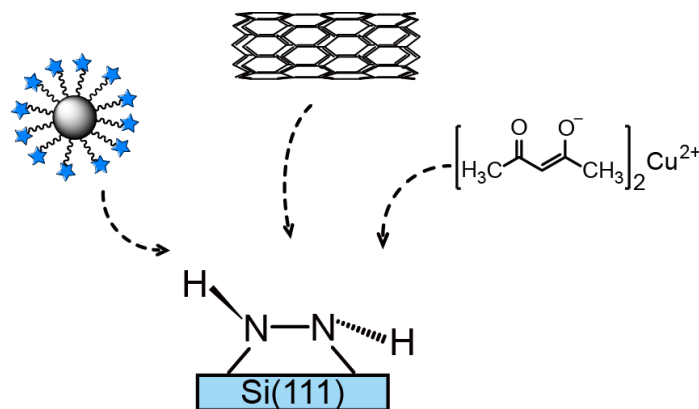


Figure 7.2 Illustration of possible reactions with the hydrazine-modified silicon surface.

In Chapter 6, we introduce a simple and precise method to modify the zinc oxide surface with gas-phase propionic acid in vacuum at room temperature. This gas-phase approach preserves the surface morphology for further modification protocols, free from the “etching” effect of acidic modifier;³ so that this design can serve as a universal method for the modular functionalization of zinc oxide surface following the initial surface preparation. Another interesting point is that the alkyne group available on the propionic acid-modified surface enables the sequential “click” reaction with azide group, which provides a new way for many other applications. For example, a porphyrin derivative containing azide group can be attached to the surface and such porphyrin structure can be incorporated into dye-sensitized solar cells, as well as used as a molecular electronics component or utilized as a supramolecular building block for other systems.⁴⁻⁵



Overall, the ability to control chemistry of surfaces and interfaces will lead to new devices, new applications, new materials and likely new concepts for designing such systems. The current research provides the foundation for these developments.


REFERENCES


1. Bent, S. F.; Teplyakov, A. V. Semiconductor Surface Functionalization for Advances in Electronics, Energy Conversion and Dynamic Systems. *J. Vac. Sci Technol. A* **2013**, *31*, 050810-1-12.
2. Gao, F.; Teplyakov, A. V. Challenges and Opportunities in Chemical Functionalization of Semiconductor Surfaces. *Appl. Surf. Sci.* **2017**, *399*, 375-386.
3. Hewlett, R. M.; McLachlan, M. A. Surface Structure Modification of ZnO and the Impact on Electronic Properties. *Adv. Mater.* **2016**, *28*, 3893-3921.
4. Walter, M. G.; Rudine, A. B.; Wamser, C. C. Porphyrins and Phthalocyanines in Solar Photovoltaic Cells. *J. Porphyrins Phthalocyanines* **2010**, *14*, 759-792.
5. Yella, A.; Lee, H.-W.; Tsao, H. N.; Yi, C.; Chandiran, A. K.; Nazeeruddin, M. K.; Diau, E. W.-G.; Yeh, C.-Y.; Zakeeruddin, S. M.; Grätzel, M. Porphyrin-Sensitized Solar Cells with Cobalt (II/III)-Based Redox Electrolyte Exceed 12 Percent Efficiency. *Science* **2011**, *334*, 629-634.

Appendix A

COPYRIGHT PERMISSION LETTERS



[Home](#) [Account Info](#) [Help](#) 

 **ACS Publications**
Most Trusted. Most Cited. Most Read.

Title: Reaction of Hydrazine with a Chlorine-Terminated Si(111) Surface
Author: Fei Gao, Andrew V. Teplyakov
Publication: The Journal of Physical Chemistry C
Publisher: American Chemical Society
Date: Dec 1, 2014
Copyright © 2014, American Chemical Society

Logged in as:
Fei Gao
Account #:
3001150772
[LOGOUT](#)

PERMISSION/LICENSE IS GRANTED FOR YOUR ORDER AT NO CHARGE

This type of permission/license, instead of the standard Terms & Conditions, is sent to you because no fee is being charged for your order. Please note the following:

- Permission is granted for your request in both print and electronic formats, and translations.
- If figures and/or tables were requested, they may be adapted or used in part.
- Please print this page for your records and send a copy of it to your publisher/graduate school.
- Appropriate credit for the requested material should be given as follows: "Reprinted (adapted) with permission from (COMPLETE REFERENCE CITATION). Copyright (YEAR) American Chemical Society." Insert appropriate information in place of the capitalized words.
- One-time permission is granted only for the use specified in your request. No additional uses are granted (such as derivative works or other editions). For any other uses, please submit a new request.

[BACK](#)[CLOSE WINDOW](#)

Copyright © 2017 Copyright Clearance Center, Inc. All Rights Reserved. [Privacy statement](#), [Terms and Conditions](#).
Comments? We would like to hear from you. E-mail us at customerscare@copyright.com



RightsLink®

Home

Account
Info

Help



ACS Publications
Most Trusted. Most Cited. Most Read.

Title:

Monolayer of Hydrazine
Facilitates the Direct Covalent
Attachment of C60 Fullerene to a
Silicon Surface

Logged in as:

Fei Gao
Account #: 3001150772

Author:

Fei Gao, Andrew V. Teplyakov

LOGOUT

Publication:

Langmuir

Publisher:

American Chemical Society

Date:

Feb 1, 2017

Copyright © 2017, American Chemical Society

PERMISSION/LICENSE IS GRANTED FOR YOUR ORDER AT NO CHARGE

This type of permission/license, instead of the standard Terms & Conditions, is sent to you because no fee is being charged for your order. Please note the following:

- Permission is granted for your request in both print and electronic formats, and translations.
- If figures and/or tables were requested, they may be adapted or used in part.
- Please print this page for your records and send a copy of it to your publisher/graduate school.
- Appropriate credit for the requested material should be given as follows: "Reprinted (adapted) with permission from (COMPLETE REFERENCE CITATION). Copyright (YEAR) American Chemical Society." Insert appropriate information in place of the capitalized words.
- One-time permission is granted only for the use specified in your request. No additional uses are granted (such as derivative works or other editions). For any other uses, please submit a new request.

BACK

CLOSE WINDOW

Copyright © 2017 Copyright Clearance Center, Inc. All Rights Reserved. [Privacy statement](#), [Terms and Conditions](#).
Comments? We would like to hear from you. E-mail us at customercare@copyright.com



RightsLink®

Home

Account
Info

Help



Title: Dehydrohalogenation
Condensation Reaction of
Phenylhydrazine with Cl-
Terminated Si(111) Surfaces

Logged in as:

Fei Gao

Account #:
3001150772

Author: Fei Gao, Andrew V. Teplyakov

LOGOUT

Publication: The Journal of Physical Chemistry
C

Publisher: American Chemical Society

Date: Mar 1, 2016

Copyright © 2016, American Chemical Society

PERMISSION/LICENSE IS GRANTED FOR YOUR ORDER AT NO CHARGE

This type of permission/license, instead of the standard Terms & Conditions, is sent to you because no fee is being charged for your order. Please note the following:

- Permission is granted for your request in both print and electronic formats, and translations.
- If figures and/or tables were requested, they may be adapted or used in part.
- Please print this page for your records and send a copy of it to your publisher/graduate school.
- Appropriate credit for the requested material should be given as follows: "Reprinted (adapted) with permission from (COMPLETE REFERENCE CITATION). Copyright (YEAR) American Chemical Society." Insert appropriate information in place of the capitalized words.
- One-time permission is granted only for the use specified in your request. No additional uses are granted (such as derivative works or other editions). For any other uses, please submit a new request.

BACK

CLOSE WINDOW

Copyright © 2017 Copyright Clearance Center, Inc. All Rights Reserved. [Privacy statement](#), [Terms and Conditions](#).
Comments? We would like to hear from you. E-mail us at customercare@copyright.com



RightsLink®

Home

Account
Info

Help



ACS Publications
Most Trusted. Most Cited. Most Read.

Title:

Carbon Nanotubes Covalently
Attached to Functionalized
Surfaces Directly through the
Carbon Cage

Logged in as:

Fei Gao

Account #:
3001150772

Author:

Mackenzie G. Williams, Fei Gao,
Ibtihel BenDhiab, et al

LOGOUT

Publication: Langmuir

Publisher: American Chemical Society

Date: Feb 1, 2017

Copyright © 2017, American Chemical Society

PERMISSION/LICENSE IS GRANTED FOR YOUR ORDER AT NO CHARGE

This type of permission/license, instead of the standard Terms & Conditions, is sent to you because no fee is being charged for your order. Please note the following:

- Permission is granted for your request in both print and electronic formats, and translations.
- If figures and/or tables were requested, they may be adapted or used in part.
- Please print this page for your records and send a copy of it to your publisher/graduate school.
- Appropriate credit for the requested material should be given as follows: "Reprinted (adapted) with permission from (COMPLETE REFERENCE CITATION). Copyright (YEAR) American Chemical Society." Insert appropriate information in place of the capitalized words.
- One-time permission is granted only for the use specified in your request. No additional uses are granted (such as derivative works or other editions). For any other uses, please submit a new request.

BACK

CLOSE WINDOW

Copyright © 2017 Copyright Clearance Center, Inc. All Rights Reserved. [Privacy statement](#), [Terms and Conditions](#).
Comments? We would like to hear from you. E-mail us at customercare@copyright.com



RightsLink®

Home

Account
Info

Help



ACS Publications
Most Trusted. Most Cited. Most Read.

Title:

Chemical Protection of Material
Morphology: Robust and Gentle
Gas-Phase Surface
Functionalization of ZnO with
Propiolic Acid

Logged in as:

Fei Gao

Account #:

3001150772

LOGOUT

Author:

Fei Gao, Soraya Aminane, Shi
Bai, et al

Publication: Chemistry of Materials

Publisher: American Chemical Society

Date: May 1, 2017

Copyright © 2017, American Chemical Society

PERMISSION/LICENSE IS GRANTED FOR YOUR ORDER AT NO CHARGE

This type of permission/license, instead of the standard Terms & Conditions, is sent to you because no fee is being charged for your order. Please note the following:

- Permission is granted for your request in both print and electronic formats, and translations.
- If figures and/or tables were requested, they may be adapted or used in part.
- Please print this page for your records and send a copy of it to your publisher/graduate school.
- Appropriate credit for the requested material should be given as follows: "Reprinted (adapted) with permission from (COMPLETE REFERENCE CITATION). Copyright (YEAR) American Chemical Society." Insert appropriate information in place of the capitalized words.
- One-time permission is granted only for the use specified in your request. No additional uses are granted (such as derivative works or other editions). For any other uses, please submit a new request.

BACK

CLOSE WINDOW

Copyright © 2017 Copyright Clearance Center, Inc. All Rights Reserved. [Privacy statement](#), [Terms and Conditions](#).
Comments? We would like to hear from you. E-mail us at customer@copyright.com